NASA/TM—2014-218395

Development and Experimental Evaluation of Passive Fuel Cell Thermal Control

Anthony J. Colozza and Ian J. Jakupca
Vantage Partners Inc., Brookpark Ohio

Charles H. Castle
ZIN Technologies, Middleburg Heights, Ohio

Kenneth A. Burke
Glenn Research Center, Cleveland, Ohio

December 2014

NASA STI Program . . . in Profile

Since its founding, NASA has been dedicated to the advancement of aeronautics and space science. The NASA Scientific and Technical Information (STI) program plays a key part in helping NASA maintain this important role.

The NASA STI Program operates under the auspices of the Agency Chief Information Officer. It collects, organizes, provides for archiving, and disseminates NASA's STI. The NASA STI program provides access to the NASA Aeronautics and Space Database and its public interface, the NASA Technical Reports Server, thus providing one of the largest collections of aeronautical and space science STI in the world. Results are published in both non-NASA channels and by NASA in the NASA STI Report Series, which includes the following report types:

- TECHNICAL PUBLICATION. Reports of completed research or a major significant phase of research that present the results of NASA programs and include extensive data or theoretical analysis. Includes compilations of significant scientific and technical data and information deemed to be of continuing reference value. NASA counterpart of peer-reviewed formal professional papers but has less stringent limitations on manuscript length and extent of graphic presentations.

- TECHNICAL MEMORANDUM. Scientific and technical findings that are preliminary or of specialized interest, e.g., quick release reports, working papers, and bibliographies that contain minimal annotation. Does not contain extensive analysis.

- CONTRACTOR REPORT. Scientific and technical findings by NASA-sponsored contractors and grantees.

- CONFERENCE PUBLICATION. Collected papers from scientific and technical conferences, symposia, seminars, or other meetings sponsored or cosponsored by NASA.

- SPECIAL PUBLICATION. Scientific, technical, or historical information from NASA programs, projects, and missions, often concerned with subjects having substantial public interest.

- TECHNICAL TRANSLATION. English-language translations of foreign scientific and technical material pertinent to NASA's mission.

Specialized services also include creating custom thesauri, building customized databases, organizing and publishing research results.

For more information about the NASA STI program, see the following:

- Access the NASA STI program home page at *http://www.sti.nasa.gov*

- E-mail your question to *help@sti.nasa.gov*

- Fax your question to the NASA STI Information Desk at 443–757–5803

- Phone the NASA STI Information Desk at 443–757–5802

- Write to:
  STI Information Desk
  NASA Center for AeroSpace Information
  7115 Standard Drive
  Hanover, MD 21076–1320

NASA/TM—2014-218395

Development and Experimental Evaluation of Passive Fuel Cell Thermal Control

Anthony J. Colozza and Ian J. Jakupca
Vantage Partners Inc., Brookpark Ohio

Charles H. Castle
ZIN Technologies, Middleburg Heights, Ohio

Kenneth A. Burke
Glenn Research Center, Cleveland, Ohio

National Aeronautics and
Space Administration

Glenn Research Center
Cleveland, Ohio 44135

December 2014

Level of Review: This material has been technically reviewed by technical management.

Available from

NASA Center for Aerospace Information
7115 Standard Drive
Hanover, MD 21076–1320

National Technical Information Service
5301 Shawnee Road
Alexandria, VA 22312

Available electronically at http://www.sti.nasa.gov

Contents

Development and Experimental Evaluation of Passive Fuel Cell Thermal Control

Anthony J. Colozza and Ian J. Jakupca
Vantage Partners Inc.
Brookpark Ohio 44142

Charles H. Castle
ZIN Technologies
Middleburg Heights, Ohio 44130

Kenneth A. Burke
National Aeronautics and Space Administration
Glenn Research Center
Cleveland, Ohio 44135

Abstract

To provide uniform cooling for a fuel cell stack, a cooling plate concept was evaluated. This concept utilized thin cooling plates to extract heat from the interior of a fuel cell stack and move this heat to a cooling manifold where it can be transferred to an external cooling fluid. The advantages of this cooling approach include a reduced number of ancillary components and the ability to directly utilize an external cooling fluid loop for cooling the fuel cell stack. A number of different types of cooling plates and manifolds were developed. The cooling plates consisted of two main types; a plate based on thermo-pyrolytic graphite (TPG) and a planar (or flat plate) heat pipe. The plates, along with solid metal control samples, were tested for both thermal and electrical conductivity. To transfer heat from the cooling plates to the cooling fluid, a number of manifold designs utilizing various materials were devised, constructed, and tested. A key aspect of the manifold was that it had to be electrically nonconductive so it would not short out the fuel cell stack during operation. Different manifold and cooling plate configurations were tested in a vacuum chamber to minimize convective heat losses. Cooling plates were placed in the grooves within the manifolds and heated with surface-mounted electric pad heaters. The plate temperature and its thermal distribution were recorded for all tested combinations of manifold cooling flow rates and heater power loads. This testing simulated the performance of the cooling plates and manifold within an operational fuel cell stack. Different types of control valves and control schemes were tested and evaluated based on their ability to maintain a constant temperature of the cooling plates. The control valves regulated the cooling fluid flow through the manifold, thereby controlling the heat flow to the cooling fluid. Through this work, a cooling plate and manifold system was developed that could maintain the cooling plates within a minimal temperature band with negligible thermal gradients over power profiles that would be experienced within an operating fuel cell stack.

1.0 Introduction

Initial work was previously performed on the analysis of the cooling plate and manifold concept (Ref. 1). The subsequent design and testing discussed here was performed to evaluate both individual components as well as an integrated system to further investigate the concept of utilizing conductive plates to cool a fuel cell. This concept differs from conventional fuel cell stack thermal control which utilizes the flow of a cooling fluid within the fuel cell stack. By providing a means of transferring heat out of the fuel cell stack to an external cooling loop, this approach has a number of potential benefits:

- Reduced stack complexity (elimination of internal seals and internal fluid passages)
- Reduced Stack Volume (the cooling plates are designed to be thinner than the present cooling passages)

- Reduced Stack Mass (There is a potential mass savings by designing a system based around high conductivity cooling plates)
- Reduced Ancillary Components (a simplified cooling system may eliminate the need for a dedicated fuel cell stack cooling loop)

The experimental evaluation of the cooling plate/manifold concept was conducted in three main phases: cooling plate design and evaluation, cooling manifold design and evaluation and integrated cooling plate/manifold testing and evaluation. The first step involved determining the requirements for the thermal and electrical conductivity for the different types of plates and different methods of plate construction. The ideal cooling plate would have both high thermal and electrical conductivity. High thermal conductivity provides better thermal control of the fuel cell stack by providing a more rapid response to changes in output power. It also enables the plate to maintain a more uniform temperature distribution that minimizes internal thermal stresses, improves cell performance, and can potentially provide longer operational life. The cooling plates must also be electrically conductive so that current can flow from one cell to the next within the fuel cell stack. As a source of stack inefficiency, the electrical resistance of the cooling plates will directly affect the overall efficiency of the fuel cell. Baseline electrical and thermal conductivity tests were performed with copper and stainless steel plates to both verify the testing facility and method as well as provide a comparison to the other types of cooling plates being evaluated. Two main types of high thermal conductivity cooling plates were tested; thermo-pyrolytic graphite (TPG) based plates and planar (or flat-plate) heat pipes. The results from this testing were used to characterize the various cooling plate designs and to select the best plate design for use in the subsequent manifold testing.

In addition to the thermal and electrical conductivity tests, a series of operational tests were performed on the flat plate heat pipes under different orientations and condenser areas. Rather than using conduction to transfer thermal energy like the TPG plates, heat pipes utilize nucleated heat transfer to carry thermal energy from the evaporator to the condenser utilizing a working fluid, which boils in the evaporator section and condenses in the condenser section. This is a much different heat transfer mechanism than the material thermal conductivity utilized in the TPG plates that were tested. Therefore, a series of tests were performed to evaluate the operation of the heat pipe under different orientations and condenser areas to determine their operating limits. The condenser area consists of the area of the heat pipe surface in direct contact with the cooling manifold. The evaporator area is in contact with the active area within the fuel cell stack. It is within this area the internal working fluid of the heat pipe is condensed back to a liquid. The heat pipe operational evaluation was performed to determine any orientation sensitivity or condenser area requirements of the heat pipe so that they could be applied in the subsequent development and testing.

The second phase evaluated a number of cooling plates installed in a manifold through which a cooling fluid was circulated. The ability for the cooling plates to move heat into the cooling fluid was evaluated under various heating loads, provided through electric surface-mount pad heaters, and coolant flow rates and temperatures. The objective of this testing was to determine the rate and distribution of heat transfer from the cooling plates through the manifold wall into the cooling fluid.

The manifold tests also were used to evaluate different manifold designs and materials. The manifold provides the main thermal connection between the cooling plates and the cooling fluid. Therefore, its design has a significant impact on the overall performance of the cooling plates and the fuel cell stack. The manifold is also required to be electrically isolating between the cooling plates to avoid creating an electrical short in the fuel cell stack. Each individual cooling plate is electrically conductive, at unique electrical potentials, and in contact with the cooling manifold. The main objective of the manifold design is to enable a high heat flux between the cooling plates and the cooling fluid. The manifold design that provided the greatest heat transfer was used in the subsequent integrated control testing.

The third and final phase of the testing was an integrated control test. This testing evaluated the ability of the cooling plate system to react to varying thermal loads. Two types of control valves were utilized during the control testing. The first type was an active control valve that regulated the coolant water flow based on temperature feedback from the cooling plates. The second type of valve was a passive thermostatic valve that automatically opened and closed based on the coolant water temperature. Different valve designs were evaluated to determine what valve characteristics provided the greatest amount of thermal control. The objective of the control testing was to minimize the temperature fluctuation of the cooling plates as the thermal load varied.

These three phases of the cooling plate/manifold design and evaluation provided a means of fully assessing the concept and developing it to the level where it could be incorporated into an operational fuel cell stack.

2.0 Cooling Plate Design, Materials and Construction

Cooling plates are used as a means of removing heat from the interior of the fuel cell stack, rejecting it to an external heat exchanger, and transferring the heat to an external radiator to be dissipated to the surroundings. The characteristics and capabilities of the cooling plates are critical to the overall feasibility of this fuel cell thermal control concept. The main requirements for the cooling plates are listed below.

- The cooling plates have to be electrically conductive for the fuel cell to operate effectively. Since the cooling plates are located between each cell, or grouping of cells, within a fuel cell stack, current must flow through the cooling plates to complete the internal circuit within the fuel cell. The electrical resistance of each cooling plate will need to be as low as possible to reduce the resistance losses associated with this current flow.
- The cooling plates need to be thermally conductive. The higher the thermal conductivity of the cooling plates, the more effectively the heat will be transferred out of the fuel cell and the more uniform the internal temperature distribution will be. The smaller the thermal gradient within the fuel cell the better its performance and lifetime will be.
- The cooling plates need to be as lightweight as possible. The required cooling plate thickness will ultimately be driven by the thermal conductivity of the cooling plate and the heat load on the plate. The higher the thermal conductivity, the thinner the plates can be for a given heat load. Also, the lower the density of the cooling plate material the lower the mass of the cooling plates. Minimizing mass and thickness of the cooling plates reduces the volume and specific mass of the fuel cell system.

Two types of cooling plates were identified that could meet the requirements listed above. These consisted of plates based on a thermal pyrolytic graphite (TPG) and a planar (or flat plate) heat pipe.

2.1 Thermal Pyrolytic Graphite Cooling Plates

Thermal pyrolytic graphite (TPG), shown in Figure 2.1, is similar to conventional graphite in composition, however it differs in the bonding between the internal layers of graphene. It is produced through a process of high temperature vacuum deposition and can be constructed into very thin sheets. Due to the bonding mechanism during its formation, pyrolytic graphite has cleavage planes similar to those seen in Mica. Also, the surface finish is not flat in relation to the assembly tolerances required by the fuel cell stack and has slight peaks and valleys due to the same cleavage planes. The surface roughness for two sample pieces of TPG (sample TPG plate 1 and 2), which were similar to that shown in Figure 2.1, was tested. The average surface roughness for each of the samples was 2.013 and 2.160 μm, respectively. Because of the cleavage plane, surface irregularities, and the general brittle nature of the material, its surface needs to be covered or coated to improve its handleability.

Figure 2.1.—TPG Sample (9.8- by 9.8- by 0.05-cm)

TABLE 2.1.—THICKNESS CHARACTERISTICS
OF THE 8.9- BY 8.9-cm TPG SAMPLES

Plate	1	2
Average thickness, mm	0.368	0.371
Maximum thickness, mm	0.381	0.384
Minimum thickness, mm	0.361	0.358
Percent variation	1.6%	2.1%

In addition to the surface roughness, another aspect of the plate construction is the uniformity in thickness. The two sample plates were measured at various points over their surface to determine the thickness profile for the plate. This thickness profile is plotted in Figure 2.2 and Figure 2.3 for TPG sample plate 1 and 2, respectively, and given in Table 2.1. From this data it can be seen that although there is a variation in the thickness over the plate it is fairly small and well within the acceptable limits of 0.1 mm for the fuel cell cooling application.

A larger series of TPG plates was also utilized, shown in Figure 2.4. These plates were fabricated with a series of holes along the edge, rounded corners, and the heat extraction area was recessed slightly from the full plate length. These plates were designed for use within an operational fuel cell and measured 18.9- by 9.8- by 0.5-cm. The construction drawing for these plates is shown in Appendix A. As with the smaller TPG plates there was some variation in the plate thickness from plate to plate and over the plate surface. This variation for a 12-plate sample is given in Table 2.2 and the thickness distribution plots are given in Appendix B.

To improve the handleability and structural integrity of the TPG cooling plates, various surface coverings and coatings were tried. Each approach utilized a TPG sample similar to that shown in Figure 2.1 as the base material and then the coating or covering was applied to its surface.

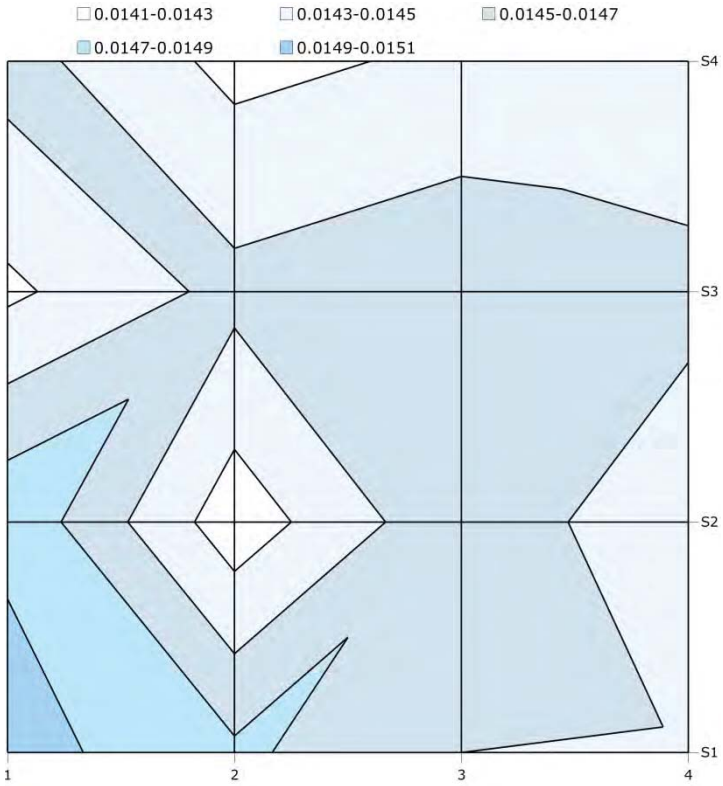

Figure 2.2.—TPG Sample 1 Plate Thickness (inches)

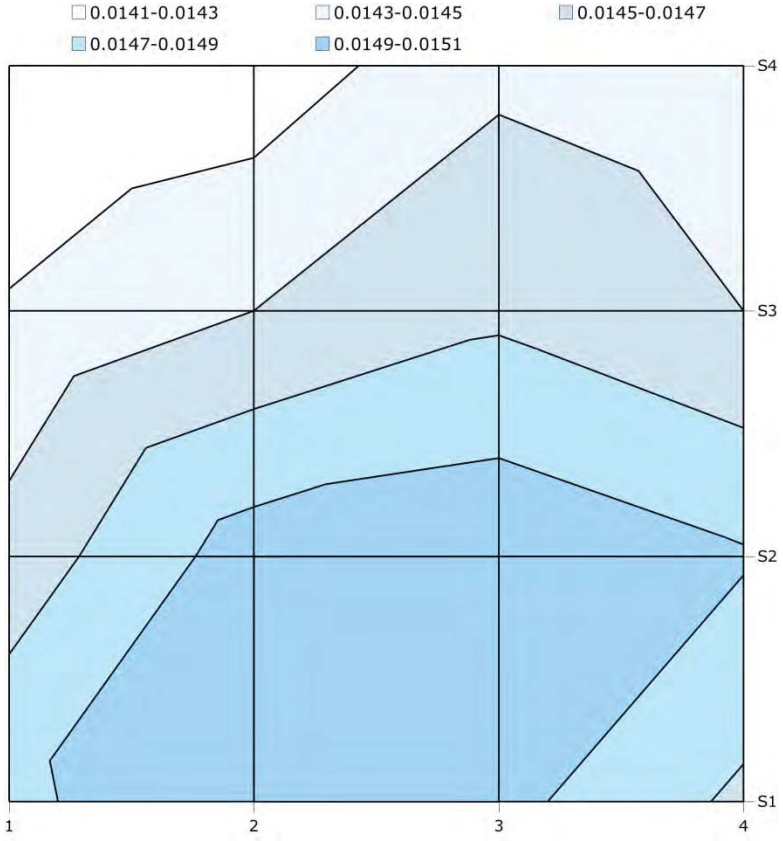

Figure 2.3.—TPG Sample 2 Plate Thickness (inches)

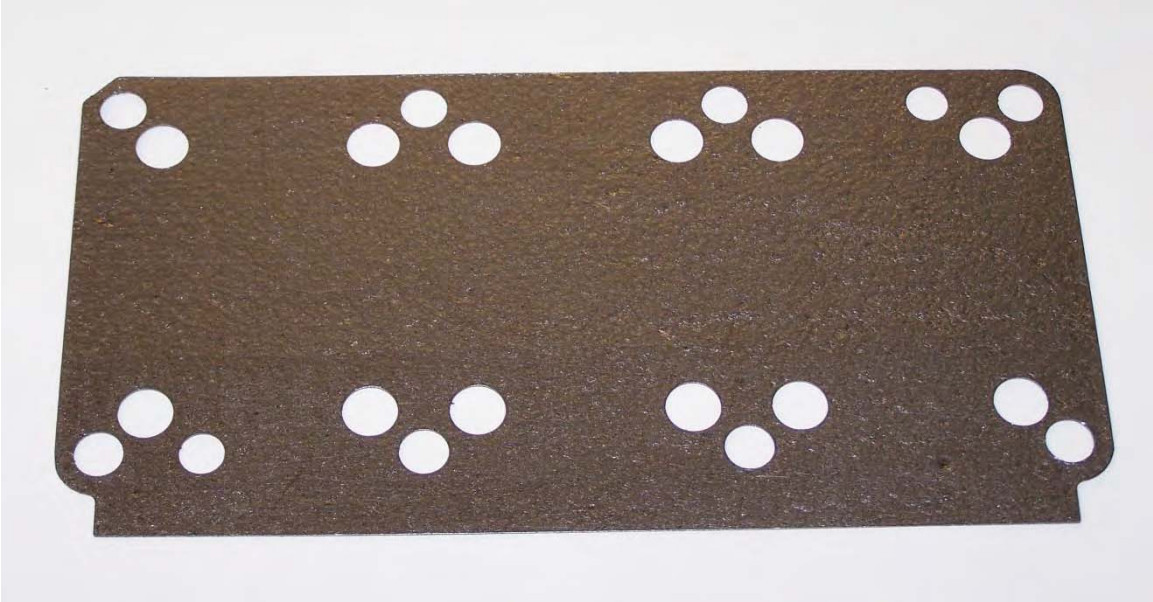

Figure 2.4.—TPG Fuel Cell Cooling Plate (18.9- by 9.8-cm)

TABLE 2.2.—THICKNESS CHARACTERISTICS OF THE 18.9- BY 8.9-cm TPG SAMPLES

Plate number	Average thickness, mm	Maximum thickness, mm	Minimum thickness, mm	Percent variation
1	0.53	0.55	0.52	1.8
2	0.53	0.56	0.51	3.1
3	0.55	0.57	0.53	1.4
4	0.55	0.57	0.52	2.1
5	0.53	0.55	0.52	1.6
6	0.54	0.57	0.52	2.6
7	0.50	0.53	0.47	3.2
8	0.52	0.55	0.51	1.6
9	0.55	0.58	0.53	2.1
10	0.53	0.55	0.51	1.9
11	0.51	0.55	0.48	3.3
12	0.52	0.55	0.49	2.8
Average	0.53	0.56	0.51	2.3

2.1.1 Diffusion Bonded Steel With TPG Core

This type of cooling plate utilized two 316 steel plates. These plates had a central region machined out to form a recess equivalent to the thickness of the TPG plate. The TPG plate was placed in this recess and the top and bottom steel halves were diffusion bonded together. A number of these plates were constructed, one of which is shown in Figure 2.5. Their dimensions were 10.15- by 10.15- by 0.11-cm.

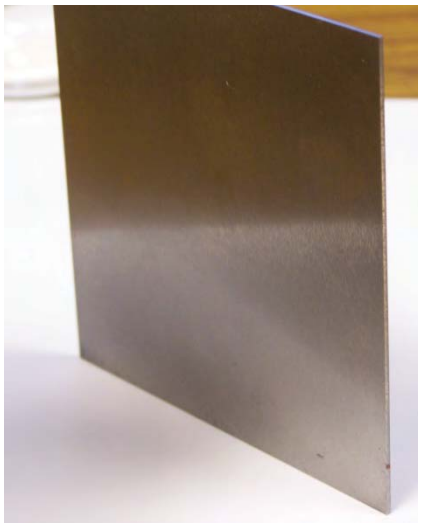

Figure 2.5.—Diffusion Bonded Steel
with TPG Core Cooling Plate

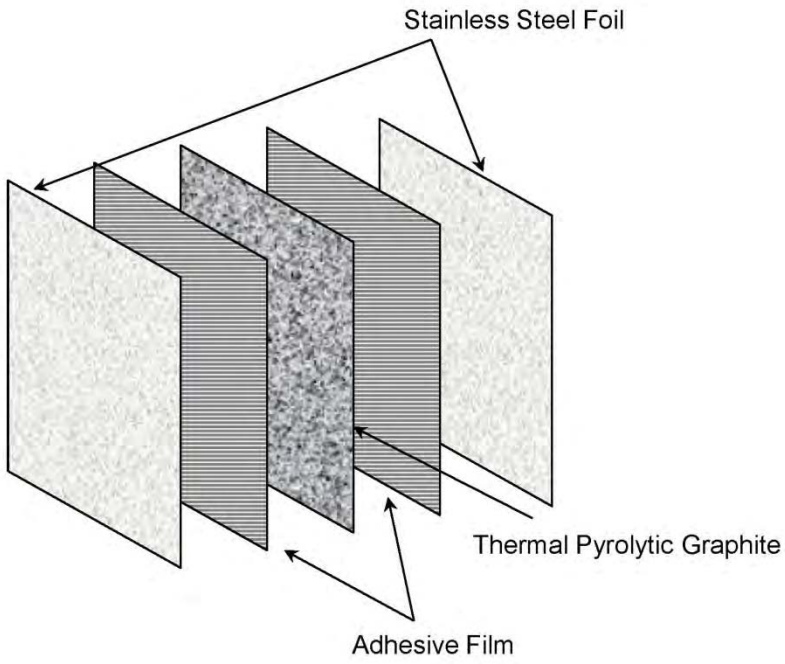

(Note Adhesive thickness on the order of 3 mil)

Figure 2.6.—Stainless Steel Clad TPG Plate Lay-up

2.1.2 Metal Clad TPG

In order to reduce the thickness of the diffusion bonded plates, a number of stainless steel clad TPG plates were constructed. These plates were constructed with two layers of 316 stainless steel foil 0.05-mm thick over a core TPG plate. The outer foil layers were attached to the TPG using a polyester film adhesive approximately 0.076-mm thick, as illustrated in Figure 2.6. To construct the plates the layers were assembled and the plates were then placed in a heated press. A press pressure of 8,900 N (2,000 lb) and temperature of 170 °C was applied to the plate for approximately 1 hr.

To improve upon the electrical and thermal conductivities of the stainless steel clad TPG plate, a copper clad TPG plate was constructed. Since copper has a higher thermal and electrical conductivity than stainless steel it provided a lower thermal and electrical resistance to the TPG and thereby improved the plate's performance. The copper clad plate, shown in Figure 2.7, was constructed using the same process and adhesive as the stainless steel one except that copper foil was used for the outer layer instead of stainless steel, as illustrated in Figure 2.6.

To further improve the performance of the copper clad TPG plates, two types of electrically and thermally conductive film adhesives from Btechcorp (Ref. 2) were evaluated, ATTA (advanced thermal transfer adhesive) LM-2 and TP-1 ACF (Anisotropic Conductive Film). ATTA LM-2 utilizes graphite fibers oriented normal to the plane of the graphene ("z" direction) held within an epoxy resin. The adhesive is activated under pressure at 130 °C for 1 hr. The second conductive adhesive, TP-1 ACF, utilizes nickel fibers in a thermoplastic film adhesive. This adhesive is activated under a compressive load at 170°C within a vacuum environment.

The copper clad plates utilizing the ATTA LM-2 adhesive were constructed in the heated press held at a pressure of approximately 8,900 N (2,000 lb) and a temperature of 130 °C for 1 hr. The copper clad plates utilizing the TP-1 ACF adhesive were placed inside a vacuum bag within the press. A pressure of 8,900 N (2,000 lb) was applied and the temperature was raised to 170 °C. Once at temperature the heaters were turned off and the plated was allowed to cool under pressure and in vacuum.

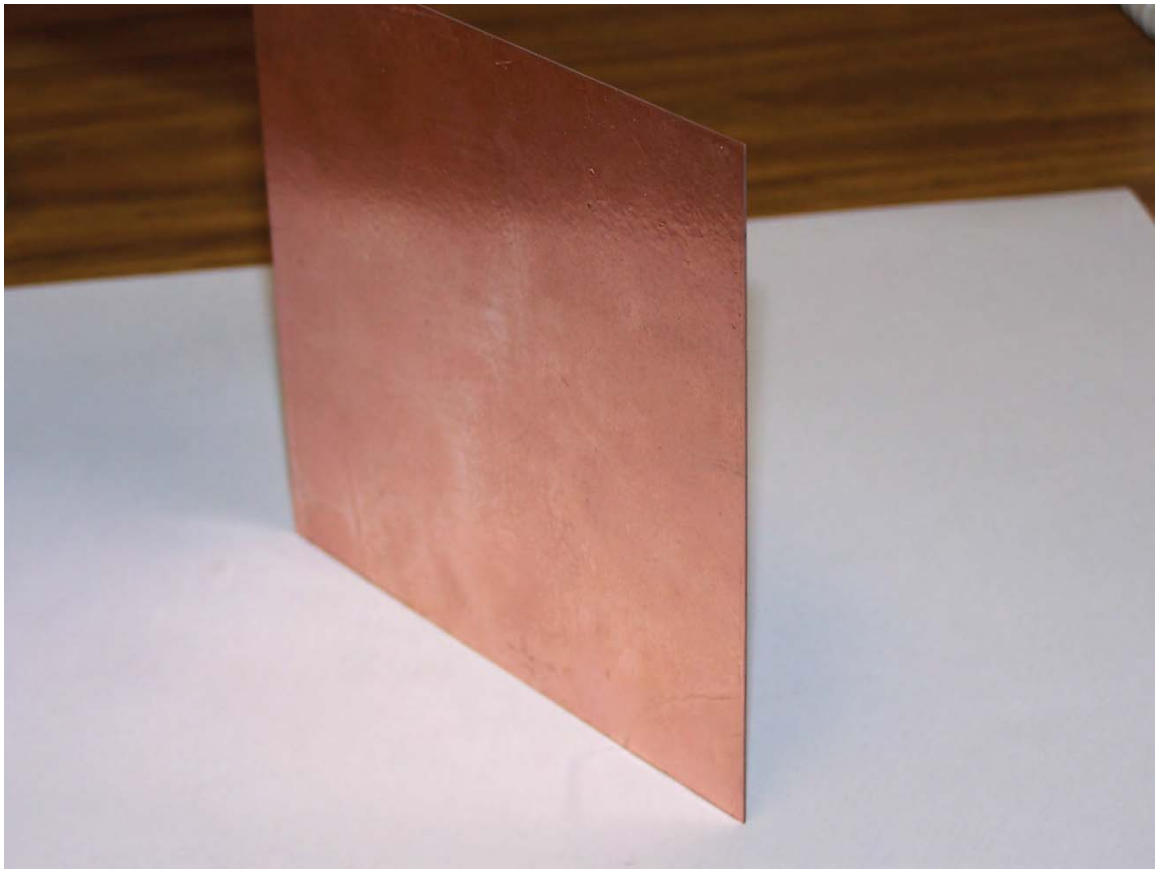

Figure 2.7.—Copper Clad TPG Cooling Plate

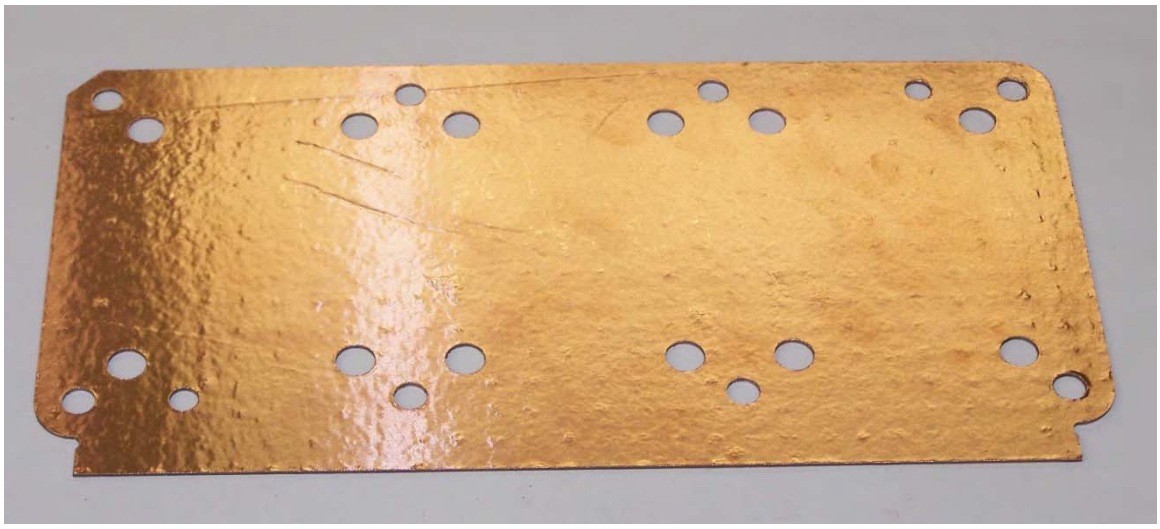

Figure 2.8.—The 18.9- by 8.9-cm Fuel Cell Copper Clad TPG Cooling Plate

A number of the larger area copper clad TPG plates were also constructed with the 18.9- by 9.8-cm TPG plates. These larger copper clad plates, shown in Figure 2.8, were all constructed with the TP-1 adhesive. They were constructed using the same process as the smaller square copper clad plates. The larger plates have holes distributed over their surface, as seen in Figure 2.8 and Figure 2.10. For a fuel cell application, the reactant gasses will pass from cell to cell through these holes. To seal these ports and minimize the potential for a chemical reaction between the reactant gasses and the cooling plate material, stainless steel washers were used as a liner for the holes in the plates and to support the o-rings. During the manufacturing process, the washers were held in place with the TP-1 adhesive.

2.1.3 Painted TPG

As a means of simplifying the construction process and potentially providing a thinner, lighter weight plate, two types of conductive paint applied directly to the TPG plate were evaluated; a carbon paint and a silver paint both manufactured by SPI (Ref. 3). The carbon paint contained micro-graphite particles to provide enhanced electrical and thermal conductivity. The silver paint has a high concentration of fine silver particles within a polymer adhesive.

Initially, the paint was brushed onto the TPG plates by hand. This resulted in inconsistent paint thickness and surface finish which would occasionally flow over and fill in the larger irregularities on the plate's surface. To provide a more consistent and uniform coat, an air-pressurized spray gun was used to apply the paint using isopropyl alcohol as a diluting agent. The spray application provided a very controllable, repeatable, and uniform coating. The paint thickness applied to the TPG plates was approximately 0.04 mm. Both the smaller square (9.8- by 9.8-cm) and the larger fuel cell plates (18.9- by 9.8-cm) were produced with the painted surface.

Both types of paint adhered very well to the TPG, with no peeling or flaking of the paint noted on any of the plates. The majority of the painted plates utilized the silver conductive paint due to its better electrical conductivity properties. A carbon painted TPG plate is shown in Figure 2.9 and the silver painted TPG plate is shown in Figure 2.10.

Figure 2.9.—Carbon Painted TPG Plate (9.8- by 9.8-cm)

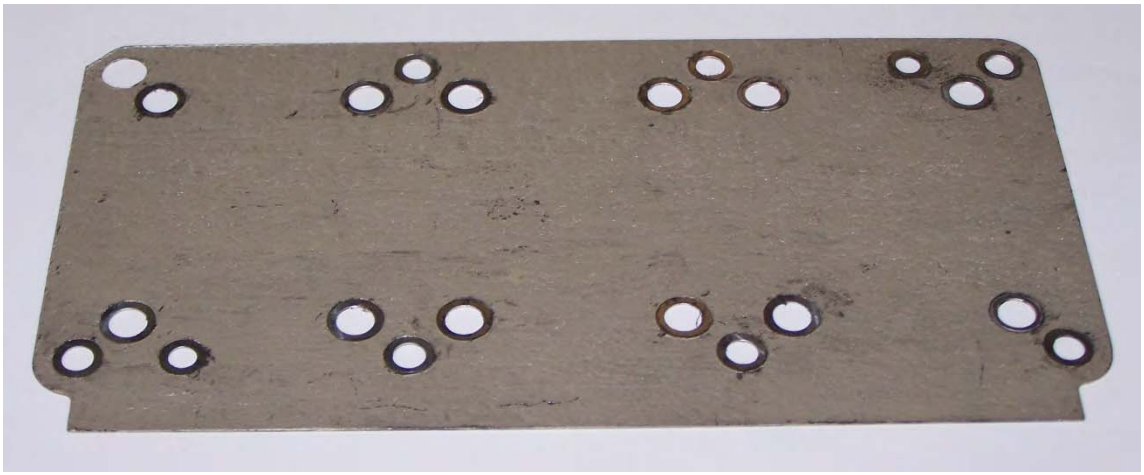

Figure 2.10.—Fuel Cell Silver Painted TPG Cooling Plate (18.9- by 9.8-cm)

2.1.4 Metal Plated TPG

Another means of providing a uniform finish with considerable control over the coating thickness is through plating or sputtering process. An electroplating process was initially tried to place a layer of copper onto the TPG. Copper was successfully deposited onto the TPG but the adhesion was very poor. To possibly increase the adhesion a thin layer of copper was sputtered onto the TPG surface. The sputtered copper was on the order of a few angstroms thick, and adhered well to the surface. Additional copper was then plated over the sputtered copper layer. However, once the copper plating was applied the sputtered layer along with the copper plating began to peel off. No successful copper plated TPG plates were constructed.

2.2 Flat Plate Heat Pipes

The second type of cooling plate tested was a planar, or flat plate, heat pipe. A heat pipe transfers heat through the process of an internal fluid liquid to gas phase change, which differs significantly from the purely conductive TPG plates described previously. A heat pipe utilizes an internal fluid that moves heat

from one location on the heat pipe (evaporator) to another location (condenser) through capillary action, differential internal pressures, and phase change of the working fluid. The difference in heat transfer mechanisms result in different operating properties from the conductive plates. Due to the phase change of the internal working fluid, heat pipes have a much greater capacity to move heat and maintain a single operating temperature. Heat pipes are designed to operate over a small-specified temperature range: this temperature range is based on the characteristics of the internal working fluid and the internal pressure. Outside of this operating temperature range, the heat pipe will not function. In addition, because fluid is moving internally within the heat pipe during operation, a heat pipe can be sensitive to orientation.

For the fuel cell cooling application, water is a good working fluid for the heat pipe. A water heat pipe can be designed to transfer heat within the temperature range 273 to 643 K (Ref. 4). This temperature range is an overall range for water as a working fluid. A specific heat pipe design will function over a much smaller temperature range. Typically heat pipes are cylindrical in shape. Fluid is carried from the condensing section to the evaporator section through a wick structure located along the inside surface of the cylinder wall. The central portion is hollow and allows for vapor transport from the evaporator to the condenser section. A diagram of the basic heat pipe operation is shown in Figure 2.11.

This cylindrical shape is not ideal for integration into a fuel cell as a cooling plate. Therefore a different geometry based on a flat plate was utilized (Refs. 5 and 6). This planar, or flat plate, heat pipe operates in a similar fashion as the cylindrical type, shown in Figure 2.11. Other than the geometry, one of the main differences in operation over the conventional cylindrical design is that the heat input occurs over a large portion of the surface area, approximately 75 percent. The heat transfer surface area to internal volume ratio for a flat plate heat pipe is on the order of 10 times greater than that for a conventional cylindrical design. A diagram showing the layout of the flat plate heat pipe is shown in Figure 2.12.

Utilizing this planar heat pipe design, two initial planar heat pipes were constructed. These flat plate heat pipes, shown in Figure 2.13, were made of copper with water as a working fluid. To improve upon these and reduce their weight and thickness, a second generation of heat pipes was then constructed. These second-generation flat plate heat pipes, shown in Figure 2.14, were constructed of titanium. A final set of six titanium flat plate heat pipes, shown in Figure 2.15, was constructed for use within a prototype fuel cell stack for testing and evaluation. To work in the fuel cell stack, the shape of these flat plate heat pipes was different than the initial copper or titanium ones. They were also painted with SPI silver paint to improve their electrical conductivity properties and eliminate oxidization of their surface. The characteristics of each of the heat pipes constructed are summarized in Table 2.3 (Refs. 7 and 8).

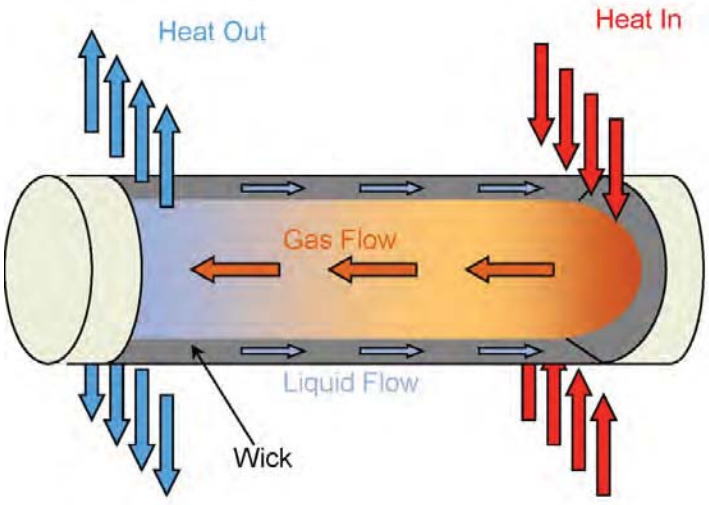

Figure 2.11.—Conventional Tubular Heat Pipe Operational Diagram

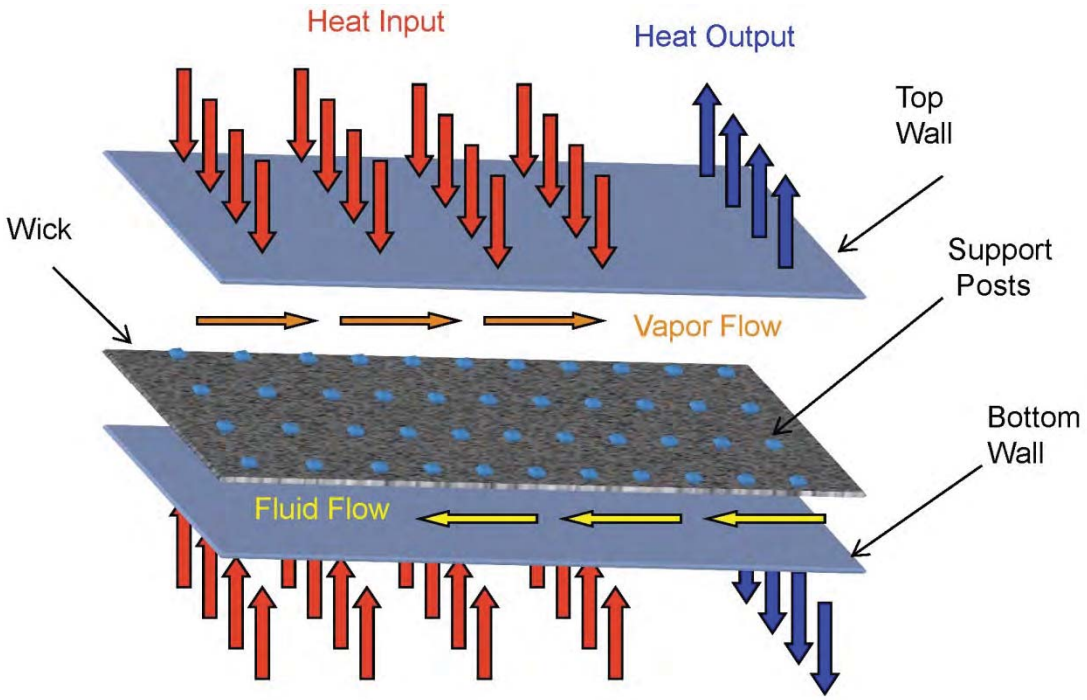

Figure 2.12.—Flat Plate Heat Pipe Operational Diagram

Figure 2.13.—Copper Flat Plate Heat Pipe

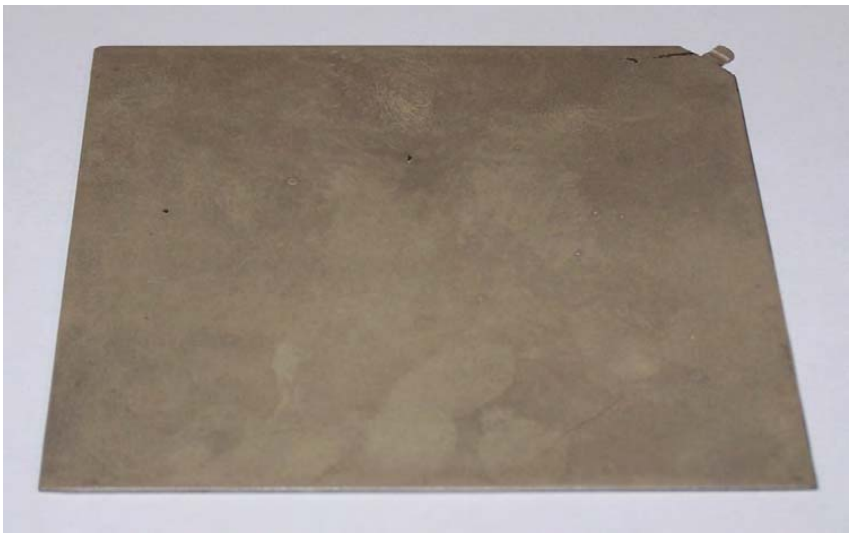

Figure 2.14.—Titanium Flat Plate Heat Pipe with Silver Paint Coating

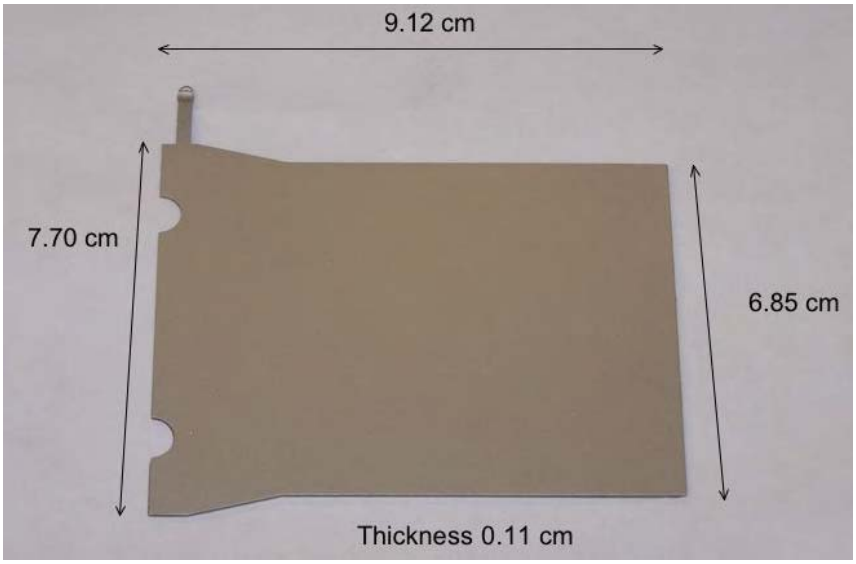

Figure 2.15.—Flat Plate Titanium-Water Stack Heat Pipe with Silver Paint Coating

TABLE 2.3.—CONSTRUCTED FLAT PLATE HEAT PIPE CHARACTERISTICS

Item	Maximum dimensions, (mm by mm)	Thickness, mm	Mass, g
Copper Heat Pipe 1	102.1 by 102.0	1.85	81.93
Copper Heat Pipe 2	101.6 by 102.0	1.85	83.98
Titanium Heat Pipe 1	95.3 by 95.3	0.86	N/A
Titanium Stack Heat Pipe 2	95.8 by 95.5	1.11	15.88
Titanium Stack Heat Pipe 4	95.8 by 95.5	1.11	17.85
Titanium Stack Heat Pipe 5	95.8 by 95.5	1.11	15.78
Titanium Stack Heat Pipe 6	95.8 by 95.5	1.11	16.39

3.0 Cooling Plate Thermal Conductivity Testing

Thermal conductivity is the key characteristic in the effectiveness of the cooling plates. With a higher thermal conductivity, the plates have a greater ability to remove heat and provide a uniform internal temperature distribution. To assess the effectiveness of the cooling plates, their thermal conductivity was measured. Because the plates are made of a uniform material, are fairly thin, and constructed homogeneously, it was necessary to only measure conductivity in one direction along the plate. This also had the benefit of simplifying the test setup.

The method used for measuring the thermal conductivity of the different types of cooling plates was based on Fourier's equation for heat conduction along one axis which equates the thermal energy ( ) as a function of time (*t*) to the change in temperature ( ) over a distance ( ), given by Equation (3.1). This equation states that the change in heat flow over time is equal to the change in temperature multiplied by the cross sectional area ( ) and thermal conductivity of the material ( ). The equation given assumes heat transfer only in one direction ( ).

$$\frac{}{t} = - \quad \frac{}{} \tag{3.1}$$

To measure the thermal conductivity, the heat flux and temperature change must be known and measurable. Using this method the cooling plate was positioned between two heaters on one end and two cooling blocks on the opposite end. Thermocouples were placed on the plate surface in a grid pattern between the heated and cooled ends. A diagram of the test setup is illustrated in Figure 3.1.

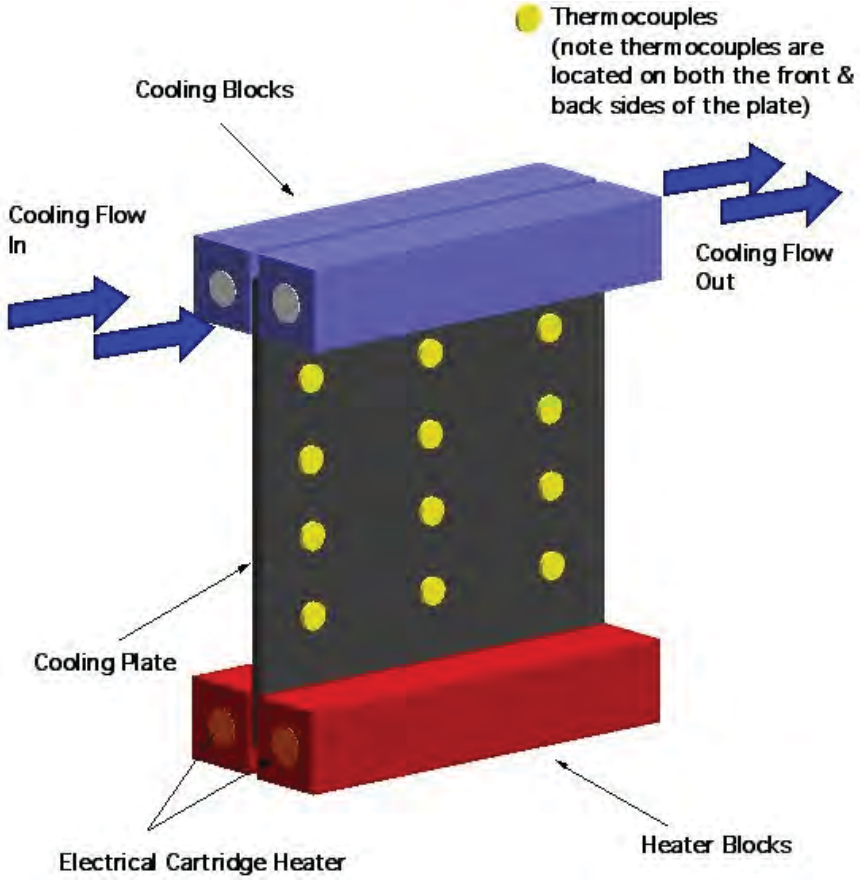

Figure 3.1.—Flat Plate Conductivity Measurement Setup Diagram

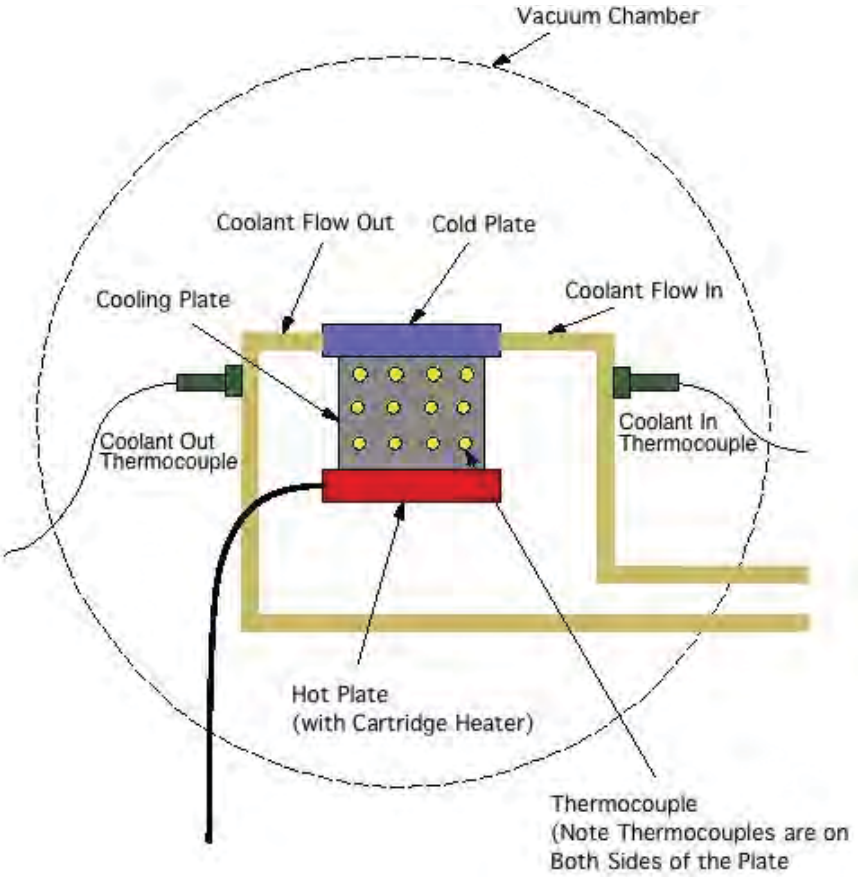

Figure 3.2.—Thermal Conductivity Test Layout Diagram

The operation of this type of thermal conductivity measurement system is outlined below and a diagram of the test setup is shown in Figure 3.2.

- The temperature of the hot and cold plates are accurately (± 1 °C) controlled.
- Power into the system is known by measuring the voltage and current supplied to the electrical heater.
- The temperature along the sample is measured by a series of thermocouples.
- To provide minimal convective heat transfer to the surroundings, the thermal conductivity testing was performed in a vacuum.
- Both the test sample and the heater blocks were insulated from the tank and support structure to limit any conductive heat transfer to the surroundings.

To determine the cooling plate's thermal conductivity, a fixed amount of power was provided to the pad heater while coolant was flowing through the cooling blocks. A chiller was used to maintain the coolant temperature at 19 °C and pump it through the cooling blocks. The temperature of the thermocouples was monitored until a steady-state temperature distribution was reached along the cooling plate. This provided a conductivity value for the plate. This process was repeated for at least five different power levels for each plate and the results averaged to determine the plate's thermal conductivity.

Performing the test in vacuum and thermally isolating the heating and cooling blocks from the tank support structure significantly reduced any heat transfer to the surroundings. The only heat transfer mechanism, other than conducting the heat down the plate to the cooling fluid, was through radiation to the vacuum tank walls. The radiation heat loss ( ) from the heater blocks and cooling plate can be calculated by Equation (3.2) where σ is the Stephan-Boltzmann constant with a value of 5.67×10^{-8} W/m^2K and ε is the emissivity of the stainless steel tank walls with an estimated value of 0.14. The steady state temperature profile along the plate as well as the heater block temperature was used to estimate this heat loss.

$$= \sum_{i=0}^{i=n} \sigma \ \varepsilon\left({}_i^4 - {}_w^4 \right) \tag{3.2}$$

$$= \frac{L}{n} \tag{3.3}$$

The plate and heater block was broken down into a number of segments (*n*). The surface area ( ) of each segment is given by Equation (3.3) where is the width of the cooling plate and *L* is the plate length between the heating and cooling blocks. A linear curve fit of the thermocouple steady state temperature data was used to estimate the temperature ($_i$) of each segment along the plate. The tank wall temperature ($_w$) was measured and remained constant throughout the testing at around 19 °C. The coolant temperature was set at the tank wall temperature of 19 °C to eliminate any radiation heat transfer to or from the coolant blocks with the surroundings.

The amount of heat loss to the tank walls varied from 0.04 to 0.4 W depending on the total power supplied to the heaters. The higher the heater power level, the higher the cooling plate steady state temperature which resulted in a higher heat loss to the surroundings. However, the total heat loss to the surroundings was a small percentage of the total heat applied to the system, ranging from 0.4 to 1.2 percent of the total power applied. Although small, the heat transferred through the plate was adjusted to account for this radiation loss from the plate to the surroundings.

The sample test plates were constructed of different materials and then tested. These plates include control samples of copper and stainless steel as well as various types of the thermally conductive plates under development. The description of each plate type and the thermal conductivity, determined through the testing, are listed in Table 3.1 and shown graphically in Figure 3.3 and Figure 3.4.

As discussed previously, the heat pipes tested do not transfer heat in the same fashion as the conductive plates therefore the thermal conductivities for the heat pipes are not completely representative of their performance capabilities. The heat pipes, as described in Section 2.2, transfer heat through the vaporization and condensation of an internal working fluid. Therefore, their heat transfer capability is much more sensitive to operating temperature and heat flux where the pure conductive plates depend upon differential temperature and material property. The effective thermal conductivity values for the heat pipes, given in Table 3.1 and Figure 3.3, provides a good means of comparing their performance to the other types of conductive plates under similar operating conditions.

TABLE 3.1.—TESTED PLATED AND THEIR THERMAL CONDUCTIVITY

Plate no.	Plate name	Description	Average conductivity (W/m K)
1	Steel –TPG Diff	Diffusion bonded steel plate with thermal pyrolytic graphite (TPG) core. (10.1- by 10.1- by 0.1 cm)	521
2	Stainless Steel -TPG	Stainless Steel Clad TPG with a polyester glue	874
3	Copper HP 1	Copper - water flat plate heat pipe	6,813
4	Copper HP 2	Copper - water flat plate heat pipe	3,596
5	Graphite Plate	Fuel Cell Bi-Polar Graphite Plate (12.5- by 11.7- by 0.5-cm, hollow interior with cooling passages)	47
6	Copper	Pure copper plate.	454
7	316 Stainless Steel	Stainless steel plate	25
8	Bare TPG	TPG plate, no covering	1,355
9	Copper -TPG	Copper Clad TPG with TP-1 conductive adhesive top and bottom grain perpendicular (8- by 8-cm)	1,315
10	Copper -TPG	Copper clad TPG with TP-1 conductive adhesive top and bottom grain parallel (8- by 8-cm)	1,364
11	Copper -TPG	Copper clad TPG with LM-2 conductive adhesive (8- by 8-cm)	1,230
12	Titanium HP	Titanium-water flat plate heat pipe	3,629
13	Titanium HP 1	Titanium-water stack heat pipe	2,462
14	Titanium HP 2	Titanium-water stack heat pipe	3,710
15	Titanium HP 3	Titanium-water stack heat pipe	5,032
16	Titanium HP 4	Titanium-water stack heat pipe	6,290
17	Titanium HP 5	Titanium-water stack heat pipe	5,577
18	Titanium HP 6	Titanium-water stack heat pipe	3,485

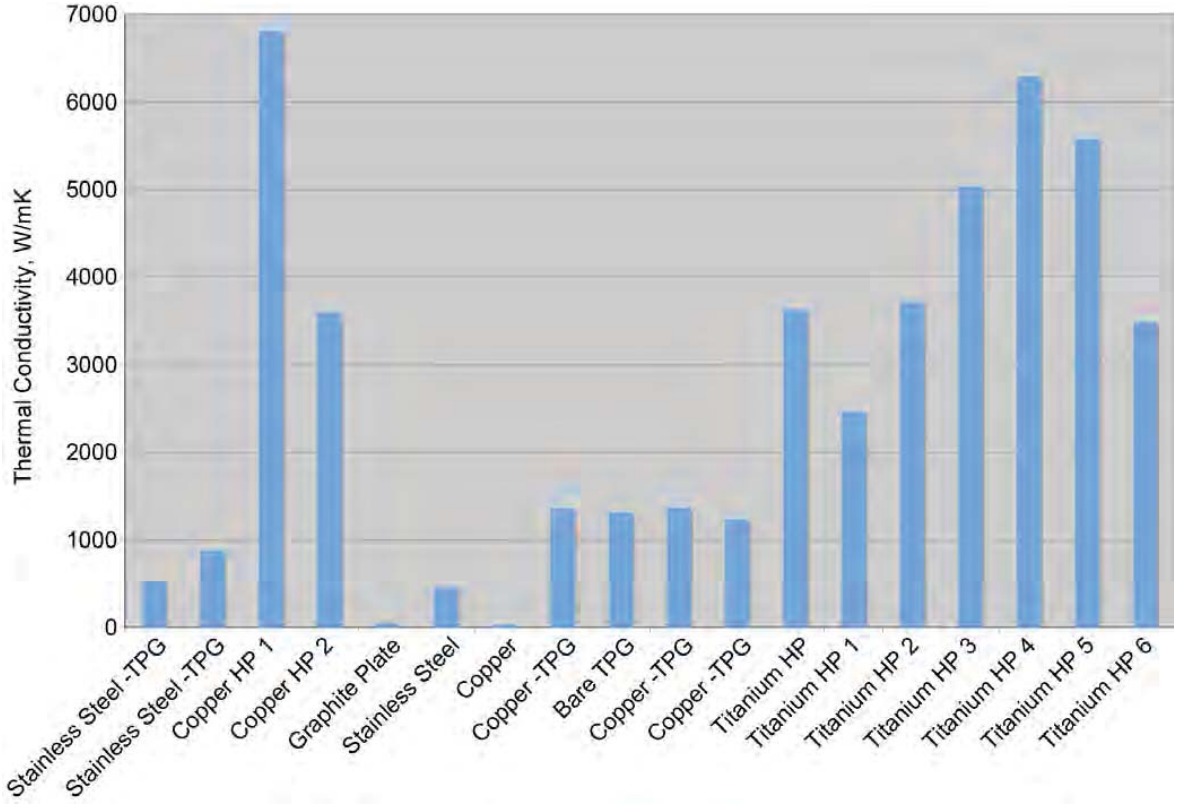

Figure 3.3.—Thermal Conductivity of Various Plate Types

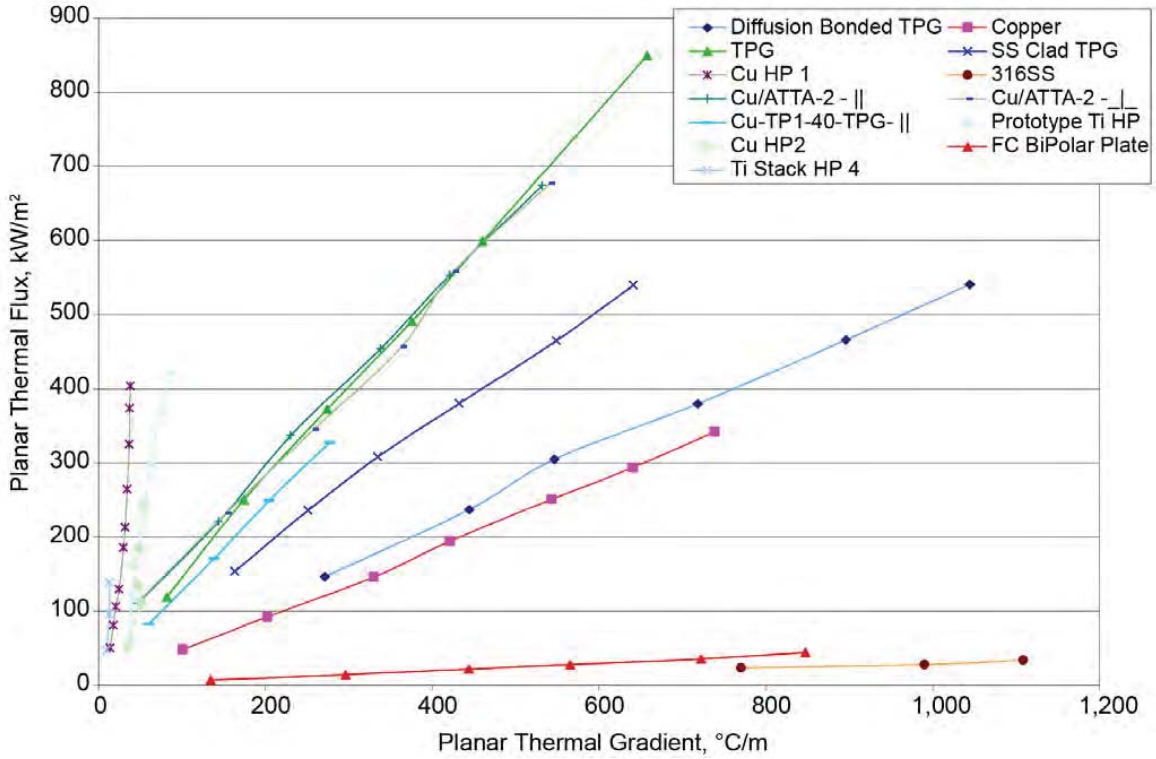

Figure 3.4.—Conductivity Curves for Various Cooling Plates

The test data for some of the plates is also plotted out in Figure 3.4. This figure shows the thermal flux through the plate as a function of the thermal gradient along the plate. The thermal flux (kW/m^2) versus the temperature gradient (°C/m) curves produced for each of the plates tested are fairly linear. This indicates consistent performance of the plates over the range of power levels tested. Also this shows that the test method used provided consistently reproducible results.

Figure 3.5 is an example of the variation in performance of the heat pipes with changing heat flux. In this figure, the heat pipe effective thermal conductivity is plotted as a function of the thermal input power. For the three heat pipes shown, there is an increase in thermal conductivity with increasing input power. This type of behavior is consistent with nucleated heat transfer. Within the heat pipe, there is a liquid/vapor front where the balance between evaporation and condensation is maintained. As more heat is put into the system, more energy becomes available to vaporize the working fluid which reduces its vaporization time, thereby increasing the effective performance of the heat pipe and moving the liquid/vapor front towards the heat pipe condenser. However, it should be noted that if the input power becomes too great, the liquid/vapor front will enter the condenser, terminate the nucleated heat transfer mechanism and the heat pipe will effectively shut off. This maximum heat flux is dependent on the heat pipe design. Therefore, unlike a conductive plate, there is an upper limit to the heat carrying capacity of the heat pipes.

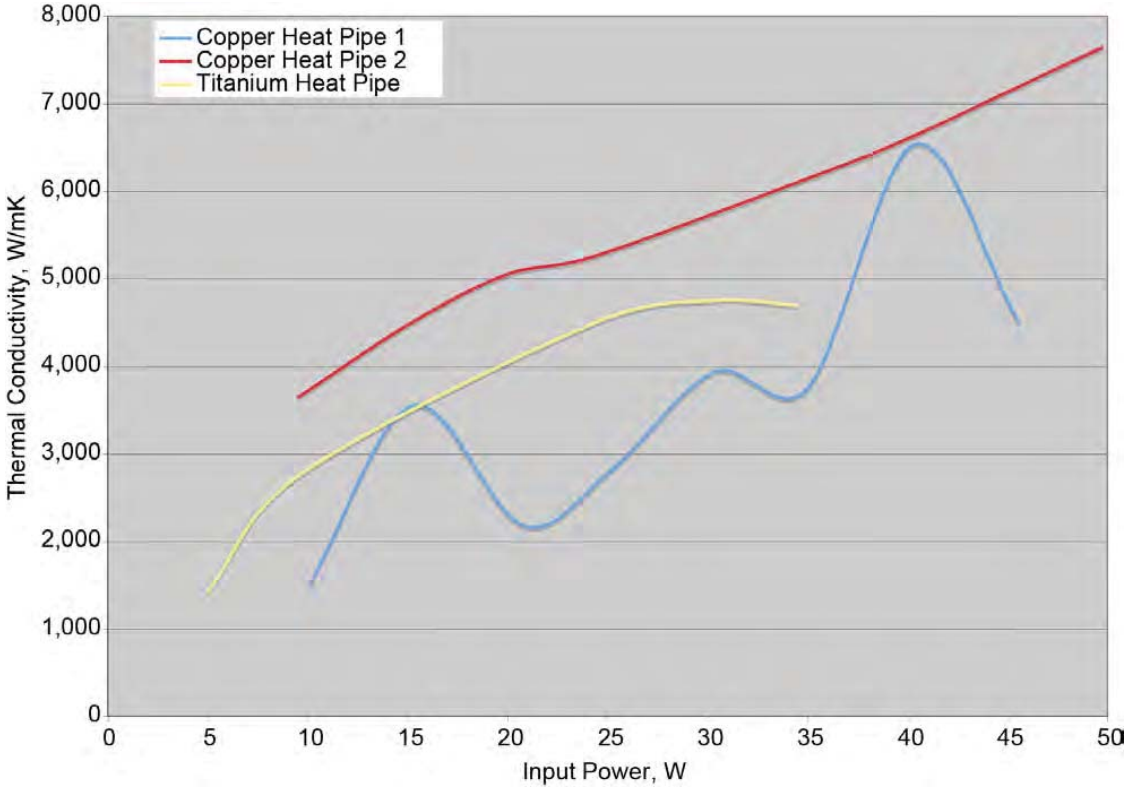

Figure 3.5.—Heat Pipe Effective Thermal Conductivity Over a Range of Input Power

4.0 Cooling Plate Electrical Conductivity Testing

For the fuel cell to operate efficiently, electrical current needs to flow from cell to cell with as little resistance as possible: this ability will be based on the plate's electrical conductivity Since the cooling plates are placed between each cell and considering the large number of cells in a typical fuel cell stack, their ability to conduct current is critical to the overall efficiency of the fuel cell.

A test was devised to evaluate the electrical conductivity of the sample cooling plates. The test setup was designed to mimic the conditions within the fuel cell that would have an effect on the electrical conduction through the plane of the cooling plate. The test setup utilized a hydraulic press with copper conducting plates, a high current power supply, and a precision potentiometer. This setup is shown in Figure 4.1 and Figure 4.2. The hydraulic press has heated platens allowing both the internal fuel cell stack pressure and temperature to be simulated. The sample cooling plate was placed between the two 12 mm thick copper plates. The copper plates were connected to the positive and negative terminals of the power supply. Due to the very low electrical resistance of copper (1.68×10^{-8} Ω-m)^2 the plates provided a uniform distribution of the current through the cooling plate. A DC power supply was used to supply up to 60 A of current through the cooling plate being tested. This high current level simulated the current flow that would be experienced within the fuel cell stack. The voltage drop across the cooling plate was monitored and recorded for each test case. This voltage drop was then converted into a resistance utilizing Equation (4.1).

$$R = — \qquad (4.1)$$

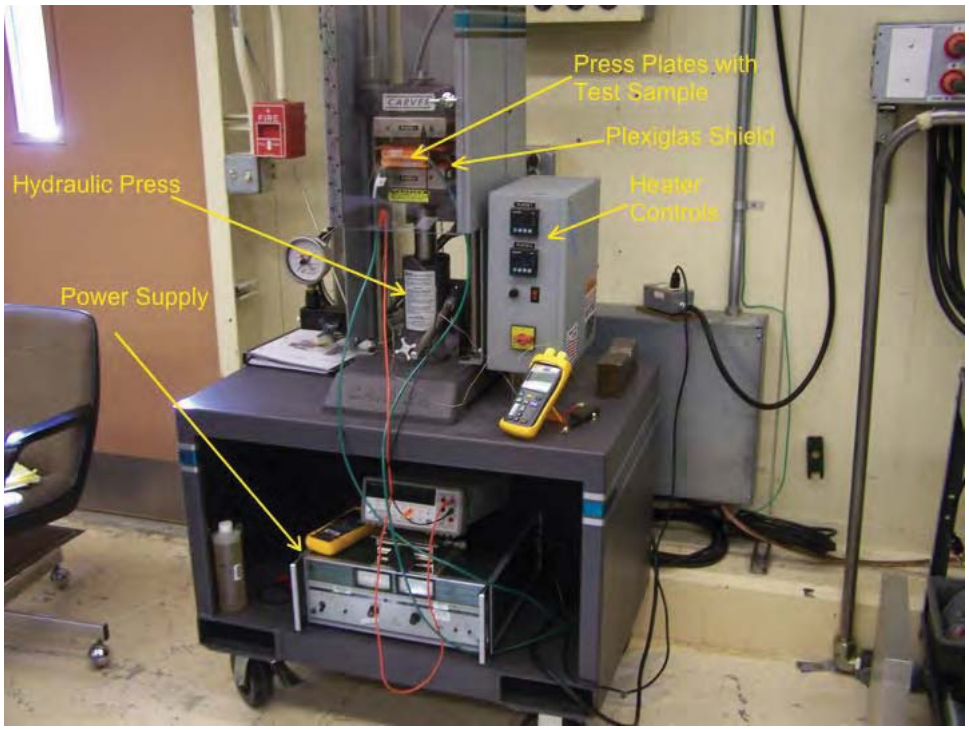

Figure 4.1.—Electrical Conductivity Test Setup

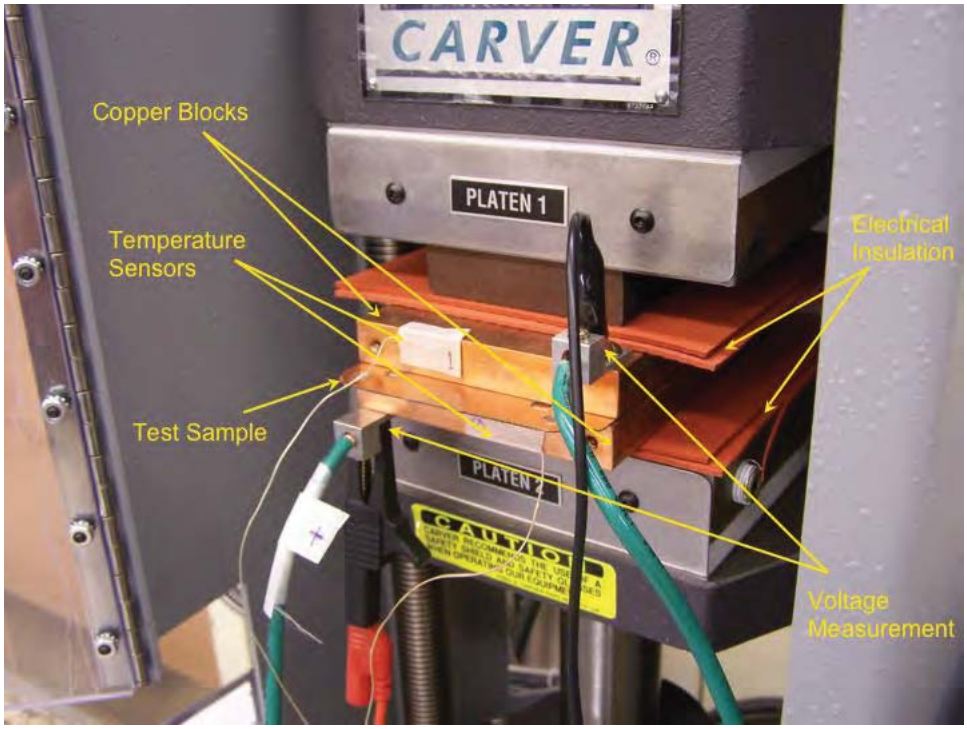

Figure 4.2.—Cooling Plate Installation for Electrical Conductivity Test

The cooling plates that were tested were either constructed from the thermal pyrolytic graphite (TPG) or were titanium-water heat pipes. The cooling plates utilizing the TPG were constructed using a variety of different techniques and materials. The heat pipes utilized were all titanium-water with different surface preparations. The plates tested are listed in Table 4.1.

TABLE 4.1.—COOLING PLATES USED IN ELECTRICAL CONDUCTIVITY TESTING

Plate type	Description
Clad TPG	A TPG plate clad with thin copper sheets using hot melt adhesive to adhere the copper to the TPG
Clad TPG	A TPG plate clad with thin copper sheets using TP-1 conductive adhesive to adhere the copper to the TPG
Painted TPG	A TPG plate painted with SPI electrically conductive silver paint applied
Painted TPG	A TPG plate painted with SPI electrically conductive silver paint applied and then sanded to improve surface finish
Titanium-water heat pipe	Bare titanium-water heat pipe with no surface preparation
Titanium-water heat pipe	Bare titanium-water heat pipe surface polished
Titanium-water heat pipe	Bare titanium-water heat pipe surface cleaned with tarnish remover

A range of forces was applied to the conductor plates, ranging from 0 N (0 lb) (just the weight of the upper copper conductor plate) up to 8,896 N (2,000 lb) to simulate the compressive loadings that would be experienced within a fuel cell stack. The subsequent loading on the plate, in pounds per square inch, was based on this force and the area of the plate of the sample cooling plate within the press. Since different sized cooling plates were tested, using the force per area on the plate was a uniform way to compare the electrical conductivities as a function of the force applied.

4.1 TPG Electrical Conductivity Test

The TPG plate geometry is shown in Figure 2.1. To improve the handleability and electrical conductivity of the TPG, it had to be encapsulated, as described in Section 2.1.2, Metal Clad TPG, or coated, as described in Section 2.1.3, Painted TPG. The construction method for the cladding and the paint application are described in more detail in Section 2.0.

The results from the electrical conductivity testing of the TPG plates with an area of 103 cm^2 (16 in^2) are shown in Figure 4.3. This graph shows the plate electrical resistance over a range of compressive loads applied to the plate. For the various TPG based plates tested, the lowest resistance curve shows the electrical resistance due to the contact resistance between the copper plates. Data for this curve was generated without a cooling plate between the copper plates and is labeled “no cooling plate” on the graphs. This curve represents a minimum resistance that could be achieved during the testing. A bare TPG plate (no paint or cladding) was tested to show what effect the application of the cladding or painting had on TPG resistance itself. From this figure it can be seen that the bare TPG electrical resistance falls off quickly with increasing compressive load. However, its electrical resistance is still fairly poor when compared to some of the encapsulated plates. This is due to the surface roughness of the TPG and its hard ceramic composition. The surface roughness limits the contact area between the TPG and copper conductor plates, which increases the contact resistance to the copper plates.

The clad TPG with the hot melt adhesive had a significantly higher resistance over the complete range of compressive loads than the clad TPG with the TP-1 conductive adhesive. This result should be expected since, even though the hot melt glue thickness was only on the order of 0.05 mm, it is an insulator. Therefore it increased the plate resistance over the TPG with the electrically conductive TP-1 adhesive.

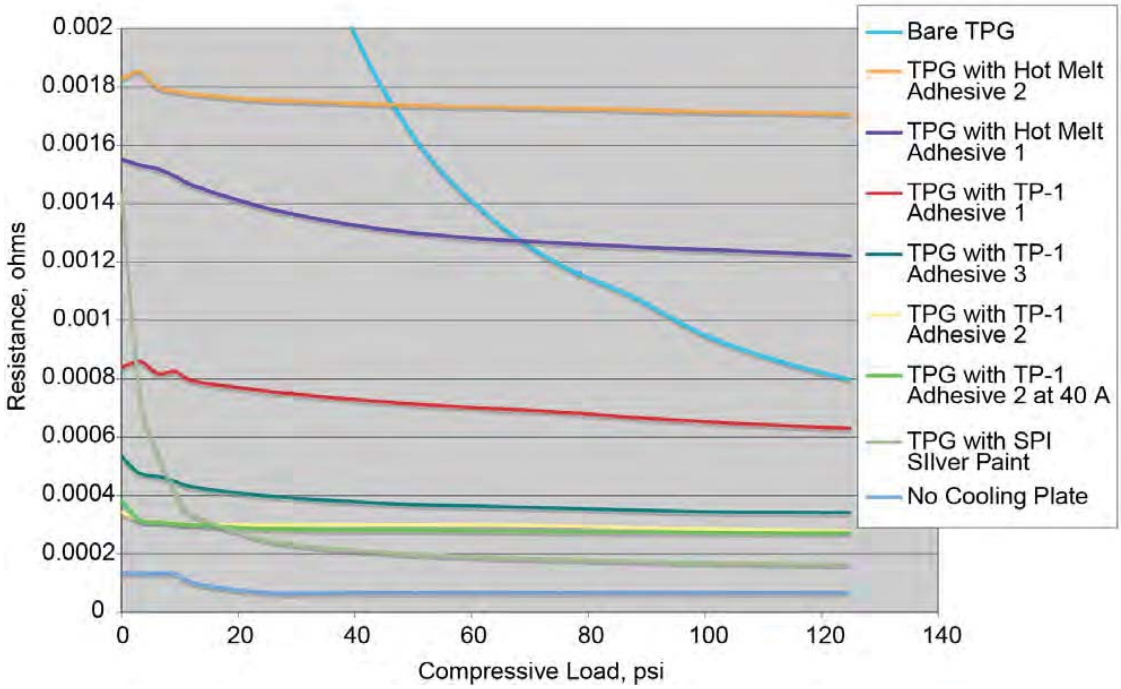

Figure 4.3.—Electrical Resistance for TPG Cooling Plates

The TPG with the TP-1 adhesive showed low electrical resistance, below 0.8 μΩ and two of the three plates constructed in this fashion had resistances below 0.4 μΩ. Also, the TPG with TP-1 adhesive, plate number 2, was run at both 30 A (the current level at which all of the plates were tested) and 40 A. The increased current had no effect on the plate resistance. This suggests that the plate's resistance should be fairly constant over the range of operational powers a fuel cell would run.

The silver painted plate had the lowest resistance of all the TPG plates tested. Its resistance was below 0.2 μΩ at the compressive loads that would be experienced within a fuel cell stack. The electrical resistance of the carbon painted TPG plate was very high, on the order of 0.03 Ω. This was significantly higher than the all of the other plates tested. Therefore the results from the carbon plated TPG plate were not plotted in Figure 4.3.

Additional electrical resistance testing was performed on a series of larger sized TPG based cooling plates, 155 cm^2 (24 in^2) in area, as shown in Figure 2.8 and Figure 2.10. The results for four copper clad TPG plates with TP-1 adhesive are shown in Figure 4.4.

The results from the larger TPG cooling plates shown in Figure 4.4 show a lower level of resistance (all below 0.2 μΩ) than the similar, smaller area plates whose results are shown in Figure 4.3. These results indicate that there is some variability in the electrical resistance of the cooling plates of similar construction. This variability is most likely due to material and manufacturing variations. The results from Figure 4.4 are very close to, and in the case of plate number 1, better than that for the silver painted TPG plate, as shown in Figure 4.3.

The electrical resistance results from testing a series of larger (155 cm^2) silver brush painted TPG plates are shown in Figure 4.5. As with the previous testing, there is variation in the results even for similarly prepared plates. Overall, these plates showed a higher resistance than the silver painted plate results given in Figure 4.3, and a slightly higher resistance than the copper clad plates of similar size, shown in Figure 4.4. These results show that for the painted plates, sanding the painted surface to provide a smoother finish increased the surface resistance of the plates. It is believed that this occurred because the paint provides a somewhat elastic plate covering. This elasticity allows it to flow into voids on the plate surface when under the applied compressive load, which increases the contact area thereby reducing bulk contact resistance between the cooling plate and conductor plate. Sanding the surface reduces this elasticity resulting in increased contact resistance and therefore higher electrical resistance.

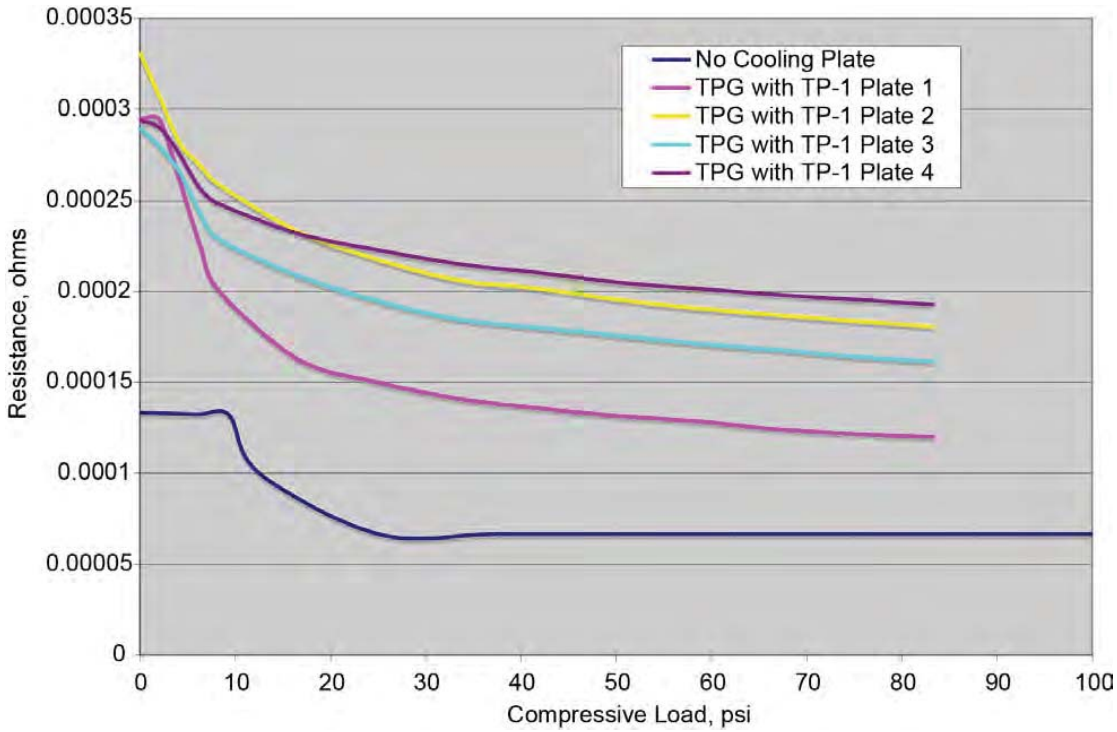

Figure 4.4.—Electrical Resistance of 155 cm^2 TPG Cooling Plates with TP-1 Adhesive

In addition to sanding, another treatment method was tried with plate number 4 that did reduce its electrical resistance. After brush painting and the initial electrical resistance testing, this plate was heated in the hydraulic press to 75 °C under a compressive load of 8,896 N (2000 lb). This pressure heating resulted in a lower overall resistance (approximately 33 percent lower) for the plate over the complete pressure range tested. This treatment also minimized the variation in resistance over the total pressure range.

A second set of silver painted 155 cm^2 TPG cooling plates were produced. The paint was applied utilizing the compressed air spray gun instead of being brushed on. The paint had to be thinned with isopropyl alcohol to work with the spray gun. Three coats of paint were applied to each side of the TPG plate. The electrical resistance results for the silver spray painted plates are given in Figure 4.6.

The results for the sprayed on silver painted plates show an overall higher electrical resistance then for the brushed on silver painted plates. The electrical resistance of some of the plates (plates S01, S07, S05, S04 and S06) is close to that for the bare TPG plate. It is believed that this is due to the overall thicker layer of paint applied through the brushing process. Also the brushing process applies a larger volume of paint to a given area of the plate. This allows the paint to spread out and better fill depressions and surface irregularities in the plate as discussed previously. The silver paint has a very short drying time. Spraying the paint on in a very thin layer further promotes this drying. Because of this accelerated drying, the paint does not have time to flow over the surface and fill in any irregularities. The brush method has a longer drying time, which increases the paints ability to fill in the surface irregularities, and therefore reduces the bulk electrical contact resistance.

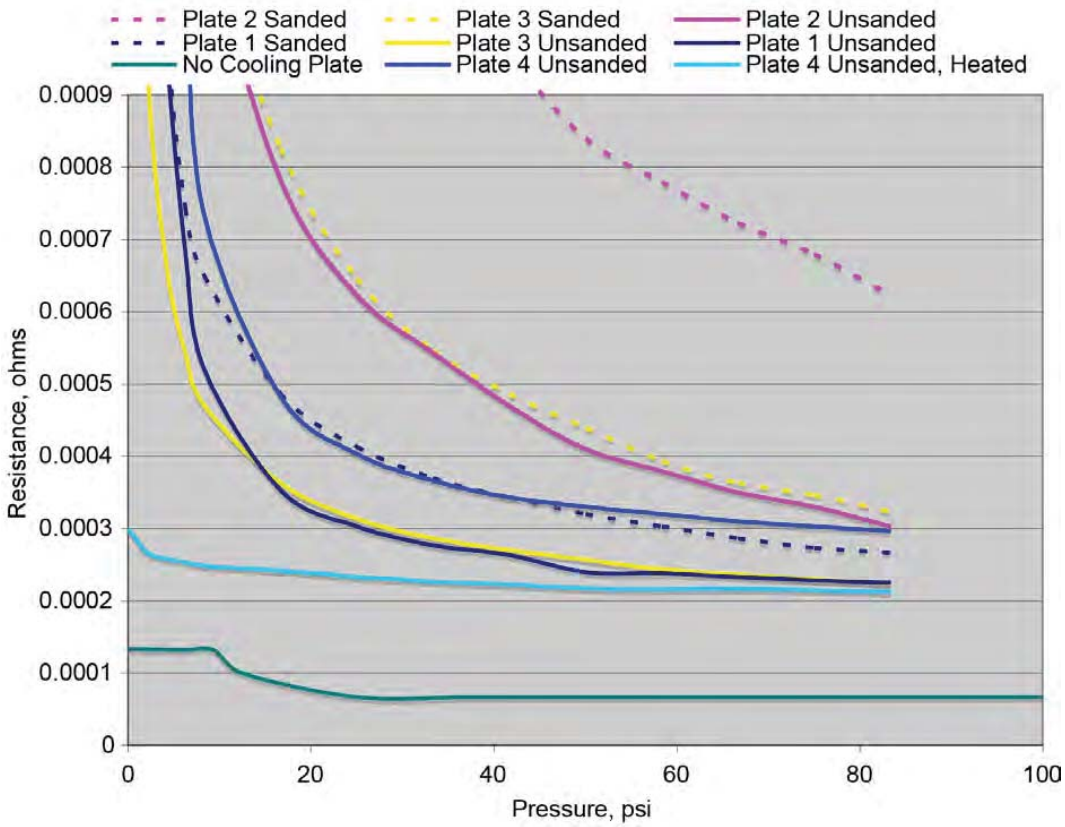

Figure 4.5.—Electrical Resistance of 155 cm^2 TPG Cooling Plates with Silver Paint

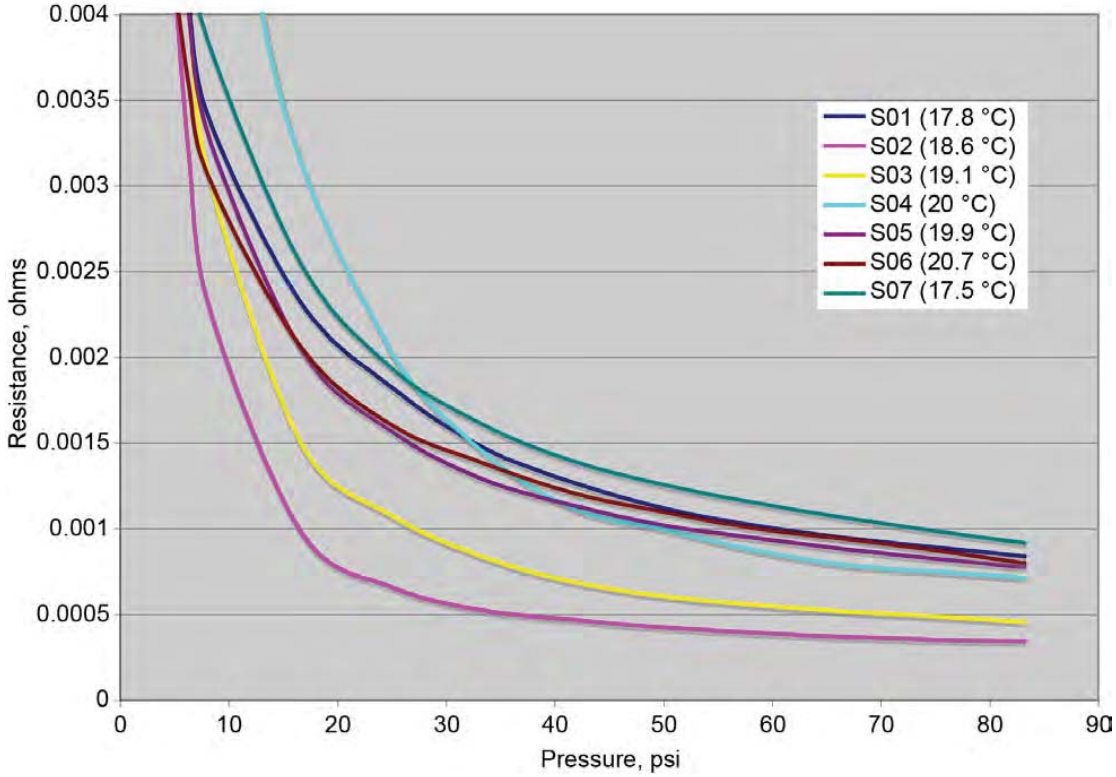

Figure 4.6.—Electrical Resistance of 155 cm^2 TPG Cooling Plates with Sprayed on Silver Paint

4.2 Heat Pipe Electrical Conductivity Test

The second type of cooling plates, the titanium-water heat pipes, was also tested to evaluate their electrical resistance. The electrical resistance of the two square, first-generation prototype titanium heat pipes, shown in Figure 2.13, were evaluated first. A third, first-generation square heat pipe was polished to provide a better finish than the other two used in this testing. The heat pipes had a surface area of 103 cm^2 (16 in^2). The results from the electrical resistance testing for these heat pipes is shown in Figure 4.7

As shown in Figure 4.7, the initial electrical resistance for the first two heat pipes tested (titanium heat pipe 1 and 2) was fairly high. As a means of reducing this resistance the heat pipes were cleaned with a tarnish remover. The original two heat pipes had been in storage for approximately 6 months. Over this time, the bare, not cleaned titanium surface had built up a layer of oxidization. As titanium oxide is not a good electrical conductor, it was believed that cleaning the surface might reduce the electrical resistance of the heat pipes. The electrical resistance of the cleaned heat pipes was significantly lower than that from the original not cleaned heat pipes. The resistance dropped ~75 percent from 4 to 5 mΩ (412 to 515 mΩ·cm^2) down to ~1 mΩ (103 mΩ·cm^2). It should be noted that the initial resistance with the not cleaned heat pipes, showed a difference of ~1 mΩ (103 mΩ·cm^2) between the two heat pipes whereas after cleaning the difference between the two heat pipes was negligible. This indicates that the original difference was due to different surface oxidation levels of the heat pipes.

The initial electrical conductivity results of the polished heat pipe were lower than the initial testing of the two not cleaned heat pipes. However, after cleaning all the heat pipes had similar electrical resistance. This indicates that polishing the surface did not provide any electrical resistance benefit and the main influence on the electrical conductivity was the surface oxidation level.

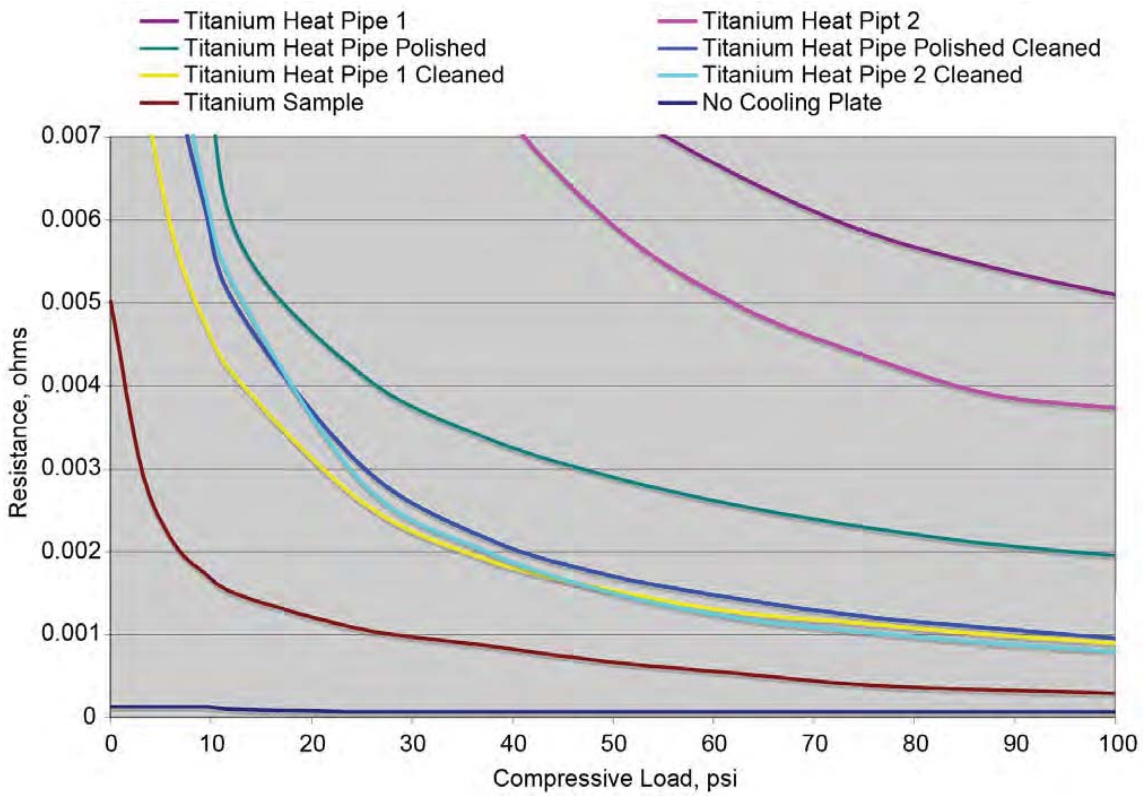

Figure 4.7.—Electrical Resistance of 103 cm^2 Titanium-Water Heat Pipes

A titanium square was also tested as a control sample to establish the lowest resistance that could be expected from the heat pipes. The cleaned heat pipes had over twice the resistance of the titanium sample. This indicates that there is an internal mechanism within the heat pipe that increases its electrical resistance. This could be due to the heat pipe design, fabrication process, or internal oxidization. Since the heat pipe has a hollow internal vapor chamber surrounded by a wicking structure, it is possible that the internal surfaces of the heat pipe have oxidized similarly to the unfinished outer surface. It is possible that contact between these oxidized surfaces, the internal wick, and support structure would restrict current flow and thus increase the resistance of the plate.

As an attempt to reduce the electrical resistance by protecting the surface from oxidization, the polished heat pipe was cleaned and then painted with the SPI conductive silver paint. The electrical conductivity results for the polished plate, as it was received, cleaned, and after painted are given in Figure 4.8. This figure shows that at each step in this process the electrical resistance decreased. Adding the silver paint significantly decreased the electrical resistance at lower compressive loads, following very closely the curve generated for the solid titanium sample plate. These results demonstrate that the addition of the conductive paint can reduce the plate's electrical resistance as well as provide protection from oxidization of the plate's surface.

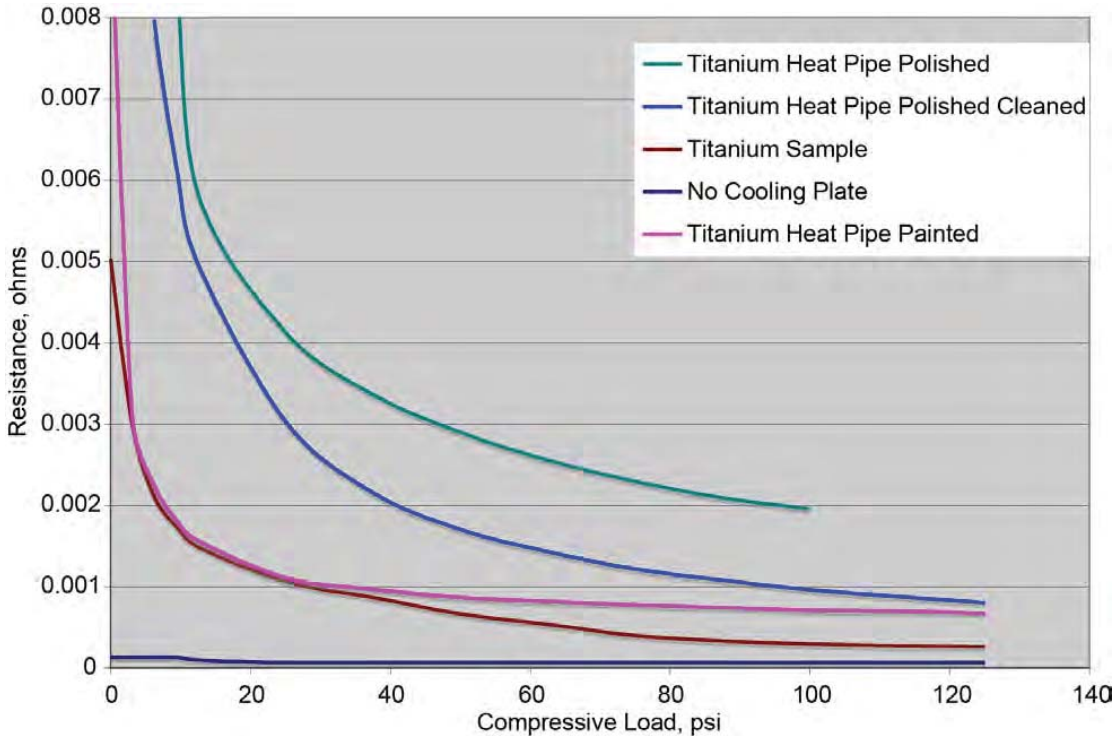

Figure 4.8.—Electrical Resistance of Polished Titanium Heat Pipe with Various Surface Processing

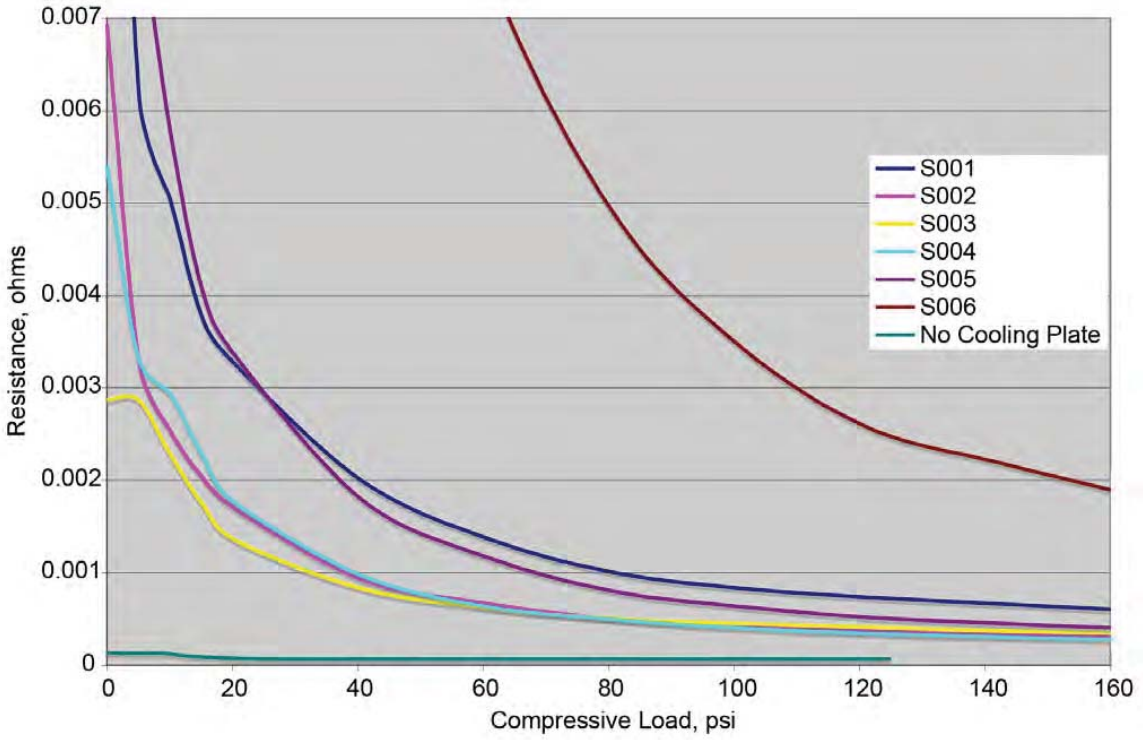

Figure 4.9.—Electrical Resistance of 64 cm^2 Titanium-Water Heat Pipes

A second generation of titanium-water heat pipes, shown in Figure 2.15, was constructed. These heat pipes used the same materials and manufacturing techniques as the initial generation but differed in size and shape. The second generation heat pipes had an area of 64 cm^2 (9.875 in^2). The electrical resistance for these heat pipes is shown in Figure 4.9. This electrical resistance data is for the bare titanium surface without any cleaning or other surface preparation. The electrical resistance is much lower on these heat pipes than the initial generation prior to any surface cleaning and painting. Five of the six heat pipes tested had resistances below 1 mΩ, most were below 0.5 mΩ. One of the heat pipes had a resistance near 2 mΩ. It is believed that this resistance variation between the heat pipes is due to surface oxidization since no cleaning was performed on any of these heat pipes prior to testing.

It should be noted that these second generation heat pipes were tested approximately 1 month after being manufactured compared to the first generation ones that had been stored for approximately 6 months after being manufactured. This reduced time between manufacturing and testing could account for the resistance difference between the two sets. Since the oxidization process takes time to occur, the resistance of the second-generation heat pipes may increase over time as the oxidization layer builds up, especially if it is occurring on the interior surfaces.

4.3 Electrical Conductivity Test Summary

The electrical resistance testing on both the TPG plates and the titanium heat pipes has provided some insight into the processing and construction that can minimize electrical resistance across the plates. Based on the test results for both types of plates the following items are worth noting:

TPG Cooling Plates

- Because of its surface finish, the bare TPG requires some type of surface treatment (coating or cladding) to provide low electrical resistance.

- Electrically conductive adhesive is required in the cladding process to provide a low resistance plate.
- Conductive silver paint provides as low or lower resistance as the clad plates when properly applied.
- Brush painting the silver paint reduced the resistance over spray painting the plates
- Sanding a painted surface increases its resistance and is not recommended for this application.
- A variation in electrical resistance exists from plate to plate. This is most likely due to slight variations in material and manufacturing.

Titanium Heat Pipe Plates

- Surface oxidation on the heat pipe significantly increases its electrical resistance.
- Surface polishing did not provide a benefit in reducing the electrical resistance
- Surface cleaning provided a significant benefit in reducing electrical resistance
- The internal structure of the heat pipe imposes a level of electrical resistance.
- Painting the heat pipe surface with the conductive silver paint is recommended after cleaning the surface. This painting reduces its electrical resistance and will provide a barrier to oxidization.
- A variation in electrical resistance exists from plate to plate. This is most likely due to slight differences in manufacturing.

5.0 Heat Pipe Operational Evaluation

The prototype titanium water heat pipes designed for use within an operational fuel cell, as shown in Figure 2.15, were tested and evaluated to assess their performance. Based on the initial results, the flat plate heat pipes did not operate as predicted. The heat pipe temperatures, at low heater input power levels, were much higher than expected. This indicated that there was a problem with either the heat pipes themselves or with the interface between the heat pipes and the cooling fluid.

Additional testing was done under ambient conditions to further evaluate the operation of the heat pipe. Initially each of the five titanium-water heat pipes was evaluated to assess their basic operation. The heat pipes were placed in a bath of hot water and the condenser side was monitored for any temperature change. Each heat pipe provided a rapid condenser temperature rise indicating that the heat pipe was operating properly. After this initial assessment, a further evaluation, outlined in Table 5.1, was performed utilizing a heated/cooled hydraulic press to characterize the effects of heat pipe installation on performance.

The hydraulic press platens contain internal cooling fluid passages used to maintain their temperature at a desired level. A cooling fluid was circulated through the platens maintained at 19 °C by a chiller. To perform the evaluation, a titanium-water heat pipe was instrumented with ten-thermocouples on one side and a flexible heating pad, with an approximate resistance of 158 Ω, on the other. Data from the thermocouples was collected to provide the heat pipe surface temperature distribution. The bulk heat pipe temperature was determined by averaging the ten-thermocouples. Power was supplied to the pad heater from a DC power supply. This test setup is shown in Figure 5.1. The heat pipe was placed horizontally between the cooled press platens as shown in Figure 5.2. Test runs were made using a press force of 60, 80, 100 and 120 lb with the heat pipe condenser length of 5 mm and a heater power of 5.4 W (30 V, 0.18 A). It should be noted that the condenser length represents the linear distance along the edge of the heat pipe that is in direct contact with the cooled press platens. It is within the heat pipe condenser area that the internal working fluid will condense. These results are shown in Figure 5.3. These results show the initial rise in the heat pipe temperature when the heater is turned on. After a few minutes the rise in heat pipe temperature levels off and the heat pipe reaches a steady-state operational temperature for the

heater power supplied. The curves also show the subsequent drop in the heat pipe temperature once the heater power is turned off.

At a press pressure of 60 lb, the heat pipe is held securely in the platens but still can be slid within the platens. This force level represents a mild interference fit between the heat pipe and the cooling platens. At press forces above 27 N (60 lb) the heat pipe was not moveable.

These results show that there was little effect of the press force on the temperature profile of the heat pipe. This indicated that sufficient thermal contact was being made between the heat pipe and the press even at the lowest press force utilized. The operating temperature of the heat pipe was approximately 42 °C which correlates well to the heat pipe design temperature of 40 °C.

TABLE 5.1.—EVALUATION TESTS PERFORMED ON THE TITANIUM WATER HEAT PIPES

Test variable	Implementation
Cooling plate pressure	Platen pressure varied between 60 to 120 lb
Cooling fin depth	Depth of the heat pipe held by the cooling platens, varied between 0 and 15 mm
Thermally conductive compound	Evaluation with and without conductive compound
Heat pipe orientation	Horizontal and vertical heat pipe orientation
Cooling plate material	Bare press platens, copper plates, and D5506 LCP conductive plastic

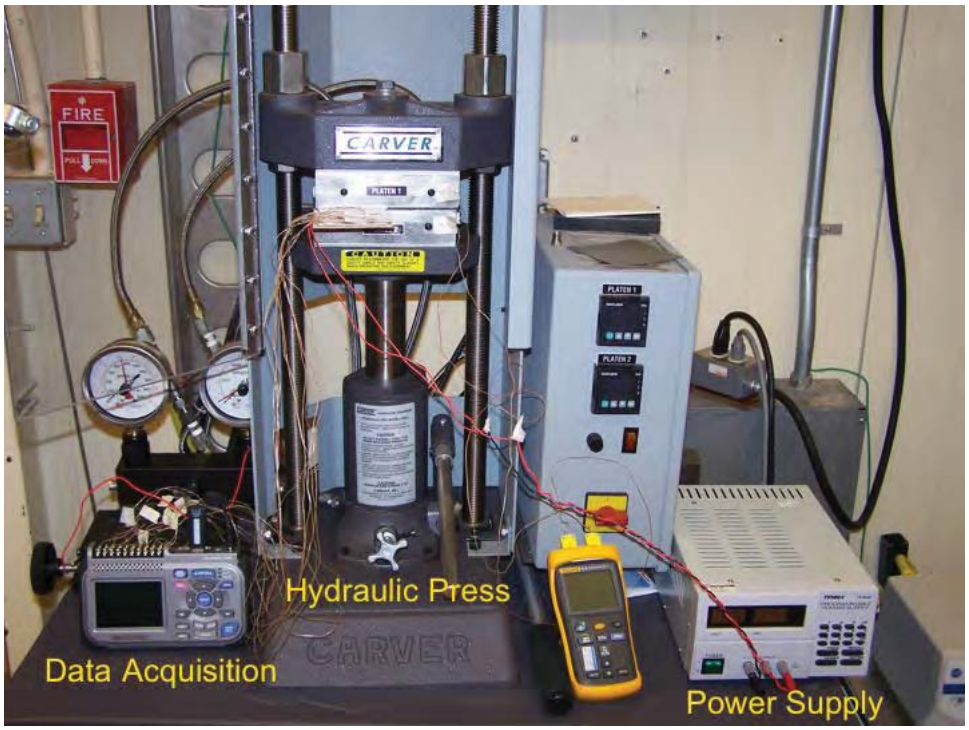

Figure 5.1.—Hydraulic Press Heat Pipe Test Setup

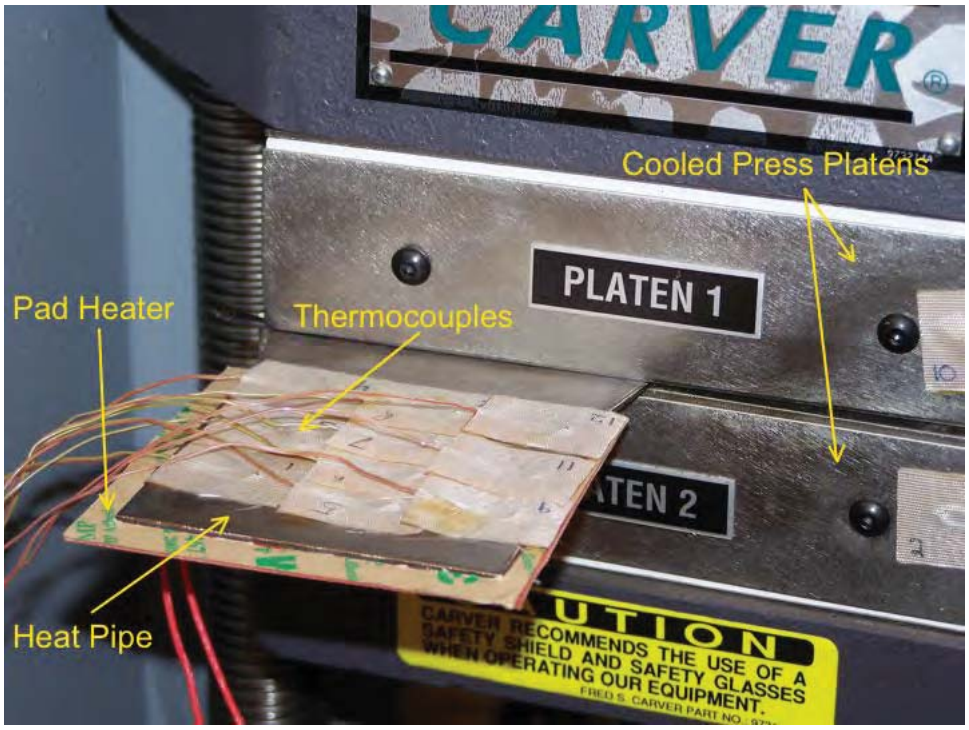

Figure 5.2.—Instrumented Heat Pipe Installed Horizontally in the Press

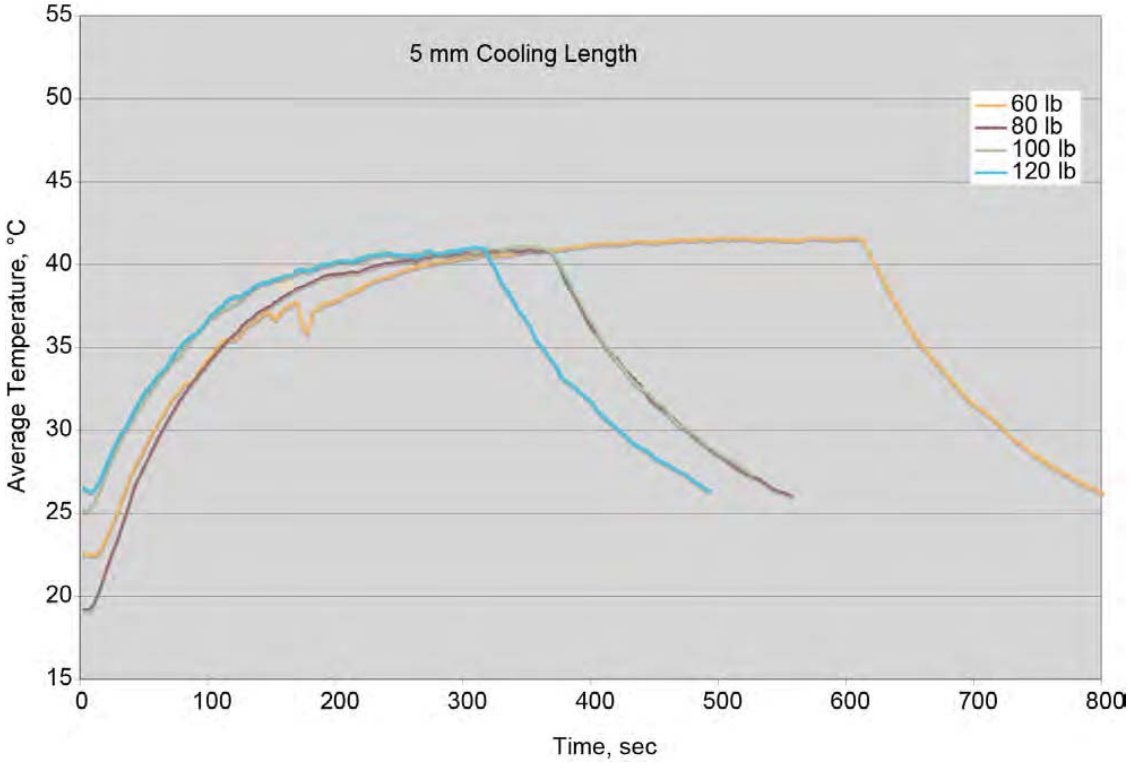

Figure 5.3.—Heat Pipe Temperature for various press forces at 5 mm cooling fin length

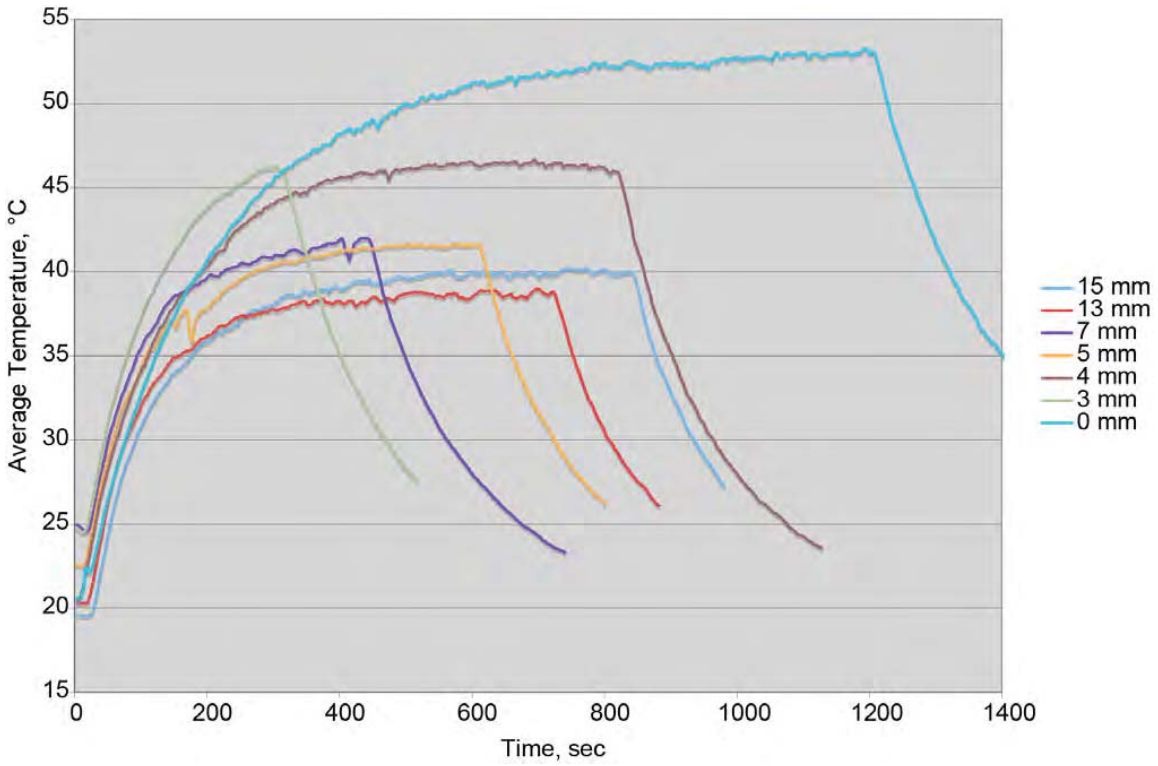

Figure 5.4.—Heat Pipe Temperature for various condenser length at 60 lb press force

Additional testing was performed utilizing a press force of 60 lb over a range of condenser lengths. Prior to placing the heat pipe into the press, a test was run with the instrumented heat pipe in air, with only natural convective cooling. This control test was performed to determine the worst case cooling condition defined as 0 mm condenser length. The results from this testing are shown in Figure 5.4.

These results indicate that the heat pipe condenser length affects the steady state operating temperature of the flat plate heat pipe. In general as the condenser area is increased, the steady state operating temperature decreased. This verifies that significant heat was being conducted to the press platens by the heat pipe. The design operating temperature of the heat pipe limits the reduction of the achievable steady state temperature.

5.1 Horizontal Heat Pipe Testing With Copper Blocks

In the next series of tests a set of copper plates, each 12 mm thick, were placed between the press' platens and the heat pipe was placed between these, as illustrated in the test setup diagram shown in Figure 5.5. For these initial tests, there was no insulation on the heat pipe as it is shown in the figure. The copper plates were used as a means of placing additional thermal resistance between the heat pipe and cooling plates and as a means of more evenly distributing the force from the press onto the heat pipe. A series of tests were run, utilizing the copper plates, to evaluate the heat pipe temperature at different press forces with a condenser length of 5 mm. The first set of data was performed with a similar configuration as that shown in Figure 5.2, except for the addition of the copper plates. These results are shown in Figure 5.6.

These results, shown in Figure 5.6, illustrate that there is little change in the temperature profile of the heat pipe with increasing press pressure. The maximum average equalized heat pipe temperatures are approximately 4 °C higher than those shown in Figure 5.3. This temperature increase is due to the addition of the copper plates, which imposes an additional thermal contact resistance between the platens, copper blocks, and heat pipe, compared to the previous test.

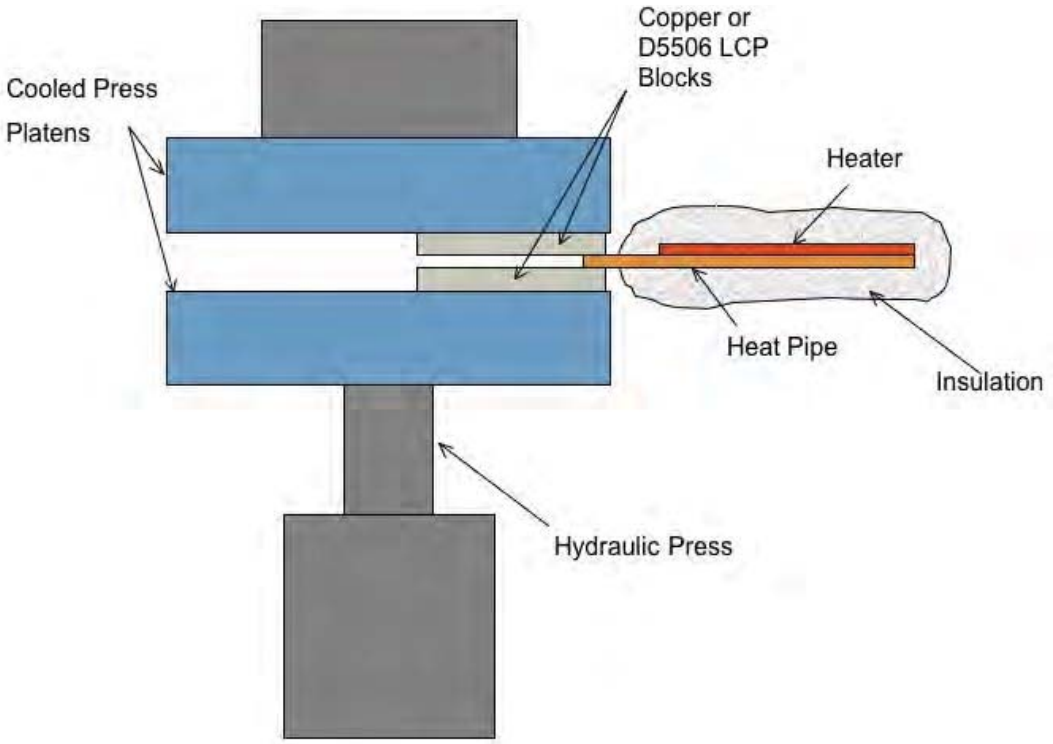

Figure 5.5.—Horizontal Heat Pipe Test Diagram

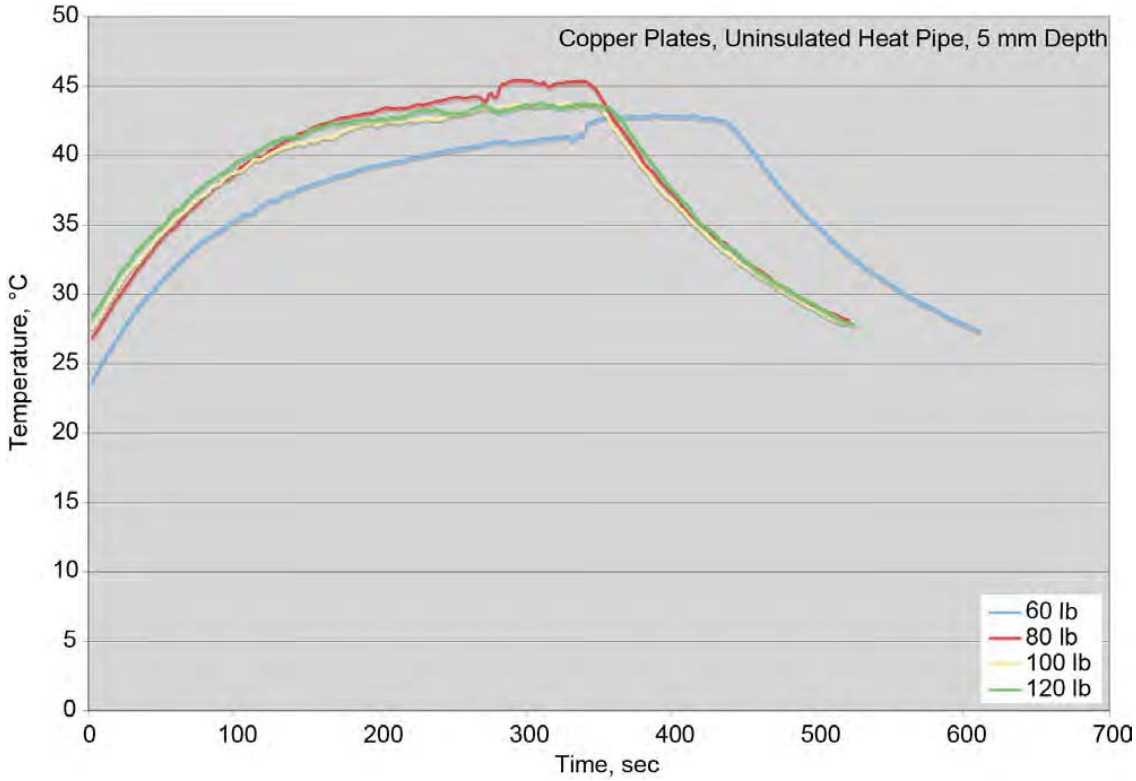

Figure 5.6.—Heat Pipe Temperature for various press forces at 5 mm cooling fin length with copper plates in the press

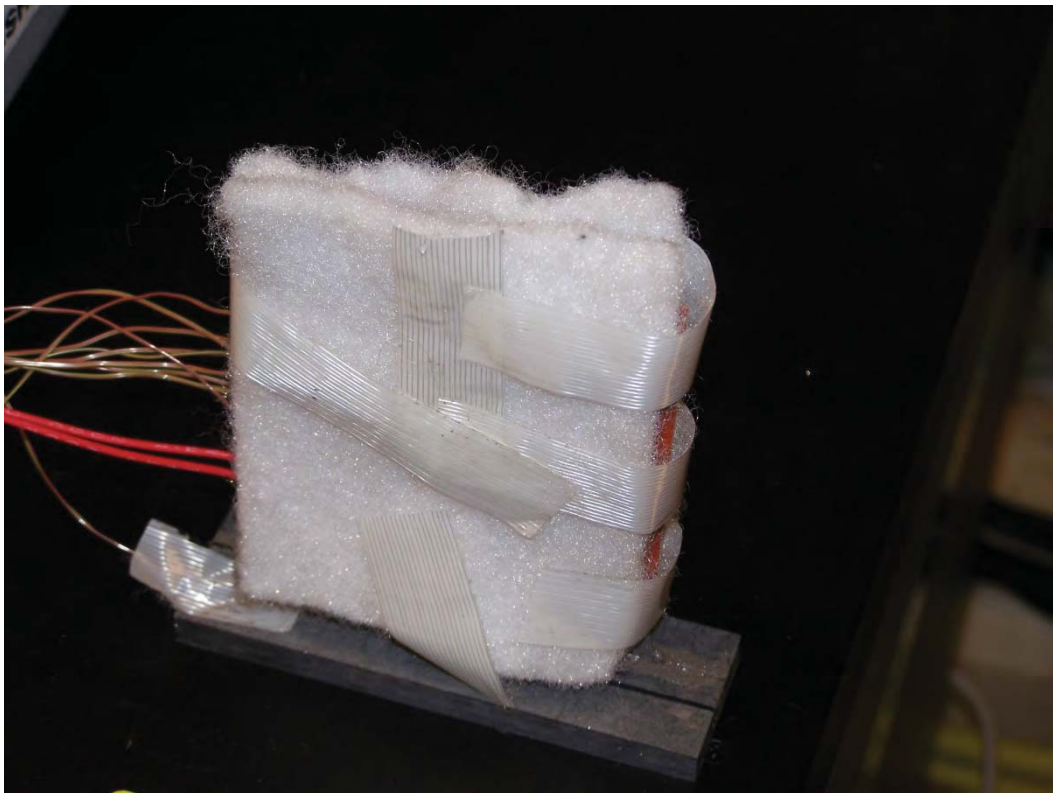

Figure 5.7.—Insulated Heat Pipe

To provide better accuracy in the heat pipe testing, as well as to better simulate the heat pipe operation within a fuel cell stack, polyester fiber insulation was placed around the outer heated and instrumented portion of the heat pipe. This insulation reduced the convective heat loss from the heat pipe to the surroundings. A picture of the insulated heat pipe is shown in Figure 5.7. The cases shown in Figure 5.6 were rerun with the insulated heat pipe. An additional case was added with a press force of 400 lb. These results are given in Figure 5.8.

From Figure 5.8 it can be seen that as with the previous tests, the heat pipe operating temperature is not dependent on the press pressure. Also, the added insulation significantly reduced the heat transfer to the surroundings resulting in temperature curves, which are much smoother and converged better than those from the results shown in Figure 5.6. The operating temperature of the additional case at 182 N (400 lb) of press force leveled off near the same temperature as the other trials. This demonstrates that sufficient heat transfer is occurring at the mild interference fit of 27 N (60 lb) of press force and additional press pressure does not enhance the heat transfer. It should be noted that the steady-state temperature of the heat pipe was around 51 °C. This is approximately 5 °C higher than the temperature shown in Figure 5.6. This increase in temperature is due to the insulation on the heat pipe limiting heat transfer to the surroundings and therefore increasing the heat pipe operating temperature.

5.2 Horizontal Heat Pipe Testing With LCP Blocks

The next step in the heat pipe operational evaluation was to replace the copper blocks with two D5506 LCP thermally conductive plastic blocks, each 10 mm thick. This material is used in the construction of some of the manifold designs. The plastic has a relatively high thermal conductivity (10 W/m K) while maintaining electrical isolation. As discussed in Section 4.0, these characteristics are required for operation of the fuel cell.

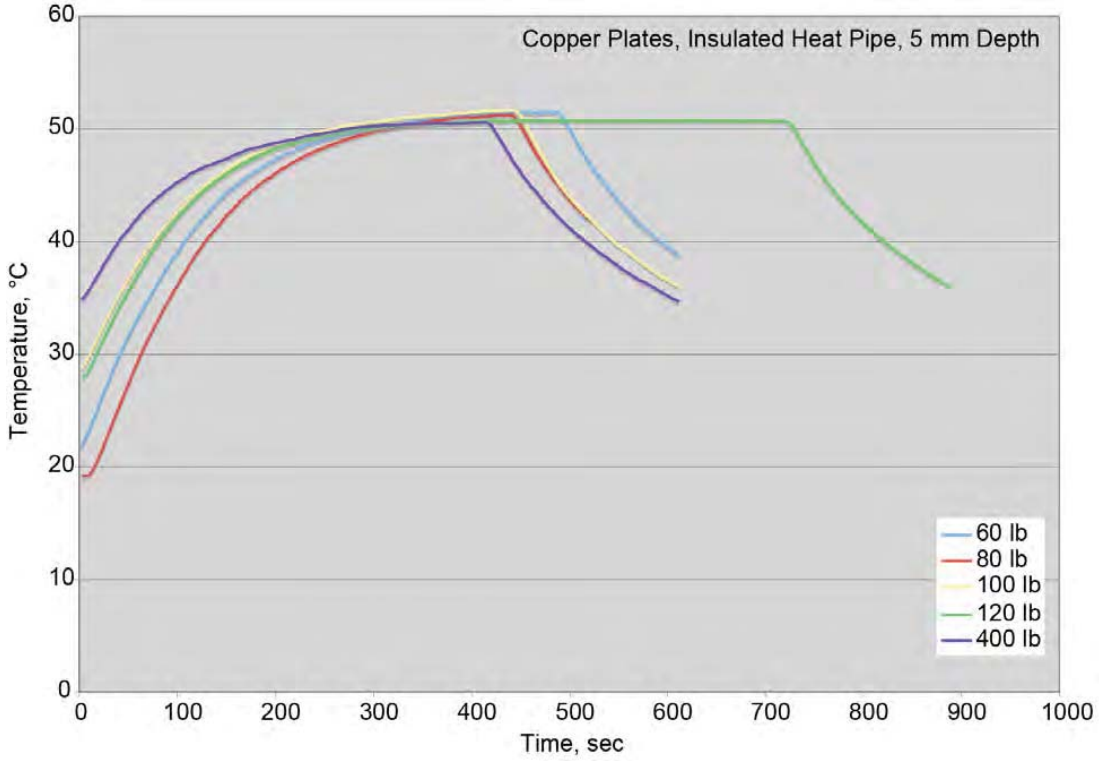

Figure 5.8.—Insulated Heat Pipe Temperature for various press forces at 5 mm cooling fin length with copper plates and 5.4 W heater power

5.3 Horizontal Heat Pipe Testing With LCP Blocks

The next step in the heat pipe operational evaluation was to replace the copper blocks with two D5506 LCP thermally conductive plastic blocks, each 10 mm thick. This material is used in the construction of some of the manifold designs. The plastic has a relatively high thermal conductivity (10 W/m K) while maintaining electrical isolation. As discussed in Section 4.0, these characteristics are required for operation of the fuel cell.

The results from the first series of tests performed where the D5506 LCP conductive plastic replaced the copper blocks is shown in Figure 5.9. These results are for an insulated heat pipe with 5.4 W (30 V, 0.19 A) applied to the pad heater. From this figure it can be seen that there is a small (few degree) reduction in the heat pipe temperature with the increasing press force. The effect of press force on the heat pipe temperature was not a factor in the previous tests. It is believed that the effect of higher press forces was due to the significantly lower thermal conductivity of the conductive plastic compared to the copper (400 W/m K) or bare platens. Because of the lower conductivity of the plastic the increased heat transfer due to reduction in thermal resistance between the heat pipe, plastic and platens, from the higher press forces became evident. Also it should be noted that with the D5506 LCP plastic the heat pipe operating temperature increased approximately 5 °C over the results with the copper plates. Again this is due to the reduced thermal conductivity of the plastic.

To enhance the heat transfer while utilizing the plastic plates, a conductive thermal compound, Arctic Silver 5 (manufactured by Arctic Silver Inc.) a high-density polysynthetic silver thermal compound, was used to decrease the thermal resistance between the heat pipe and plastic plates. The results using the plastic plates with the Arctic Silver thermal compound are shown in Figure 5.10.

From these results it can be seen that the thermal compound reduced the heat pipe operating temperature to the levels seen with the copper plates, given in Figure 5.8. Also the effect of press force was reduced. The heat pipe operated a few degrees hotter at the lowest press force, 60 lb. However at the higher press forces the operating temperature was similar for all cases run.

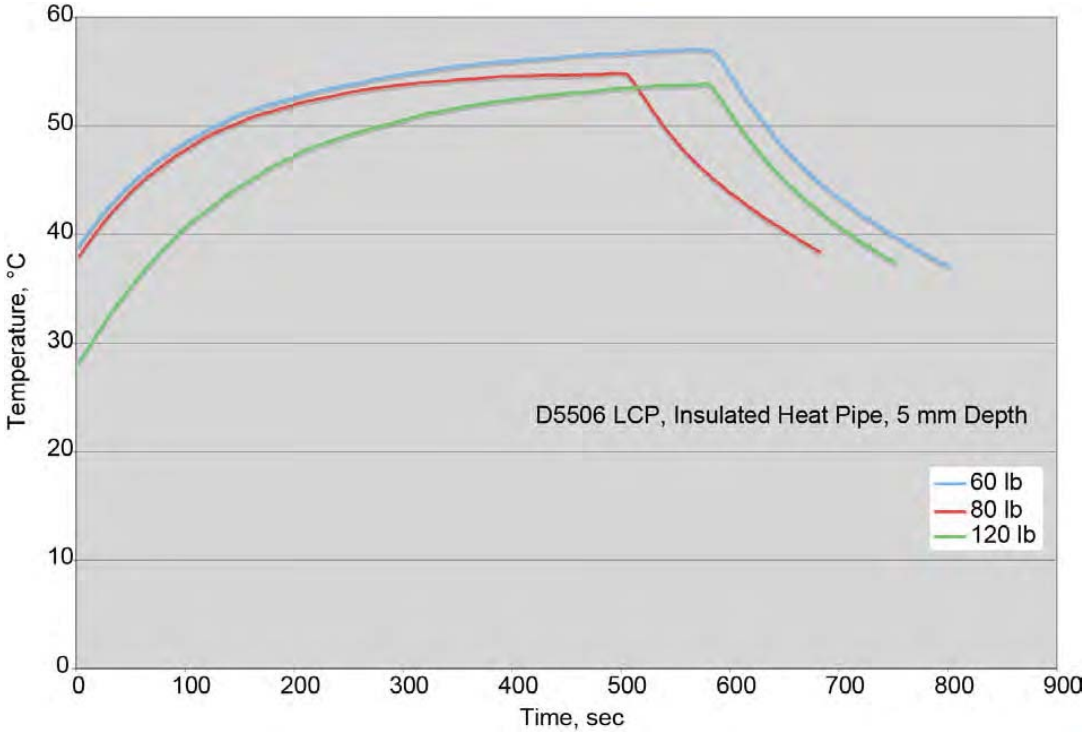

Figure 5.9.—Insulated Heat Pipe Temperature for various press forces at 5 mm cooling fin length with D5506 LCP plastic plates and 5.4 W heater power

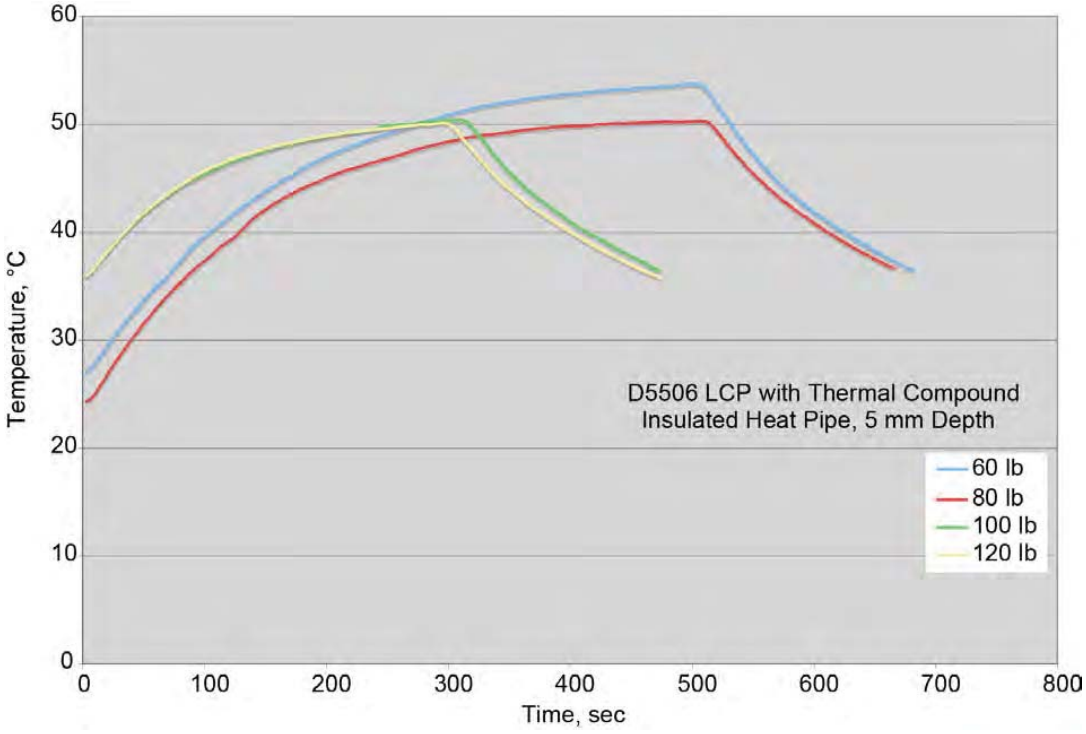

Figure 5.10.—Insulated Heat Pipe Temperature for various press forces at 5 mm cooling fin length with D5506 LCP plastic plates with thermal compound and 5.4 W heater power

5.4 Vertical Heat Pipe Testing

The last series of tests were run to evaluate orientation effects on heat pipe performance. The heat pipe was placed vertically in a slot within a D5506 LCP plastic manifold, as shown in Figure 5.11. The slot was filled with Arctic Silver 5 thermal compound to enhance the heat transfer from the heat pipe to the plastic. The heat pipe depth into the slot was approximately 5 mm which corresponds to the slot depth of previous horizontal tests. The slot width with the thermal compound provided a secure interference fit between the heat pipe and plastic. The heat pipe and plastic manifold piece were placed within the press and the press platen was used as a means of cooling the heat pipe. The test setup is shown in Figure 5.12. This test setup was used to evaluate the heat pipe in two orientations, vertical with the heat pipe condenser on the top and vertical with the heat pipe condenser on the bottom: both orientations are shown in Figure 5.13. As with some of the previous tests the heat pipe was insulated to limit any heat transfer by convection to the surroundings.

The press applied minimal force to hold the heat pipe setup. The heat pipe operating temperature results for these two orientations are given in Figure 5.14. From this figure it can be seen that there is a significant operating temperature difference between the heat pipe oriented vertically with the condenser on the top and with the condenser on the bottom. With the condenser on the top the heat pipe temperatures are lower than the lowest operating temperatures seen in previous testing (oriented horizontally). The operating temperature was much higher for the heat pipe oriented with the condenser on the bottom and were comparable to the insulated heat pipe operating horizontally in air with little heat transfer from the condenser area. This indicates that, with the condenser on the bottom, the heat pipe is not operating. This heat pipe as designed is not capable of transporting the condensed fluid back up into the heat pipe against gravity.

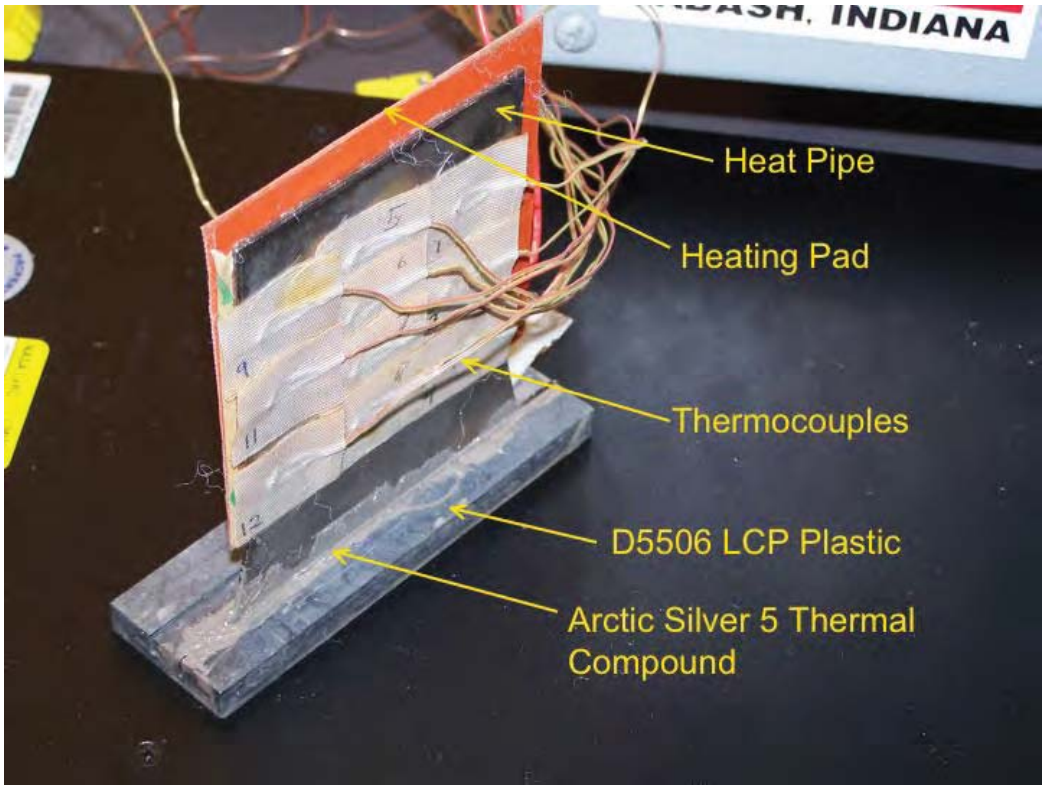

Figure 5.11.—Heat Pipe Installed in a D5506 LCP Manifold for Vertical Testing

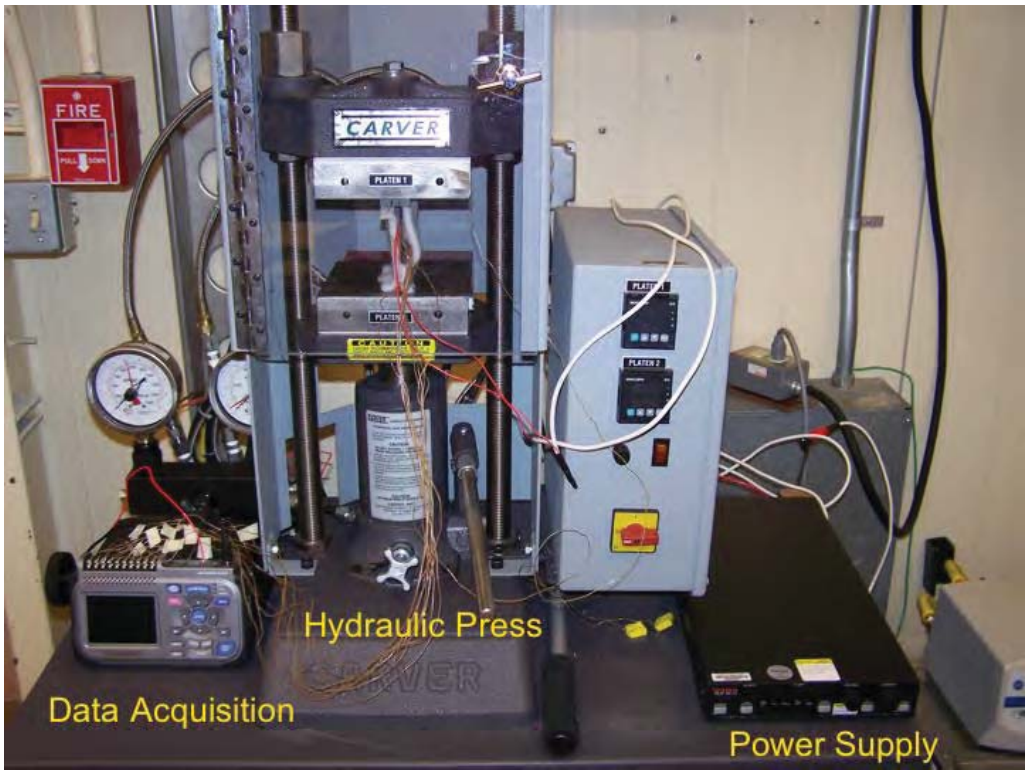

Figure 5.12.—Test Setup with Heat Pipe Installed Vertically

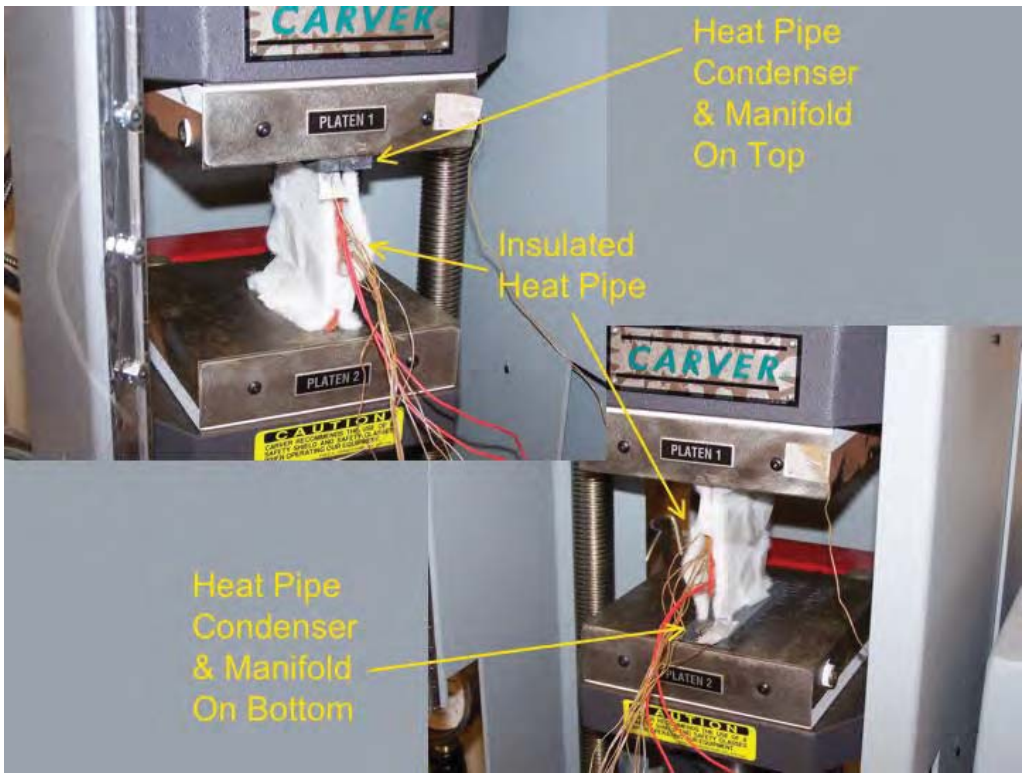

Figure 5.13.—Test Setups with Heat Pipe Condenser on Top and Bottom

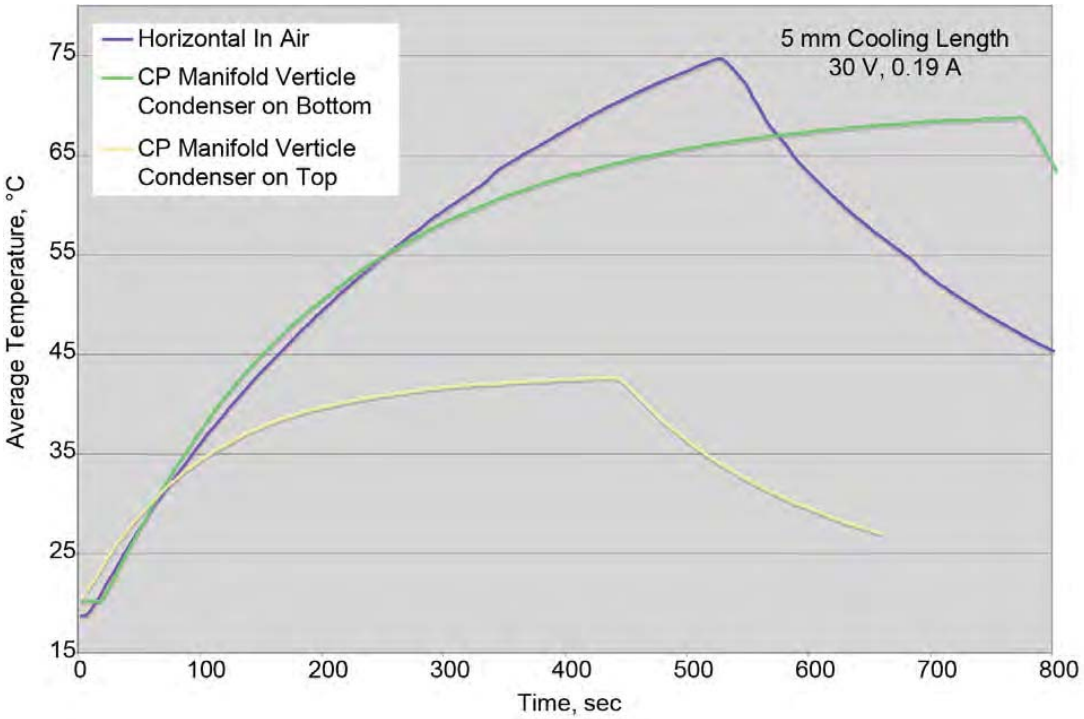

Figure 5.14.—Vertically Orientated, Insulated Heat Pipe Temperature Results, With D5506 LCP plastic manifold and 5.4 W of Heater Power

In addition to the average bulk heat pipe temperature shown throughout the previous section, the heat pipe surface temperature distribution is also of interest. The steady-state temperature distribution provides an indication of the operation of the heat pipe and its ability to maintain a uniform temperature distribution over its surface. This temperature distribution can be seen by plotting the steady-state temperature of each thermocouple on the heat pipe. The location of each thermocouple is shown in Figure 5.15.

The steady-state temperature distribution for the titanium-water heat pipe, horizontally held between the copper plates (as illustrated in Figure 5.5), is given in Figure 5.16. This figure shows a fairly uniform temperature distribution along the heat pipe for all the cases shown. Thermocouple 6 has the highest temperature for all of the cases and is approximately 3 °C higher than the lowest temperature for any given case. This location is centrally located and its increased temperature could be due to non-uniform output in the heater pad. It should be noted that the typical error for a type K thermocouple is ±1.5 °C for the temperature range of this testing. Therefore the temperature differences that were measured between the thermocouples are approaching the error tolerance for the thermocouples. The remaining thermocouples show fairly uniform temperature over the surface of the heat pipe. The variations seen, on the order of 1 °C or less is within the experimental error of the testing. This figure also shows about a 5 °C temperature rise in the heat pipe between the insulated and non-insulated tests. The insulation limited heat transfer to the surroundings and therefore increased the operating temperature of the heat pipe. The insulated heat pipe is more representative of the operation within the fuel cell, where the only meaningful heat transfer from the heat pipe will be through the condenser edge.

Similar results were generated using the D5506 LCP plastic plates instead of the copper plates, shown in Figure 5.17. The temperatures were produced with an insulated heat pipe with and without the Arctic Silver 5 thermal compound between the heat pipe and plates. All of the cases show a variation of 1 to 2 °C in temperature over the heat pipe surface with the peak coming at the thermocouple 6 location. There is a significant drop in temperature of 3 to 4 °C with addition of the thermal compound. This drop is

consistent over all the cases. These results illustrate that there is some dependence on the press force with the D5506 LCP plates. For the lowest press force, the temperatures are approximately 3 °C higher than those at the higher press forces. For the cases without the thermal compound, there is still a more moderate reduction in temperature with increasing press force. However for the cases with the thermal compound, after the initial 60 lb force level, there is little decrease in temperature with increasing force.

The final set of temperature distribution data is for the heat pipe orientated vertically. This data, which shows the temperature distribution for the heat pipe with the condenser on the top, bottom and with the heat pipe in air (no cooling plate), is plotted in Figure 5.18.

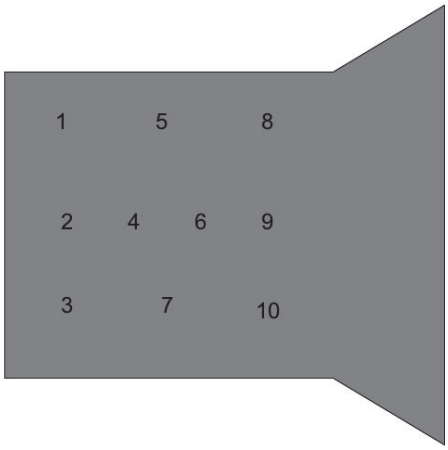

Figure 5.15.—Thermocouple Layout on Heat Pipe

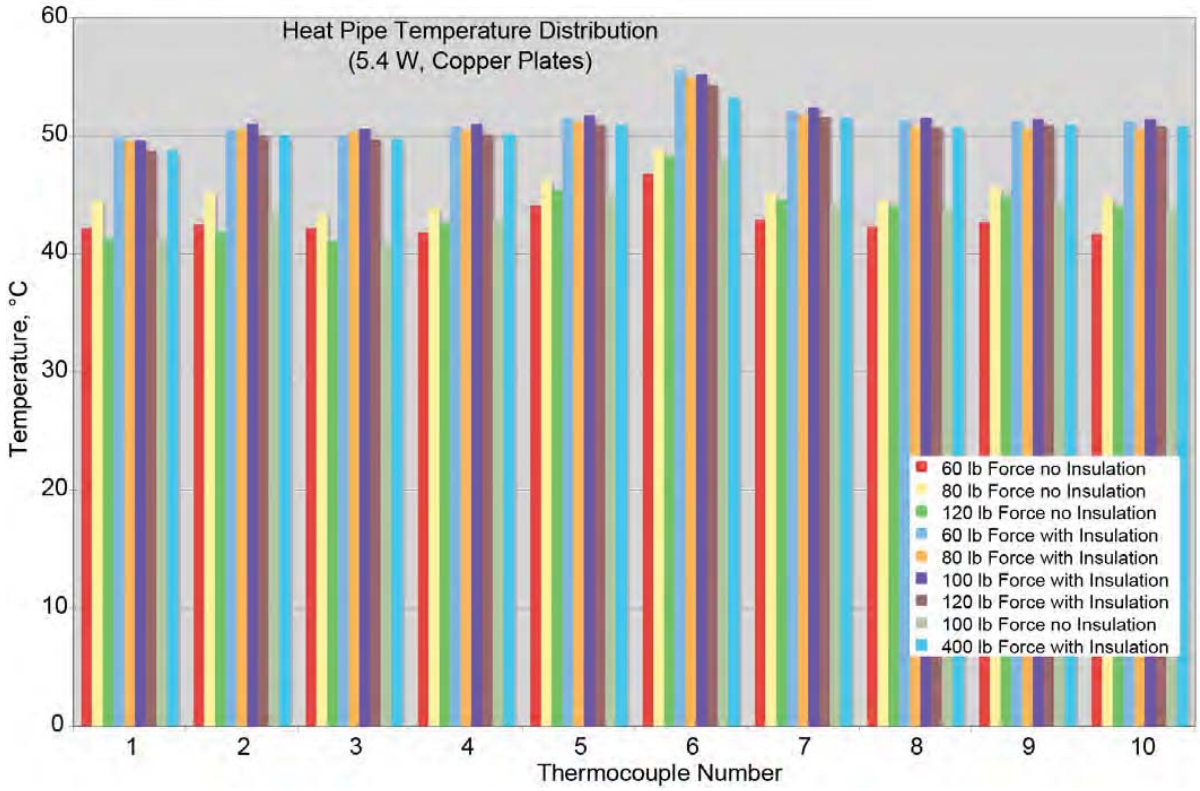

Figure 5.16.—Steady-State Heat Pipe Temperatures, Cooper Plates, 5.4 W Input Power

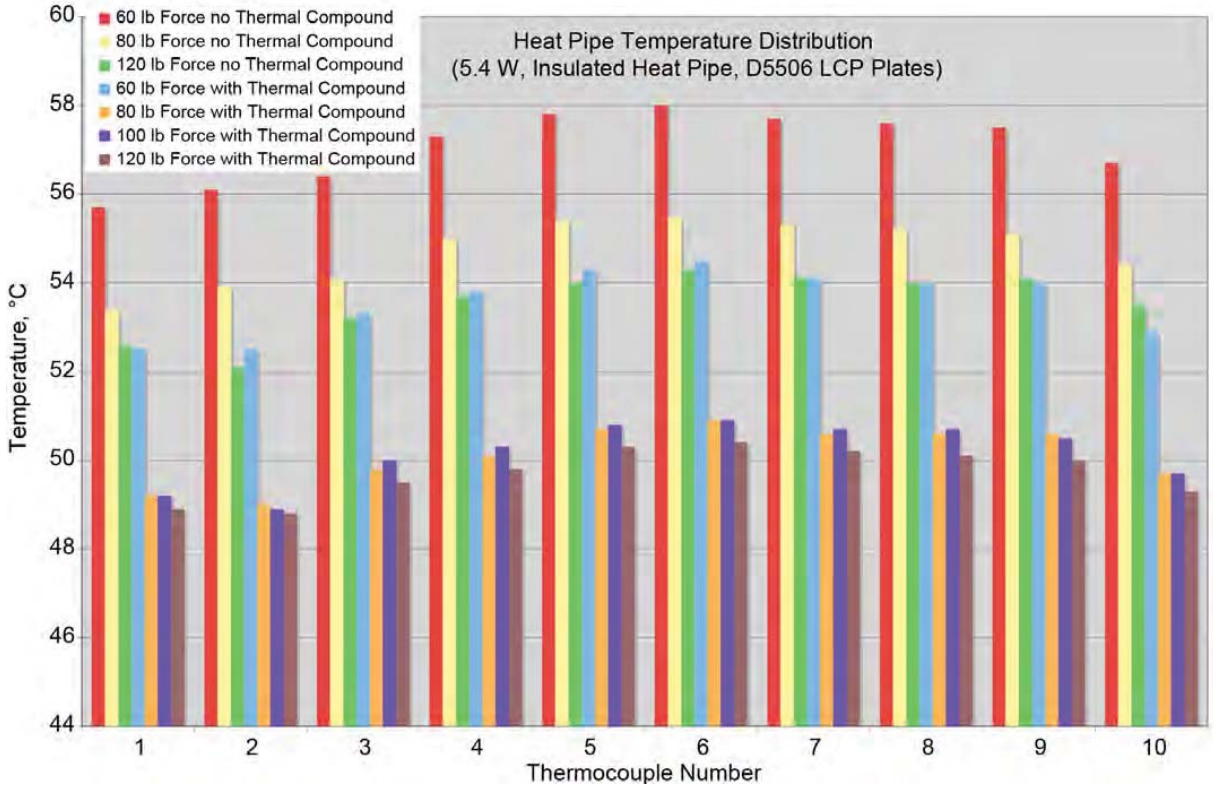

Figure 5.17.—Steady-State Heat Pipe Temperatures, D5506 LCP Plates, 5.4 W Input Power

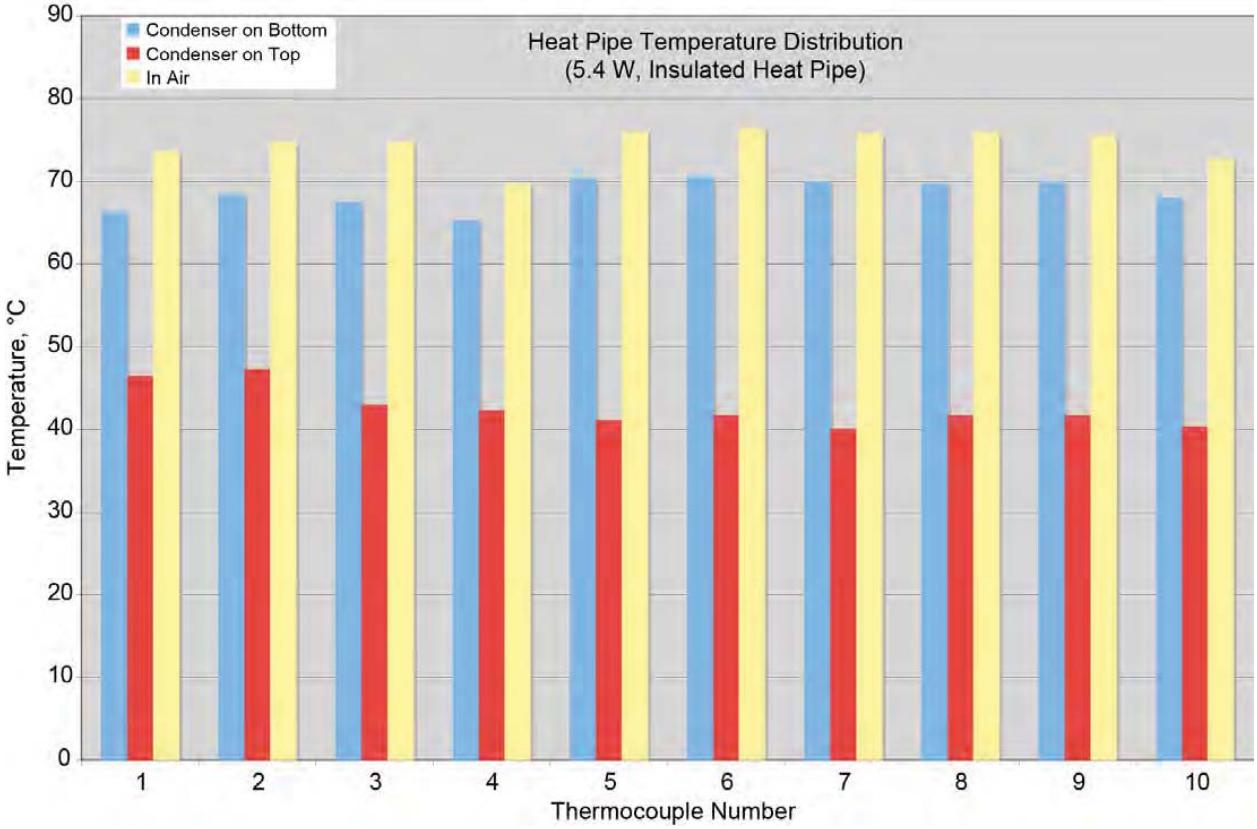

Figure 5.18.—Steady-State Heat Pipe Temperatures, Vertical Heat Pipe in D5506 LCP Manifold

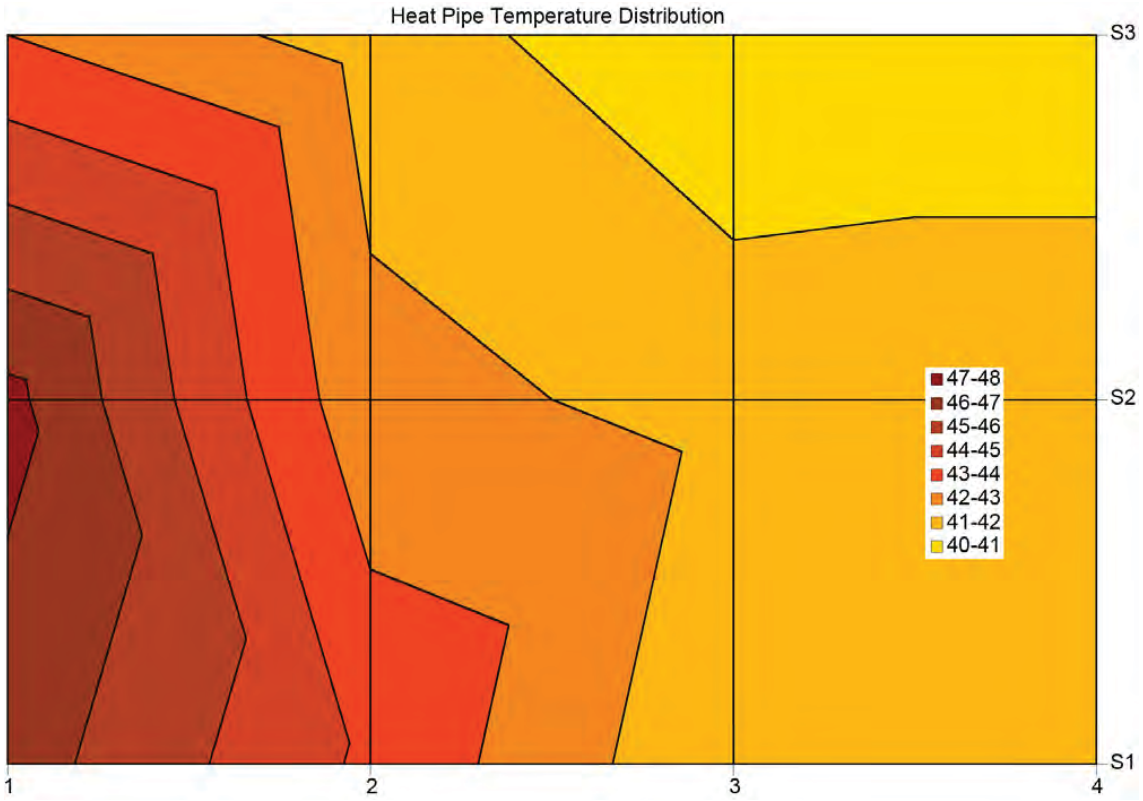

Figure 5.19.—Vertical Heat Pipe Surface Temperature Distribution with Condenser on Top

From Figure 5.18, it can be seen that there is a significant difference in the temperature profile with the condenser on the top versus on the bottom. For the case with the condenser on the top, the heat pipe temperature is fairly uniform except for the area furthest from the condenser where there is a rise of approximately 5 °C. This temperature profile over the heat pipe with the condenser on the top is further illustrated in Figure 5.19. Overall, the temperatures with the condenser on the top are about 25 °C lower than with the condenser on the bottom. Also the temperature values and distribution with the condenser on the bottom is similar to that with the heat pipe held in air (no active cooling). This indicates that the heat pipe was not functioning properly in that orientation probably due to its inability to move the internal working fluid against gravity back to the evaporator portion of the heat pipe.

5.5 Heat Pipe Operational Test Summary

The heat pipe evaluation testing has provided some insight into the successful operation of the heat pipes. The main items of note are:

- The heat pipes will operate with the 5506 LCP conductive plastic as an interface between the heat pipe and the cooling source.
- The thermal compound provides additional thermal benefits and enhanced heat transfer between the 5506 LCP plastic and the heat pipes.
- The heat pipes as designed must be operated vertically with the condenser on the top or horizontally to work properly.
- The gripping force between the heat pipe and cooling surface is not a critical factor as long as a sufficient interference fit is maintained.
- The cooling length or fin length on the heat pipe should be at least 5 mm to insure good heat transfer and operation of the heat pipe.

6.0 Manifold Design, Materials and Construction

The cooling plates conduct the internal heat from the fuel cell stack to a portion of the plate extending beyond the stack. Heat must then be removed from this exposed portion of the cooling plate in order to provide the desired cooling of the fuel cell stack. To achieve this, a cooling manifold must interface with the cooling plate and provide a path for the heat to flow from the cooling plate to an external cold sink.

The cooling manifold design is critical to the performance of the cooling plates as well as the ability to control the internal fuel cell stack temperature. If not properly designed, any thermal resistance added by the cooling manifold could introduce a significant time lag into the response of the system to changes in internal temperature. This response time will be dependent on the manifold design, fuel cell stack design, and cooling fluid flow properties. The greater this thermal response lag, the more difficult it will be to accurately control the internal fuel cell temperature. In this application, the main requirements for the cooling manifold design are related to its thermal and electrical properties. The basic cooling manifold requirements are listed below.

- The cooling manifold must provide electrical isolation between cooling plates. For the fuel cell stack to operate efficiently, the cooling plates have to be electrically conductive in order to allow current to flow from cell to cell within the stack. However, because the manifold will contact more than one cooling plate, it has to be an electrical insulator otherwise it would short out the fuel cell stack. Therefore the cooling manifold would need to have the unique property of being thermally conductive as well as an electrical insulator.
- The cooling manifold has to provide good thermal contact between the cooling plates and the external cooling fluid loop. The manifold design will need to minimize the thermal contact resistance between the cooling plates and the cooling fluid and provide a good thermally conductive path for the heat flow from the cooling plates to the cooling fluid.
- To minimize overall system mass, the cooling manifold will need to be as lightweight as possible. Utilizing lightweight materials that meet the thermal and electrical requirements and minimizing the size of the manifold will be needed to achieve this.

A number of different types of cooling manifolds were designed and constructed. An important characteristic of the manifold is the Reynolds number of the internal cooling fluid. This Reynolds number will indicate whether the fluid flow is laminar or turbulent. Turbulent flow will have a much greater heat transfer capability between the surface through which the heat is being transferred and the cooling fluid. Once turbulent flow is achieved, however, the increased heat transfer will tend to be fairly constant regardless of increases in the flow rate. The transition between laminar and turbulent flow results in a sharp increase in heat transfer rate. This in turn will cause a significant drop in both the manifold and cooling plate temperatures. Another aspect of turbulent flow is that it will increase the pressure drop through the manifold. This increase in pressure drop will require an increase in pumping power in order to maintain the desired flow rate. Because of these issues, it is desirable to have laminar flow through the cooling chamber and over the range of cooling flow rates to be used. Laminar flow will enable the heat transfer, and therefore cooling plate temperature, to be more easily controlled through variations in the cooling fluid flow rate through the manifold as well as minimize pumping power.

The Reynolds number (Re) through the cooling channel of the manifold is based on the temperature-dependent density and viscosity of the cooling fluid (ρ, μ), the diameter of the coolant passage ( ) and the velocity of the cooling flow ( ) The Reynolds number for flow through the cooling manifold is given by Equation (6.1).

$$\mathrm{Re} = \frac{\rho(\quad)}{\mu(\quad)} \tag{6.1}$$

Because the maximum operating temperature of the cooling plates and therefore manifold will be less than 100 °C, water was chosen as the cooling fluid for the manifolds. The viscosity and density of water are not constants and vary with the water temperature ( ). Since the inlet and outlet temperature of the coolant water can be significantly different expressions for the density and viscosity of water as functions of temperature were used. These are given in Equations (6.2) and (6.3), respectively (Ref. 5).

$$\rho(\quad) = -404.87 + 14.121\quad - 0.0507\quad^{2} + 7.79\times10^{-5}\quad^{3} - 4.63\times10^{-8}\quad^{4} \tag{6.2}$$

$$\mu(\quad) = 4.5\times10^{13}\quad^{-5.7342} \tag{6.3}$$

For manifolds that do not have circular cooling passages an effective cooling passage diameter ($_{eff}$) was used in place of the standard diameter ( ). The effective diameter is calculated based on the hydraulic diameter ($_{h}$) of the passage, the height (h) to width (w) ratio of the passage and its friction constant (f_{Re}) as given by Equations (6.4) to (6.6) (Ref. 6).

$$_{eff} = \frac{64}{f_{\mathrm{Re}}}\quad_{h} \tag{6.4}$$

$$_{h} = \frac{2wh}{w+h} \tag{6.5}$$

$$f_{\mathrm{Re}} = 95.705 - 121.22\left(h/w\right) + 132.75\left(h/w\right)^{2} - 50.416\left(h/w\right)^{3} \tag{6.6}$$

6.1 Metal Manifold Design

The initial manifolds were constructed out of metal. These manifolds were designed as test articles whose intended use was to demonstrate the ability to remove heat from the edge of the cooling plates. Three sets of metal manifolds were constructed. Each set was identical in design but constructed out of different metals; copper, 6061-T6 aluminum and 316 stainless steel. These manifolds were designed to work with the TPG cooling plates. The specifications on these metals and the thermally conductive plastic D5506 LCP are given in Table 6.1. The three manifolds (aluminum, stainless steel, and copper) are shown in Figure 6.1 and the design drawing for the metal manifolds is shown in Figure C.1 of Appendix C.

TABLE 6.1.—MANIFOLD MATERIAL PROPERTIES

Material	Density, g/cm^3	Thermal conductivity, W/mK	Specific heat capacity, J/g °C	Coefficient of linear thermal expansion, ×10^{-6}/°C
C10100 Copper	8.94	391	0.4	16.9
316 Stainless Steel	7.96	16.3	0.5	18
6061-T6 Aluminum	2.7	167	0.9	23.6
Anodized 6061-T6 Aluminum	2.7	167	0.9	23.6
D5506 LCP	1.8	10	1.0	116.2 parallel 5.6 perpendicular

These metals were selected because they represented a range of thermal conductivities that were used to determine how the thermal conductivity of the manifold affects the cooling plate temperature and performance. In order to use these metal manifolds in an actual fuel cell stack, the ends of the cooling plates inserted into the manifold would need to be electrically insulated to avoid shorting out the cells within the fuel cell stack. This adds to the complexity of the cooling plate design. Another drawback to

the metal manifolds is their density. To minimize the overall cooling system mass, it would be beneficial to utilize a material with the lowest density that is capable of transferring heat effectively from the cooling plates to the cooling fluid. The cooling flow Reynolds number for these metal manifolds for various flow rates over a range of cooling fluid temperatures is shown in Figure 6.2.

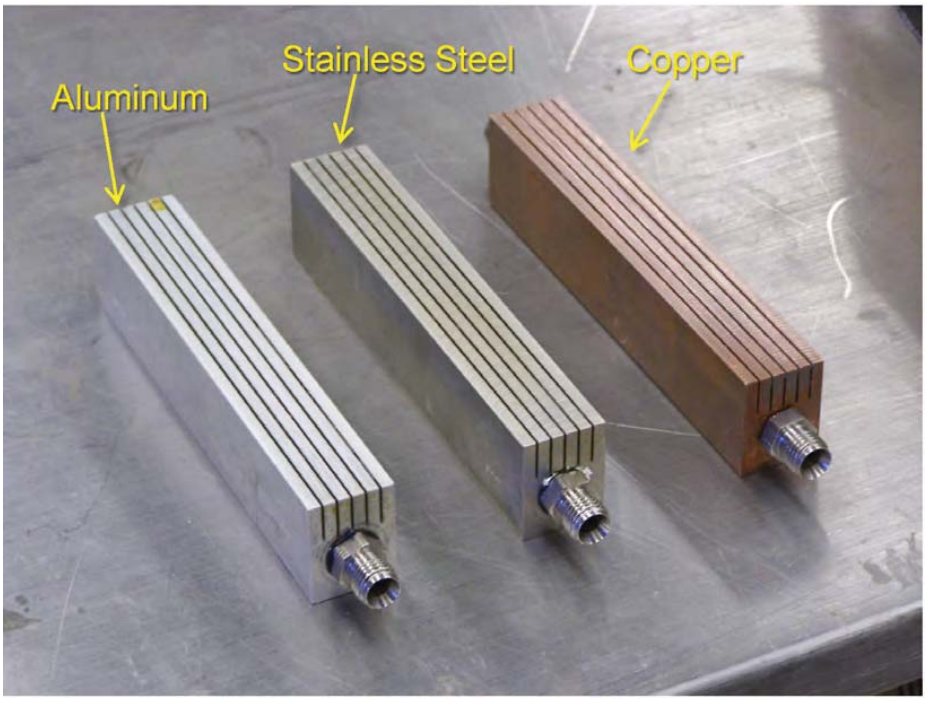

Figure 6.1.—Aluminum, Stainless Steel and Copper Metal Manifolds

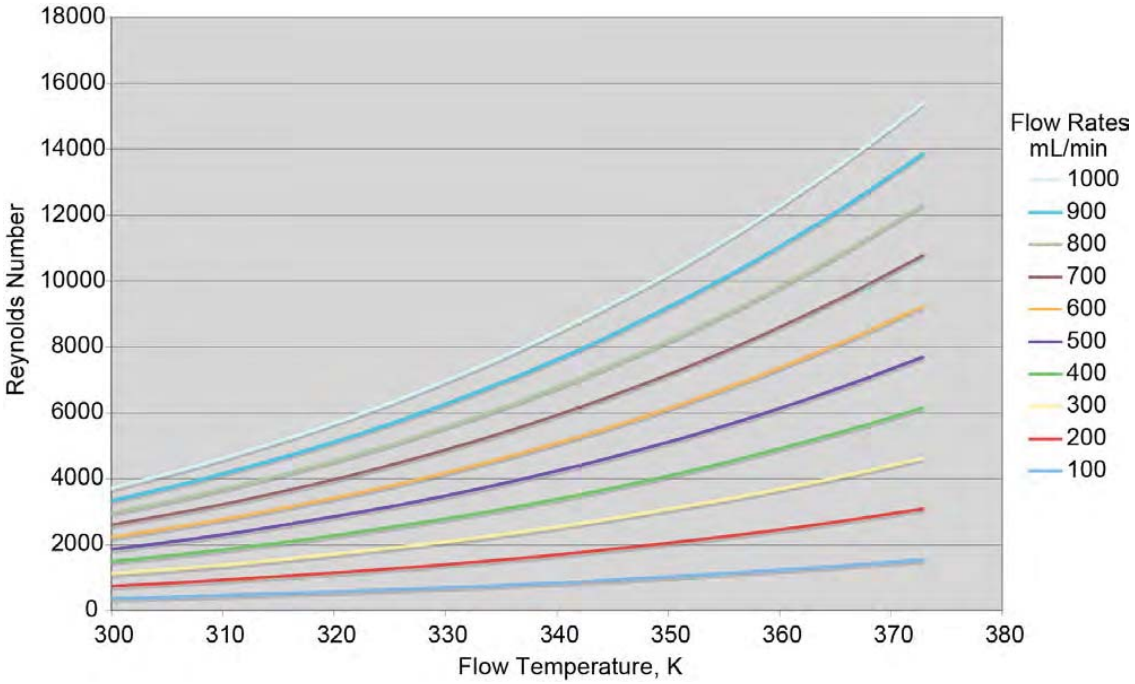

Figure 6.2.—Metal Manifold Reynolds Number for Different Flow Rates Over a Range of Cooling Fluid Temperatures

For the circular fluid passage in the manifolds the Reynolds number for transition from laminar to turbulent flow is approximately 2300. Figure 6.2 shows that at room temperature operation, the flow will be laminar up to approximately 700 mL/min flow rate. As the fluid temperature increases, this transition occurs at lower flow rates due to the temperature dependent properties of water.

6.2 Aluminum Channel/LCP Manifold Design

To provide both higher thermal conductivity and no electrical conductivity, the next series of manifolds were constructed out of an electrically nonconductive material, D5506 thermally conductive liquid crystalline polymer (LCP). This was done to test a manifold that could eliminate the need to electrically insulate the edge of the cooling plates. This easily machined material, which can be extruded or molded, has a thermal conductivity of 10 W/mK. This thermal conductivity is low compared to metals but high relative to other electrically isolating materials. The data sheet from the manufacturer on D5506 LCP material properties is in Reference 9.

The first series of manifolds using the D5506 LCP material were constructed in two segments. A block of LCP had groves machined in it to accommodate the edges of the cooling plates. This block was then glued onto an aluminum channel through which the cooling fluid would flow, as shown in Figure 6.3. The construction diagram for the LCP block is shown in Figure C.2 of Appendix C. The LCP was attached to the aluminum with an adhesive, as shown in Figure 6.4. Two versions of this manifold were constructed, one for the TPG cooling plates and one for the heat pipe cooling plates. The only difference between them was the groove thickness needed to accommodate each type of plate and the number of plate grooves. The manifolds made for the TPG plates had four grooves, to hold four plates, whereas the manifolds for the heat pipe plates had two grooves, for holding two plates.

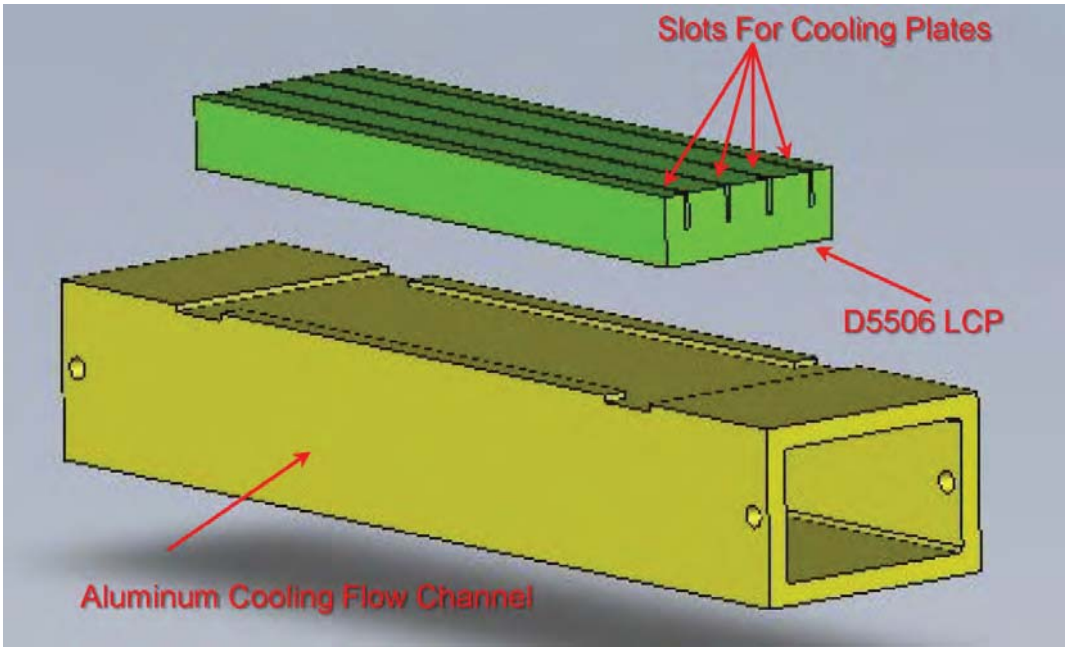

Figure 6.3.—D5506 LCP Manifold Components and Arrangement

Figure 6.4.—D5506 LCP and Aluminum Cooling Manifolds

Initially a thermally conductive gap filler adhesive compound, (3500S35, see the data sheet in Ref. 10) was utilized, to adhere the LCP to the aluminum. This compound had a thermal conductivity of 3.6 W/mK. The compound worked well initially and bonded the LCP to the aluminum. However, under vacuum conditions the bond weakened and the LCP separated from the aluminum. Because of this a number of other adhesives were tested to determine which would provide the best bond between the LCP and aluminum as well as being capable of operating within a vacuum and at temperatures potentially exceeding 100 °C.

Five adhesives, given in Table 6.2, were tested to identify an adhesive which would provide the strongest bond between the LCP and aluminum. These adhesives were not as thermally conductive as the gap filler compound previously used but were applied as a very thin layer between the LCP and aluminum to minimize any thermal resistance they would impart.

Lap joint specimens of LCP bonded to aluminum were made with each type of adhesive, as shown in Figure 6.5. All surfaces were cleaned with ODC free degreaser before any surface preparation was applied. To prepare the aluminum surfaces for bonding, it was roughened with fine grit emery prior to any surface preparation required by the adhesive. The LCP surface was left as received. Once cured, the test samples were tested to estimate the force needed to break the joint. The rankings listed in Table 6.2 correspond to the force needed to separate the adhesive. The JB Weld epoxy required the greatest force and therefore was ranked 1 as the LPC material failed before the adhesive.

A second version of the LCP and aluminum cooling manifold was also constructed, as shown in Figure 6.6. This manifold was for use with the larger size cooling plates, shown in Figure 2.10. The cooling passage for the LCP and aluminum channel manifold was significantly larger than the passage for the metal manifolds. The channel was rectangular with a width of 3.5 cm and a height of 2 cm. Because of this larger cooling passage size, the Reynolds numbers for the cooling flow through the LCP and aluminum channel manifolds, shown in Figure 6.7, are much lower than those for the metal manifolds for similar flow rates and coolant temperatures.

TABLE 6.2.—ADHESIVES TESTED IN THE BONDING OF THE LCP AND ALUMINUM

Adhesive	Surface Preparation		Ranking best to worst (1 to 5)
	Aluminum	LCP	
Plastic Welder II Epoxy	None	None	4
Plastic Welder II Epoxy	Lord AP134 Primer	Lord 7701 Primer	3
Bondit B-45TH Epoxy	Lord AP134 Primer	Lord 7701 Primer	2
JP Weld Epoxy	Lord AP134 Primer	Lord 7701 Primer	1
Loctite 680 Retaining Compound	7649 Primer	7649 Primer	5

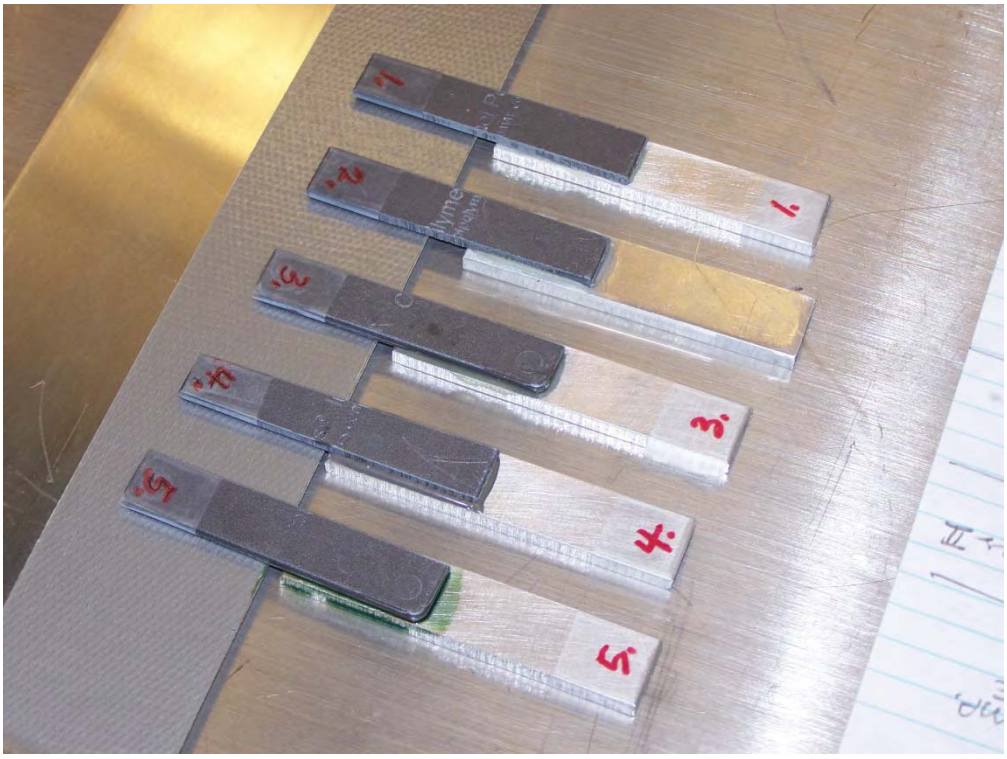

Figure 6.5.—LCP and Aluminum Adhesive Test Samples

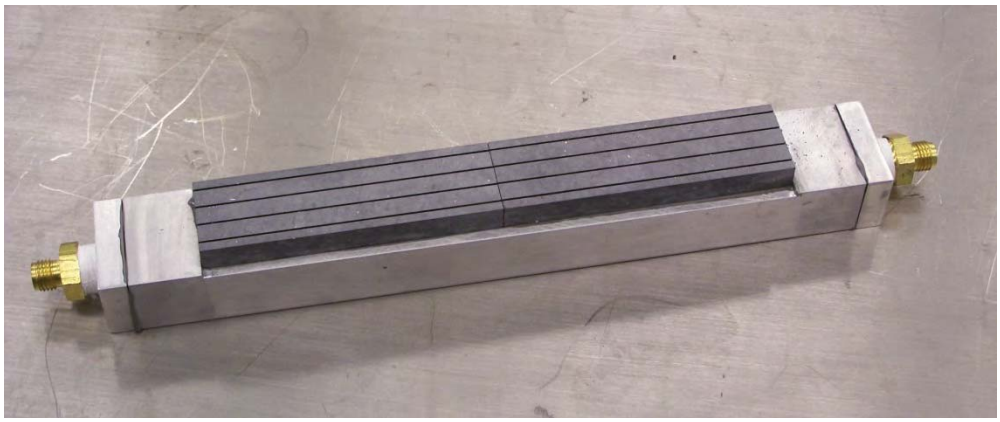

Figure 6.6.—Larger Size LCP and Aluminum Cooling Manifold

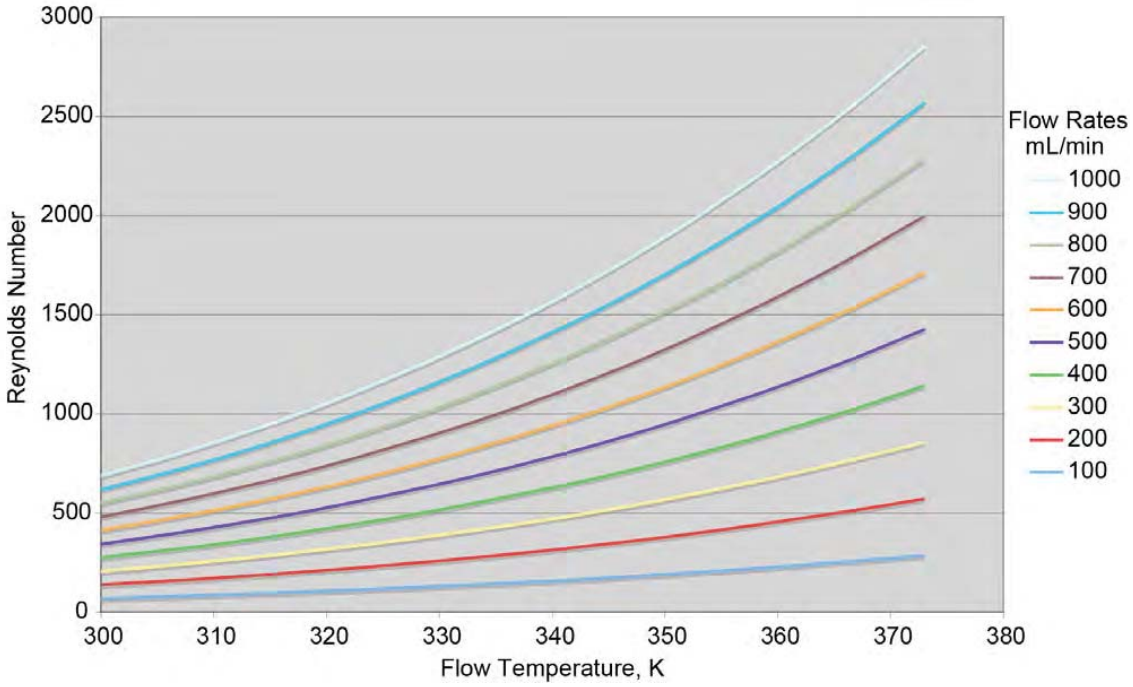

Figure 6.7.—Reynolds Number for the LCP and Aluminum Channel Manifolds Over a Range of Flow Rates

From Figure 6.7 it can be seen that for almost the complete ranges of flow rates and coolant temperatures the Reynolds number is below the initial transition point (Re = 2,300) between laminar and turbulent flow. Therefore for this manifold design, laminar flow can be maintained under almost all operating conditions.

6.3 LCP Manifold With Integral Fluid Channel

The next series of manifolds that were constructed were designed to enhance the heat transfer from the cooling plates to the cooling fluid by integrating the cooling fluid passages directly through the LCP material, as shown in Figure 6.8. Aluminum end caps were used to connect the external cooling fluid lines to the channels in the LCP manifold. An illustration of the LCP manifold with the integral cooling passages is shown in Figure 6.9. Based on the previous adhesive testing results, JP Weld epoxy was used to adhere the aluminum end caps to the LCP manifold. The constructed LCP manifold with integral cooling passages is shown in Figure 6.10.

As with the metal manifolds, the coolant passageways through LCP are fairly small. They are elliptical in shape with a height of 0.664 cm and a width of 0.477 cm. Flow through these channels will produce higher Reynolds numbers than the flow through the LCP and aluminum manifold as shown in Figure 6.11 for a range of flow rates and coolant temperatures.

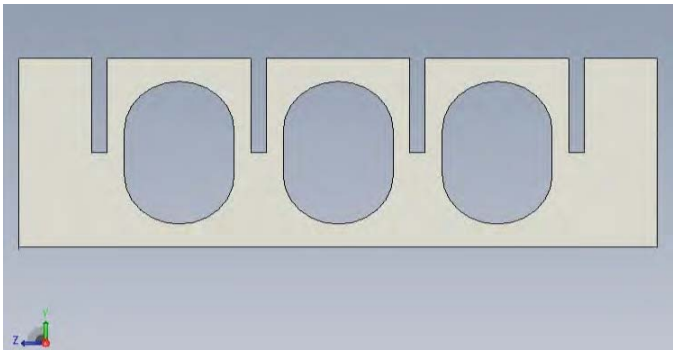

Figure 6.8.—Cooling Fluid Passages in the all LCP Manifold

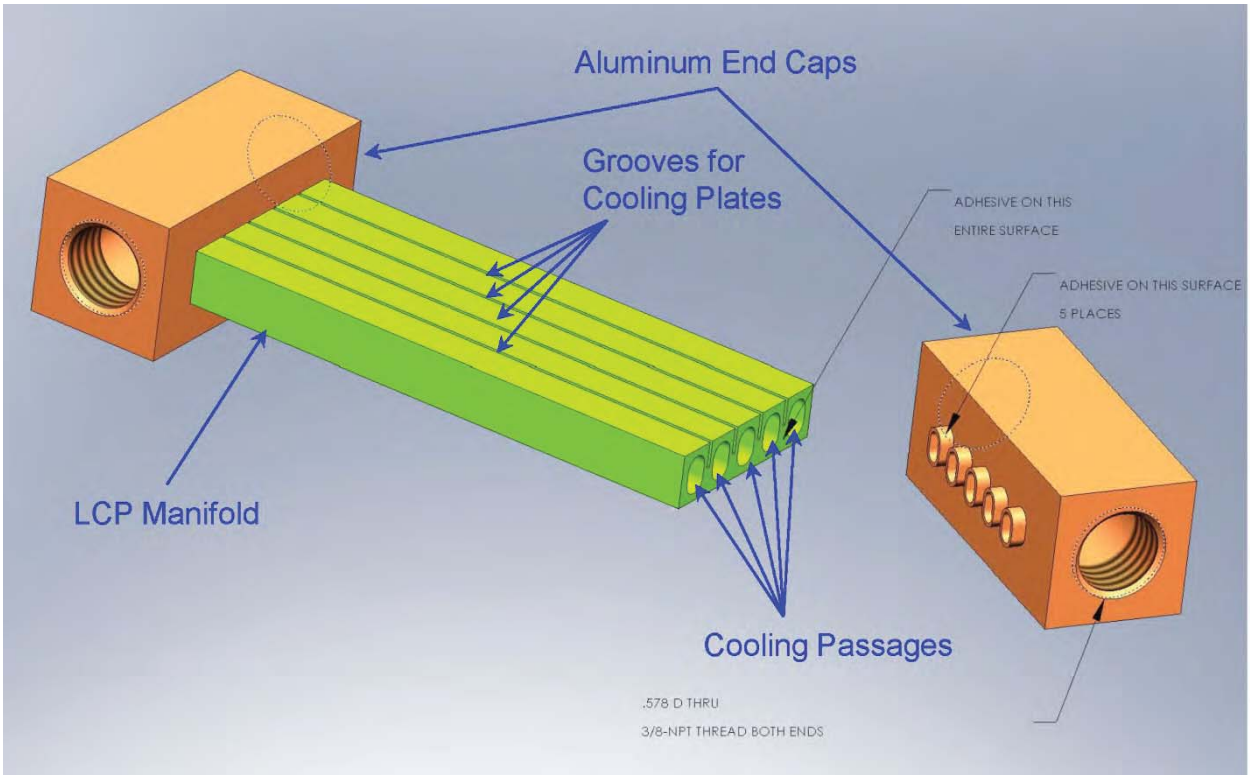

Figure 6.9.—LCP Manifold with Integral Cooling Passages Diagram

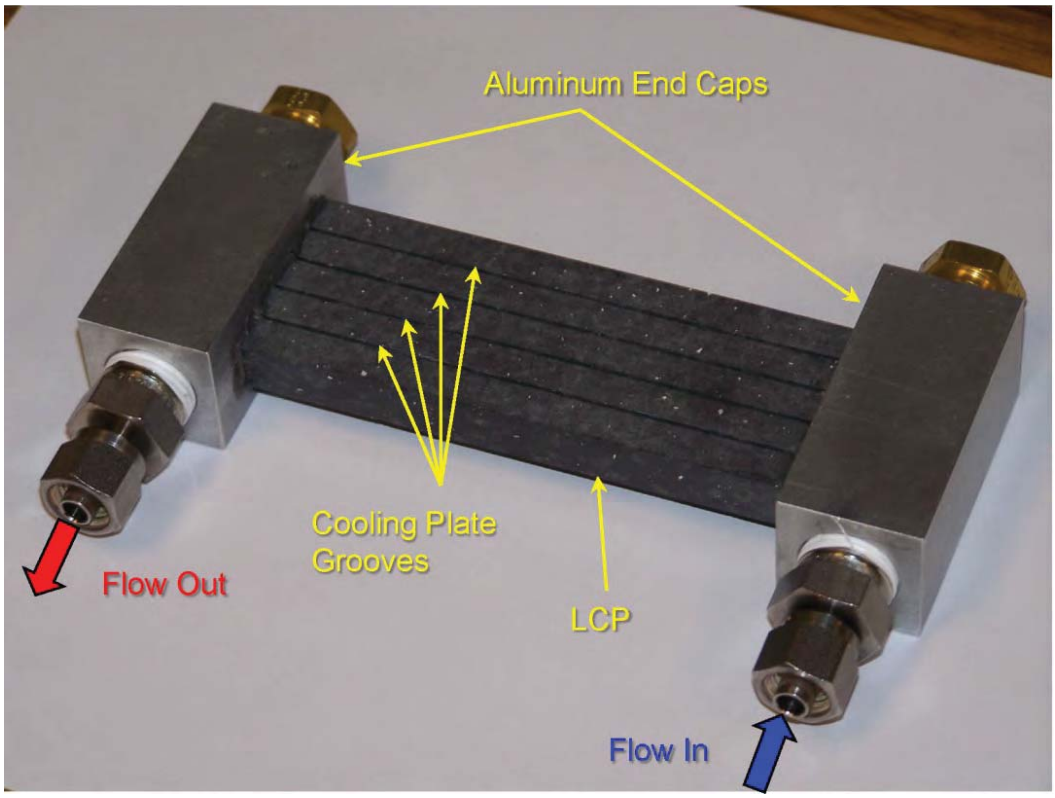

Figure 6.10.—LCP Cooling Manifold with Integral Cooling Passages Assembly

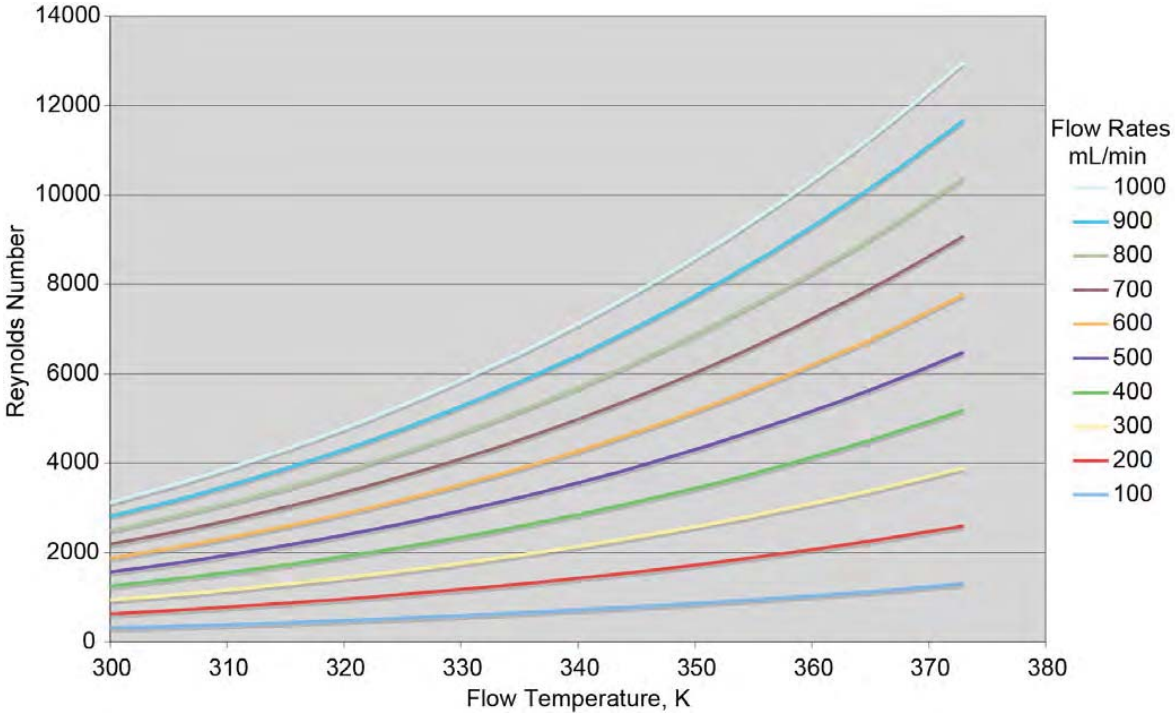

Figure 6.11.—Reynolds Number for the LCP Manifold with Integral Cooling Passages Over a Range of Cooling Flow Temperatures for Various Flow Rates

6.4 Anodized Aluminum Manifold With Integral Cooling Passages

The last type of test manifold was constructed entirely from aluminum. It was based on the design of the LCP manifold with the integral cooling passages using anodized aluminum instead of the LCP material. This manifold provided the same coolant flow capability as the LCP manifold with a wear-resistant electrically nonconductive surface over a more thermally conductive material. Since the anodized layer is harder than both the base aluminum and TPG cooling plates, it will resist wear and scratching during the insertion and removal of the cooling plates. The main concern with anodizing the aluminum was the ability to maintain the groove thickness tolerance for the cooling plates since anodizing will accumulate on the aluminum surface thus changing its dimensions. To account for this, the grooves were machined slight larger than desired. The higher thermal conductivity of the aluminum, compared to the LCP material, enhances the heat transfer to the cooling fluid, which increases the performance of the manifold. Because of the change in materials, the cooling passage geometry in the aluminum manifold was different than the LCP. To enable easier machining, circular cooling holes with a diameter of 0.47 cm were used instead of the oval ones used with the LCP. The cooling passage hole geometry for the aluminum manifold is illustrated in Figure 6.12 and the anodized all-aluminum manifold is shown in Figure 6.13. The construction drawing for the manifold is shown in Figure C.3 of Appendix C.

The cooling passage hole diameter for the aluminum manifold is the same as that used for the metal manifolds described previously. Therefore because of the similar geometry, the Reynolds number for the cooling flow through the anodized aluminum manifold will be the same as that of the metal manifolds, as given by Figure 6.2, at similar coolant flow rates and temperatures.

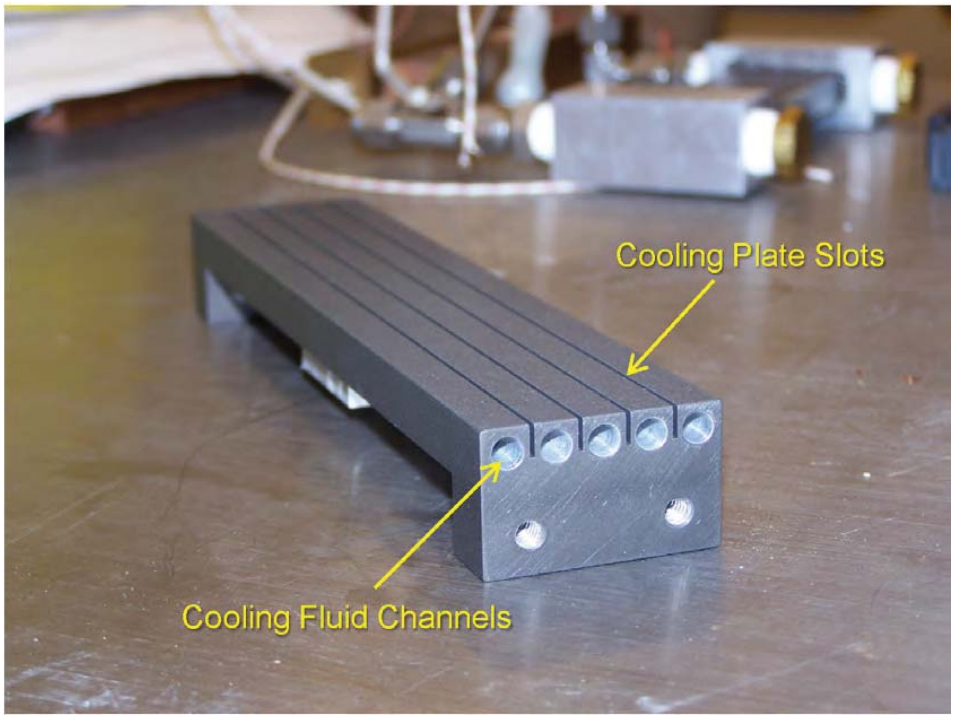

Figure 6.12.—Cooling Passage Geometry for Anodized Aluminum Manifold

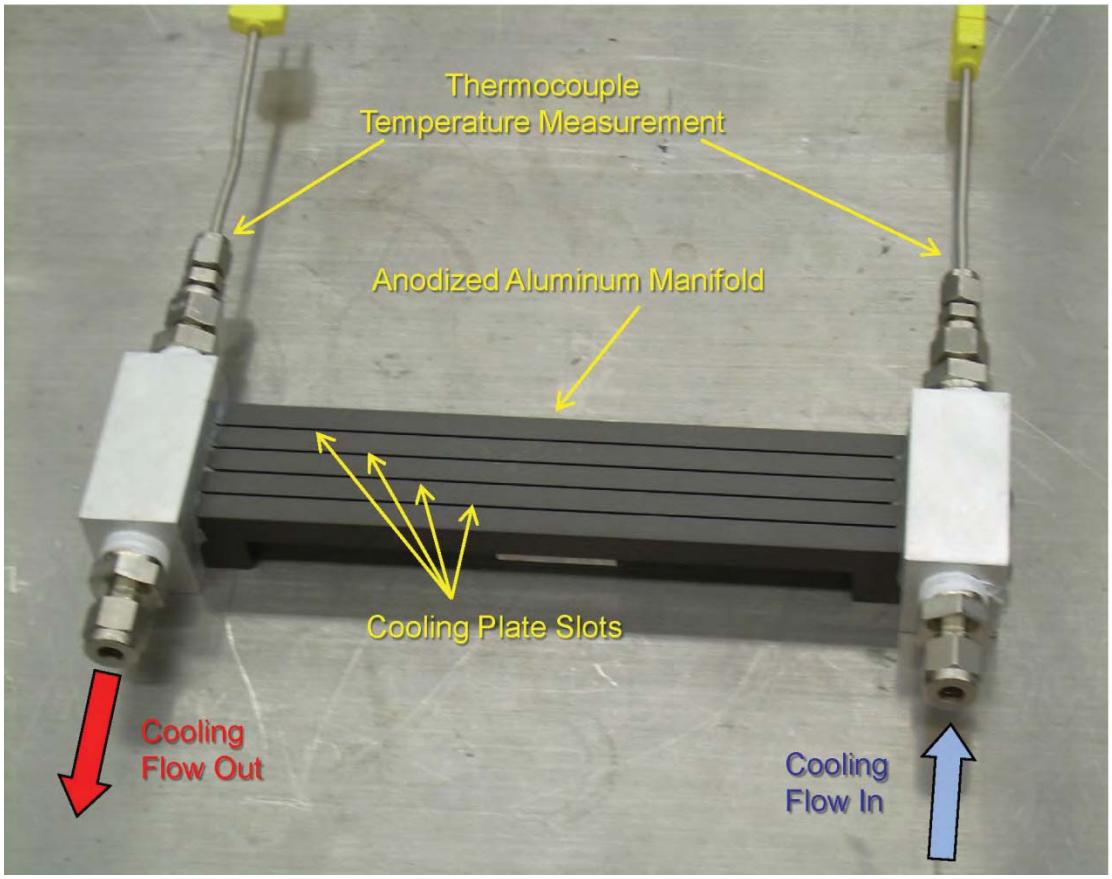

Figure 6.13.—Anodized Aluminum Manifold Assembly

7.0 Manifold Cooling Tests

The testing of the cooling plate manifolds was performed within a vacuum tank facility to minimize any convective heat loss to the surroundings. The test setup utilized the existing hardware and data collection system from the single plate conductivity tests.

The objective of the manifold tests is to assess their ability to remove heat from the cooling plates and maintain a fairly uniform temperature along the edge of each cooling plate. The temperature was determined by monitoring and collecting data from a series of thermocouples affixed to the surface of the cooling plates. The same cooling plates were utilized for each of the initial manifold test. The manifolds included in these tests were the metal manifolds, shown in Figure 6.1 and in Figure C.1 and the aluminum channel/LCP manifold shown in Figure 6.3 and Figure 6.4 and Figure C.2. Utilizing the same cooling plates for all manifold tests eliminated some experimental variability and enabled a more accurate performance comparison between the different manifolds.

The all LCP plastic cooling manifold, shown in Figure 6.8 to Figure 6.10, was included in the initial manifold tests. However, when exposed to vacuum, the LCP material became porous to water and began to leak the cooling water into the vacuum chamber. A number of unsuccessful attempts were made to seal the plastic with various water sealants. Although the all LCP manifold would have been capable of operation under ambient conditions, test in vacuum was necessary to reduce the heat losses to the surrounding. This would minimize the experimental error in evaluating the heat transfer capabilities of the manifolds. Due to the material's porous behavior under vacuum conditions, the all LCP manifold was not included in the manifold testing.

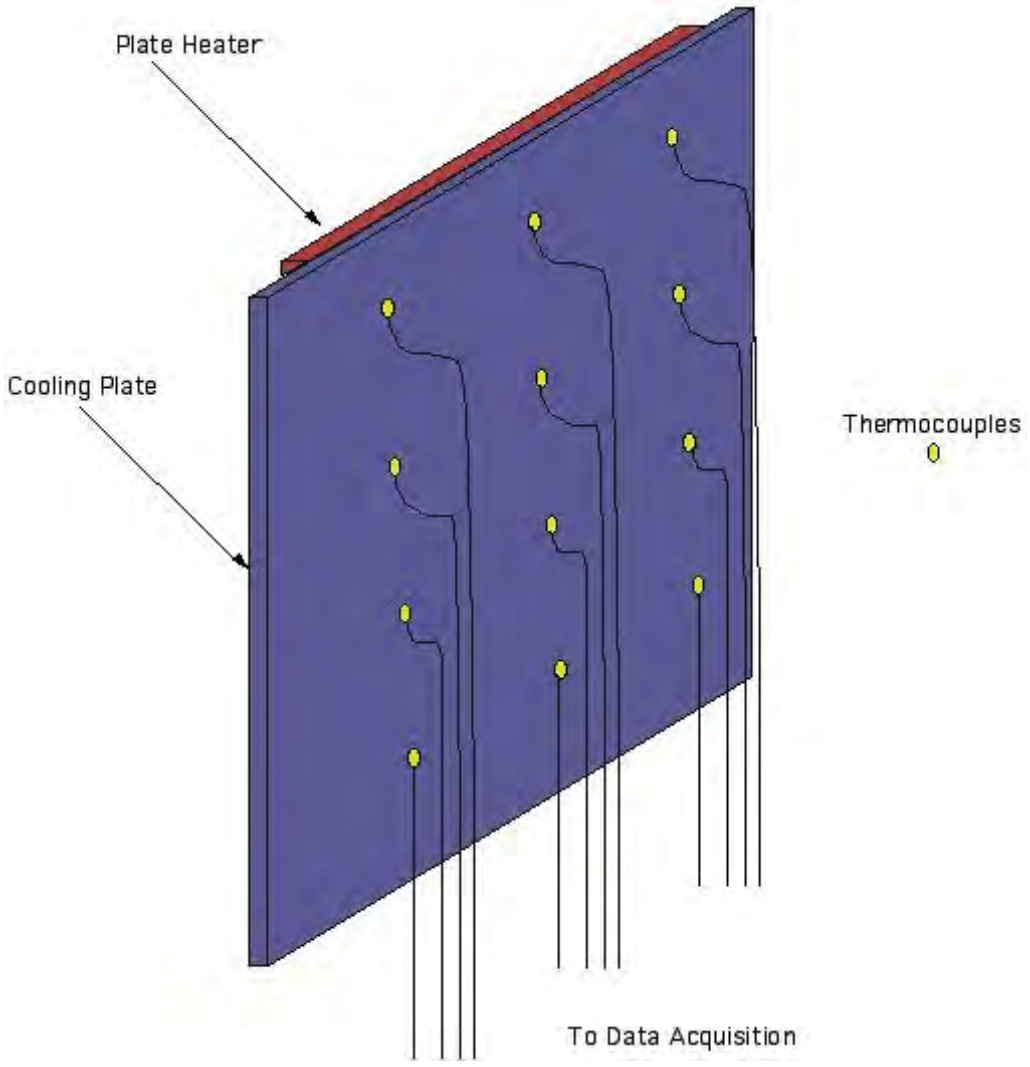

Figure 7.1.—Heater and Thermocouple Arrangement

A flat plate heater was used to simulate the heat output of a single cell or multiple cells into the cooling plate. The cooling plates were instrumented with thermocouples on the side opposite the heater. The heater and thermocouple example arrangement is illustrated in Figure 7.1.

7.1 Metal Manifold Steady State Cooling Test

The initial manifold tests, with the metal manifolds shown in Figure 6.6, utilized four cooling plates. The cooling plates each contained 12 thermocouples (as illustrated in Figure 7.1). The test set-up with the thermocouples taped to the surface of the cooling plate as shown in Figure 7.2 and Figure 7.3.

For these initial manifold tests, cooling manifolds on opposing edges were used to extract heat from the plates. The cooling manifolds and plate arrangements are illustrated in Figure 7.2 and Figure 7.3, respectively. The copper clad TPG plates, as shown in Figure 2.7, were used in the metal manifold tests.

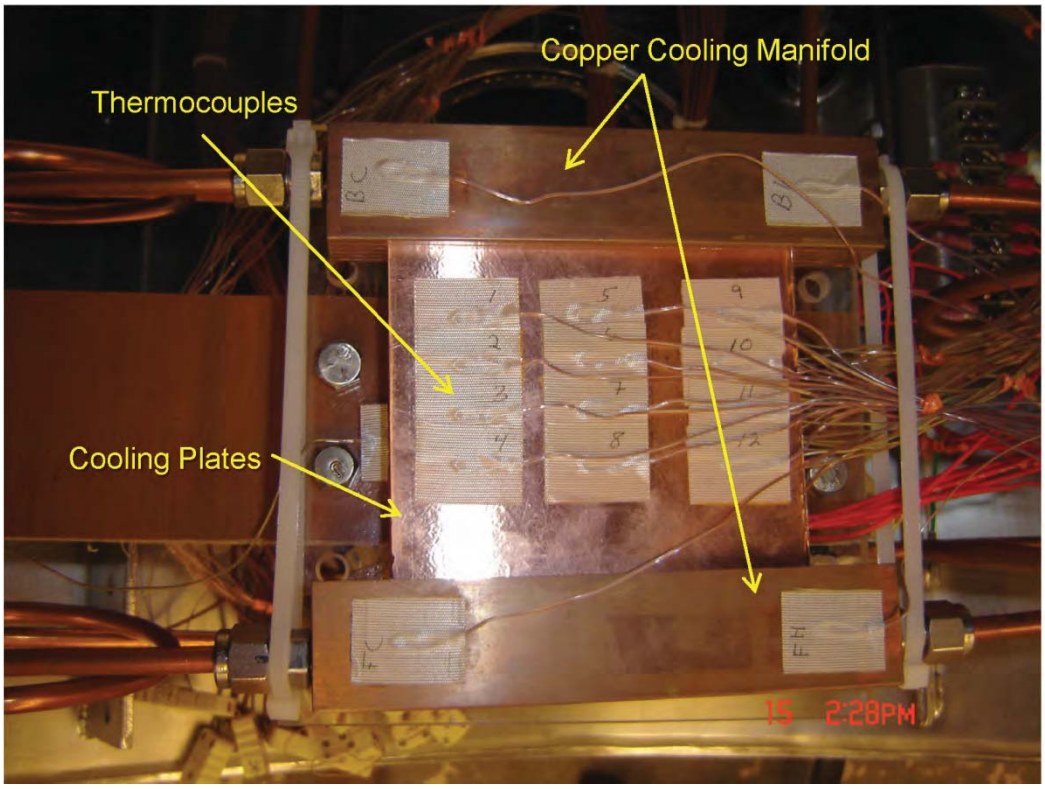

Figure 7.2.—Installed Cooling Plate Instrumented with Thermocouples

The manifold testing was performed under vacuum conditions to minimize any convective heat loss from the plates ensuring that the heat generated by the flat plate heaters would be transferred to the cooling manifolds. The main test components for the initial manifold testing included the following;

- Manifold and Plate assembly (as illustrated in Figure 7.2)
- Vacuum Tank Facility (Shown in Figure 7.5)
- Heater Plate Power Supply
- Chiller and Coolant Lines (for coolant flow to the manifolds)
- Flow Controller
- Data Acquisition System (collecting data on thermocouples and flow rate)

A diagram of the test layout showing the main components of the testing setup is illustrated in Figure 7.4 and the installation of the copper manifold/cooling plate system in the test chamber is shown in Figure 7.5.

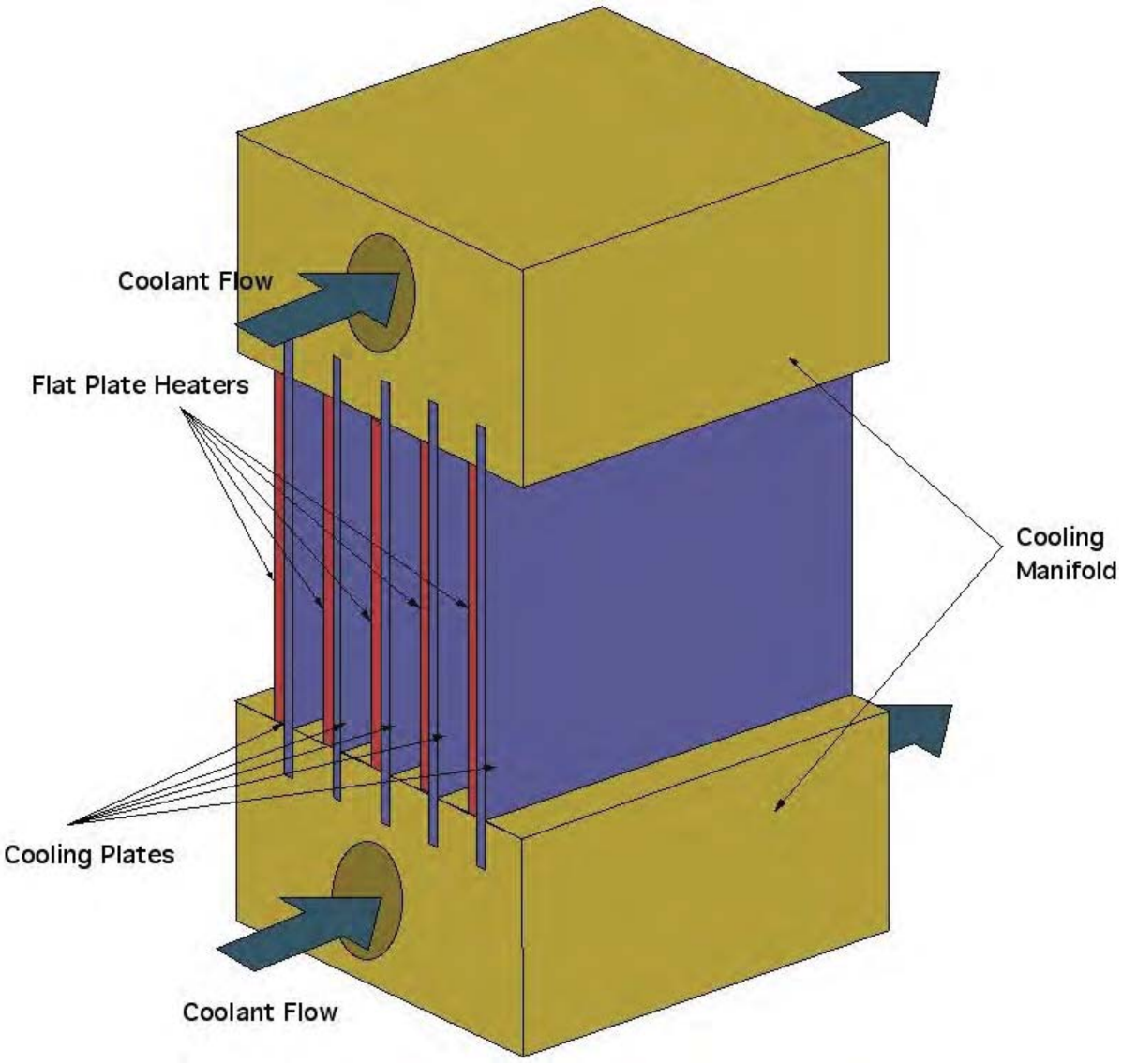

Figure 7.3.—Cooling Manifold and Plate Test Arrangement

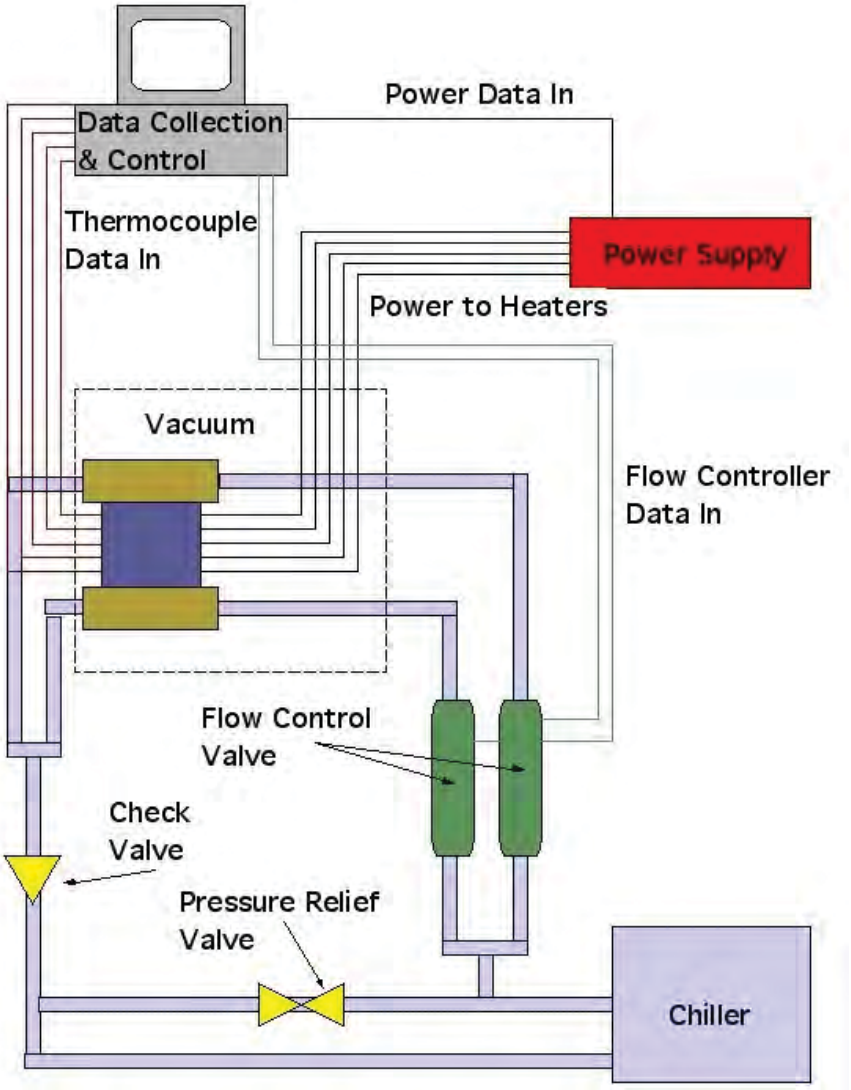

Figure 7.4.—Manifold Cooling Test Diagram

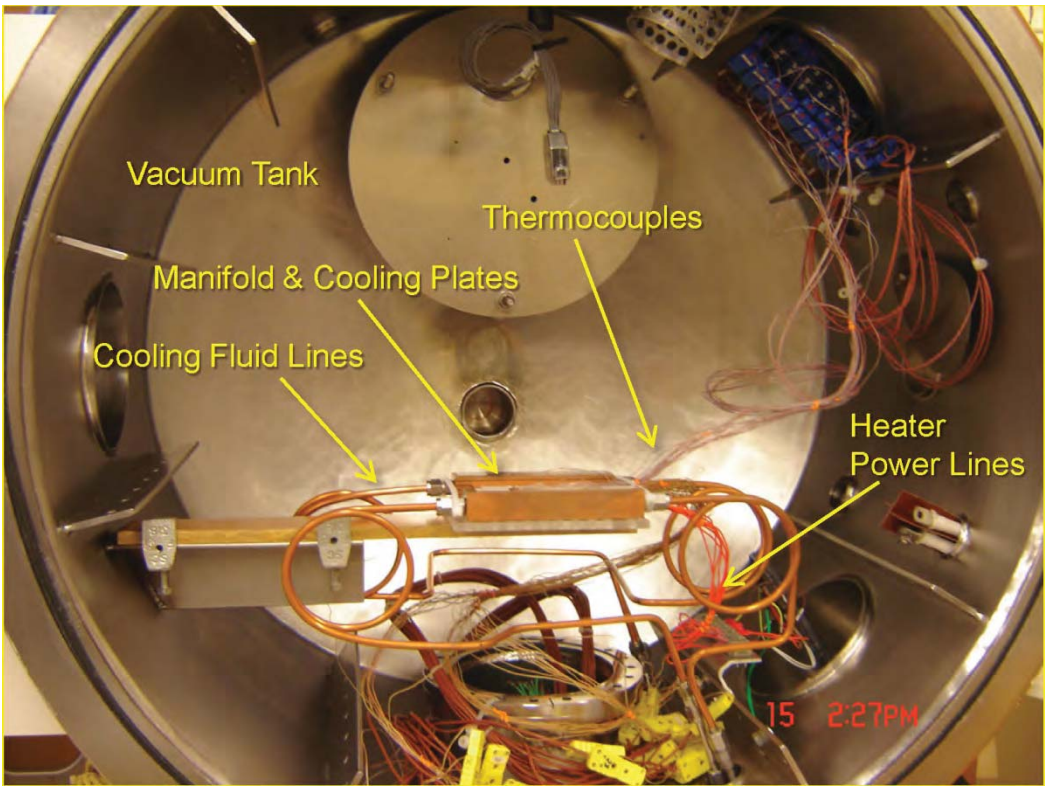

Figure 7.5.—Copper Manifolds with Cooling Plates Installed in the Test Vacuum Chamber

Utilizing the test layout illustrated in Figure 7.4, the temperature distribution for each cooling plate, the heater power supplied and the coolant flow rate were all monitored and recorded. A test matrix of heater power and flow rates was used to provide a complete map of the manifolds performance. The tests with the three- (3) metal manifolds and copper clad TPG cooling plates were performed both with and without Apiezon H-Grease, a vacuum rated thermally conductive grease was used to enhance the heat transfer between the plates and the cooling manifold.

The test protocol involved supplying power to the heaters at a given cooling flow rate and waiting until the system achieved a steady state temperature defined as a temperature rise of less than 1 °C per 5 min. Once this steady state was achieved, the heater power level was increased and the procedure was repeated. Once all of the desired heater power levels were tested for a particular flow rate, the cooling flow rate was increased and the same heater power levels were again tested for the new cooling flow rate.

Figure 7.6 shows the temperature difference between the plate and the stainless steel cooling manifold over a range of cooling flow rates (0.2 to 1.2 LPM) and power supplied to the cooling plates. The power supplied to each cooling plate and the corresponding heat flux to the plates is given in Table 7.1. The heat flux is based on the plate heater area of 49 cm^2. From this figure, it can be seen that the coolant flow rate did not significantly affect the differential temperature between the cooling plate and manifold. As should be expected, there was a smaller temperature difference of 3 to 5 °C for the tests performed with the conductive thermal grease compared to without it.

TABLE 7.1.—HEATER POWER AND HEAT FLUX
FOR THE METAL MANIFOLD TESTS

Plate heater power, W	Heat flux to each cooling plate, W/cm^2
2.5	0.05
7.5	0.15
15	0.31
22.5	0.46

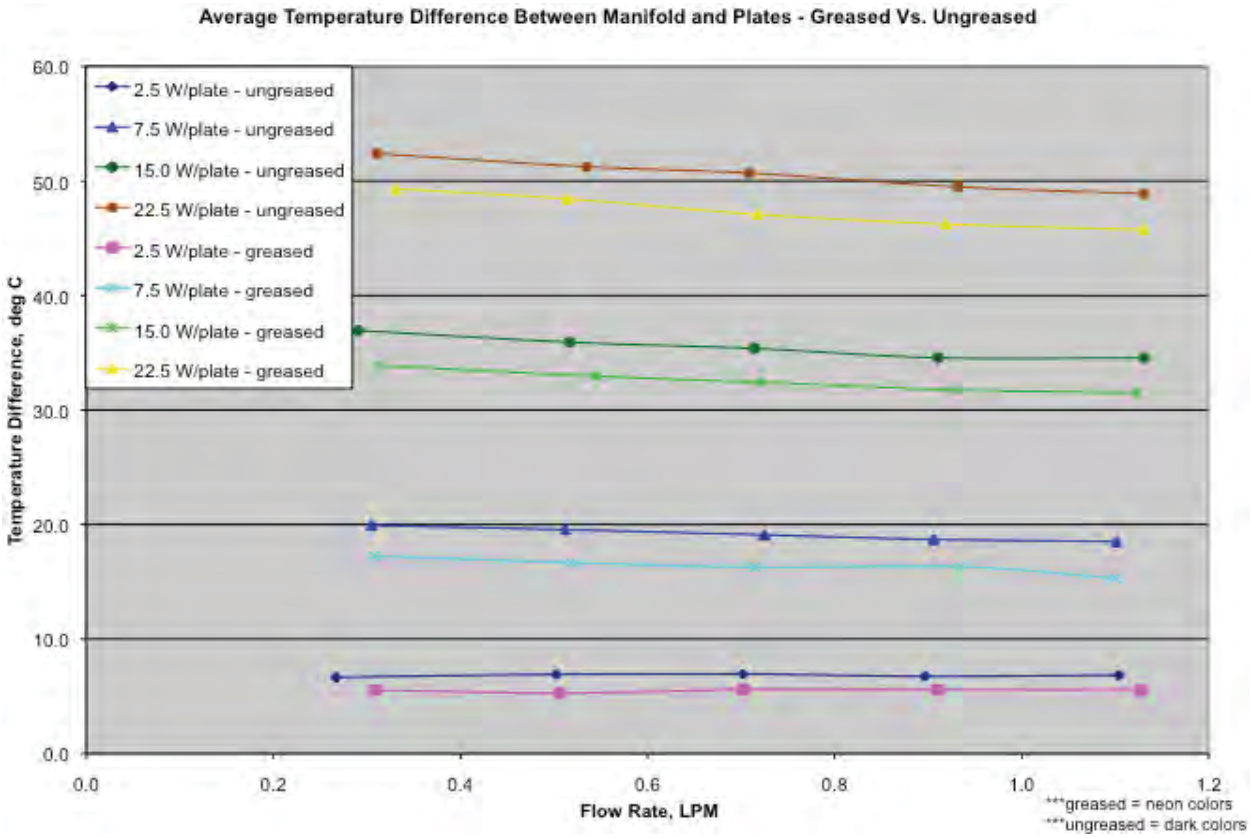

Figure 7.6.—Cooling Plate/Manifold Temperature Difference for the Stainless Steel Manifold Test

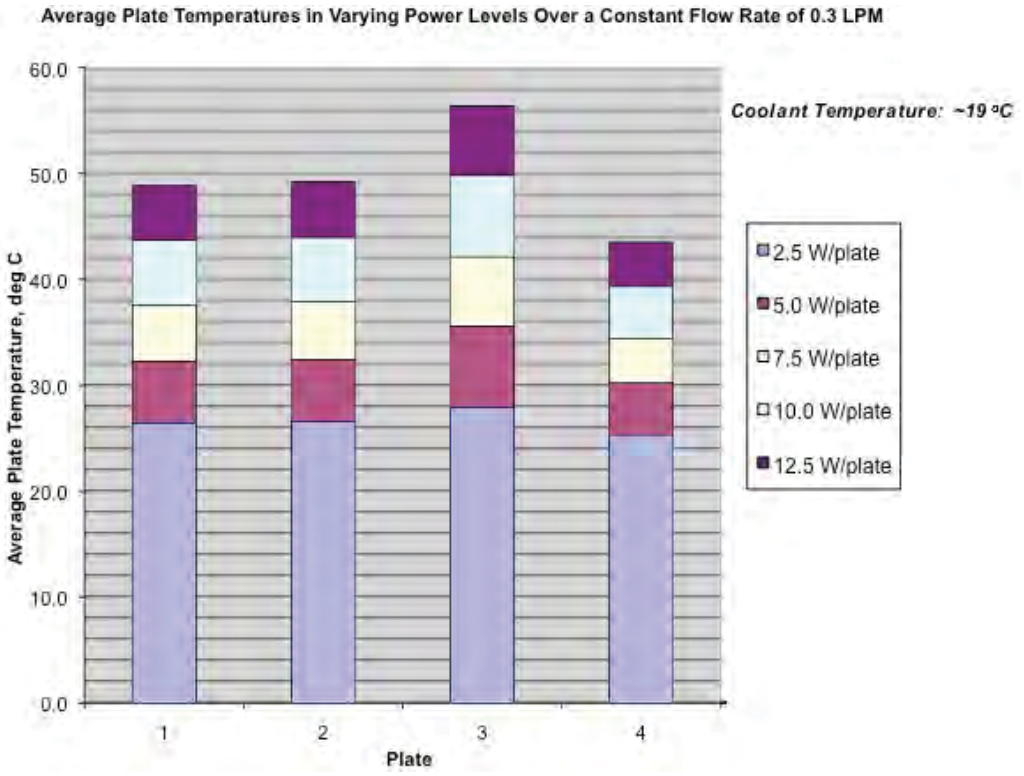

Figure 7.7.—Cooling Plate Temperature with Stainless Steel Manifold and Thermal Grease

The average plate temperatures for the stainless steel manifold with thermal grease are shown in Figure 7.7. From this figure, it can be seen that the average temperature of each plate was fairly consistent over the range of heater power utilized.

The results for the aluminum cooling manifolds are shown in Figure 7.8 and Figure 7.9. Due to the order of magnitude difference of thermal conductivity between the aluminum and stainless steel, the average cooling plate temperature was significantly less with the aluminum manifold compared to the stainless steel manifold. Also, the effect of the thermally conductive grease is significantly more pronounced with the aluminum manifold than the stainless steel, particularly at the higher heater power levels. The thermally conductive grease reduced the thermal contact resistance between the plates and manifold, which permitted more heat to flow from the plates, though the manifold, and into the cooling fluid. The effect the conductive thermal grease had on the operating temperature of the aluminum and stainless steel manifolds is due to the order of magnitude difference in thermal conductivity between these two materials, as given in Table 6.1.

The plate-to-plate average temperature, shown in Figure 7.9, was very consistent over the range of heater powers utilized. The maximum plate temperatures were around 30 °C which was approximately 20 °C cooler than the stainless steel manifold.

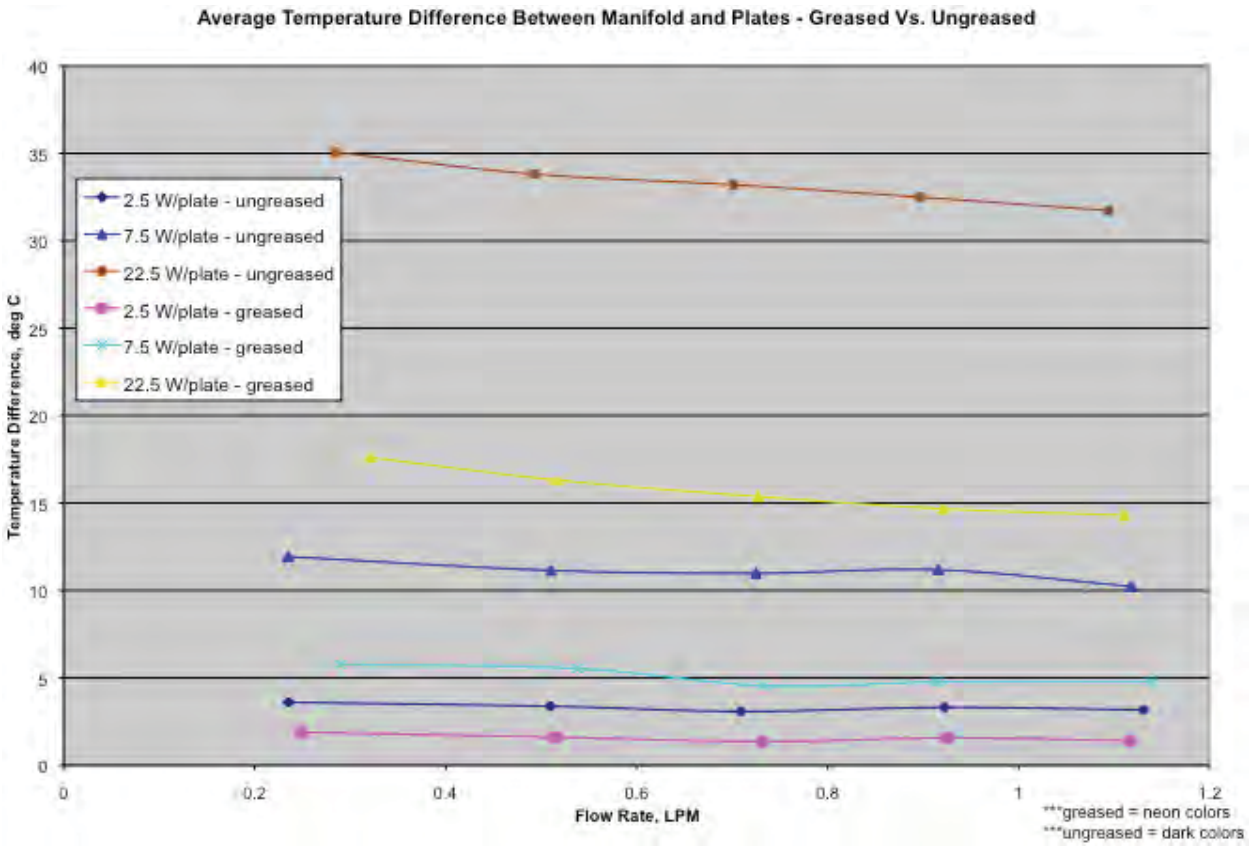

Figure 7.8.—Cooling Plate/Manifold Temperature Difference for the Aluminum Manifold Test

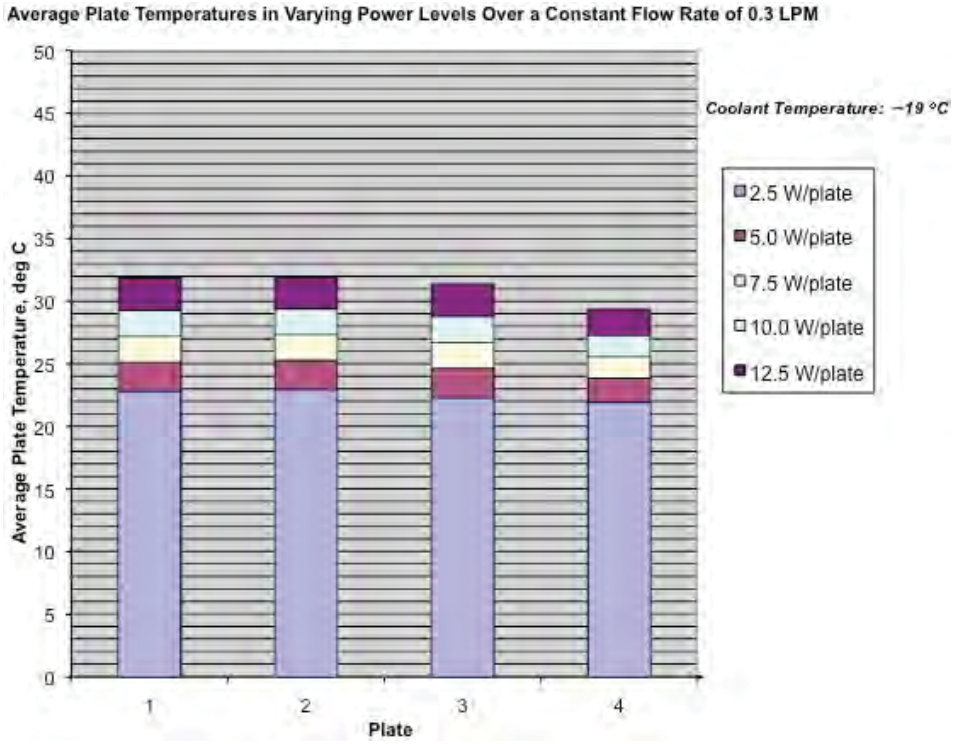

Figure 7.9.—Cooling Plate Temperature with Aluminum Manifold and Thermal Grease

The copper manifold was tested identically to the aluminum and stainless steel manifolds. The temperature difference between the cooling plate and manifold is shown in Figure 7.10 with the average cooling plate temperature data shown in Figure 7.11. Since copper has the highest thermal conductivity of the three metal manifold materials, the thermal trends between the aluminum and stainless steel manifolds were continued with the copper manifold. As with the aluminum manifold, the effect of the conductive thermal grease reduced the cooling plate temperature for each power level and reduced the temperature difference between the cooling plate and the manifold. The maximum average plate temperature was just under 30 °C which was ~ 3 °C cooler than the aluminum manifold test results and ~ 23 °C cooler than the stainless steel manifold test results.

As with the aluminum and stainless steel manifold tests, the average individual plate temperature was fairly consistent from plate to plate. The results for the three manifolds show that the manifold conductivity is inversely proportional to the change in plate temperature for a given change in heater power. For example raising the heater power from 5 to 7.5 W/plate with the stainless steel manifold caused a rise in plate temperature of 5 °C. This same input power increment with the copper manifold caused an average plate temperature change of 2 °C.

A thermally conductive compound, Arctic Silver 5, replaced the Apiezon H-Grease, to quantify the impact of reducing the thermal contact resistance on the cooling plate temperatures. The temperature difference between the cooling plates and the manifold using the Apiezon thermal grease verses the Arctic Silver-5 thermal compound with the copper manifold are shown in Figure 7.12. This figure illustrates that the higher conductivity Arctic Silver 5 thermal compound produced a lower temperature difference between the cooling plates and manifold which became more pronounced at higher heater power levels. The average cooling plate temperature, as shown in Figure 7.11 and Figure 7.13 remained fairly constant between both cases.

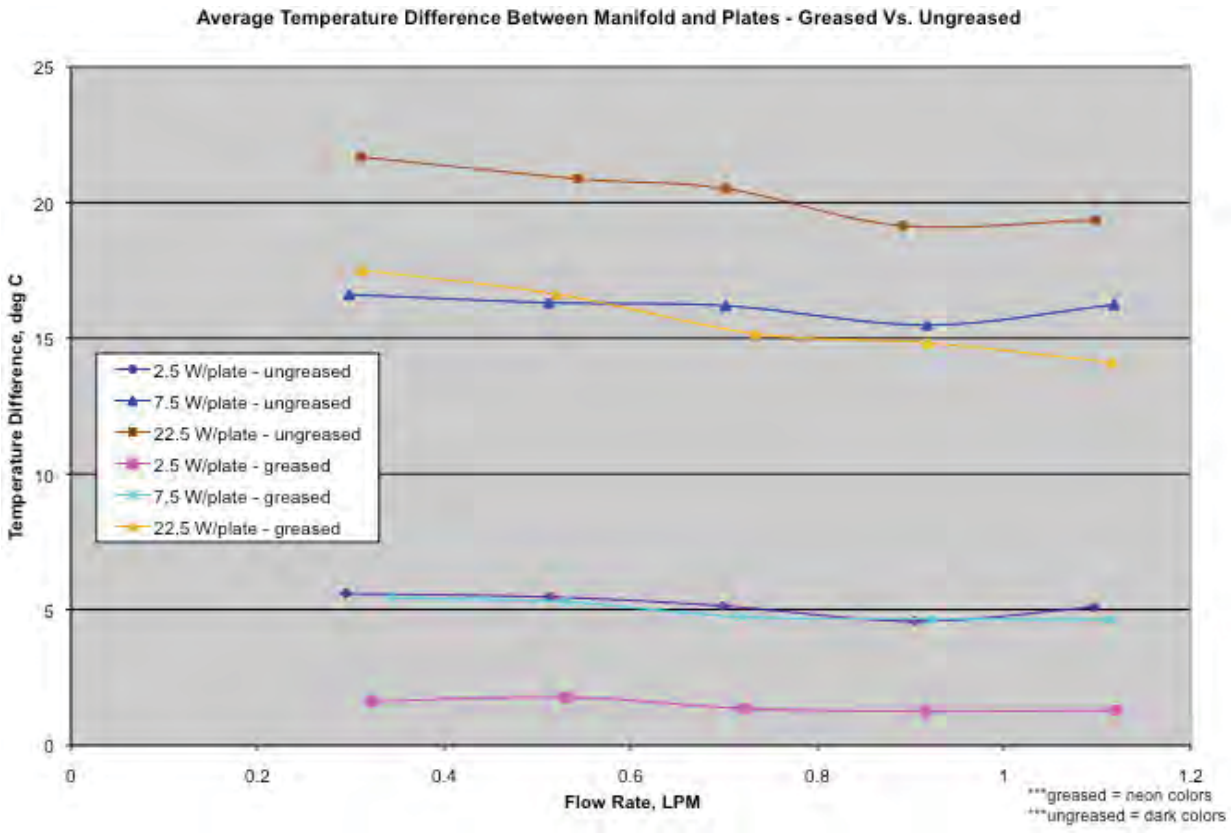

Figure 7.10.—Cooling Plate/Manifold Temperature Difference for the Copper Manifold Test

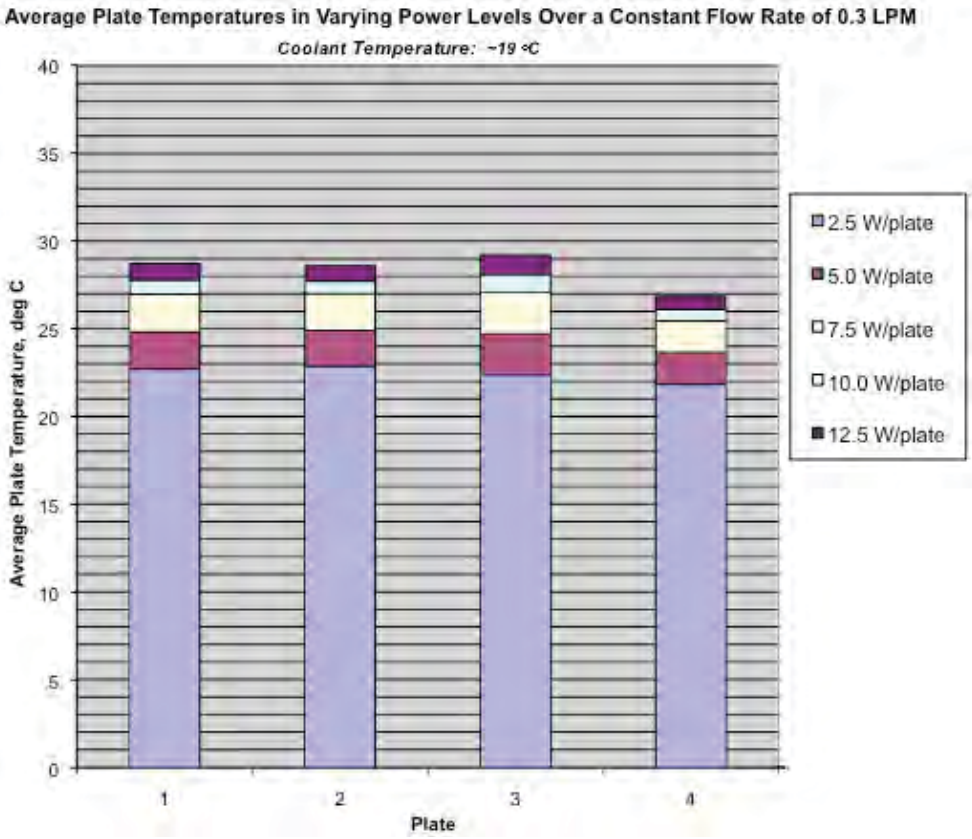

Figure 7.11.—Cooling Plate Temperature with Copper Manifold and Thermal Grease

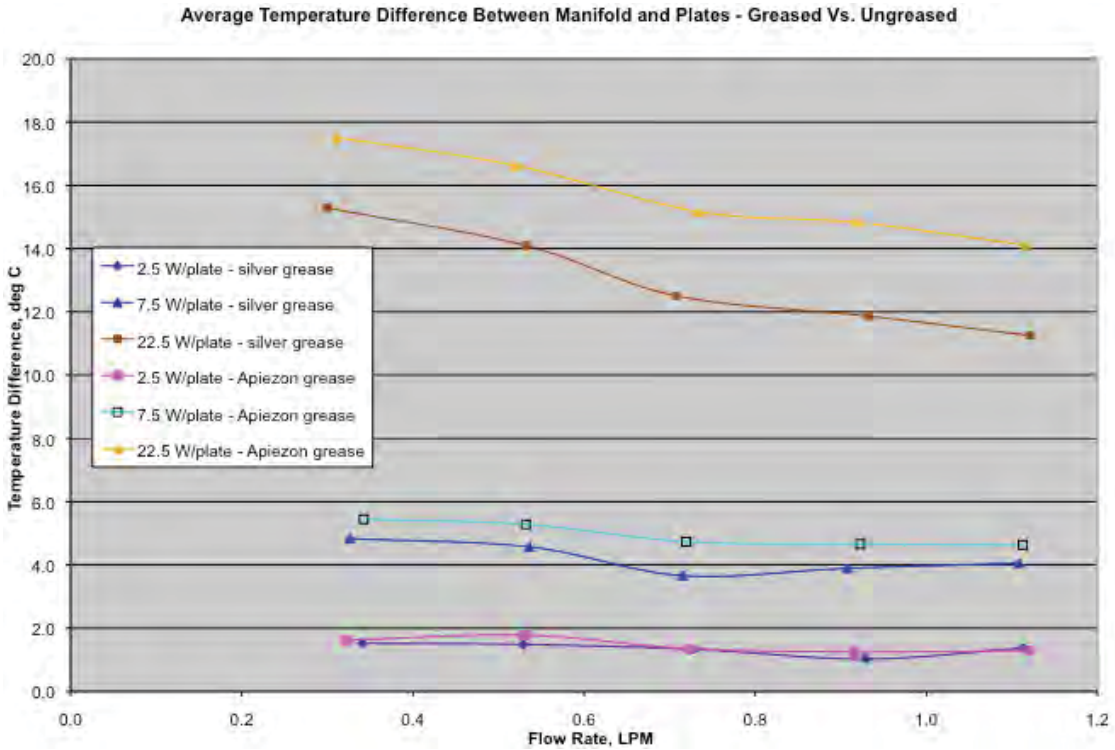

Figure 7.12.—Comparison Between the Thermal Grease and Silver Thermal Compound on Cooling Plate/Manifold Temperature Difference

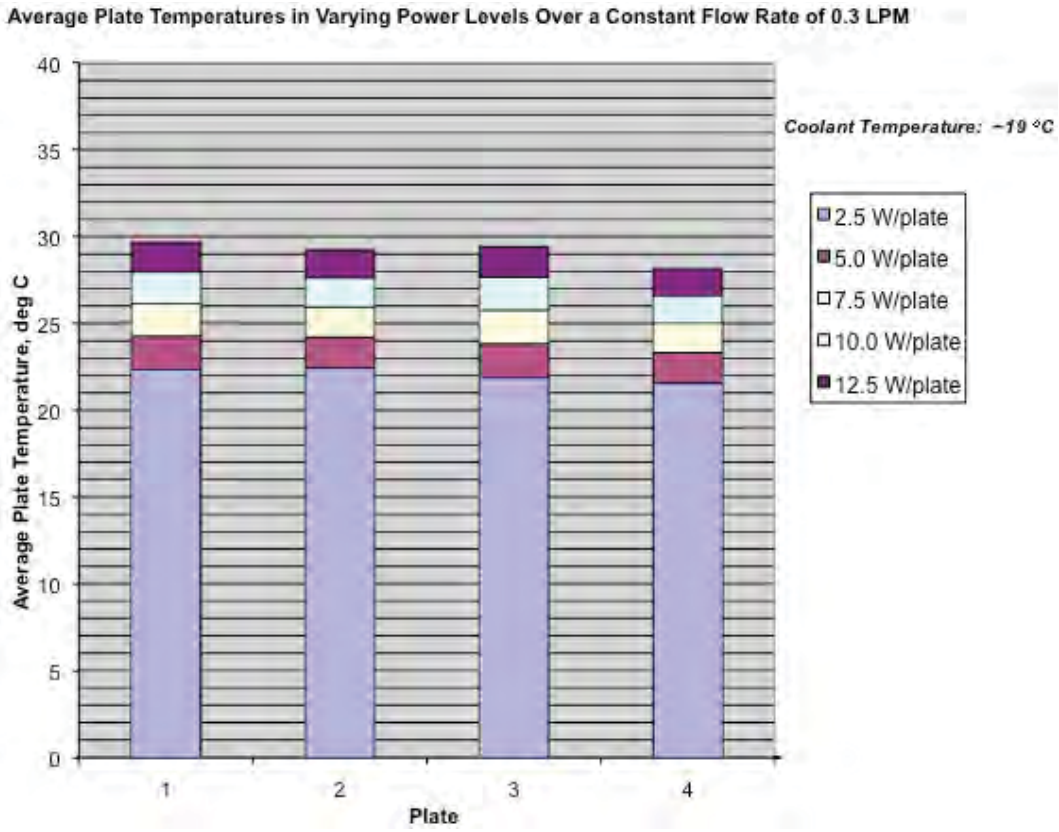

Figure 7.13.—Cooling Plate Temperature with Copper Manifold and Silver Thermal Compound

7.2 Aluminum Channel/LCP Cooling Manifold Steady State Test

The next manifold tested was the aluminum channel/LCP block manifold described in Section 6.0 and shown in Figure 6.3 and Figure 6.4. This manifold/cooling plate arrangement was similar to the previously described test with the three metal manifolds. The test setup replaced the metal manifolds with the aluminum channel/LCP manifolds, as shown in Figure 7.14. The testing with this manifold utilized the Arctic Silver-5 thermal compound between the cooling plates and the LCP.

Temperature difference comparisons between the manifold and cooling plates for the LCP based manifold for both stainless steel and copper are shown in Figure 7.15 and Figure 7.16, respectively. From these figures it can be seen that the LCP manifold had a lower manifold/cooling plate temperature difference than the stainless steel manifold but had a significantly higher temperature than the copper manifold. This is due to the relatively low thermal conductivity of the LCP and the additional thermal interface between the LCP and the aluminum channel fluid passage. The average operating plate temperature, with the standard 0.3 liters per minute coolant flow rate, maximized at between 35 and 40 °C. This was greater than the maximum temperature for both the aluminum and copper manifolds but lower that the maximum temperature for the stainless steel manifold.

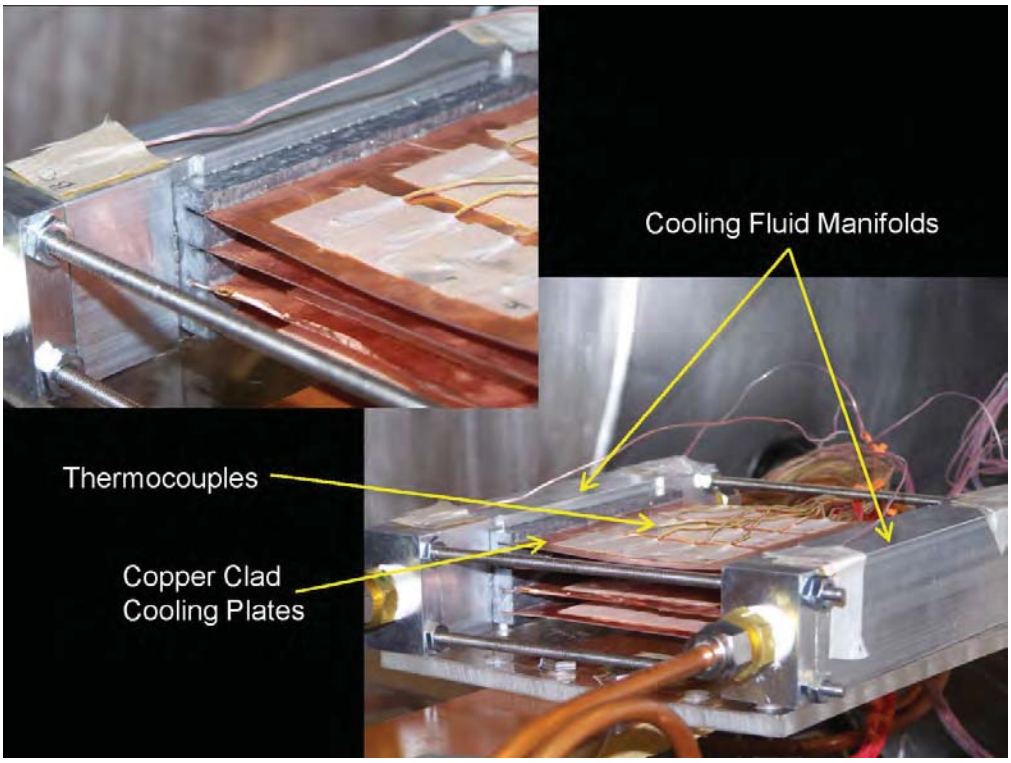

Figure 7.14.—Cooling Plates Installed Between Two Al/LCP Manifolds

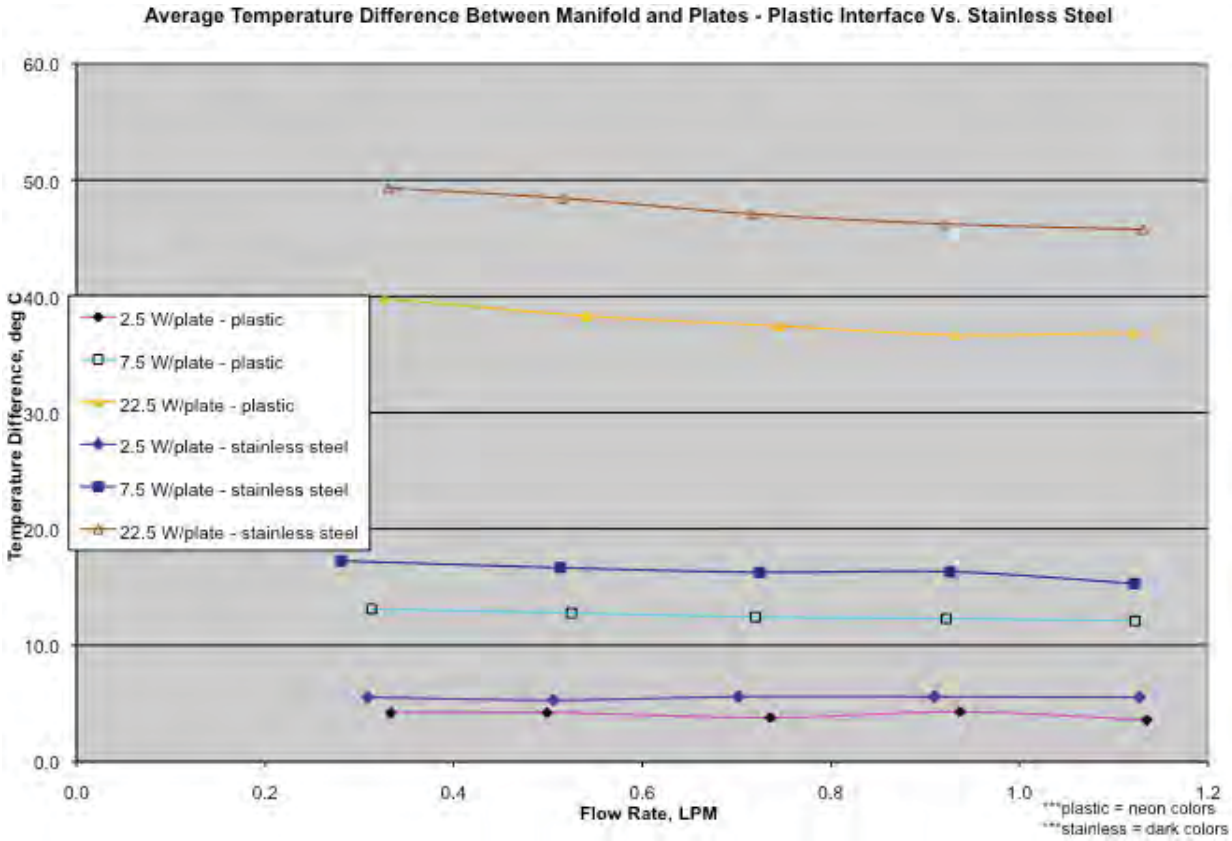

Figure 7.15.—Cooling Plate/Manifold Temperature Difference for Al/ LPC and Stainless Steel Manifolds

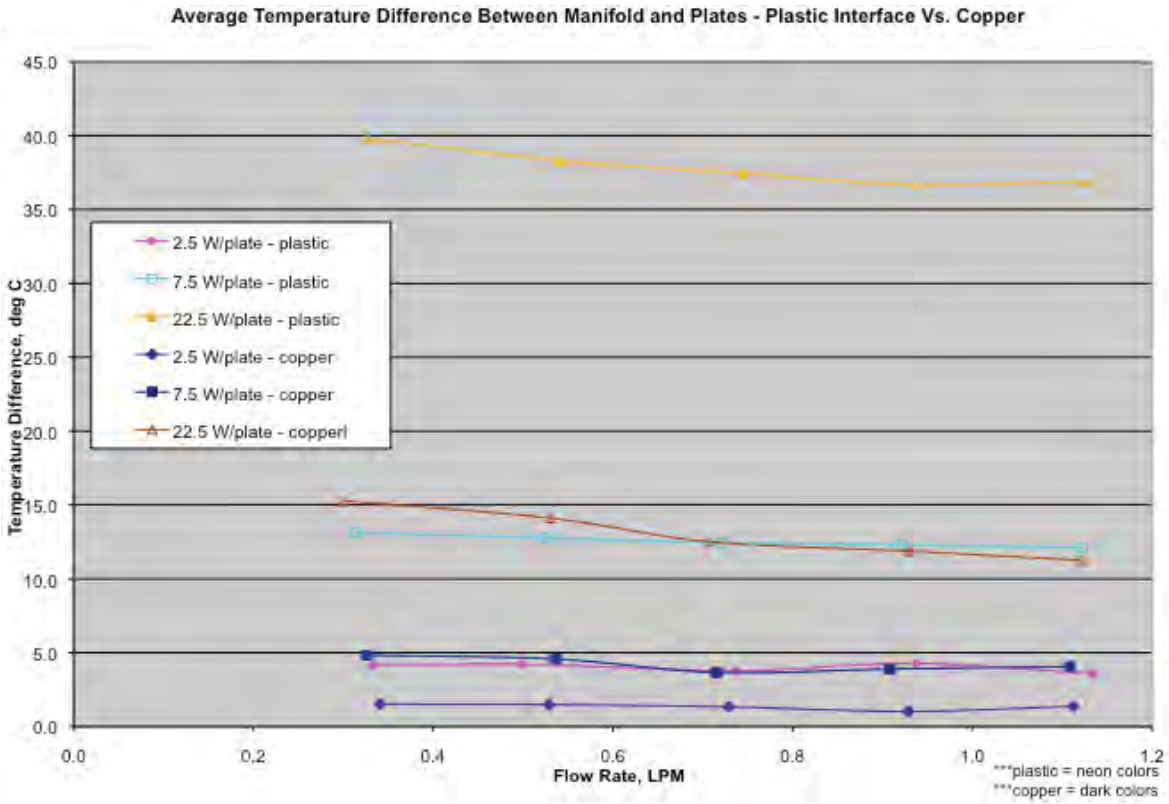

Figure 7.16.—Cooling Plate/Manifold Temperature Difference for Al/LPC and Copper Manifolds

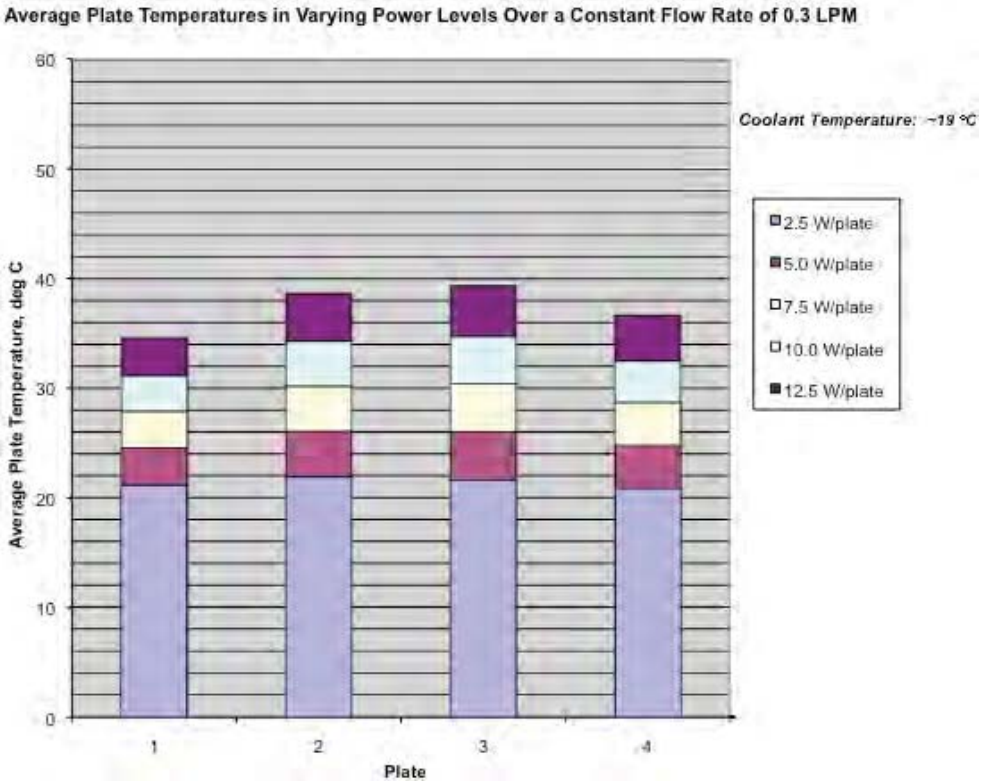

Figure 7.17.—Cooling Plate Temperature with Al/LCP Manifold and Silver Thermal Compound

The next series of manifold testing extracted heat from a single side of the cooling plates using the larger sized TPG plates, shown in Figure 2.8 and Figure 2.10. Steady state temperature tests were performed with the Al/LPC water channel manifold, shown in Figure 6.6 and with the anodized aluminum manifold shown in Figure 6.12 and Figure 6.13.

7.3 Single Sided Steady State Manifold Tests

The Al/LCP channel and anodized aluminum manifolds each held four cooling plates during the testing. Each cooling plate was instrumented with nine thermocouples distributed evenly over the surface of the cooling plate, as shown in Figure 7.18. Heaters were installed onto the side opposite of the thermocouples of each cooling plated, as shown in Figure 7.19. The heater had a surface area of 77.42 cm^2. For the testing with these larger cooling plates the heater power ranged from 7.7 to 42.3 W per cooling plate. The corresponding heat flux to the plates is given in Table 7.2. The plates were installed into the manifolds with Arctic Silver 5 thermally conductive compound to enhance the heat transfer between the cooling plates and manifolds. The test assembly was then installed into the vacuum chamber for testing, with a vacuum level of approximately 10^{-3} Torr. The Al/LCP manifold is shown installed in the chamber in Figure 7.20 while Figure 7.21 depicts the anodized aluminum manifold. As with the previous steady state manifold tests, the objective of this testing was to evaluate the effectiveness with which the single sided manifold design can remove heat from the cooling plates by monitoring and recording the temperature distribution over the cooling plate surface.

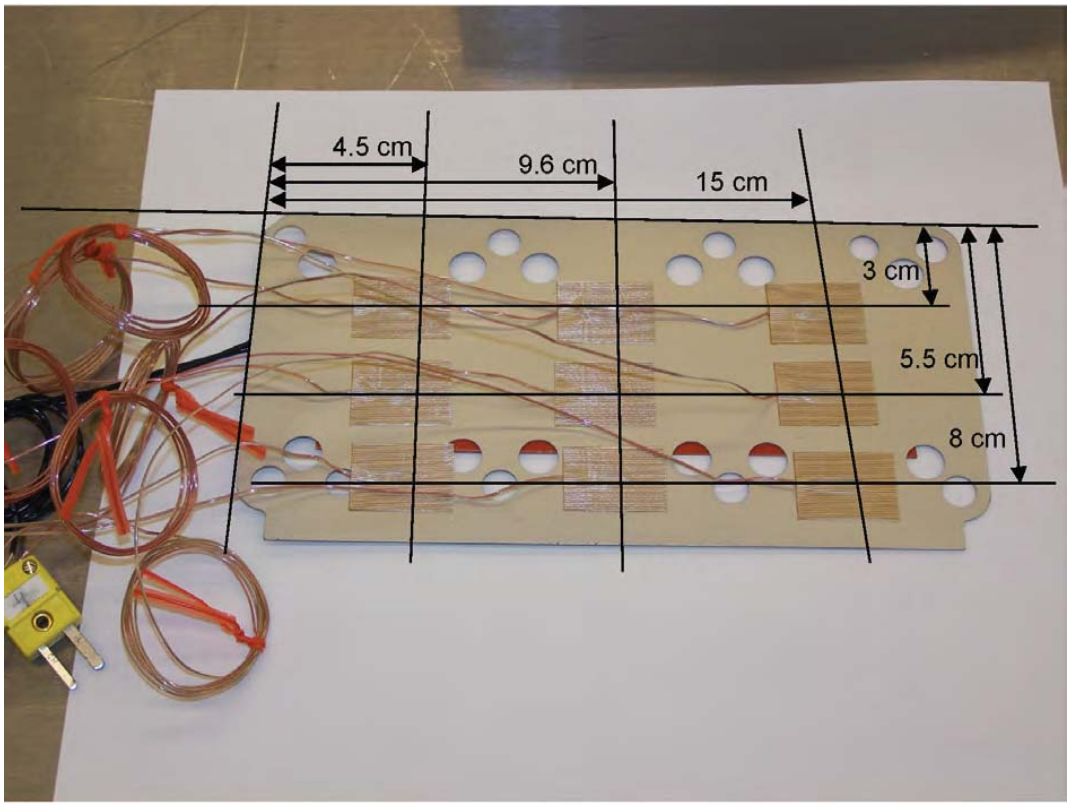

Figure 7.18.—Thermocouple Placement on the TPG Cooling Plate for the Single Side Heat Extraction Manifold Testing

TABLE 7.2.—HEATER POWER AND HEAT FLUX FOR THE SINGLE SIDED MANIFOLD TESTS

Plate heater power, W	Heat flux to each cooling plate, W/cm^2
7.7	0.09
11.5	0.15
15.5	0.20
22.4	0.29
29.9	0.39
37	0.48
42.3	0.55

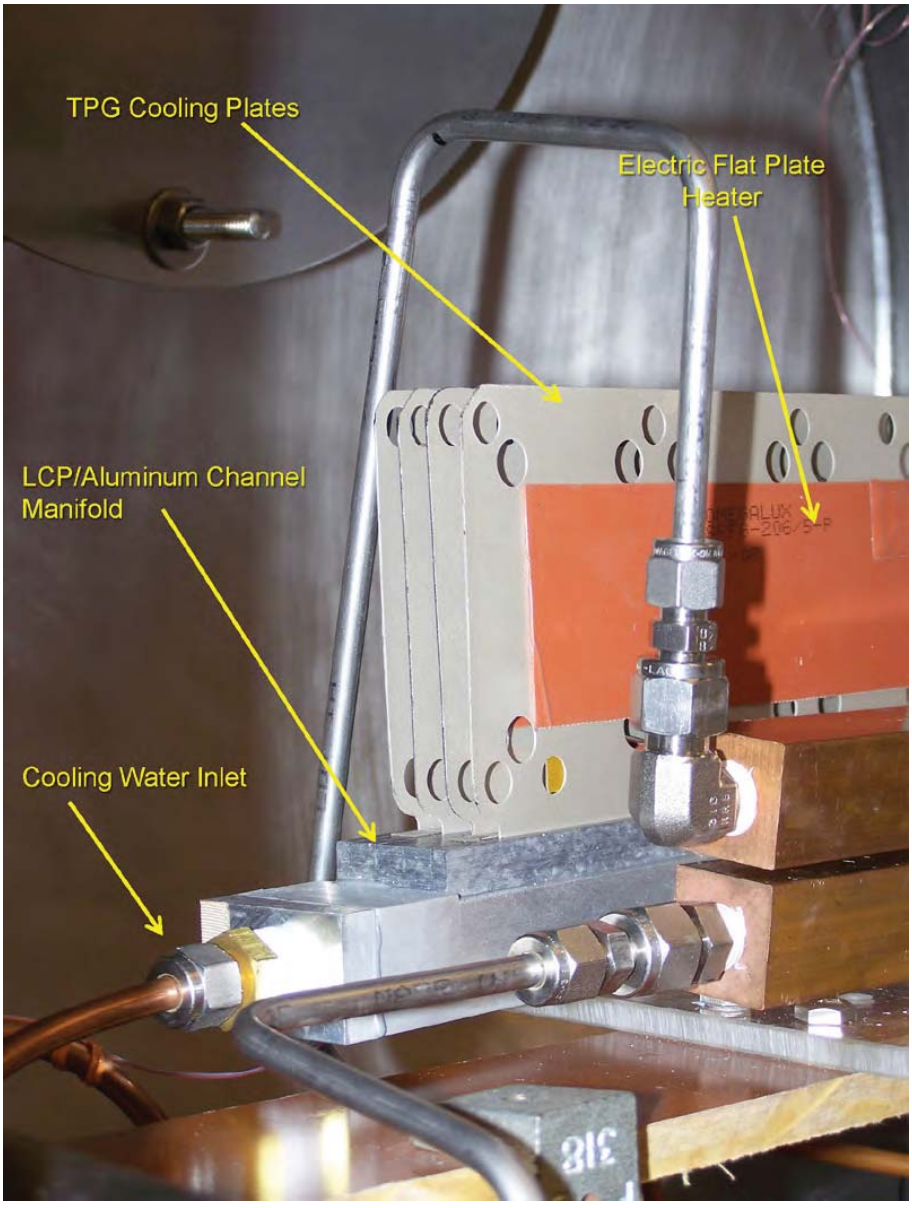

Figure 7.19.—Cooling Plate Heaters with the Cooling Plates Installed onto the Al/LCP Channel Manifold.

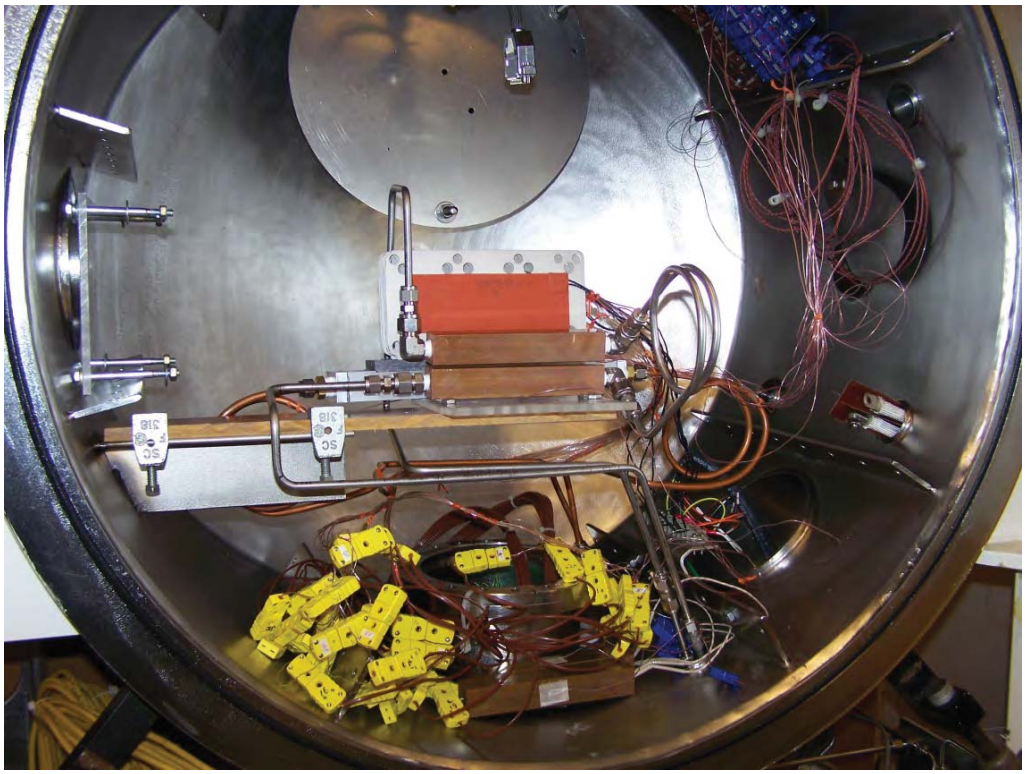

Figure 7.20.—Al/LCP Channel Manifold and Cooling Plates Installed in the Vacuum Chamber

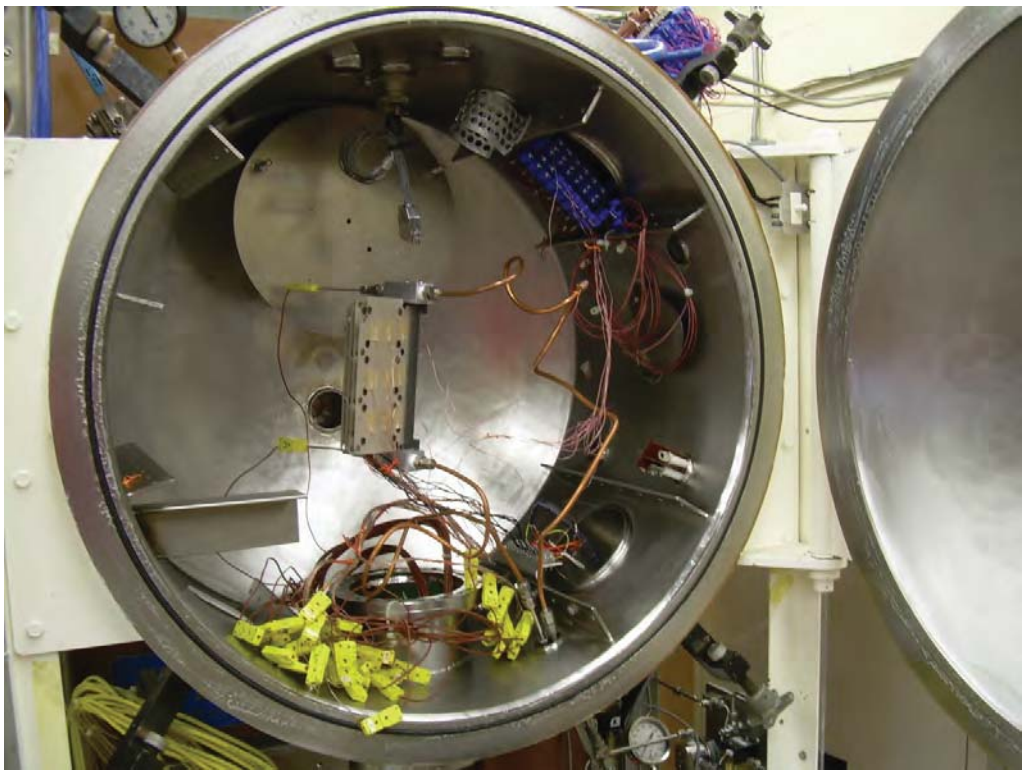

Figure 7.21.—Anodized Aluminum Manifold with Cooling Plates Installed in the Vacuum Chamber

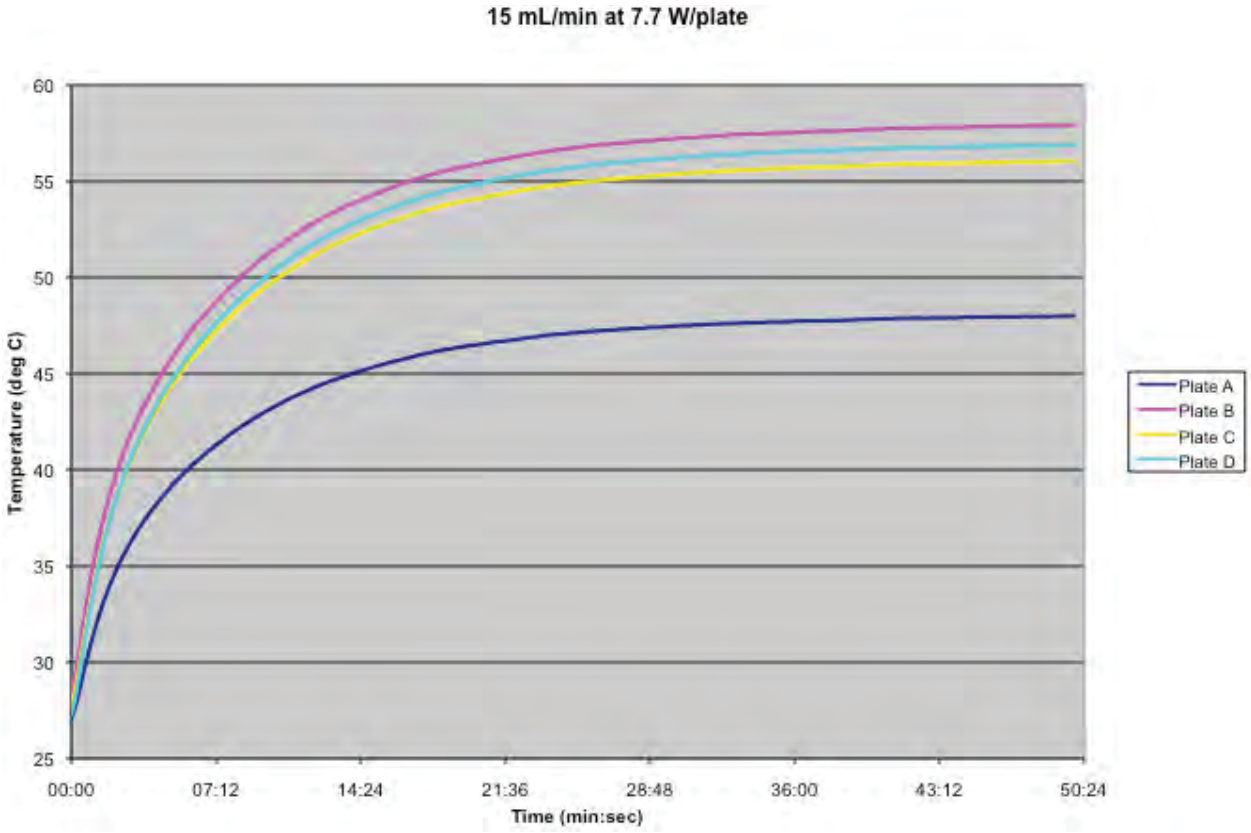

Figure 7.22.—Cooling Plate Average Temperature as a function of Time

The single manifold tests were conducted using the same protocol as the dual manifold tests described previously. The results are shown in Figure 7.22 for a cooling flow rate of 15 ml/min and power level of 7.7 W/plate.

From this figure, it can be seen that the average cooling plate temperature increased asymptotically towards a steady state value. The steady state value was achieved after approximately 40 min of constant test conditions. It should be noted that plate A operated at a much lower temperature than the other plates. This resulted from the location and orientation of the thermocouples on plate A in which its thermocouples faced the significantly cooler inner vacuum chamber wall. The thermocouple-instrumented faces of the other plates faced the heater from the adjacent plate. Therefore they received additional heat through radiation from the adjacent plate's heater. This variation in plate temperature was addressed during the control testing by insulating the entire cooling plate assembly. All of the flow rate / plate power level combinations had similar temperature rise profiles. However the main difference between the results at different flow rates was the time required to reach steady state. In general equilibrium took longer to achieve with a lower coolant flow rate.

Steady-state temperature data was plotted for both the Al/LCP and anodized aluminum manifolds for various coolant flow rates and applied heater power in Figure 7.23 for an interior cooling plate (plate B). These results represent the average steady-state plate temperature for the coolant flow and heater power specified. The coolant plate temperature was limited to 98 °C during the testing to eliminate the possibility of the coolant water boiling. Therefore test runs where the heater power and coolant flow resulted in the coolant plate temperature rising to this level were halted prior to the steady state condition being reached and are not included on the graph below.

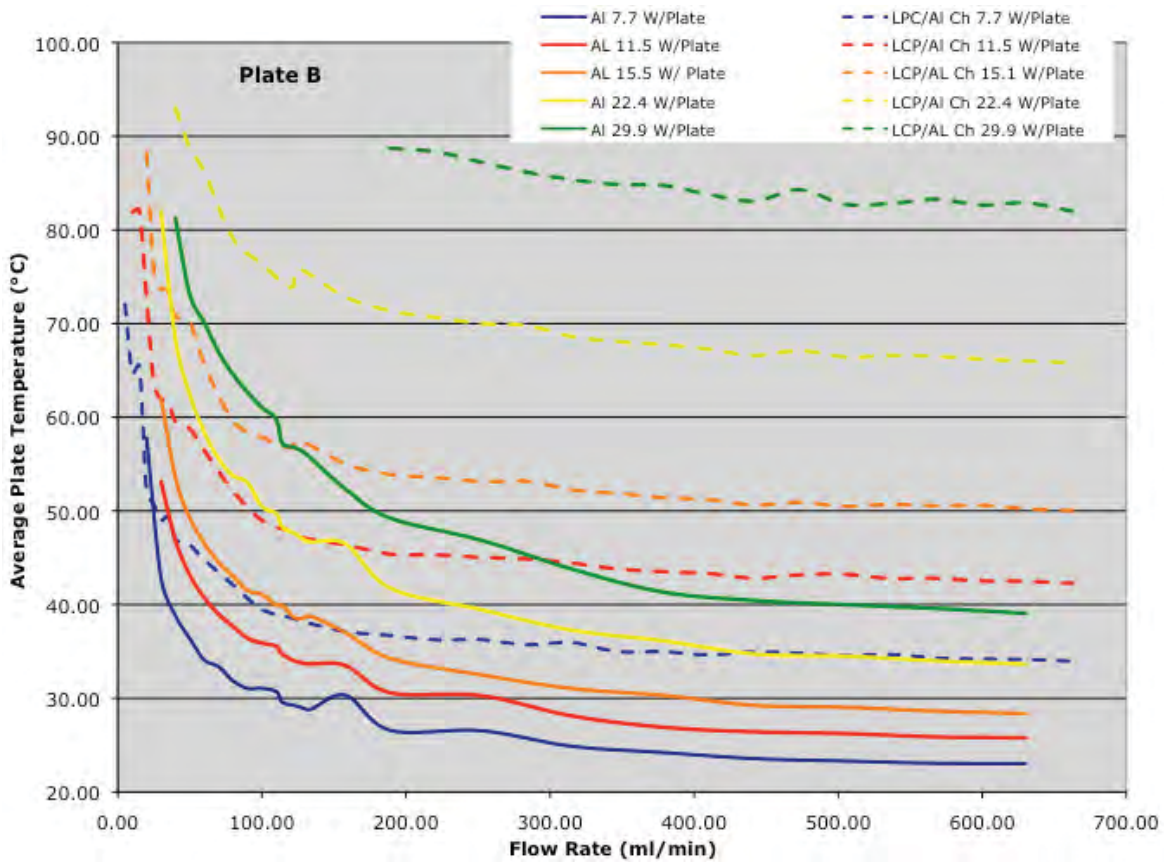

Figure 7.23.—Steady-State Coolant Plate Average Temperature for an Internal Plate for both the Al/LCP Channel and Anodized Aluminum Manifolds

These results, plotted in Figure 7.23, show that the anodized aluminum manifold operated at much lower temperatures than the Al/LCP manifold for a given flow rate and heater power. For all cases, the initial increase in flow rate produced a significant drop in the average plate temperature, up to a flow rate of approximately 100 ml/min. Beyond approximately 200 ml/min of coolant flow, the subsequent drop in average plate temperature with increasing coolant flow was significantly reduced, approaching a steady-state value in which increasing fluid flow provided no additional heat transfer capability.

Although the cooling passage channel dimensions differed greatly between the two manifolds, the Reynolds number for the coolant flow in both manifold designs remained laminar for the range of cooling flow rates tested. Figure 6.2 and Figure 6.7 show the Reynolds number for the anodized aluminum and Al/LCP channel manifolds, respectively. For flow rates below 600 ml/min, the Reynolds number for both manifolds remains below 2,300, the Reynolds number signaling the initial transition from laminar to turbulent flow, indicating the flow in both manifolds remained laminar throughout the test range. Had a transition to turbulent flow occurred, a rapid drop in cooling plate temperature would be expected, resulting from the enhanced heat transfer from the manifold wall to the cooling fluid with turbulent flow.

The lower average plate temperatures with the anodized aluminum manifold result from its greater bulk thermal conductivity and lower thermal resistance between the cooling fluid and the Al/LCP channel manifold. The enhanced heat transfer characteristics of the anodized aluminum manifold enabled greater control over the cooling plate temperature. At the highest power level of 29.9 W/Plate, the anodized aluminum manifold provided steady-state cooling plate temperatures between 80 and 40 °C, whereas the plate temperature for the Al/LCP channel manifold ranged between 90 and 80 °C for the same power levels and coolant flow range.

Another goal of the manifold test was to determine the effect of cooling fluid flow rate on the steady-state surface temperature distribution. The cooling plate surface temperature distribution appears in the cooling plate surface temperature plots in Appendix D. These plots are for interior cooling plate B with a heater power of 22.4 W with coolant flow rates of 30 to 378 ml/min. For all cases, the upper portion of the plate, furthest from the manifold, was the hottest, as should be expected. The maximum temperature gradient across the cooling plate for each flow rate is given in Table 7.3. The maximum temperature gradient across the cooling plate ranged from just under 6 °C to just over 8 °C.

7.4 Manifold Cooling Steady State Test Summary

The manifold testing results provide some insight into the effects of materials and configurations in constructing the manifold system. These are outlined below;

- Contact resistance is a key design parameter. It proportionally impacts the heat transfer rate, average plate temperature, and thermal response time. With a material of sufficient thermal conductivity, contact resistance becomes the limiting thermal transfer factor. Reducing the contact resistance between the cooling plates and manifold will significantly reduce the plate operational temperature for a given flow rate and input power level. It also decreases the response time of plate temperature to changes in input power level. However, this effect is limited by the conductivity of the manifold material. If the manifold is constructed of material with a low thermal conductivity (as with the testing performed with the stainless steel manifold), this will become the limiting factor in transferring heat to from the plates to the coolant.
- The manifold material thermal conductivity directly affects the operating temperature of the cooling plate as well as the change in plate temperature with changes in input power. The higher the thermal conductivity of the manifold, the lower the operating temperature of the cooling plates will be and the lower the increase in temperature with increasing input power.
- Large thermal transport distances between the cooling plates and cooling fluid may be mitigated by highly thermally conductive materials.

TABLE 7.3.—MAXIMUM TEMPERATURE GRADIENT ACROSS THE COOLING PLATES AT VARIOUS COOLING FLOW RATES

Flow rate, (ml/min)	Minimum temperature, °C	Maximum temperature, °C	Maximum temperature gradient
30	84.6	78.2	6.4
60	60.6	54.8	5.8
90	55.2	49.5	5.7
158	49.2	41.1	8.1
378	39.2	31.5	7.7

8.0 Thermal Control Testing

Cooling plate temperature control tests were performed with the manifold system. In the manifold cooling system, the only means of controlling the temperature of the cooling plates is by regulating the flow rate and/or temperature of the coolant through the manifold. However, under real-world operational conditions, regulating the coolant temperature is less practical than regulating the coolant flow rate to control the cooling plate temperatures. Both active and passive control valves were utilized as the means of controlling the coolant flow rate.

The objective of the control testing was to evaluate the response and determine how well the system could maintain a desired cooling plate temperature under varying heater power levels and profiles, as well as determining the thermal response time of the cooling system.

In order to reduce heat transfer from the cooling plates to the vacuum tank wall and between the plates themselves, multi-layer insulation (MLI) was used with the anodized aluminum manifold test article, shown in Figure 6.12 and Figure 6.13. MLI sheets were constructed of aluminum foil with a Teflon spacer sheet between each aluminum layer. Six layers of aluminum and five layers of Teflon were used to construct the MLI. The aluminum layers were spot welded along the edges to secure them together. MLI sheets were placed between each of the cooling plates and a single sheet was wrapped over the cooling plates and installed as shown in Figure 8.1.

A series of steady-state temperature tests were tested with the insulated plates and the anodized aluminum manifold over a range of flow rates and heater power levels to evaluate the effect the insulation had on the plate operating temperature. The results from these tests are shown in Figure 8.2. This figure compares the steady-state temperature results for Plate B with and without insulation.

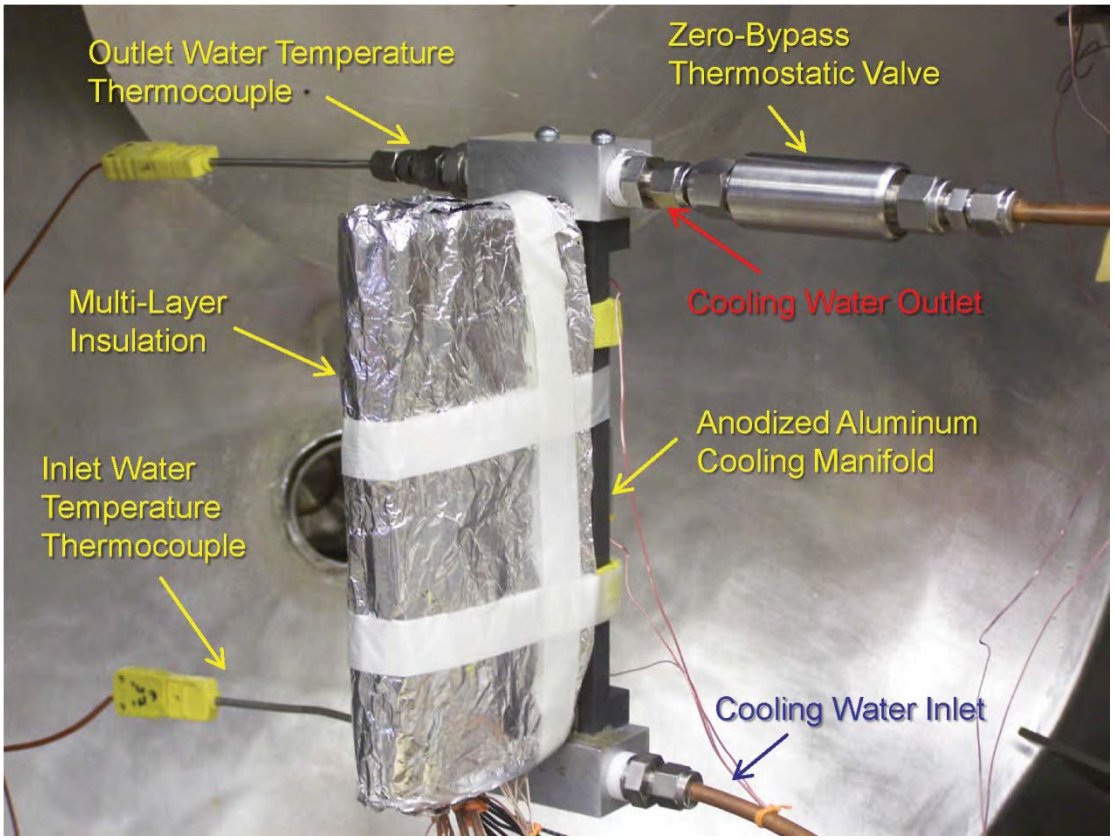

Figure 8.1.—Insulated Cooling Plates and Manifold Installed in the Test Chamber with the Zero-Bypass Thermostatic Control Valve

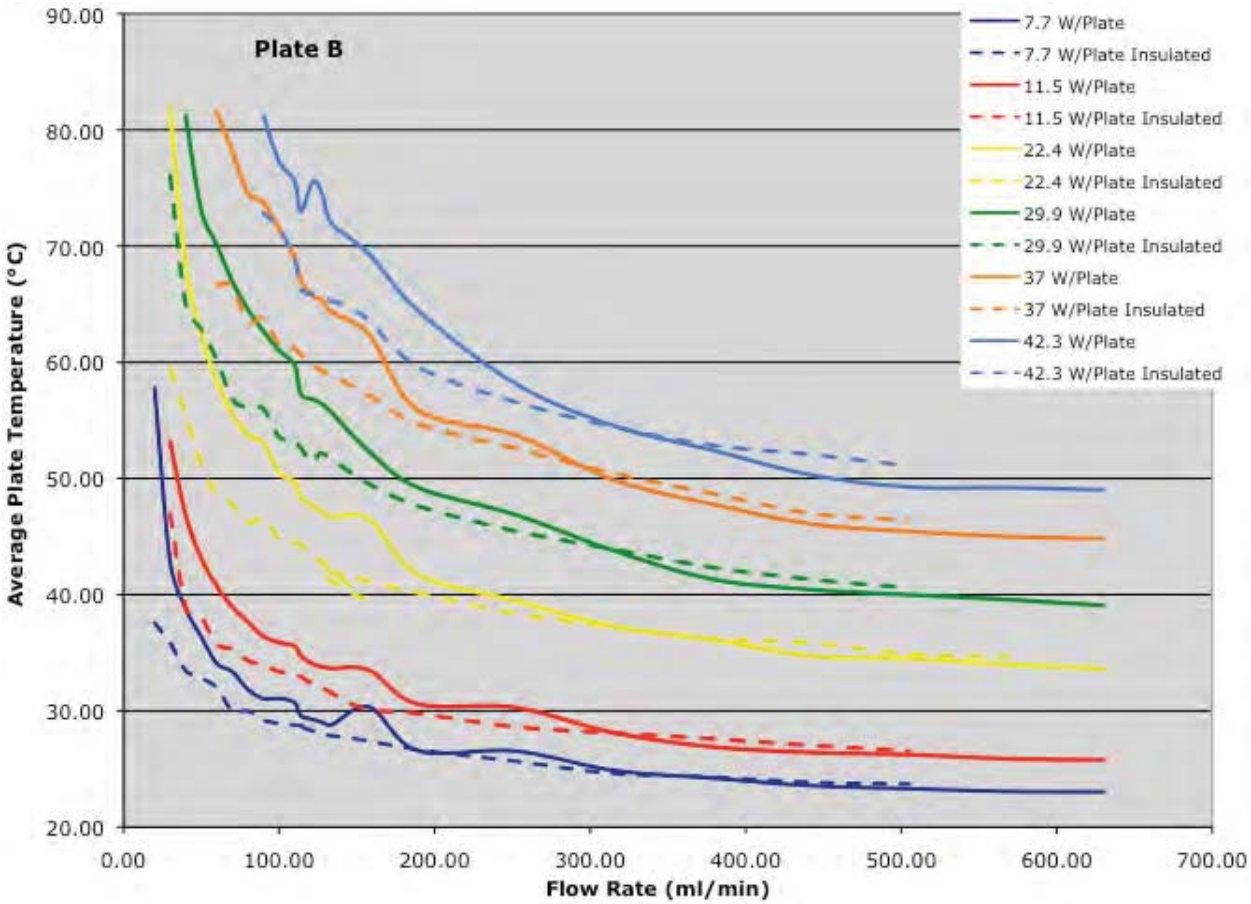

Figure 8.2.—Bare and Insulated Cooling Plate B Steady-State Temperature

At the flow rates above ~ 300 mL/min, there is little difference between the temperatures of the insulated and uninsulated cooling plate. However, at flow rates below approximately 300 mL/min, the steady state plate temperatures for the insulated and un-insulated cooling plates begin to diverge. For all of the power levels tested, the insulated cooling plate operated at a lower steady-state temperature in low cooling flow conditions. This might at first seem counter intuitive since the insulation should be limiting the heat loss from the plates to the surroundings. However, in vacuum, radiation is the only mode of heat transfer to the surroundings. This mode of heat transfer will be limited by a few factors, such as plate temperature and view factor to the tank wall. The radiation heat transfer, Equation (8.1), includes the temperature of the cooling plate ($_p$), the temperature of the surroundings ($_s$) the emissivity of the cooling plate (ε, estimated to be around 0.8), the Stefan-Boltzman constant ($\sigma = 5.67\times10^{-8}$ W/m^2 K^4), the area of the cooling plate ($_p$) and its view factor to the surrounding tank wall (v_f).

$$= \varepsilon\sigma v_f \quad _p\left(\quad _p^4 - \quad _s^4 \right) \tag{8.1}$$

Radiation heat transfer from the cooling plates produces a heat loss of around 1 W. At the average operational plate temperature, radiation heat transfer is not a significant factor. However, insulating the cooling plates did provide a barrier between the heater on one cooling plate and the thermocouples on an adjacent one. By eliminating the radiation heat transfer from one plate heater to the thermocouples of an adjacent plate, they registered a more accurate cooling plate temperature. It is the elimination of the heat

transfer from the heater on one plate to the thermocouples on the adjacent plate that accounted for the reduction in thermocouple temperature between the insulated and un-insulated cooling plate tests.

8.1 Thermostatic Control Valve Testing

The first type of control valve to be evaluated was the passive thermostatic valve. This type of control valve uses a cylinder that contains a wax that would melt at the desired operational temperature. The phase change causes the wax to expand which increases the cylinder length and actuates a variable orifice to control the fluid flow. Flow rate is therefore based on coolant temperature and wax phase change temperature, this type of valve does not require any active control.

Two different types of thermostatic valves were tested, valves with and without bypass flow. Bypass flow allows a controlled bleed of the cooling fluid through the valve when it is fully closed. There are advantages and disadvantages to having or not having a bypass flow which are summarized in Table 8.1.

The zero bypass flow thermostatic valve is shown installed with the manifold in the vacuum chamber in Figure 8.1. The thermostatic valve incorporating a bypass flow is shown installed with the manifold in the vacuum chamber in Figure 8.3.

This valve operates by allowing the coolant to flow around the thermally activated actuator. The actuator is housed in a cylinder that has small holes around the circumference at its base. When closed, a beveled edge seats against the valve housing, preventing the coolant fluid from flowing through the valve. There are small grooves in this beveled edge to provide a small controlled bleed through the valve providing the bypass flow. This enables the actuator to be heated with the coolant from the manifold as it flows through the bypass groves. A spring is used to seat the cylinder against the housing. As the actuator extends the spring is compressed and the cylinder moves toward the coolant exit end of the valve. This separates the beveled edge of the cylinder from the housing allowing the fluid to flow thorough the valve. The valve design is illustrated in Figure 8.4.

The flow rate through the valve depends on the extent of the actuator and the corresponding spacing between the beveled edge and housing. The valve is self-regulating because as the coolant heats up from the increased thermal power applied to the cooling plates, it will heat up the actuator due to the bypass flow within the valve. As the actuator heats up and extends, the flow rate through the manifold increases thereby cooling it down. The subsequently lower fluid temperature then cools down the actuator and the valve begins to close. For a given input power to the cooling plates, the valve will self-regulate the flow to a temperature within the operating range of the actuator. For this valve, the actuator begins to extend at 50 °C and is fully extended at 60 °C. The maximum travel distance of the actuator is 0.5 cm.

TABLE 8.1.—THERMOSTATIC VALVE BYPASS FLOW OPERATIONAL CHARACTERISTICS

Valve type	Advantage	Disadvantage
No bypass flow	Theoretically faster rise in system temperature with increasing power level.	Slow heat propagation to the valve. In practice, without a good heat transfer mechanism to the thermal actuator within the valve, the response time is very slow. The precise phase transition temperature and thermal gradient between the cooling plates and valve are very design specific.
Bypass flow	Enables good heat transfer to the control actuator by allowing cooling fluid to continuously flow over the actuator.	Low bypass flow rates are needed in order to avoid over cooling the system at low power levels.

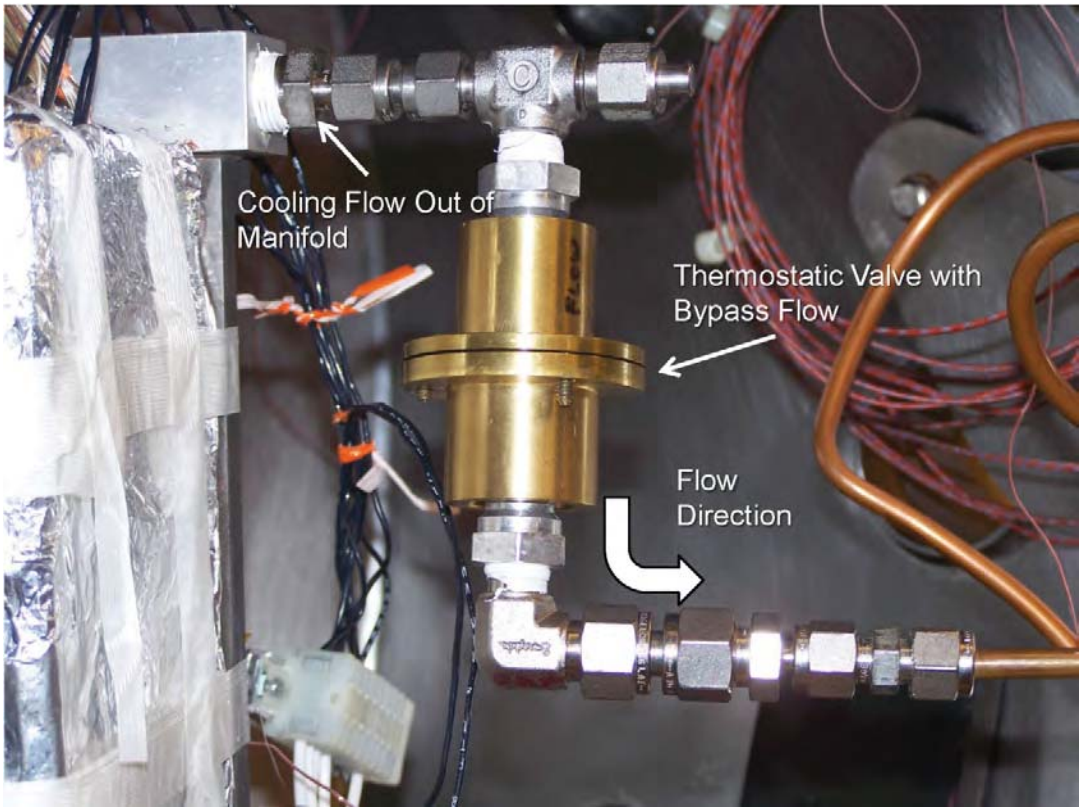

Figure 8.3.—Installed Bypass Flow Thermostatic Valve in the Test Chamber

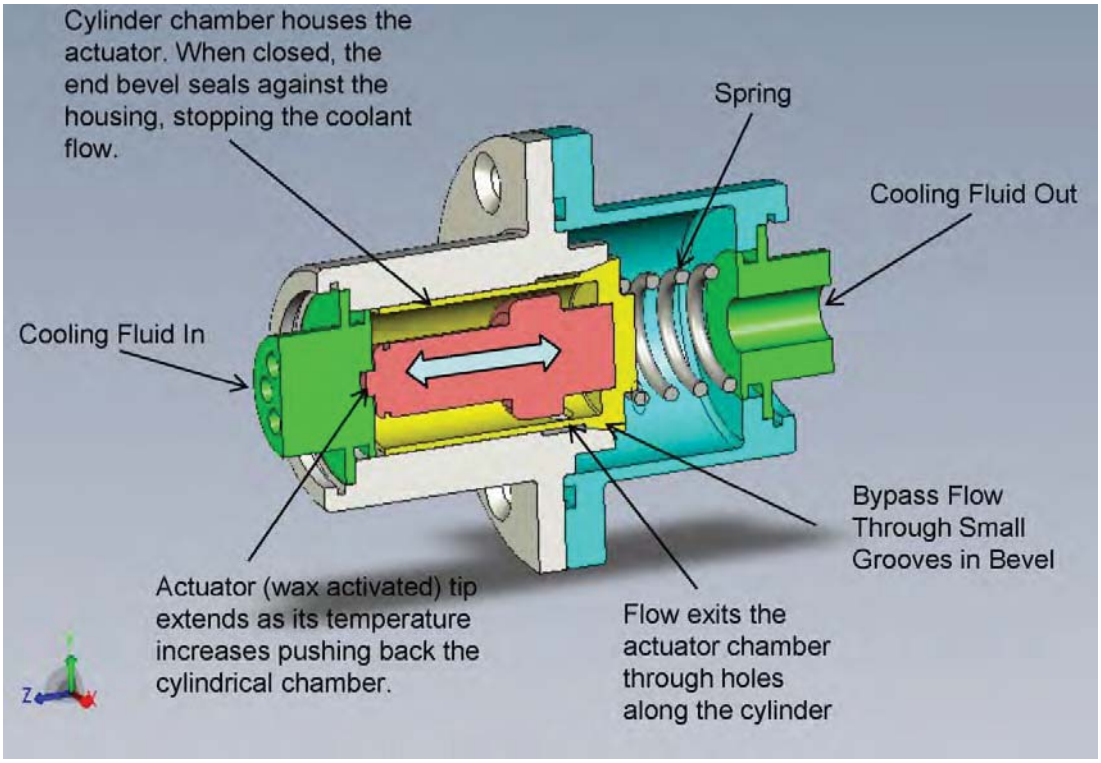

Figure 8.4.—Illustration of the Internal Components of the Thermostatic Valve with Bypass Flow

8.1.1 Thermostatic Valve Steady State Power Control Test

Initial tests were performed with both types of thermostatic valves, with bypass flow and without. These tests used a step power profile as shown in Figure 8.5. The power to the heaters was held constant for a period of time so that the cooling plates would settle out and reach temperature equilibrium. Once equilibrium was reached the heater power was increased to the next level.

In the testing of the zero bypass flow valve, there was insufficient heat transfer to the valve to enable it to open prior to the cooling plates reaching their maximum temperature of 95 °C. At this temperature, the test control system would automatically turn off the power to the heaters as a safety precaution to prevent boiling the cooling fluid. Three different no bypass flow valves with different set points were tried. These included valves that were fully open at 77, 71, and 65 °C. The valves were installed as close to the manifold as possible to maximize the heat transfer to the valve, as shown in Figure 8.1. To further enhance the heat transfer to the valve, a copper bar was attached to the manifold and clamped to the valve body. However, even with these modifications, the valves without bypass flow could not operate within the maximum temperature range of the cooling plates and therefore could not be used in the testing.

Results for the control test results of the thermostatic valves with bypass flow, shown in Figure 8.3 and Figure 8.4, using the step power profile shown in Figure 8.5 are shown in Figure 8.6. Initially, the bypass flow was approximately 30 ml/min, as can be seen from the graph. As the cooling plate temperature began to rise, the flow through the valve began to increase and the valve opened. At each increasing power level, the plate temperatures equalized at a higher temperature, reaching a maximum of near 80 °C at the power level of 42 W/plate. The coolant temperature also increased reaching a maximum of approximately 50 °C due to it reaching the design operating temperature of the thermostatic valve. The valve operated very well and maintained the coolant temperature near 50 °C by increasing coolant flow as the power increased to the cooling plates. Although the coolant temperature was maintained at 50 °C for the last three steps in the power profile, the cooling plate temperature did increase with each increase in heater power.

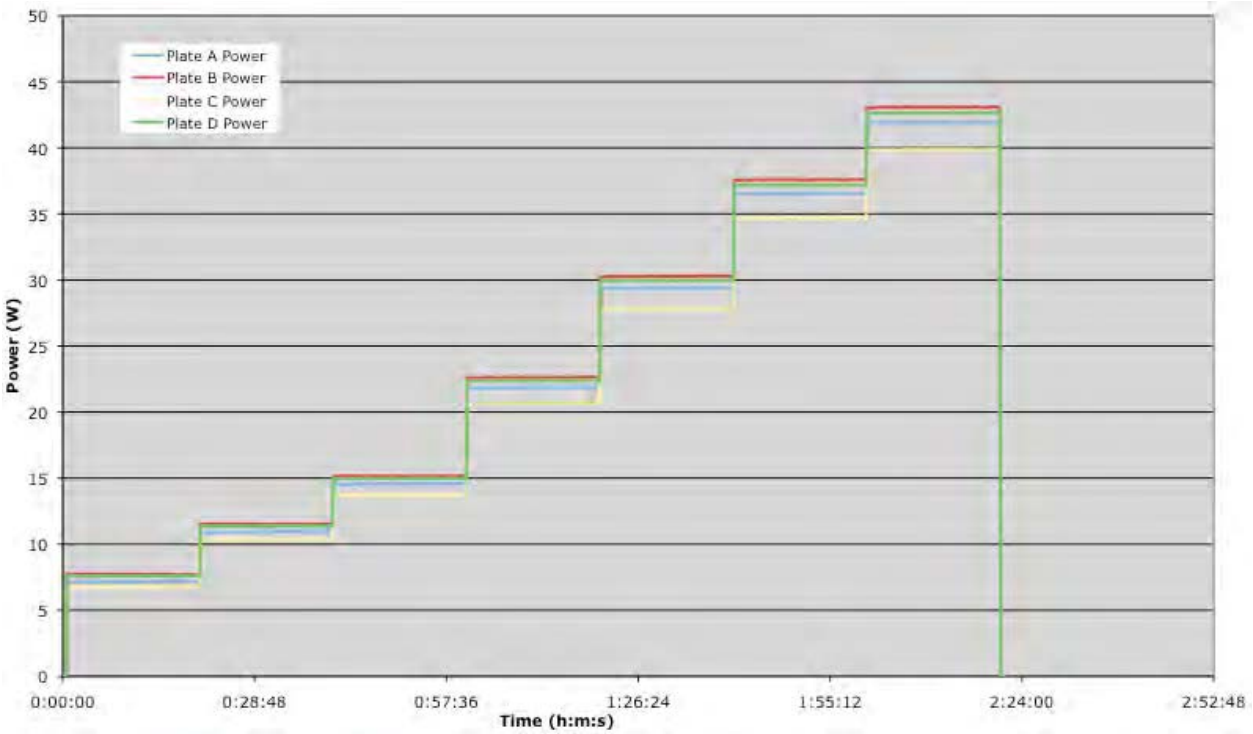

Figure 8.5.—Step Power Profile for Valve Testing

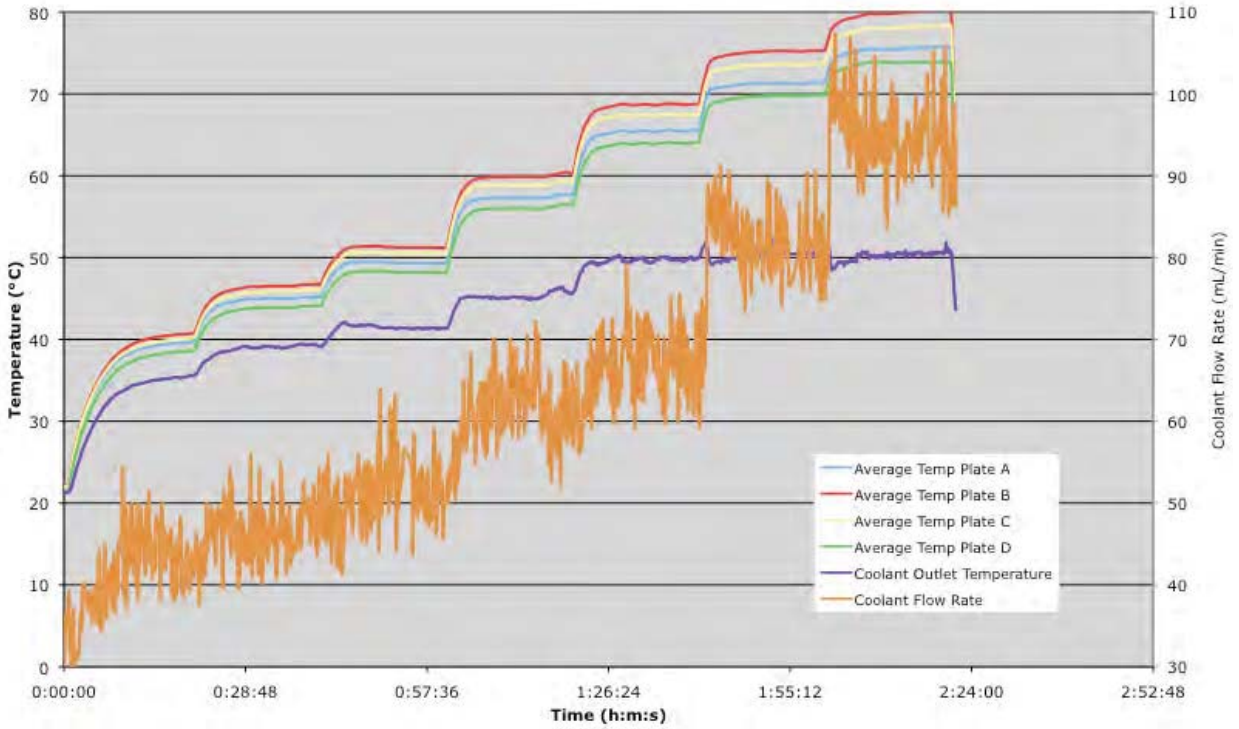

Figure 8.6.—Temperatures and Flow Rate Using the Thermostatic Valve for the Step Power Profile with 30 mL/min Bypass Flow

The plate temperature increase seen with the coolant temperature maintained at 50°C is due to the operating characteristics of the valve and the limits on the heat transfer between the cooling plates and cooling fluid. The increase in cooling plate temperature is expected since for a constant coolant temperature, any increase or decrease in power to the cooling plate will cause the plate temperature to change in order to establishing a new equilibrium. If a constant cooling plate temperature is desired, the coolant temperature would need to decrease as the power level to the plate is increased. This is not possible with a passive thermally-activated valve.

A second step power profile test was performed with a lower bypass flow to determine how the bypass flow affects the valve's response and performance at low power levels with the lower bypass flow. The bypass flow was set by physically modifying the valve to approximately 15 ml/min, half what was used in the previous test. The results from this second test are shown in Figure 8.7.

With the lower bypass flow, the initial cooling plate temperature rose more quickly. The coolant temperature reached 50°C during the second power step in the profile and remained around this level over the remainder of the test. With the lower bypass flow, the coolant temperature fluctuations and flow were much more significant than those seen with the higher bypass flow test. Except for the initial temperature rise, the overall temperature profile of the cooling plates was very similar between the two cases. The steady-state cooling plate temperature for the low bypass case was somewhat higher for all of the power steps although the difference decreased with each subsequent power step. The fluctuations in coolant temperature and flow indicate that with the lower bypass flow, the valve was oscillating between fully opened and fully closed. The higher bypass case produced a much more stable coolant temperature and much smaller swings in coolant flow rate. This large fluctuation in coolant temperature also produced smaller amplitude fluctuations in the cooling plate temperature. This is noticeable in the cooling plate temperatures shown in Figure 8.7 compared to those in Figure 8.6.

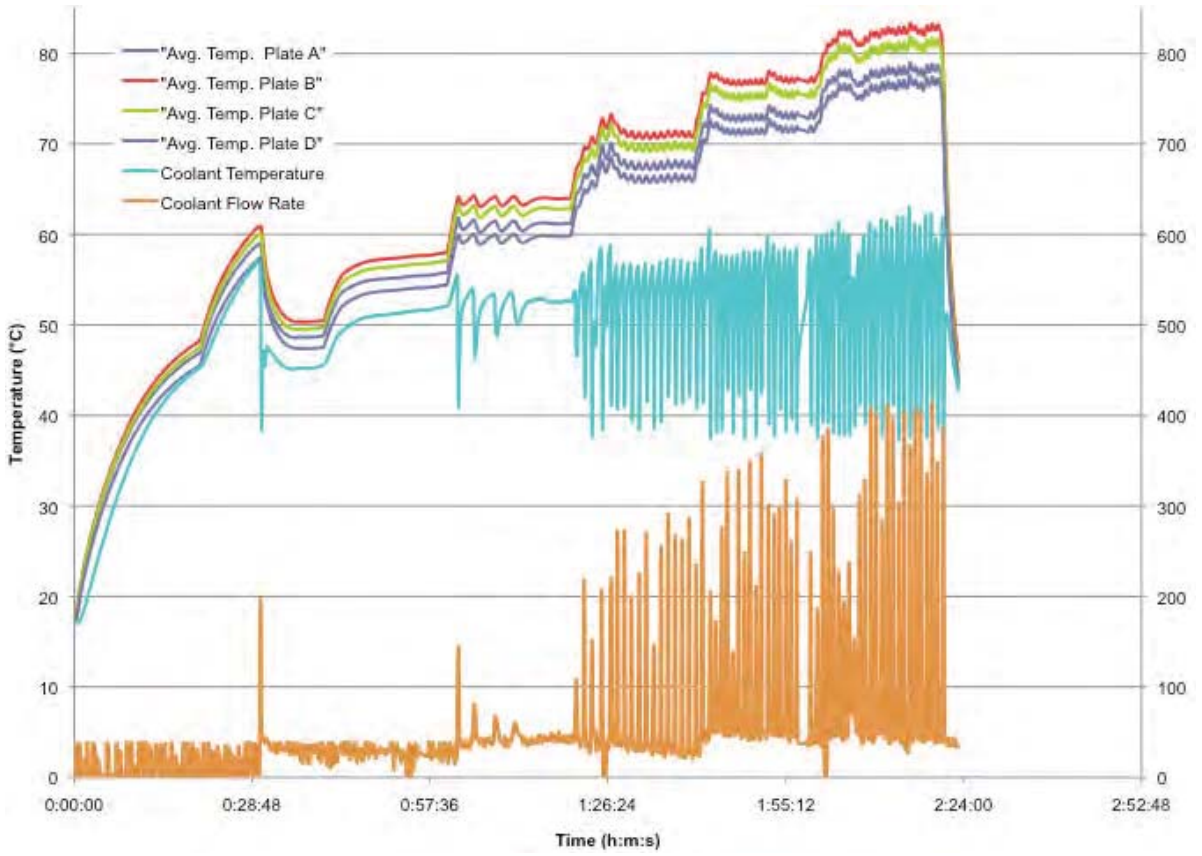

Figure 8.7.—Temperatures and Flow Rate Using the Thermostatic Valve for the Step Power Profile with 15 mL/min Bypass Flow

These results indicate that for low power operation, the lower bypass flow resulted in a higher cooling plate temperature closer to the range that would be desired for fuel cell operation. However, at higher power levels the higher bypass provided a more stable system with much less fluctuation in cooling flow and temperature.

8.1.2 Thermostatic Valve Power Profile Control Tests

The next tests evaluated the response of the 30 mL/min bypass thermostatic valve with the anodized aluminum manifold to a fuel cell test power profile. This profile consists of a number of spikes in output power, periods of steady output, and periods of power drop-off. The profile is shown in Figure 8.8. The full profile operating time was 4 hr.

The results of this test are shown in Figure 8.9. As with the results for the step power profile, this figure shows the average temperature of the cooling plates, as well as the coolant temperature and flow rate.

The system responded to changes in input power very well. There were fluctuations in the cooling plate temperature, but the valve maintained the cooling plates at around 45 °C for the majority of the test. The cooling flow rate was fairly constant at around 80 ml/min with oscillations of ± 4 mL/min. The coolant temperature was approximately 35 °C for the majority of the test. This was consistent with the coolant temperature seen with the step profile test at similar power levels.

Overall, the data from the step and power profile tests show that the passive thermostatic valve can control the coolant plate temperature under varying conditions. The valve can be tuned to maintain a controlled average temperature by selecting the appropriate bypass flow rate and the wax-based actuator operating temperature range. The system is susceptible to changes in input power and has a limited ability to maintain tight control over the cooling plate temperature. As an inherent characteristic of a passive

system, any change to an established equilibrium will cause a new equilibrium temperature. There inherent lag time between additional power being added and the valve response is due to the time required for heat transfer between the cooling plates, manifold, cooling fluid and valve. Although based on the data shown in Figure 8.7 and Figure 8.9 this lag time appears to be minimal.

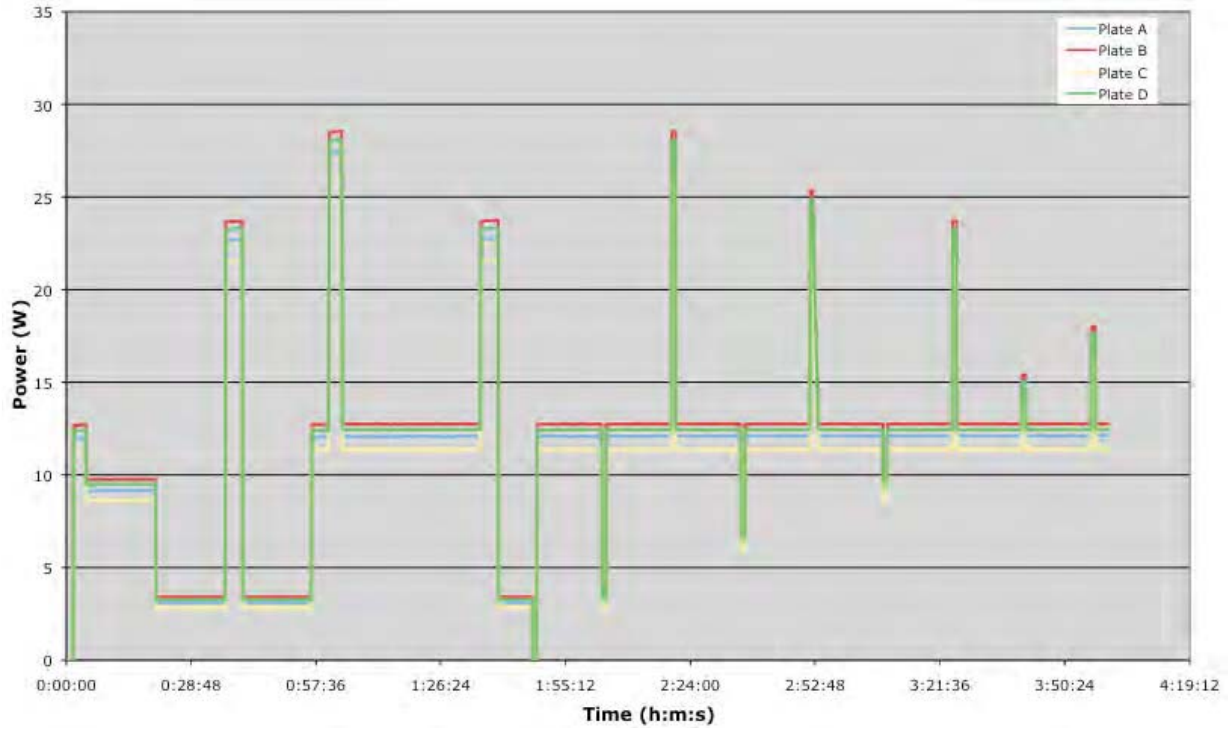

Figure 8.8.—Simulated Fuel Cell Operational Power Profile for Valve Testing

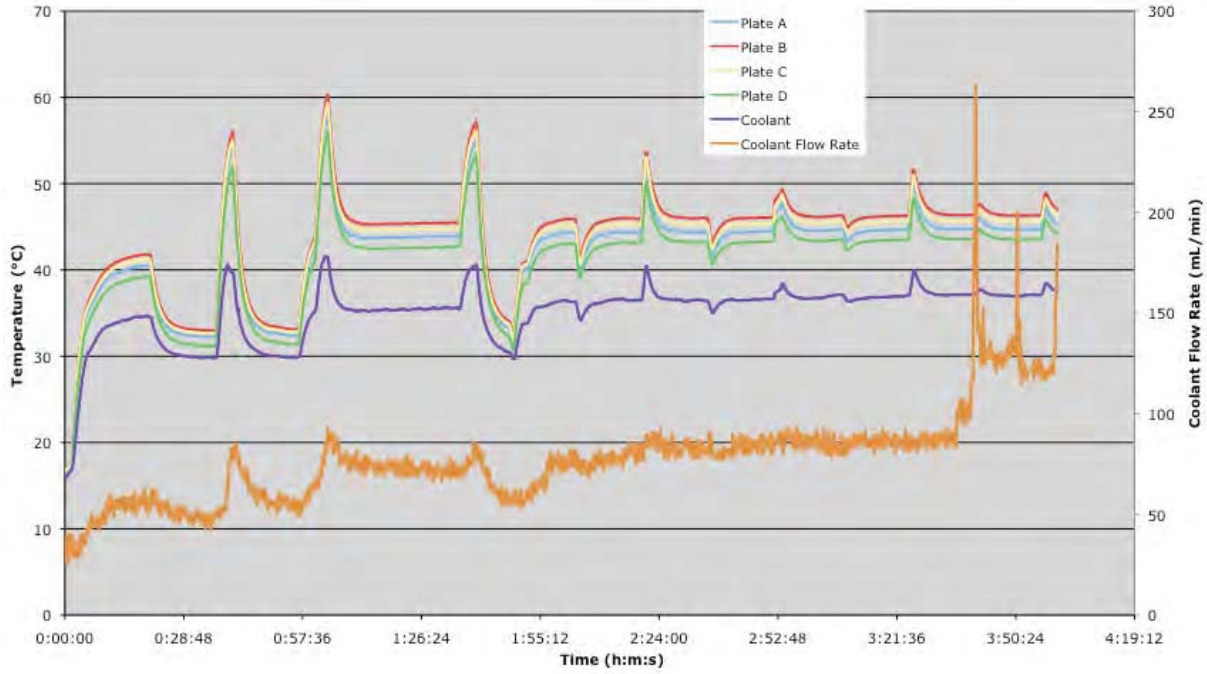

Figure 8.9.—Temperatures and Flow Rate Using the Thermostatic Valve for the Operational Power Profile with 30 mL/min Bypass Flow

8.2 Proportional Valve Control Tests

To enable the passive thermostatic valve to both maintain the cooling plates at a specified temperature and to adjust this temperature as needed, a proportional control valve was evaluated. The valve used was a Kelly Pneumatics mini-proportional valve, shown in Figure 8.10. The valve assembly actually consisted of two valves mounted on a manifold with two internal parallel channels connected to the input and output of the manifold and had a maximum listed flow range capability of approximately 500 mL/min.

The valve assembly was tested over its full flow range to characterize the valve hysteresis. The operational curve for the valve is shown in Figure 8.11 along with the valve assembly signal voltage and corresponding flow rate. The maximum flow rate was approximately 460 mL/min.

Figure 8.10.—Kelly Pneumatics Proportional Control Valve

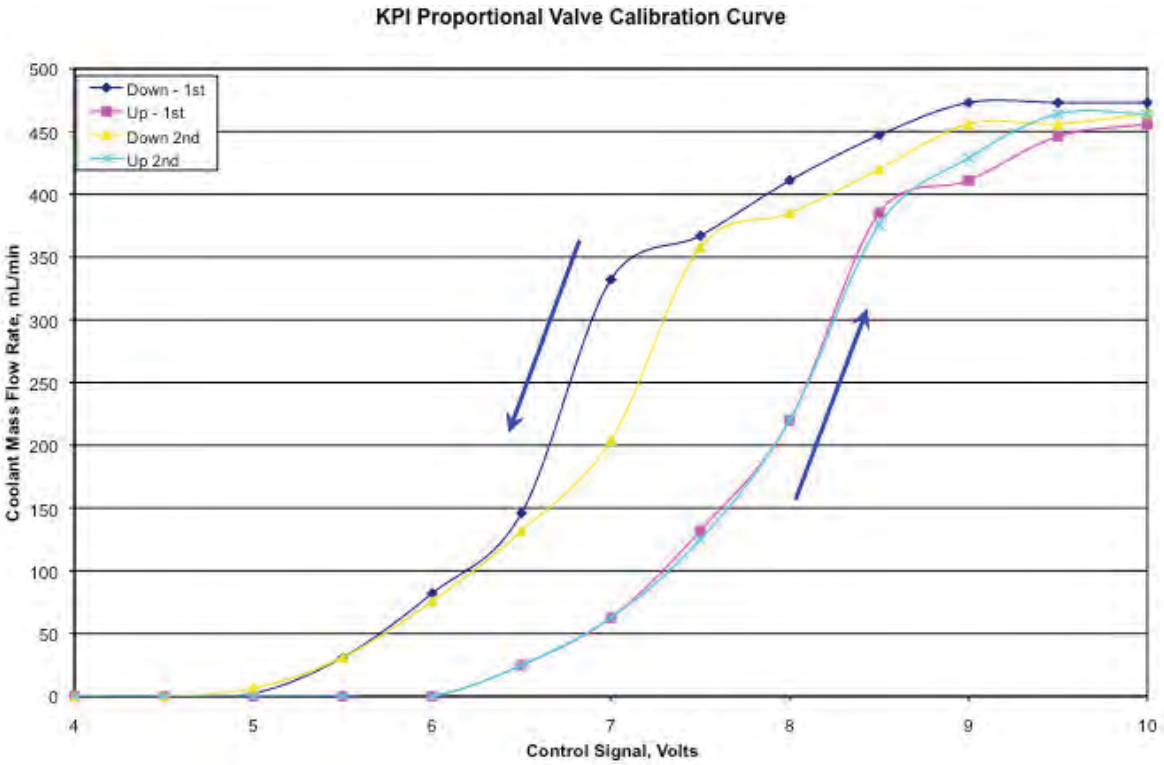

Figure 8.11.—Proportional Valve Full Flow Range of Operation

To control the flow through the manifold, the proportional valve controller used a proportional, integral and derivative (PID) control scheme using cooling plate B's average temperature taken from the n thermocouples installed on the cooling plate as the feedback signal. This approach is a single loop control where there is a desired set point (control temperature of the cooling plate) and there is the measured plate temperature (plate B's average temperature). The PID control equation has three components: a proportional term which changes linearly with the error (e) between the measured temperature ( ) and the desired temperature ($_s$), an integral term whose purpose is to eliminate offset due to a step change in the error, and a derivative term that is used to stabilize and increase the response time to changes in the error (Ref. 11). The measured and desired temperature can be translated to a percent range of opening for the valve. Therefore if the operating temperature range is 20 to 90 °C corresponding to 0 to 100 percent flow for the valve, this will correspond to a specific voltage level signal ( ). The proportional valve controller used a voltage range of 0 to 5 VDC. This voltage signal, plus the adjustment made due to the error in the desired and operational temperature, is sent to the valve ($_o$). The basic PID control relationship is given by Equation (8.2) (Ref. 11) where the control constants: system gain ( ), reset time ( ) and rate time ( ), are used to adjust the system to provide the best response.

$$_o = \pm \left(e + \frac{1}{} \int_0^t e \, t + \frac{e}{t} \right) \tag{8.2}$$

Assuming that the error changes linearly with time at a slope ( ), then the slope multiplied by time (t) can be substituted into Equation (8.2) and simplified to Equation (8.3) and expressed as a polynomial in Equation (8.4).

$$_o = + t + \frac{t^2}{2} + \tag{8.3}$$

$$_o = + _0 + _1 t + _2 t^2 \tag{8.4}$$

The constants $_0$, $_1$ and $_2$ can initially be approximated and then further refined through trial and error during the testing. From the initial testing a set of constants was determined and utilized during the subsequent tests. These are given in Table 8.2.

These values provided acceptable valve response to control the cooling plate temperature. Further refinements could be made to improve the response of the valve to changes in cooling plate temperature.

TABLE 8.2.—PID CONSTANTS USED FOR THE PROPORTIONAL VALVE TESTING

Constant	Value
$_0$	–4.7
$_1$	0.05
$_2$	0.05

8.2.1 Proportional Valve Steady State Temperature Control Tests

Using the active control setup with the proportional valve, tests were run to evaluate the temperature control band of the cooling plates. The first series of tests used a constant cooling plate heater power and increased the desired operational temperature for the cooling plates. The results for this test are shown in Figure 8.12 to Figure 8.15 for heater power levels of 7.7, 15.1, 29.9 and 42.3 W per cooling plate, respectively.

Figure 8.12 to Figure 8.14 illustrate the flow rate fluctuation needed to maintain the cooling plate set point temperature. For each case, the cooling plate temperature oscillated about the set point temperature. The oscillations tended to be larger at higher set point temperatures for all of the plate power levels. The maximum amplitude of the plate temperature oscillations was approximately 6 percent of the set point temperature. It is believed that additional optimization of the control constants for the PID controller can further damp down these oscillations.

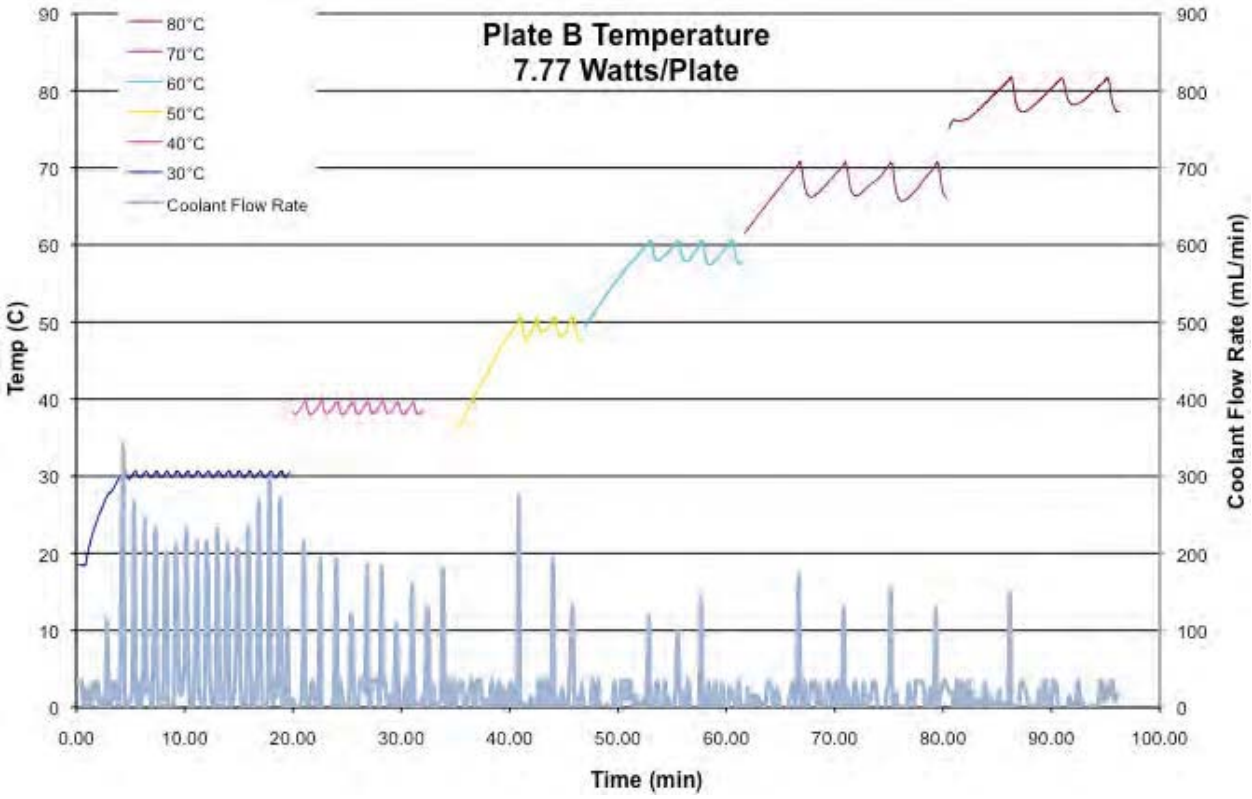

Figure 8.12.—Temperatures and Flow Rate with the Proportional Valve for 7.7 W/Plate

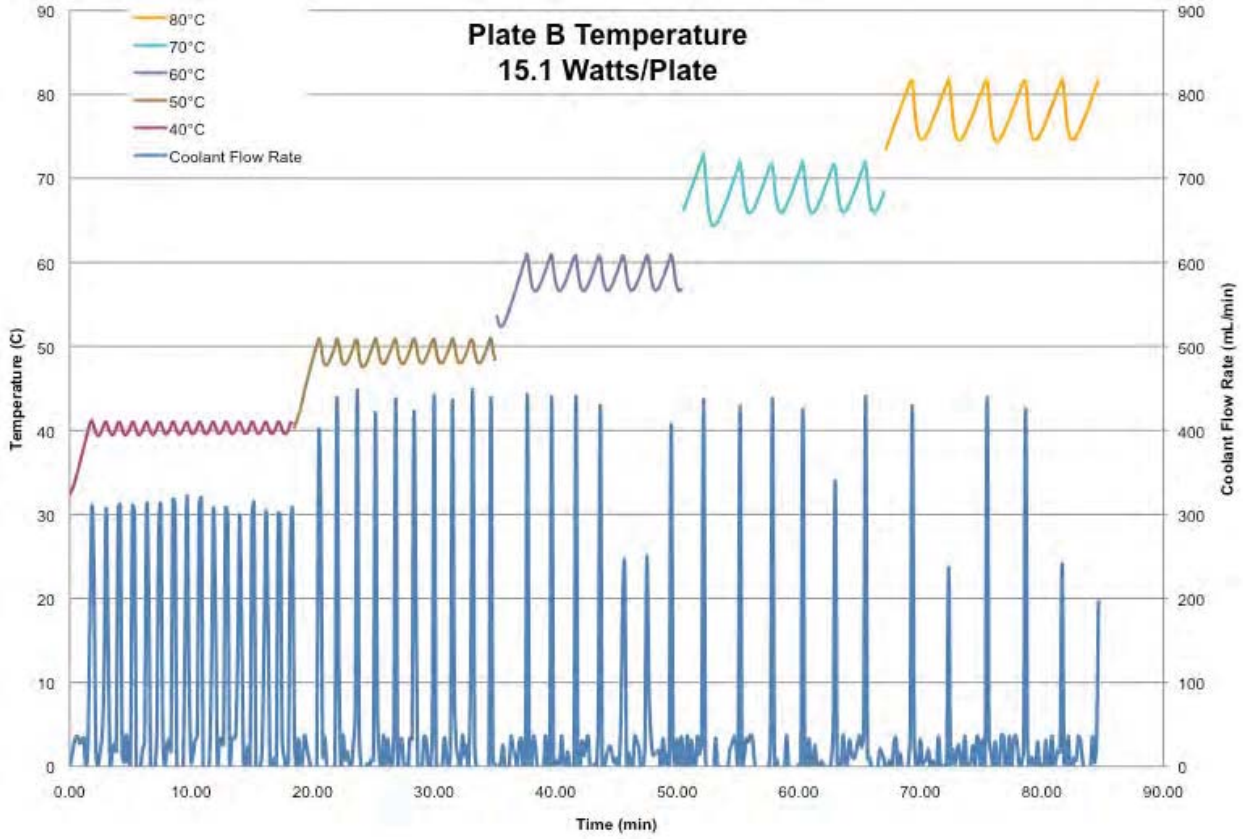

Figure 8.13.—Cooling Plate Temperature and Proportional Valve Flow Rate at 15.1 W/Plate

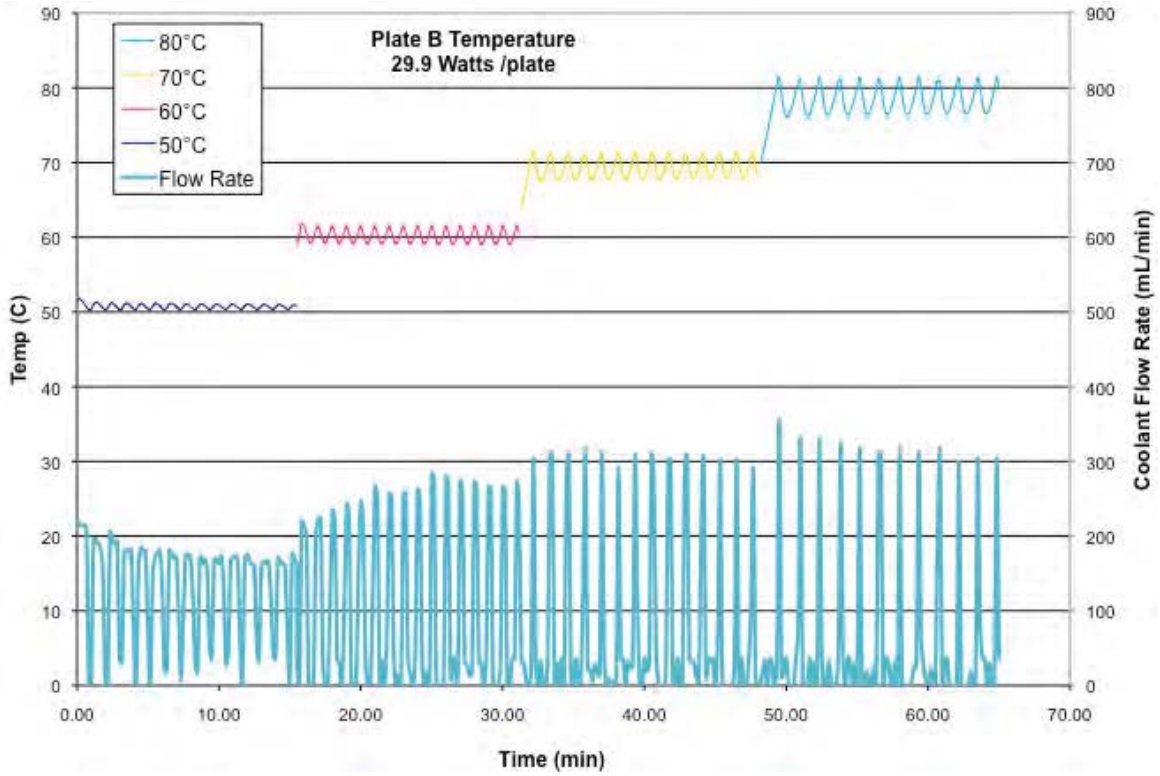

Figure 8.14.—Cooling Plate Temperature and Proportional Valve Flow Rate at 29.9 W/Plate

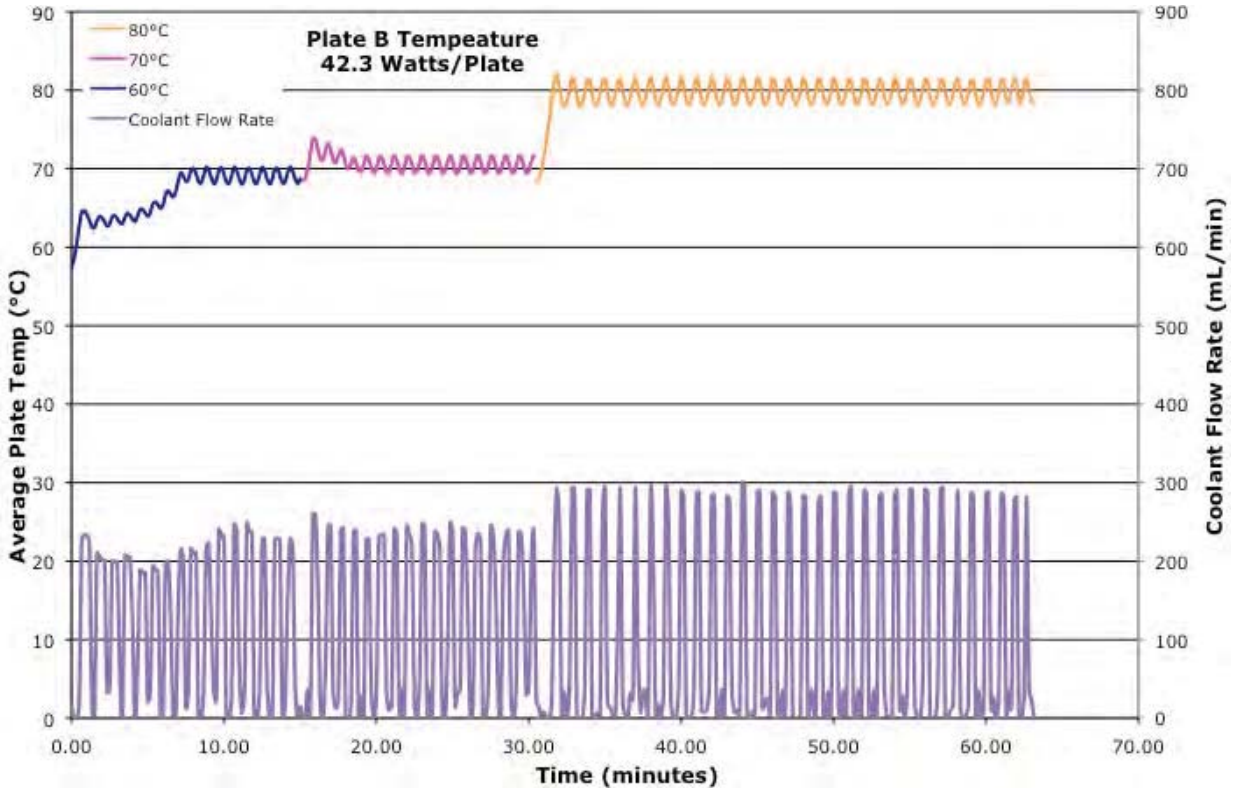

Figure 8.15.—Cooling Plate Temperature and Proportional Valve Flow Rate at 42.3 W/Plate

The temperature step control tests also illustrate how the control valve regulates the temperature. The valve continually cycles between open and closed to achieve the desired plate temperature by controlling the effective cooling flow rate. The frequency and magnitude of the valve opening varies depending on the desired temperature and plate heater power level. In all but the lowest power case, higher plate temperatures require reducing the valve frequency and increasing the valve opening amplitude. Overall, this produces a lower bulk flow rate thereby equalizing at a higher plate temperature. However, this also demonstrates why the oscillation in plate temperature is greater at the higher temperature set points. The higher magnitude oscillations in flow rate tend to overcool the plates causing the valve to almost fully close. By raising the cooling plate set-point temperature, the valve will close which in turn causes an increase in the cooling plate temperature. The plate's operating temperature responds quickly to the reduced cooling flow, causing their temperature to overshoot the set point temperature which in turn causes the valve to open allowing a high coolant flow rate. Overall, the higher the cooling plate set point temperature the faster the system will respond to changes in coolant flow.

It should be noted that the same PID control coefficients were used for all the set point temperatures and heater power levels. These coefficients worked well at the lower temperature set points where the system response time is slower. At faster response times or higher set point temperatures, different coefficients will be required to optimize the system and minimize the cooling plate temperature fluctuations.

8.2.2 Proportional Valve Power Profile Control Tests

Next, the control of the proportional valve was tested against the variable power profile, as shown in Figure 8.8 to quantify the valve's ability to maintain a set point temperature with variation in heater power. The results from this testing are shown in Figure 8.16 and Figure 8.17 for various set point temperatures.

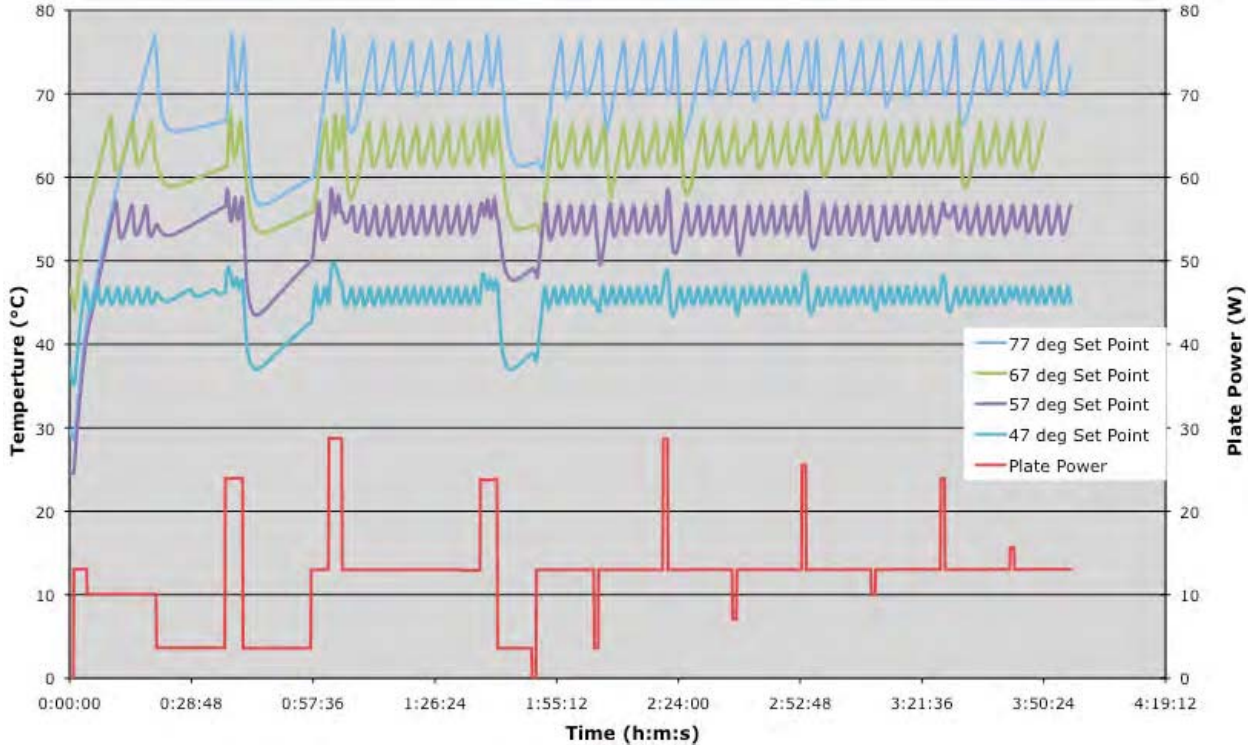

Figure 8.16.—Cooling Plate B Temperature for Various Proportional Valve Set Points with a Variable Heater Power Profile

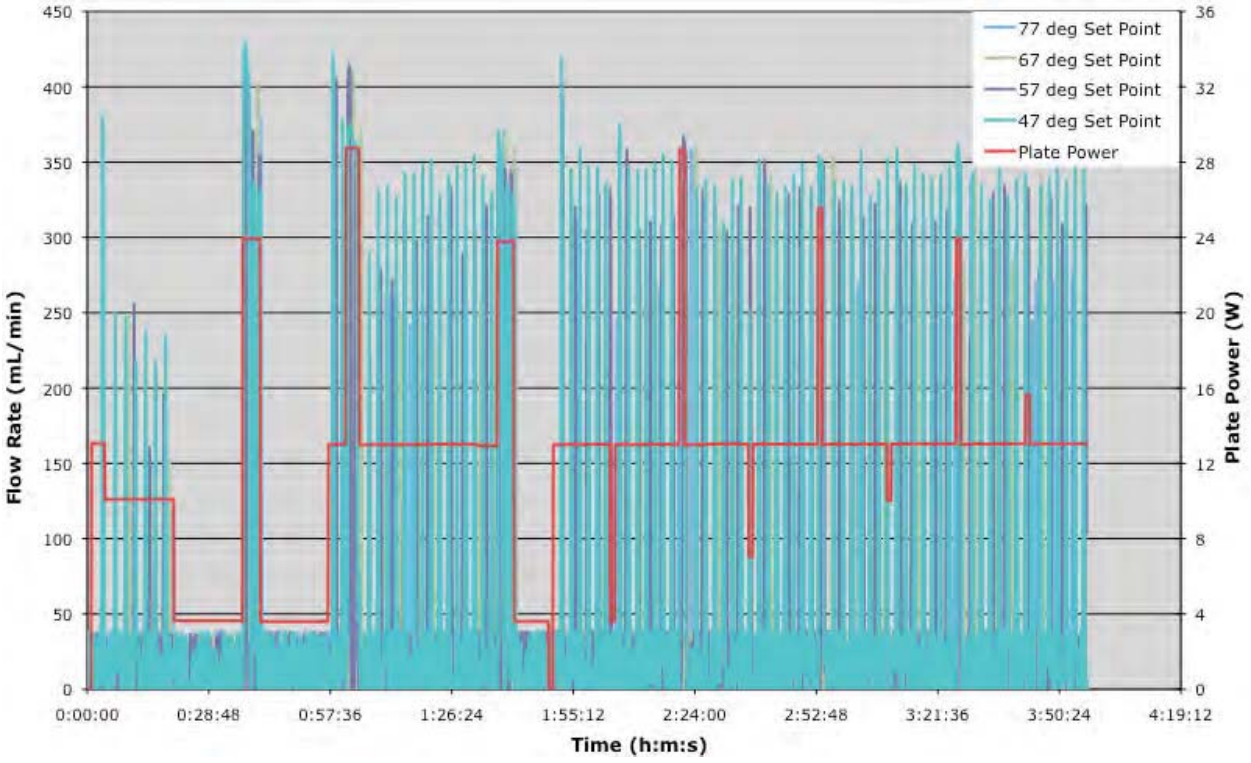

Figure 8.17.—Cooling Plate B Flow Rate for Various Proportional Valve Set Points with a Variable Heater Power Profile

The power profile test results with the proportional valve show similar trends as with the constant power tests. The valve was able to maintain the set point temperature fairly well over the duration of the test but oscillated about the set point value. Similarly, the oscillation amplitude increased with higher set point temperatures. In all cases, the drop off in heater power that occurred at approximately 40 min and again at 1 hr 40 min caused a significant drop in the cooling plate temperature to values below the set point level. The temperature remained low until the next increase in heater power that brought it back up the set-point value. During other heater power decreases that occurred during the testing, the plate temperature fluctuated outside the normal band and then recovered back to the set point quickly. The two large decreases in heater power were the largest performed during the testing and decreased the heater power to a low value below 5 W/plate. This caused the valve to effectively close with an oscillating flow below 40 ml/min, as seen in Figure 8.17. It is believed that the reason for the plate temperature drop was that the large drop in heater power caused an overcooling of the cooling plate due to the inherent lag time in the valve response. The subsequent low heater power level was not sufficient to quickly return the temperature to the set point and it therefore equalized at a lower temperature with the valve closed. It should be noted that when the valve was closed, there is still a low level of flow through the valve, as seen in Figure 8.17. The flow rates, shown in Figure 8.17 also show that the magnitude of the flow rate was similar for all of the set point temperatures. The main difference between the test runs at different set point temperatures was in the frequency in which the valve opened and closed to maintain the desired temperature.

9.0 Summary

The testing described in the previous sections was performed to evaluate the concept of extracting heat from a fuel cell through the use of passive cooling plates. The heat would ultimately be removed from an external liquid cooling loop through the use of a manifold that interfaces with the cooling plates.

Overall, the testing focused on two main types of cooling plates: those constructed of highly thermally conductive pyrolytic graphite and different types of flat plate heat pipes. Tests were performed to determine the thermal conductivity of the different types of cooling plates as well as control samples of different types of metals. The thermal conductivity of the TPG and heat pipe cooling plates was significantly higher than those of the metal test samples. The TPG cooling plates had a thermal conductivity on the order of 4 times that of a similarly sized copper plate. Whereas the flat plate heat pipes had effective thermal conductivities an order of magnitude or greater than the copper cooling plate. The TPG cooling plates needed to be coated or covered due to the brittleness of the material and that the surface would tend to rub and flake off when handled. A number of coverings were evaluated including, cladding with glued on metal sheets, diffusion bonding, plating and painting. Of these both the glued on cladding and the painting produced durable plates and limited the reduction in thermal conductivity.

The cooling plates were also tested to evaluate their electrical conductivity. Mixed results for the electrical conductivity were achieved. It was determined that the heat pipe electrical conductivity was susceptible to oxidization. This was particularly problematic for the titanium heat pipes. The TPG plates clad with electrically conductive glues had overall good electrical conductivity. The painted TPG plates, which utilized a silver paint, had the highest electrical conductivity.

Both types of cooling plates worked well in extracting heat from the fuel cell. There was an orientation issue encountered with one of the flat plate heat pipe designs. It was determined that the heat pipe could not return the internal coolant to the evaporator section against gravity, when it was oriented with the condenser below the evaporator. Under other orientations it works well.

To extract heat from the cooling plates a number of cooling manifolds were designed and tested. The cooling manifolds differed in the types of materials they were constructed from as well as the cooling fluid passage design. The manifold design that performed best consisted of a single anodized aluminum

body that had both grooves for the cooling plates and circular passages for the cooling water. This design performed best because it minimized the distance between the cooling plates and cooling fluid and also had a minimum of material interfaces between the plates and fluid. Also being constructed from aluminum provided an added benefit due to the good thermal conductivity of aluminum. However, this required it to be anodized in order to eliminate its electrical conductivity.

The last item evaluated was the control of the cooling plate temperature by varying the coolant flow through the manifold. This is necessary because in an operational fuel cell system it would be desirable to maintain a constant cell temperature over a range of power output levels, and corresponding internal heat generation levels, of the fuel cell. Two different types of control valves were evaluated to regulate the coolant flow through the manifold. These consisted of a passive type valve and an active valve. The passive valve utilized a wax cylinder that would expand or contract depending on the coolant temperature opening and closing the valve. Through a number of tests it was determined that a passive valve that utilized a small by-pass flow to provide heat to the control cylinder worked best. However, the passive valve had a lag time in its operation due to the time it took for heat from the cooling plate to effect the water temperature within the manifold. Also for the passive valve to open and increase flow rate the coolant temperature had to increase. Therefore at higher power levels where there was more waste heat, the flow rate through the passive valve would equalize at a higher temperature. So it was not possible to maintain a fixed temperature with the passive valve. The plate temperature would vary over a range depending on the amount of waste heat the needed to be removed.

The active valve operated by using a feedback loop based on the output of thermocouples located on the cooling plates. The valve would open or close based on changes in the plate temperature. The active valve responded quickly to changes in waste heat and corresponding cooling plate temperature and was able to maintain the cooling plate near a fixed temperature over a range of waste heat levels.

In summary these tests demonstrated that waste heat could be successfully removed from a fuel cell utilizing conductive cooling plates and that the temperature of the fuel cell can be controlled through these cooling plates.

Appendix A.—TPG Cooling Plate Design Drawings

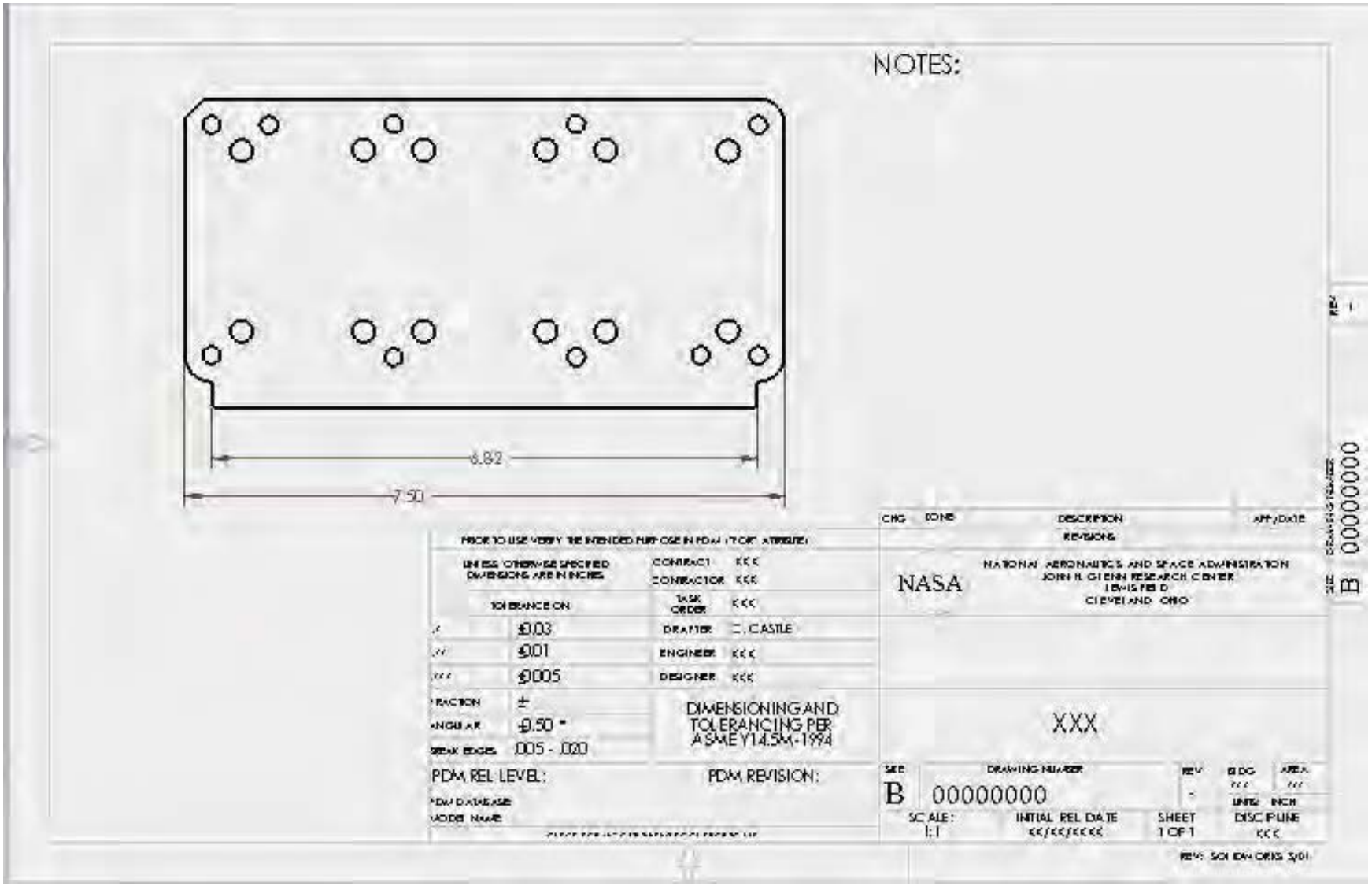

Figure A.1.—Stack TPG Cooling Plate

Appendix B.—Thickness Measurements of 12 TPG Plates

Plots of this thickness distribution are given in Figure B.1 to Figure B.12.

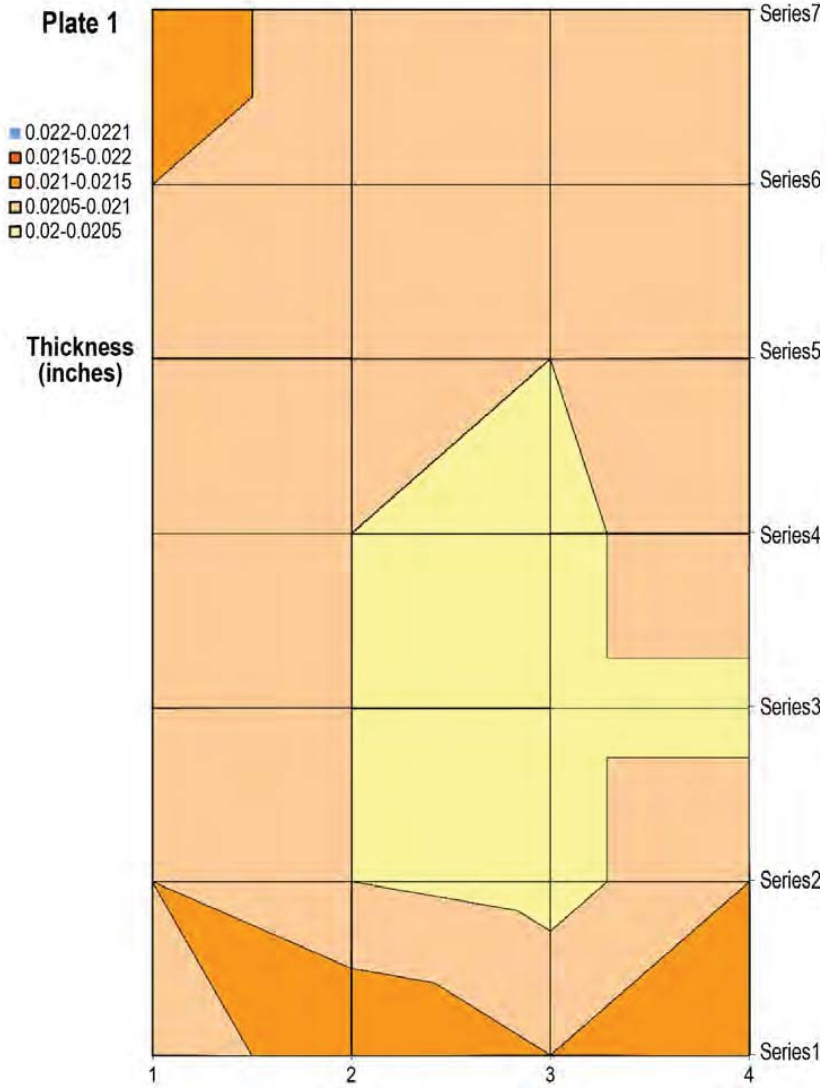

Figure B.1.—Plate 1 Thickness Profile

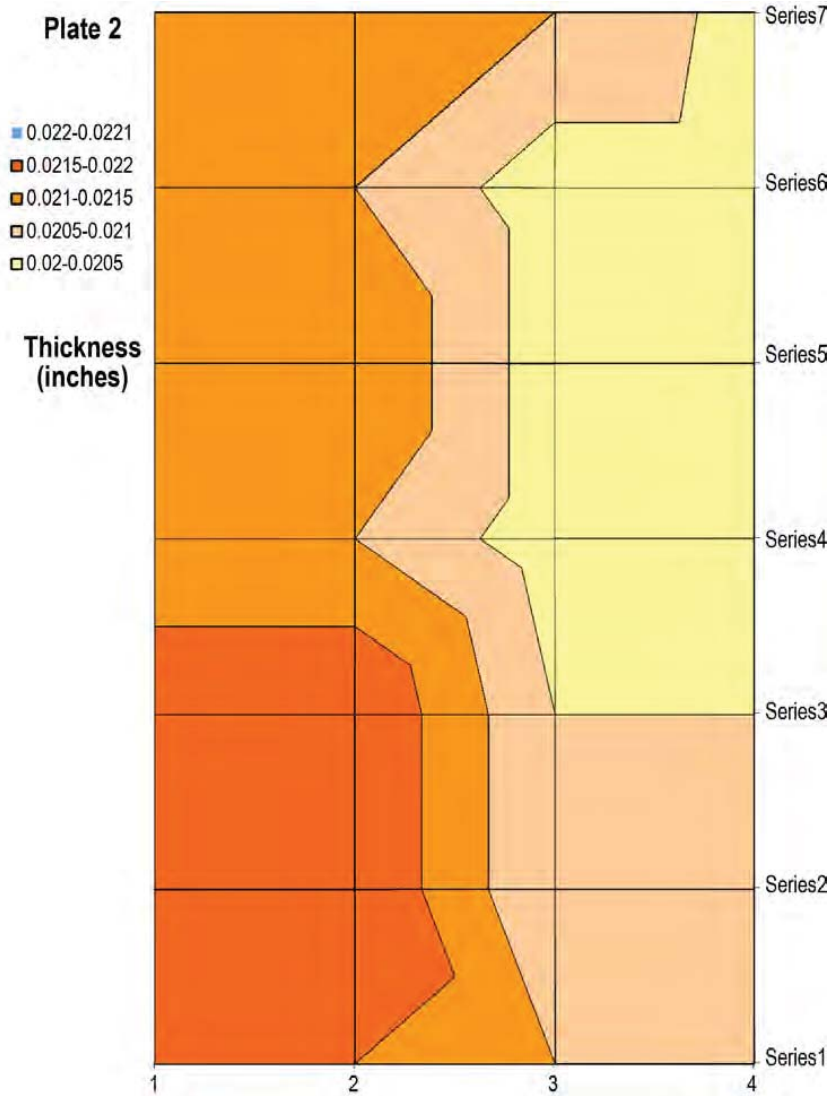

Figure B.2.—Plate 2 Thickness Profile

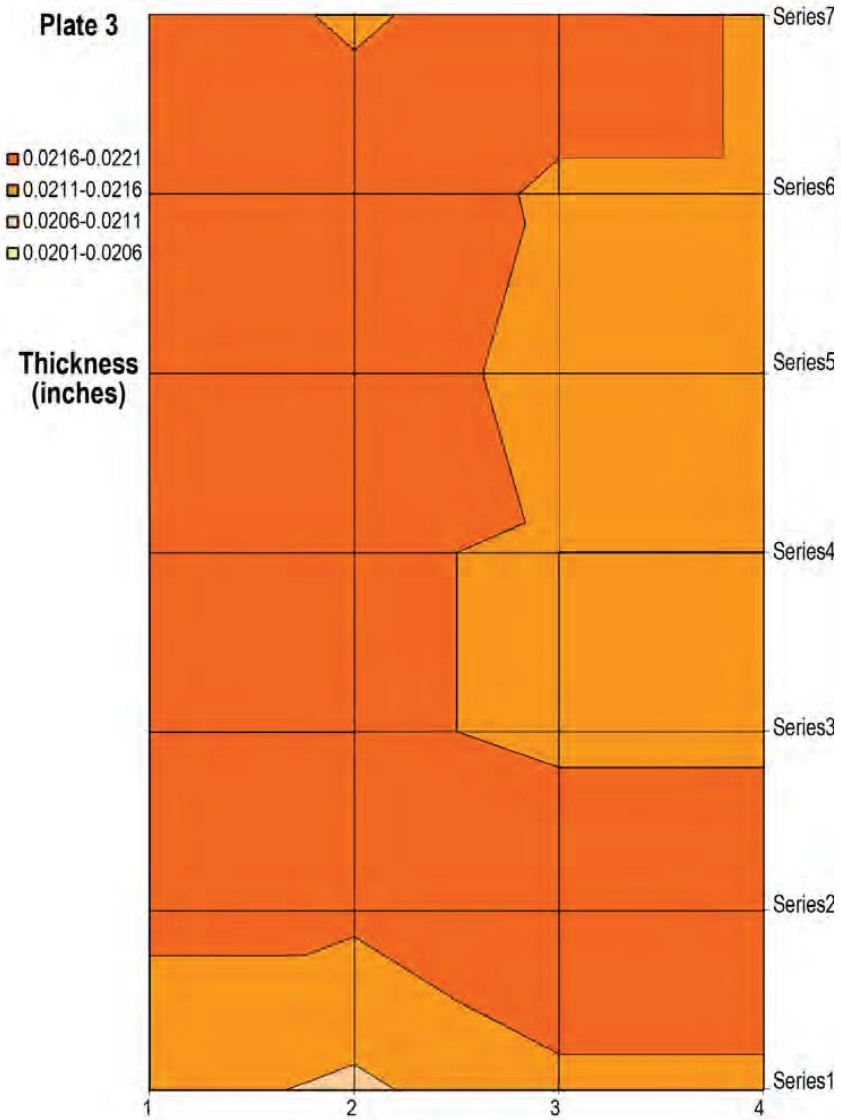

Figure B.3.—Plate 3 Thickness Profile

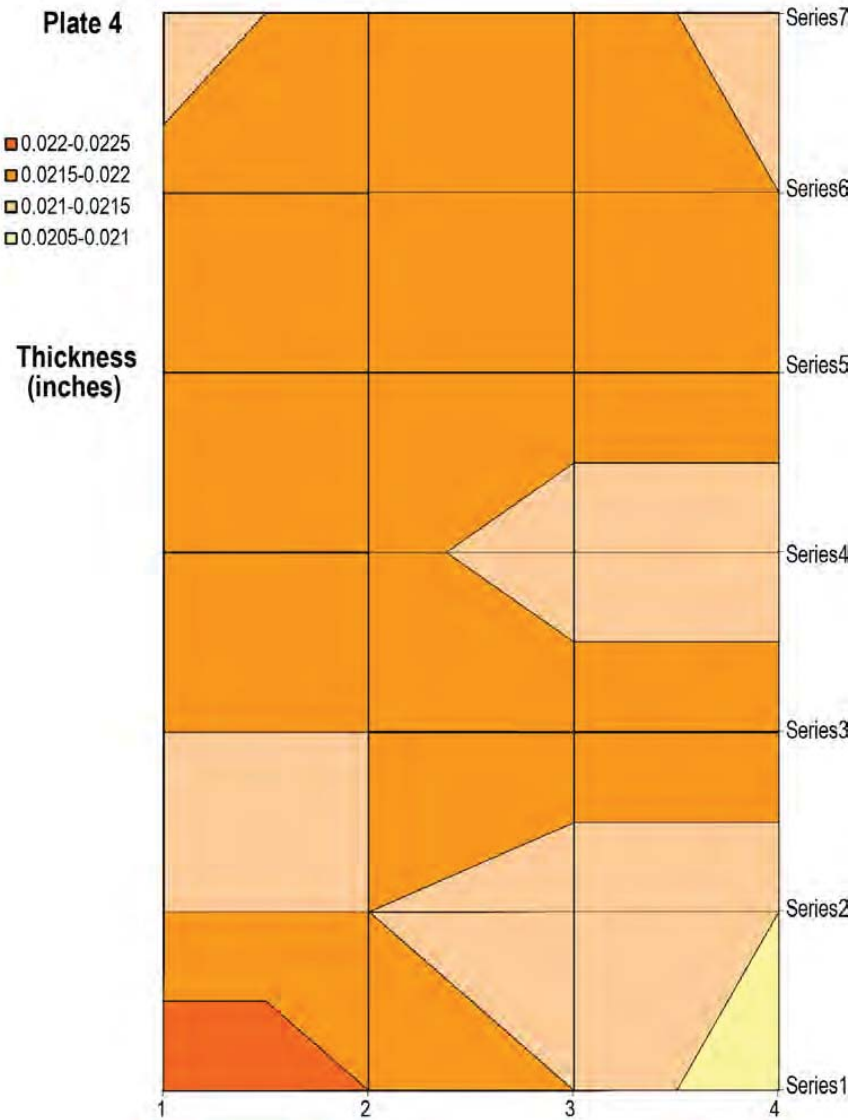

Figure B.4.—Plate 4 Thickness Profile

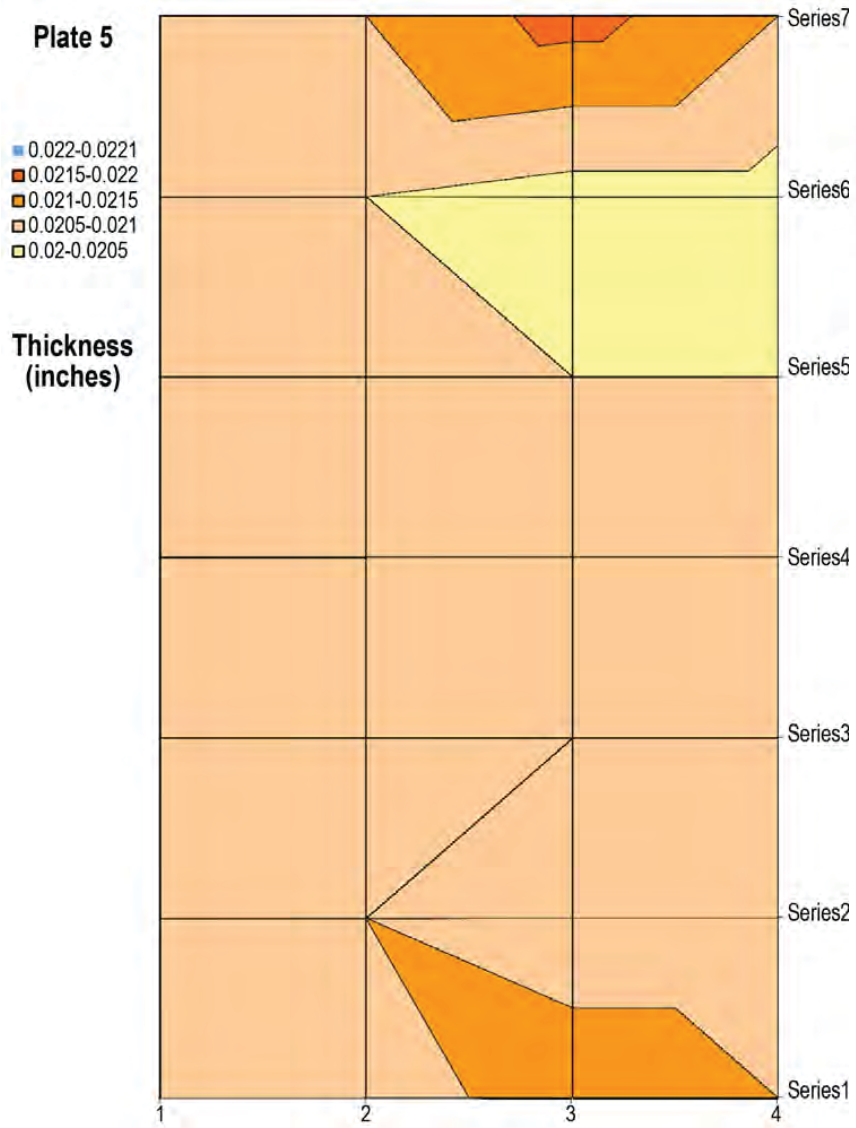

Figure B.5.—Plate 5 Thickness Profile

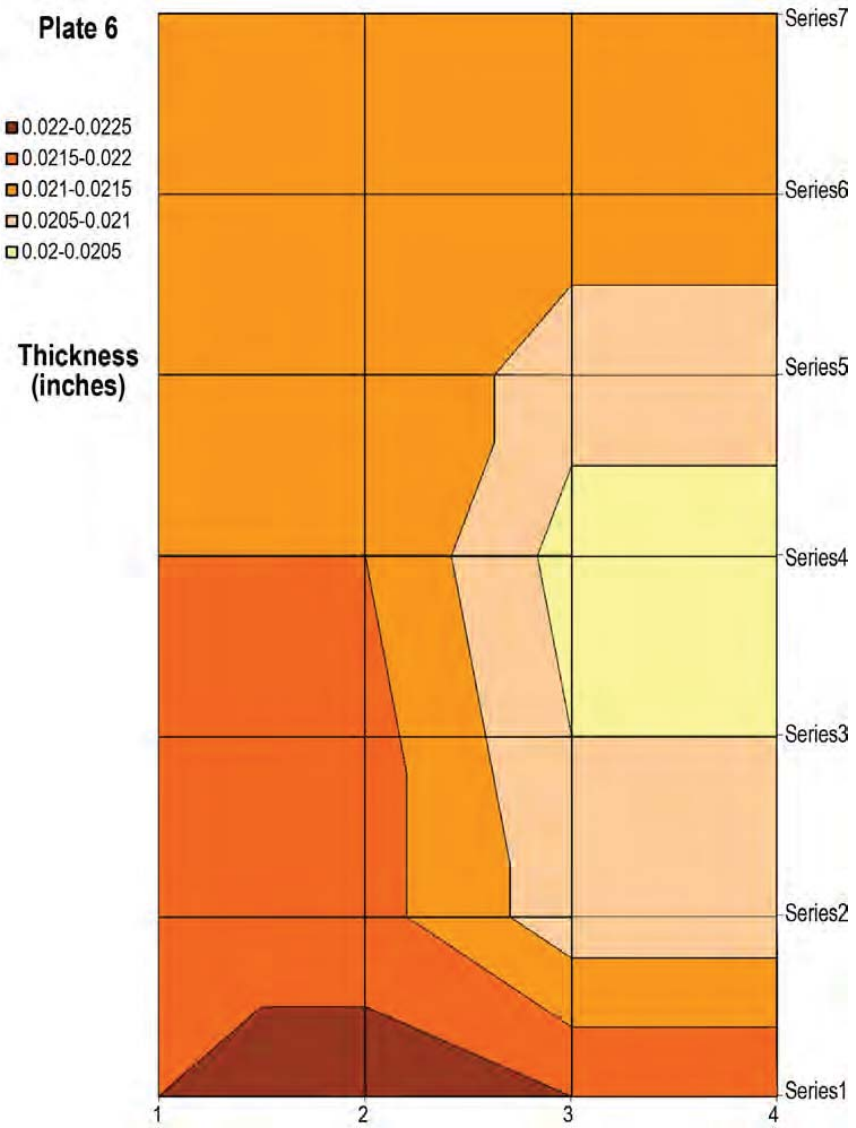

Figure B.6.—Plate 6 Thickness Profile

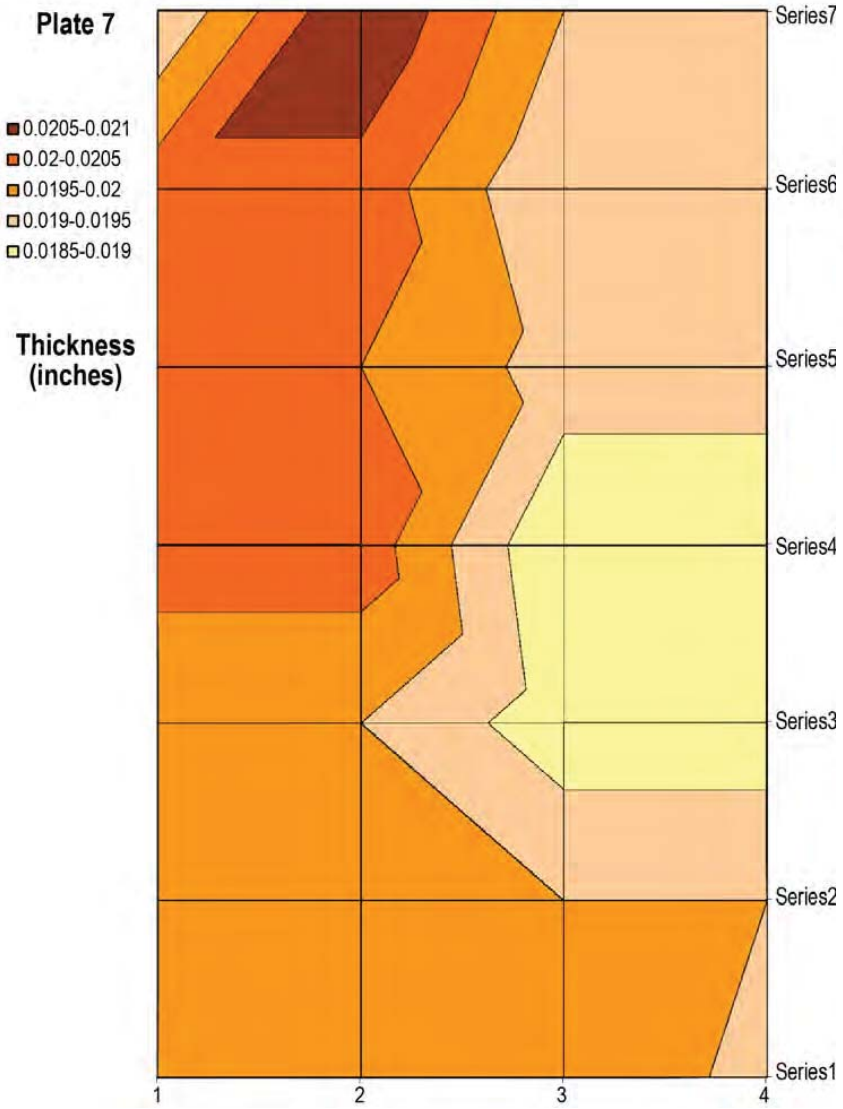

Figure B.7.—Plate 7 Thickness Profile

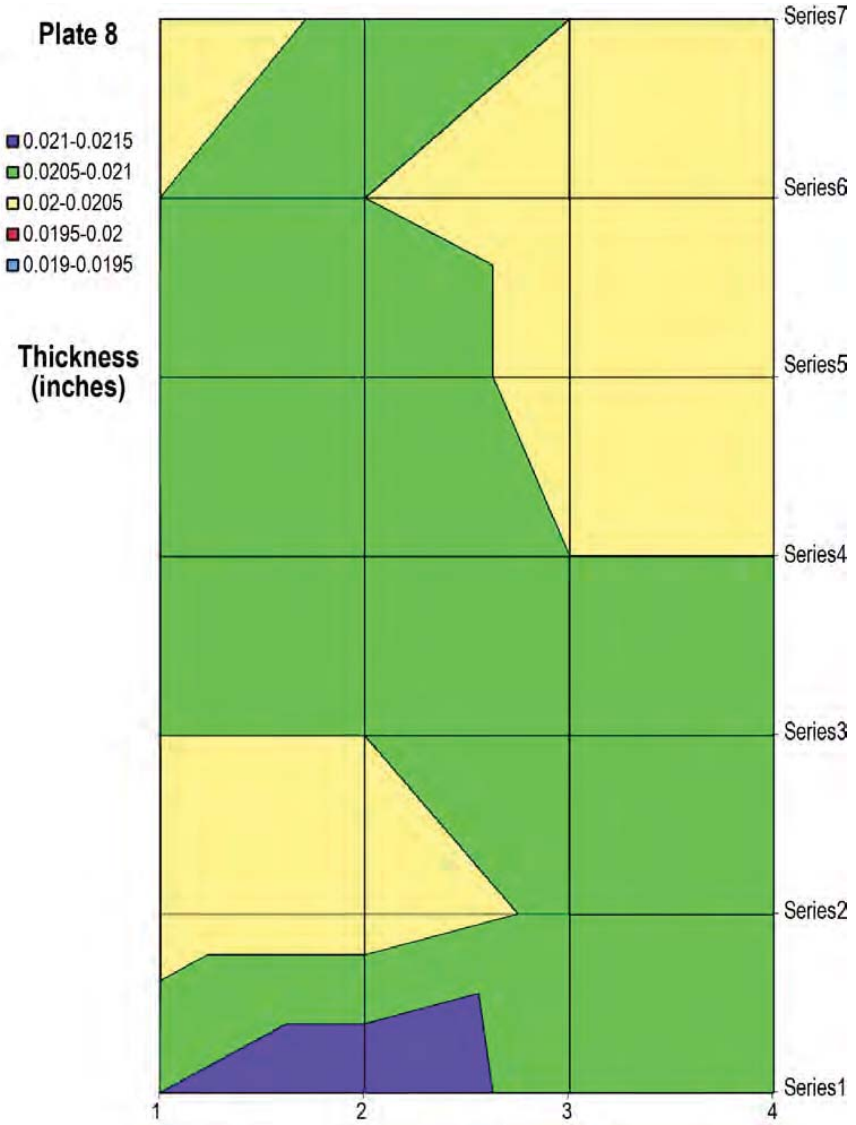

Figure B.8.—Plate 8 Thickness Profile

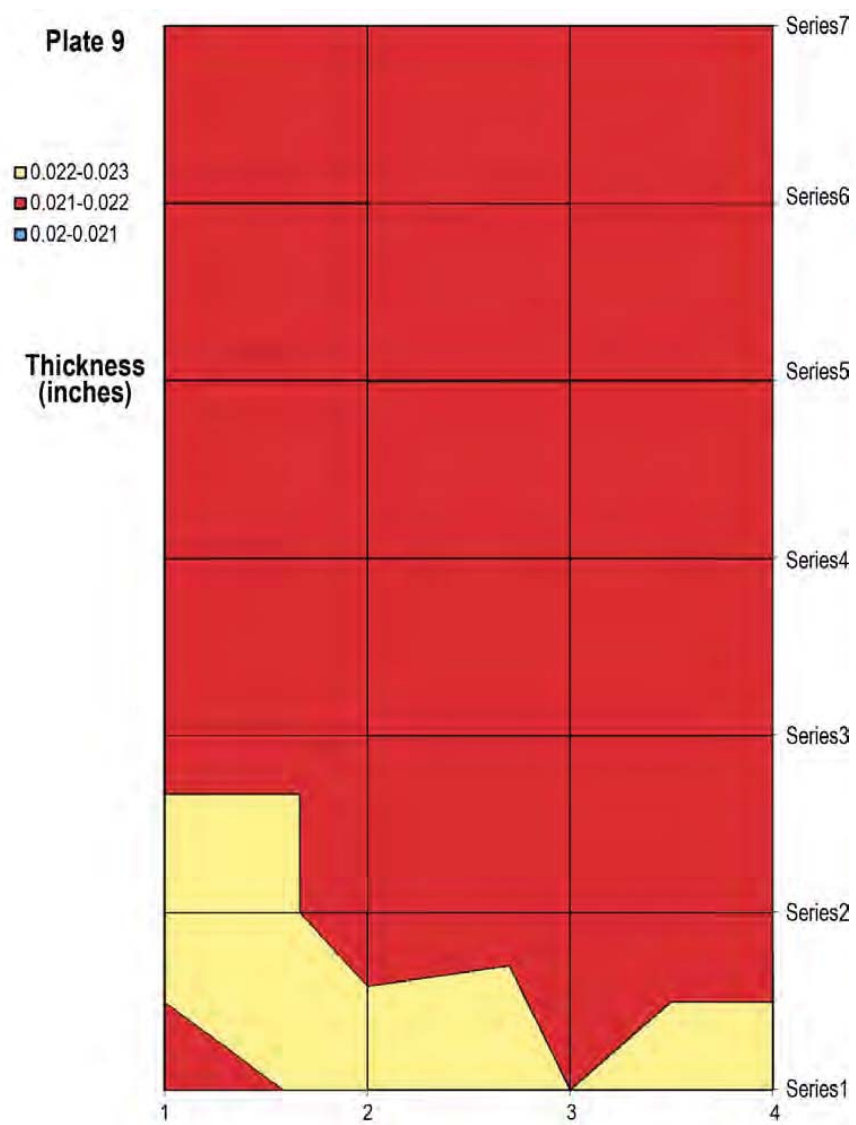

Figure B.9.—Plate 9 Thickness Profile

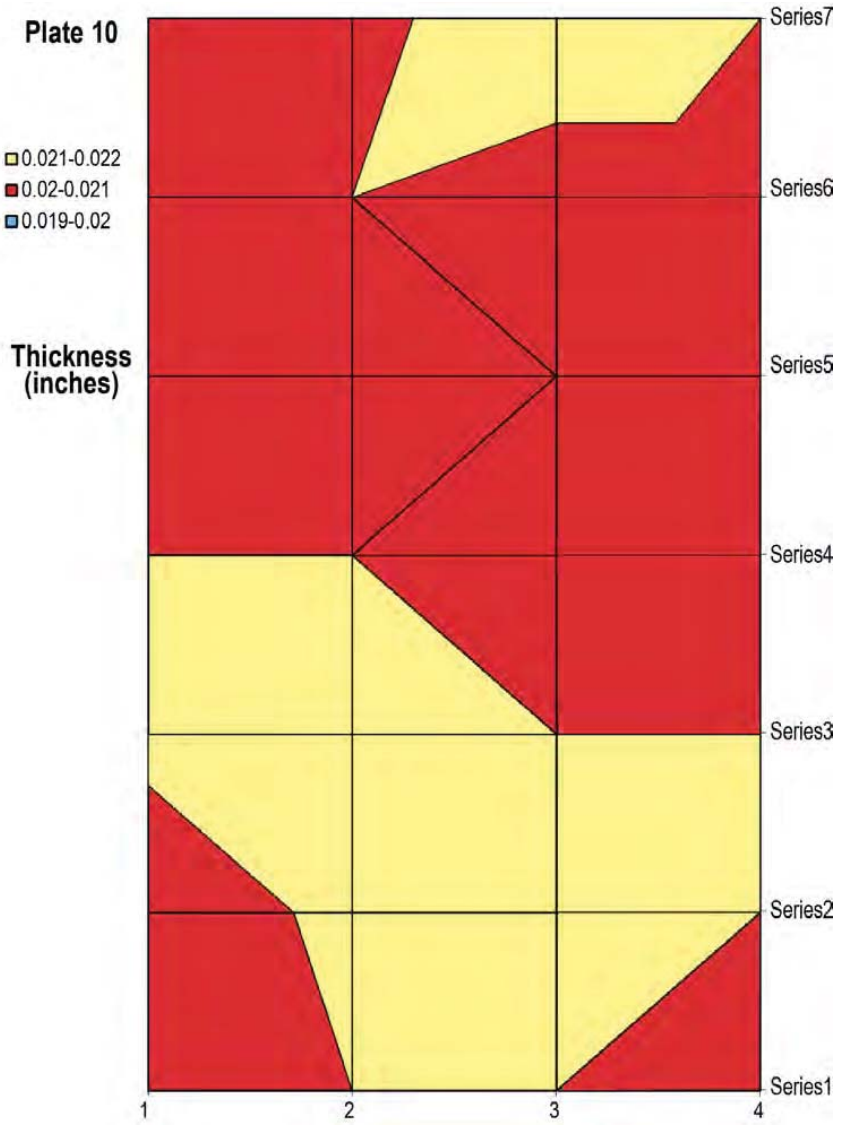

Figure B.10.—Plate 10 Thickness Profile

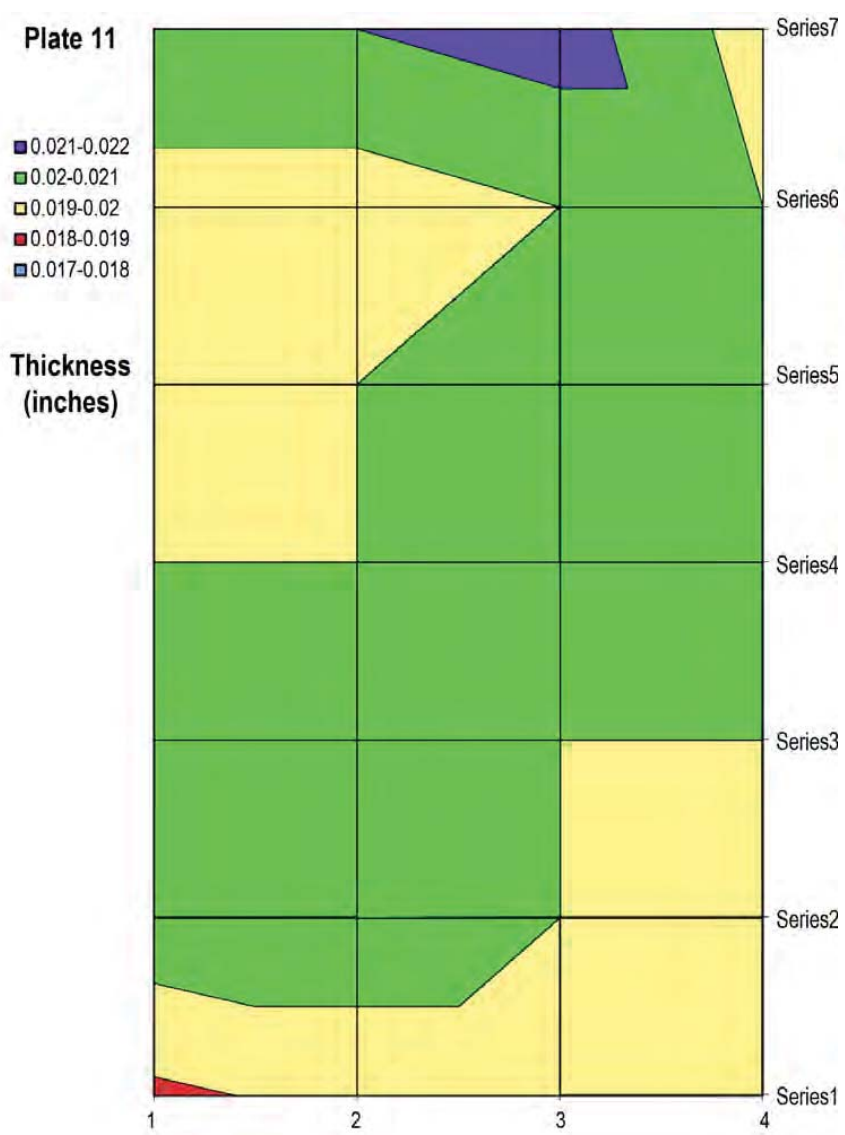

Figure B.11.—Plate 11 Thickness Profile

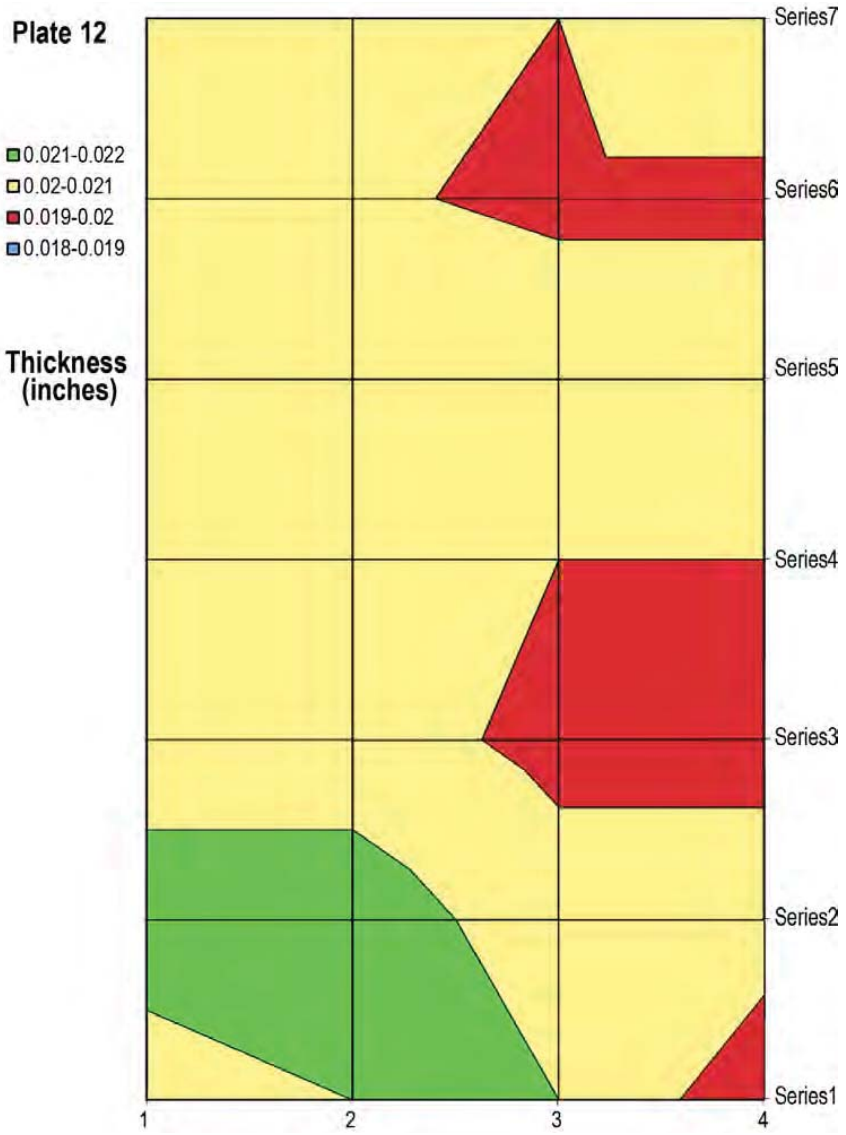

Figure B.12.—Plate 12 Thickness Profile

Appendix C.—Cooling Manifold Design Drawing

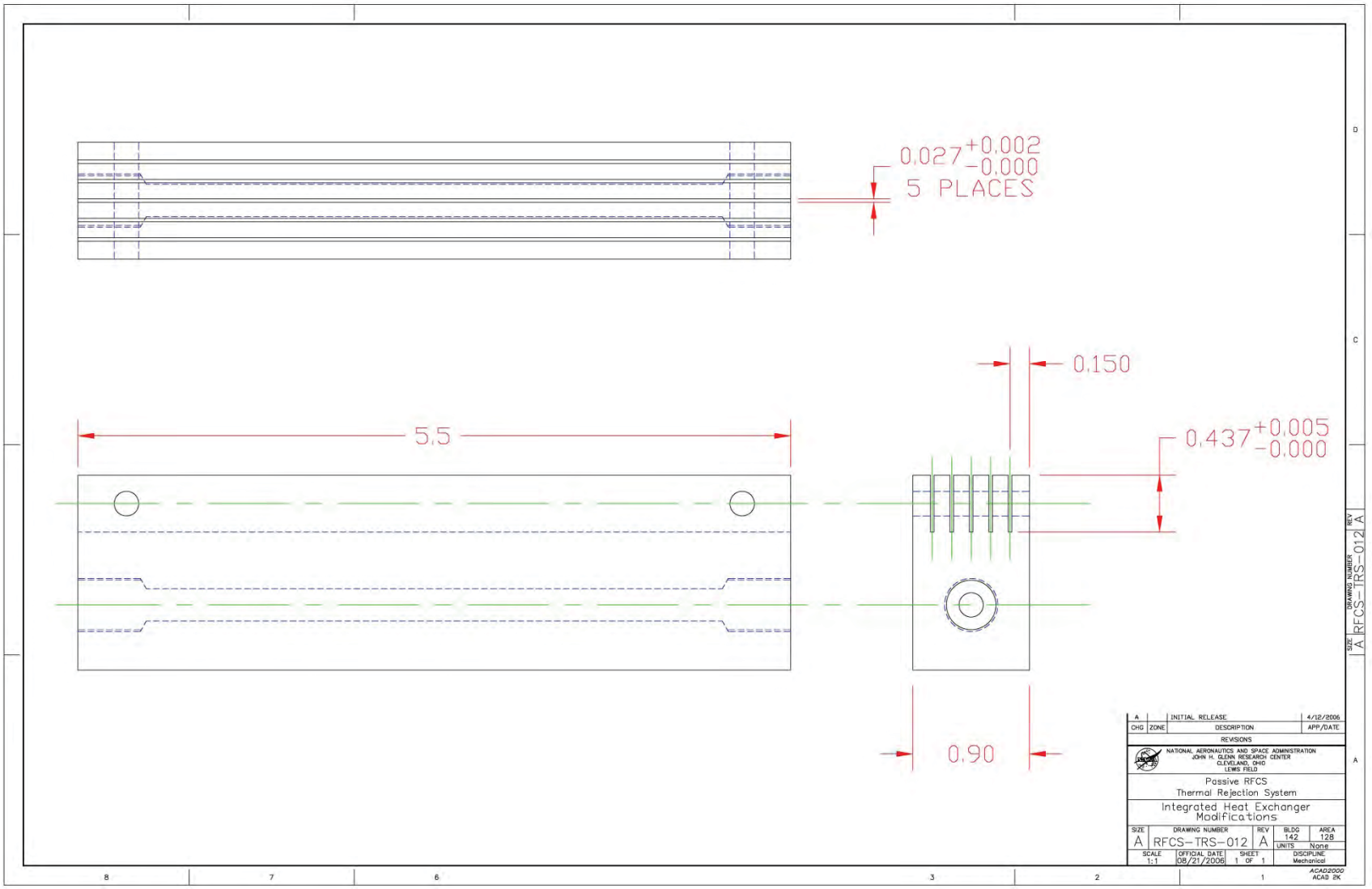

Figure C.1.—Metal Manifold Design Drawing for Use with TPG Cooling Plates

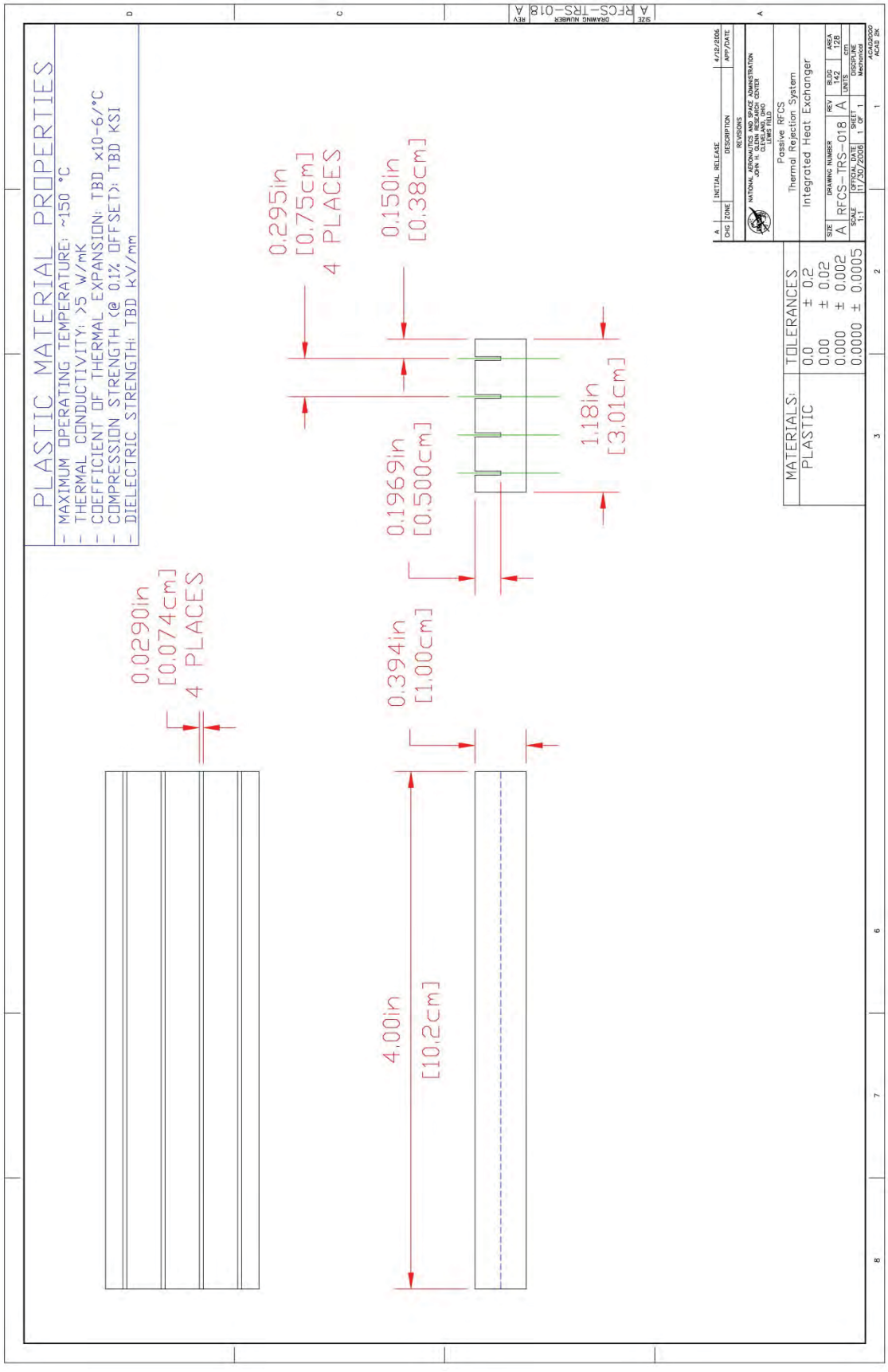

Figure C.2.—LCP Plastic Manifold Design Drawing for Use with TPG Cooling Plates

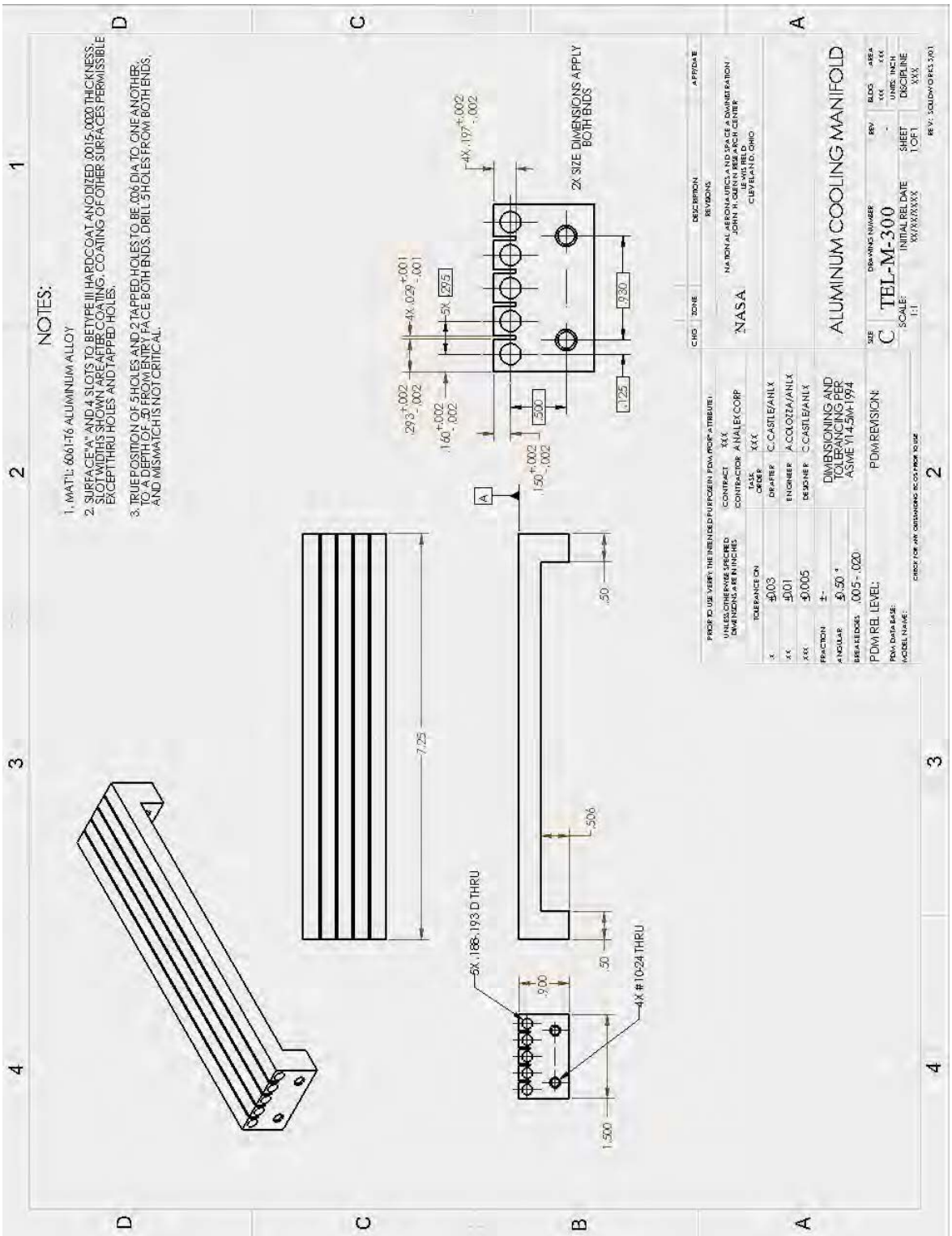

Figure C.3.—Anodized Aluminum Cooling Manifold

Appendix D.—Temperature Distribution on the Cooling Plates

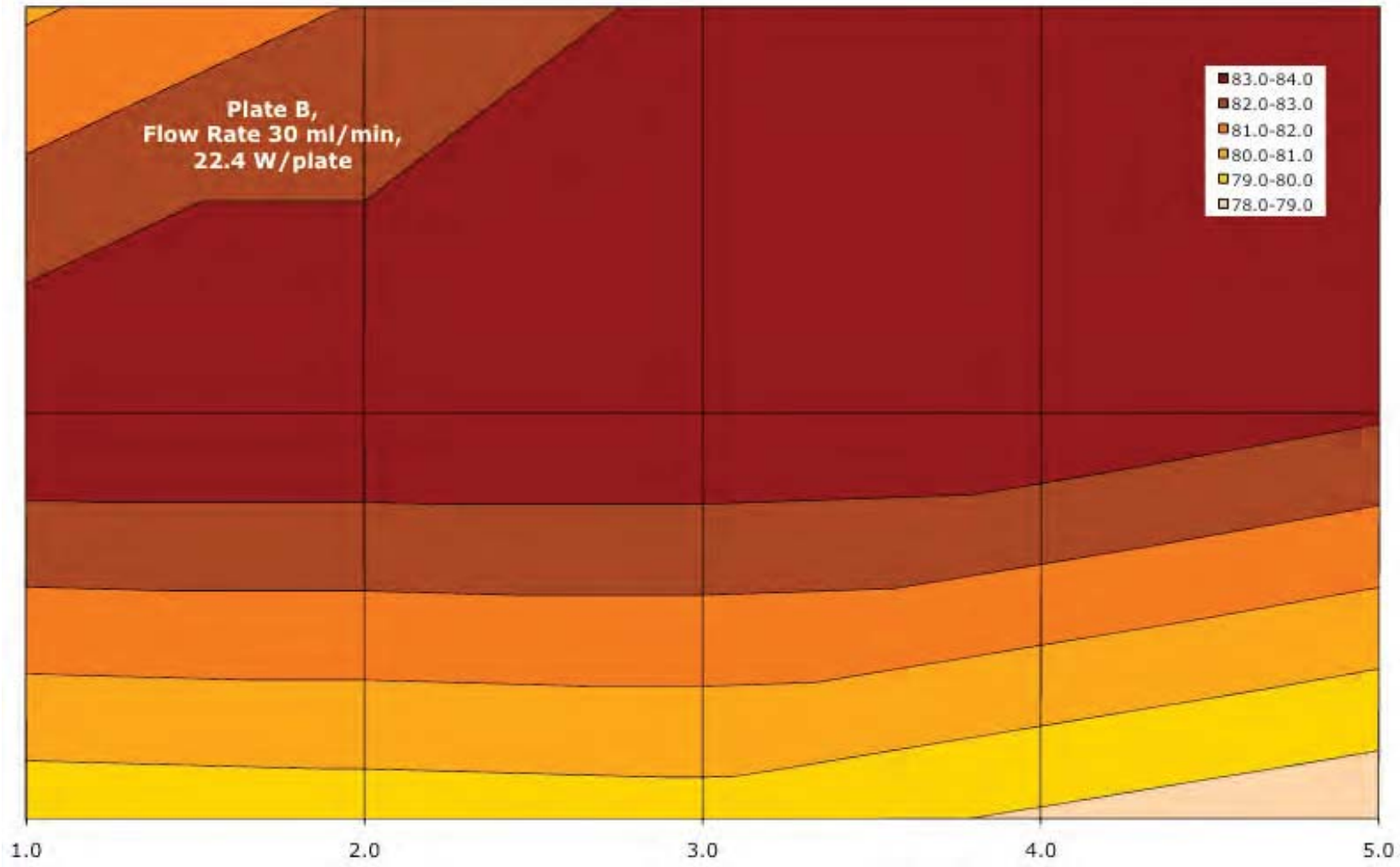

Figure D.1.—Steady State Temperature Distribution on Plate B at 22.4 W Heater Power and 30 ml/min Cooling Flow Rate

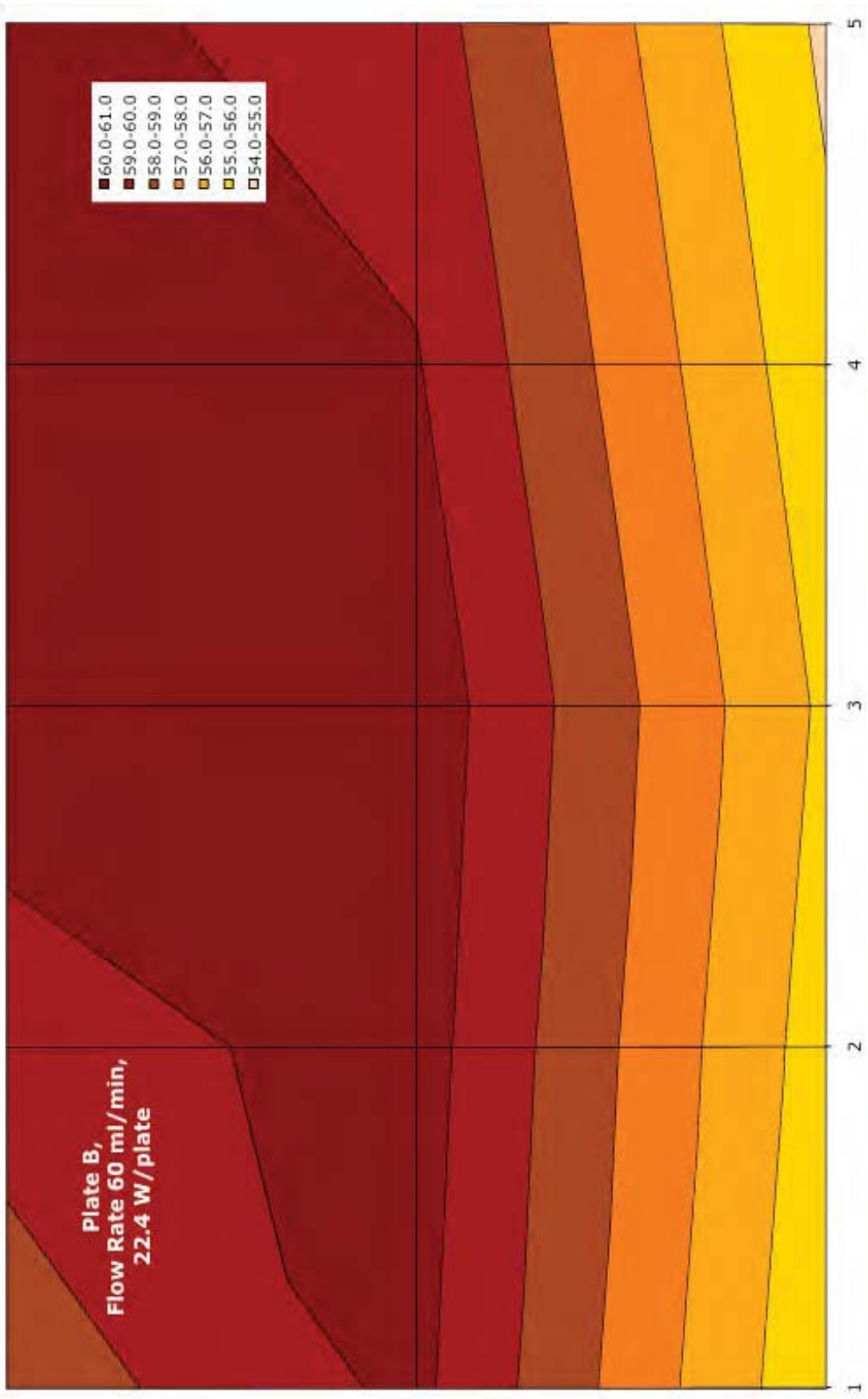

Figure D.2.—Steady State Temperature Distribution on Plate B at 22.4 W Heater Power and 60 ml/min Cooling Flow Rate

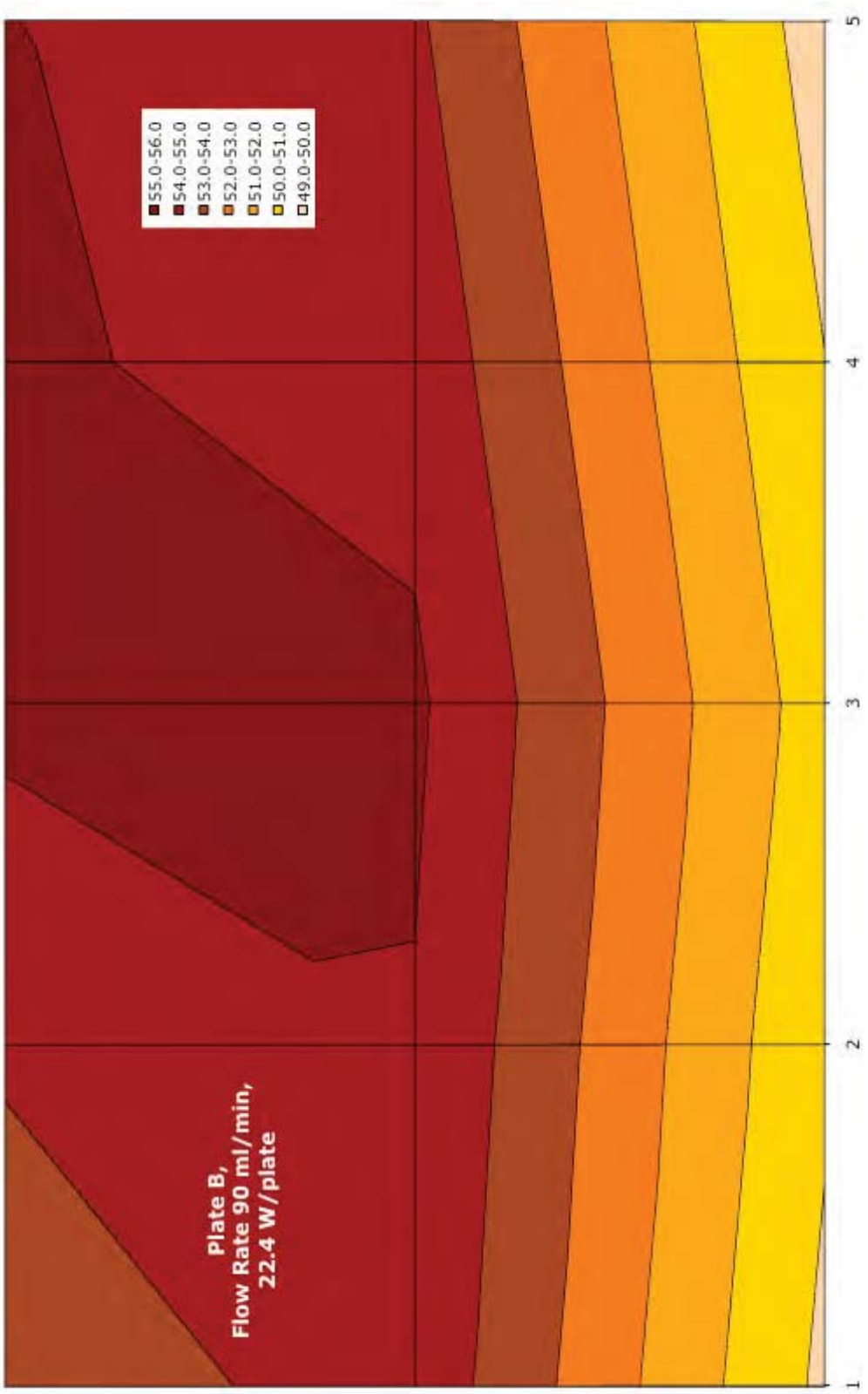

Figure D.3.—Steady State Temperature Distribution on Plate B at 22.4 W Heater Power and 90 ml/min Cooling Flow Rate

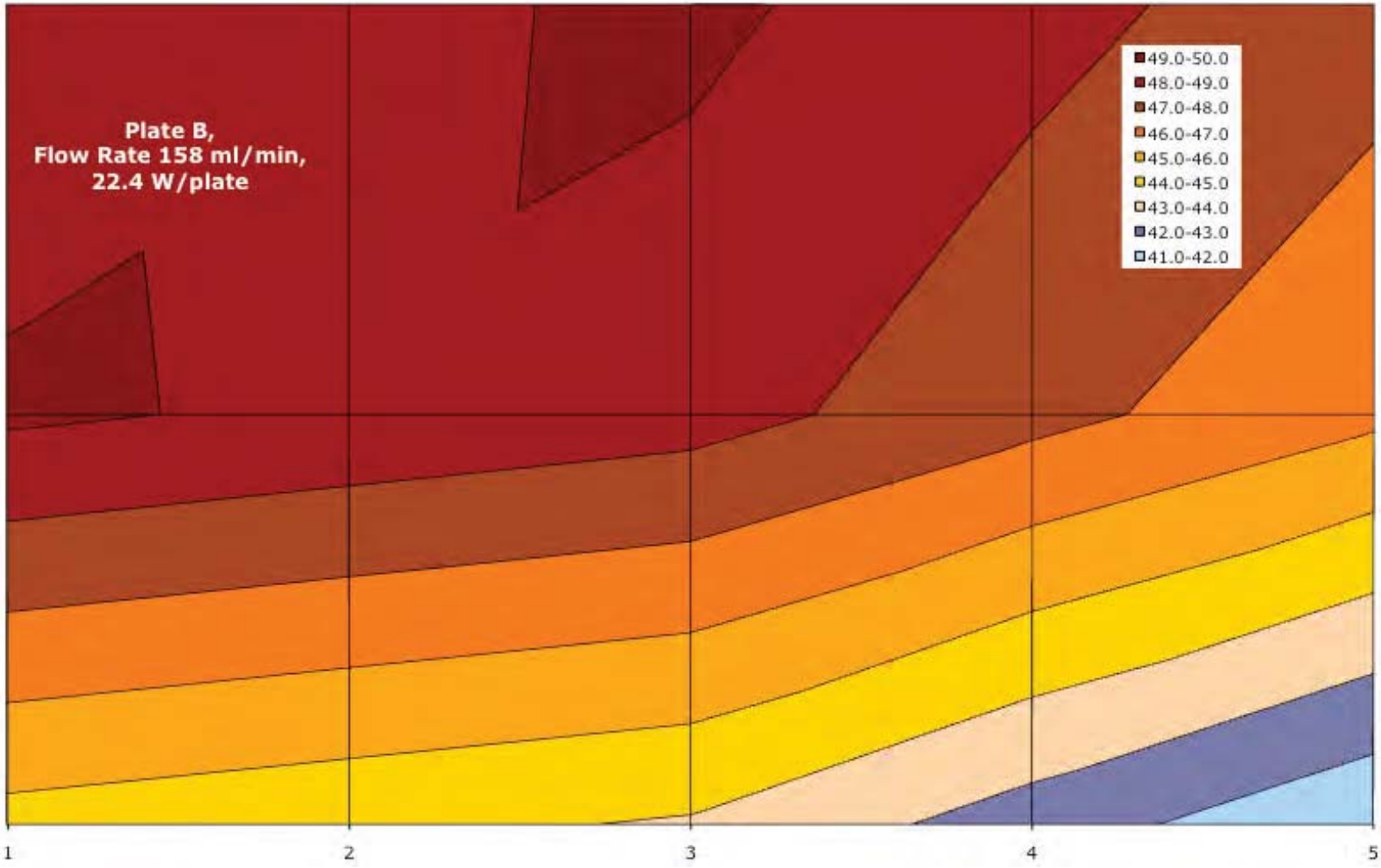

Figure D.4.—Steady State Temperature Distribution on Plate B at 22.4 W Heater Power and 158 ml/min Cooling Flow Rate

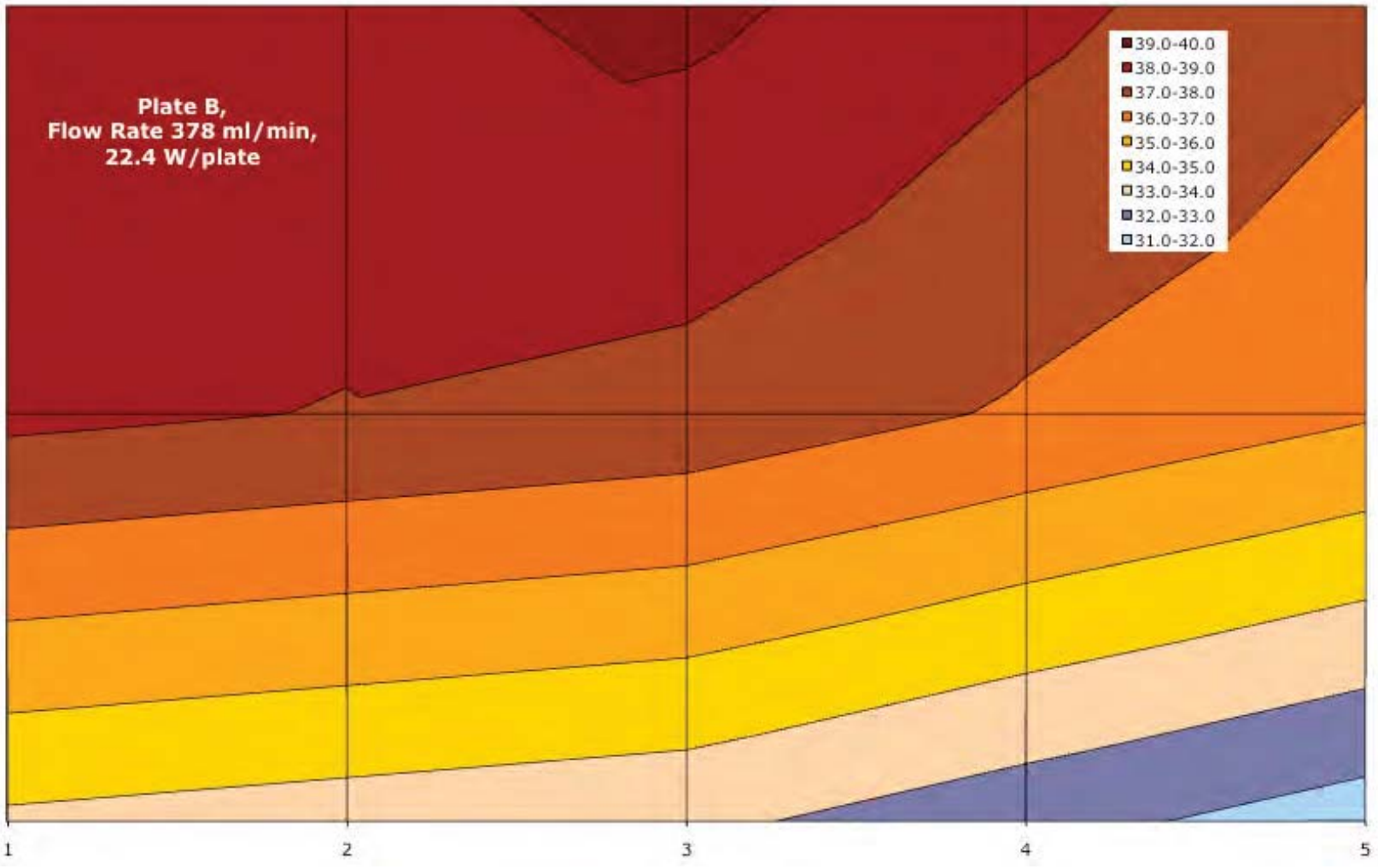

Figure D.5.—Steady State Temperature Distribution on Plate B at 22.4 W Heater Power and 378 ml/min Cooling Flow Rate

References

1. Colozza, A.J. and Burke K.A., “Fuel Cell Thermal Management Through Conductive Cooling Plates,” NASA/TM—2008-215149, May 2008.
2. Btechcorp materials web site, http://www.btechcorp.com, January 2007.
3. SPI Supplies web site, http://www.2spi.com, November 2007.
4. Bejan, A. and Kraus A.D., Heat Transfer Handbook, John Wiley & Sons Publisher, 2003.
5. Hand Book of Tables for Applied Engineering Science, 2nd Edition, CRC Press, 1973.
6. Incopera, F.P. and Dewitt, D.P., Fundamentals of Heat and Mass Transfer, 3rd Edition, 1990.
7. Semenov S.Y. and Burke, K.A., “Titanium Heat Pipe Thermal Plane,” presented at Space Technology and Applications International Forum, STAIF 2008, Albuquerque, New Mexico, 10-14 February 2008.
8. Semenov, S.Y., “Final Report: Lightweight Thin Titanium-Water Vapor Chamber Heat Pipes for APWR PFC Demonstrator System,” October 2007.
9. http://www.coolpolymers.com/files/ds/Datasheet_d5506.pdf , accessed October 15, 2014
10. http://www.bergquistcompany.com/thermal_materials/gap_filler/gap-filler-4000.htm, accessed October 15, 2014.
11. Love, J., Process Automation Handbook, Springer-Verlag London, 2007.